

Pathomechanisms of AMPA receptor signalling in chronic CNS inflammation

Dissertation
to Fulfill the Requirements for the Degree of
doctor rerum naturalium (Dr. rer. nat)

**Submitted to the Council of the Faculty of Medicine
of the Friedrich Schiller University Jena**

**by Dipl. biol. Holger Uwe Haselmann
born on 23rd March 1985 in Lichtenfels**

Gutachter (*akademischer Grad, Vor- und Nachname sowie Wirkungsort*)

1. Prof. Dr. med. Christian Geis, Klinik für Neurologie,
Universitätsklinikum Jena
2. Prof. Dr. med. Otto W. Witte, Klinik für Neurologie,
Universitätsklinikum Jena
3. Prof. Dr. med. Dipl. phys. Stefan Hallermann, Carl-Ludwig-Institut für
Physiologie, Universität Leipzig

Tag der öffentlichen Verteidigung: 06.03.2018

I Table of Contents

| | | |
|-------|------------------------------------------------------------------------------------------------------------------|-----|
| I | Table of Contents | 1 |
| II | GLOSSARY | 3 |
| III | Summary..... | 5 |
| IV | Zusammenfassung | 6 |
| 1 | Introduction | 7 |
| 1.1 | Discovery of autoimmune encephalitis as a new entity of autoimmune disorders in the central nervous system | 7 |
| 1.2 | Testing the pathogenic relevance of autoantibodies to synaptic antigens..... | 8 |
| 1.2.1 | In-vitro assays | 8 |
| 1.2.2 | Animal models..... | 9 |
| 1.3 | AE aABs show a wide spectrum of synaptic antigens..... | 11 |
| 1.3.1 | Autoimmune encephalitis associated with aABs to the AMPAR | 11 |
| 1.3.2 | Autoimmune encephalitis associated with aABs to the NMDAR..... | 13 |
| 2 | Objectives of this work..... | 16 |
| 3 | Manuscript overview | 17 |
| 4 | Manuscripts | 22 |
| 4.1 | Manuscript I | 22 |
| 4.2 | Manuscript II..... | 29 |
| 4.3 | Manuscript III..... | 37 |
| 4.4 | Manuscript IV | 59 |
| 4.5 | Manuscript V..... | 76 |
| 5 | Discussion..... | 139 |
| 5.1 | Experimental models for investigation of AE pathophysiology | 139 |
| 5.2 | aAB lead to internalization of the target antigen by cross-linking mechanisms..... | 142 |
| 5.3 | GluA2 AE leads to synaptic changes in vitro | 142 |
| 5.4 | GluA2 aABs lead to synaptic scaling..... | 144 |
| 5.5 | Recognition memory and anxiety like behavior is affected by GluA2 aAB | 145 |
| 5.6 | The effects of aABs to ionotropic glutamate receptors on synaptic long-term potentiation..... | 147 |
| 5.7 | Soluble ephrine-B2 is able to rescue the NMDAR AE phenotype in the osmotic pump model..... | 148 |
| 5.8 | The role of the target antigen in AE..... | 148 |

| | | |
|-----|--------------------------------|-----|
| 5.9 | Conclusion and outlook | 149 |
| 6 | References | 152 |
| 7 | Appendix | 160 |
| | Danksagung | 160 |
| | Ehrenwörtliche Erklärung | 161 |
| | Circulum Vitae | 162 |

II GLOSSARY

| | |
|----------------|-------------------------------------------------------------------------------------------------|
| aAB | autoantibody |
| AE | autoimmune encephalitis |
| AMPAR | α -amino-3-hydroxy-5-methyl-4-isoxazolepropionic acid receptor |
| AP | action potential |
| CNS | central nervous system |
| CSF | cerebrospinal fluid |
| <i>d</i> STORM | <i>direct</i> stochastic optical reconstruction microscopy |
| EPM | elevated plus maze |
| Fab | fragment antigen binding |
| fEPSP | field excitatory postsynaptic potential |
| FM1-43FX | (<i>N</i> -(3-Triethylammoniumpropyl)-4-(4-(Dibutylamino) Styryl) Pyridinium Dibromide fixable |
| GABA | gamma-aminobutyric acid |
| GAD65 | glutamate decarboxylase 65 |
| GluA1 | glutamate receptor 1 |
| GluA2 | glutamate receptor 2 |
| HEK | human embryonic kidney 293 |
| IgG | Immunoglobulin G |
| IR | infrared |
| ko | knockout |
| LTP | long-term potentiation |
| eEPSC | evoked excitatory postsynaptic current |
| ieEPSC | iontophoretically evoked excitatory postsynaptic current |

| | |
|-------|-------------------------------------------|
| mEPSC | miniature excitatory postsynaptic current |
| miR | micro ribonucleic acid |
| NASPM | 1-Naphthyl acetyl spermine |
| NMDAR | N-methyl-D-aspartate receptor |
| NOR | novel object recognition |
| NR | N-methyl-D-aspartate receptor subunit |
| nsFA | non-stationary fluctuation analysis |
| PSD95 | post synaptic protein 95 |
| TTX | tetrodotoxin |
| VGCC | voltage-gated calcium channel |
| VGLUT | vesicular glutamate transporter |

III Summary

Autoimmune Encephalitis (AE) is a new group of disorders characterized by autoantibodies (aABs) to synaptic surface antigens. Currently, there are 16 different subforms of AE described with aABs to postsynaptic and presynaptic, to vesicular proteins as well as to synaptic anchoring proteins. AE can be treated by immunotherapy, but recovery is often prolonged and takes several weeks. Intensive care is needed in severe cases. Specific treatment is difficult since for most subforms of AE the molecular mechanisms of aAB action are still unknown. This work focuses on investigating the molecular mechanisms of aABs in AE. Therefore, high resolution imaging, electrophysiological recordings, and behavioral tests in *in-vitro* models and *in-vivo* animal models were used. With these new methods, several molecular mechanisms of aAB action in AE were uncovered: In AMPA receptor AE aABs lead to synaptic scaling by replacing the synaptic AMPA receptor subunit composition leading to changes in synaptic transmission, impairment in long term potentiation, and defects in learning and memory. In an osmotic pump infusion animal model of NMDA receptor AE the internalization of NMDA receptors by aABs can be antagonized by addition of the EphrineB2 receptor agonist ephrine-B2 leading to a rescue of disease symptoms. Taken together, this work elucidates the mechanisms of different subtypes of AE and demonstrates new and antigen-specific treatment approaches that may become therapeutic options in patients in the future.

IV Zusammenfassung

Die autoimmune Enzephalitis ist eine neue Gruppe von Krankheiten die durch Autoantikörper gegen synaptische Membranproteine gekennzeichnet ist. Zum heutigen Stand sind 16 verschiedene Typen von autoimmuner Enzephalitis mit Autoantikörpern gegen postsynaptische, präsynaptische, vesikuläre und synaptische Ankerproteine bekannt. Autoimmune Enzephalitis kann durch Immunotherapie behandelt werden, die Genesung von dieser Krankheit dauert allerdings oft mehrere Wochen und in schweren Fällen ist mitunter eine intensivmedizinische Behandlung notwendig. Eine spezifische Behandlung für viele Typen der autoimmunen Enzephalitis ist schwierig, da bisher die molekulare Wirkweise der Autoantikörper noch immer unbekannt ist. Die vorliegende Arbeit fokussiert sich auf die Untersuchung der molekularen Mechanismen von Autoantikörpern mittels hochauflösender Mikroskopie, elektrophysiologischer Messungen und Verhaltenstests in *in-vitro* Zellmodellen und *in-vivo* Tiermodellen. Durch diese neuen Methoden konnten Wirkmechanismen von Autoantikörpern bei der autoimmunen Enzephalitis aufgeklärt werden: Bei der AMPA Rezeptor Autoimmunenzephalitis bewirken Autoantikörper die synaptische Reorganisation durch die Änderung der AMPA Rezeptorzusammensetzung. Dies führt zu Änderungen in der synaptischen Transmission, Störungen in der Langzeitpotenzierung und Defiziten beim Lernen und der Gedächtnisleistung. Bei der NMDA Rezeptor Autoimmunenzephalitis kann die Internalisierung von NMDA Rezeptoren durch die Gabe des EphrineB2 Rezeptor Agonisten Ephrin-B2 im Tiermodell verhindert werden. Zusammengefasst untersucht diese Arbeit die pathogenen Mechanismen von Autoantikörpern in verschiedenen Subtypen autoimmuner Enzephalitiden und zeigt erste Möglichkeiten für die Entwicklung potentieller neuer und Antigen-spezifischer Behandlungsmöglichkeiten beim Patienten.

1 Introduction

During the last ten years a new category of neurological autoimmune disorders was established that is characterized by autoantibodies (aABs) targeting synaptic antigens. The clinical spectrum of these disorders features rapidly progressive encephalitis (Graus et al. 2016), cerebellar syndromes (Smitt et al. 2000), or chronic encephalopathy resembling neurodegenerative processes (Sabater et al. 2014). All of these syndromes are associated with aAB to synaptic antigens and they are summarized as autoimmune encephalitis (AE). Currently, there are 16 subtypes of AE established that are defined by their aAB reactivity against synaptic proteins involved in synaptic signaling. These include excitatory and inhibitory neuronal receptors, or proteins involved in clustering and modulation of receptors, synaptic vesicle reuptake or synaptogenesis (Dalmau et al. 2017). Nearly all of these antigens are directly accessible for the aAB and the removal of aAB by immunotherapy leads to improvement of symptoms, suggesting a direct pathogenic role of these aABs.

1.1 Discovery of autoimmune encephalitis as a new entity of autoimmune disorders in the central nervous system

The discovery of AE evolved on research on paraneoplastic syndromes of the central nervous system (CNS) (Darnell and Posner 2003) and features some similarities to aAB mediated disorders in the peripheral nervous system, e.g. myasthenic syndromes (Waterman et al. 1997). These initial clinical descriptions of patients and case series led the cornerstone to understand aAB mediated diseases altering synaptic function in the CNS.

Paraneoplastic syndromes are autoimmune responses mediated by systemic cancer. Tumor cells express ectopic neuronal proteins which lead to the activation of an immune response. The so-called classical onconeural syndromes are characterized by aAB to intraneuronal antigens and cytotoxic T-cell responses against this onconeural antigen. Extensive cytotoxic T-cell infiltrates can activate perforin and granzyme B mechanisms causing neuronal degeneration. The associated aABs to nuclear or cytoplasmic antigens in these syndromes are mainly considered as an epiphenomenon (Bien et al. 2012).

In contrast to these syndromes it is known from the peripheral nervous system that disease-associated aABs can indeed be pathogenic and induce disease symptoms. Myasthenic syndromes are autoimmune disorders with aAB that have access to cell surface proteins (e.g. acetylcholine receptors). These aAB can alter neuromuscular function and/or lead to cross-linking and internalization of target proteins and induce prototypical disease symptoms upon

passive-transfer in experimental animals (Drachman et al. 1982, Drachman et al. 1978, Toyka et al. 1975).

In recent years an increasing number of patients has been identified who showed syndromes similar to the paraneoplastic CNS disorders, but responded to immunotherapy and had aABs to cell surface antigens (Ances et al. 2005). One of the first observations was a case study of four young women with prominent neuropsychiatric symptoms and neuronal antibodies against the NR1 subunit of the N-methyl-D-aspartate receptor (NMDAR). Three of these patients responded to immunotherapy and all of them had an ovarian teratoma (Dalmau et al. 2007). In another case series of 10 patients with typical limbic encephalitis aAB to α -amino-3-hydroxy-5-methyl-4-isoxazolepropionic acid receptors (AMPA) were found. Nine of these patients successfully received immunotherapy (Lai et al. 2009). Based on these observations a large number of different neuronal antigens were identified in several subtypes of AE. This was achieved by screening patients serum and cerebrospinal fluid (CSF) for possible antigens with immunolabeling on living cultured neurons and brain slices. Novel antigens were discovered by evaluating distinct pattern of brain reactivity together with mass spectrometry in combination with the clinical phenotype (Hutchinson et al. 2008, Dalmau et al. 2007). After identification of the target antigens cell-based assays were developed for routine diagnosis of these disorders. Since the epitopes of most of these antigens are not detectable in denatured proteins, recombinant human embryonic kidney 293 (HEK) cells expressing the target protein are used as diagnostic tools.

1.2 Testing the pathogenic relevance of autoantibodies to synaptic antigens

1.2.1 *In-vitro* assays

In-vitro assays are important tools for the examination of AE. Cell-based assays are crucial for a fast and reliable diagnosis of different antigens involved in AE. Additionally, the transfection of cell lines can be used to investigate acute effects of aABs on a single-protein level. For NMDARs the general binding epitope of aABs was shown in transfected HEK cells after transfection with different mutated forms of the NR1 subunit (Gleichman et al. 2012).

In addition to transfected cells, the preparation of dissociated neuronal cell cultures is a powerful model for studying neuronal signaling. There are several advantages of primary neuronal cell cultures in comparison of transfected cell lines. First, supporting cell types for the neuronal growth (e. g. astrocytes, glial cells) are included in a dissociated neuronal cell culture and can be modulated in their growth and activity by the culture medium. This allows

the investigation of the interplay of different neuronal cell types in a disease model. Second, neuronal dissociated cell cultures undergo a neural development including the outgrowth of neurites and establishment of active synapses. This enables studies on the synaptic localization of target proteins and their trafficking into synapses. Additionally, the quantification of synaptic clusters by immunocytochemical stainings is easy to obtain in neuronal cell cultures due to their growth as a single cell layer on the coverslips. Third, neuronal signaling and aAB induced pathogenic influence thereof can be investigated by recording synaptic transmission using electrophysiology.

However, dissociated neuronal cultures lack the developmentally determined network connectivity that can only be found in *in-vivo* preparations. Additionally, the culturing of neurons is only possible for a limited time frame, preventing the investigation of adult cultured neuronal cells. This limits the experimental possibilities in dissociated neuronal cultures to scientific questions on the single cell level or to the examination of undefined neuronal connections in young neurons. In the brain there exist several well-defined regions that are differently modulated by a plethora of regulatory proteins. This complex organization cannot be depicted by dissociated cultures of neurons. Thus, for the investigation of neuronal circuits the use of *in-vivo* models or *ex-vivo* slice preparation is essential.

1.2.2 Animal models

In-vitro assays can provide first evidence for a pathogenic role of aABs and they can be used to establish hypotheses how aABs interact with the target antigen. Still, *in-vitro* tests are insufficient to claim that aABs are crucial to evoke an autoimmune disease. Therefore, certain criteria (so called Koch-Witebsky criteria) have to be fulfilled that can only be tested by using animal models. According to the modified Witebsky postulates (Witebsky et al. 1957, Rose and Bona 1993) the pathophysiological role of an autoimmune disease can be unequivocally substantiated if

- an aAB can be detected in all cases of disease,
- the corresponding antigen can be identified,
- passive-transfer of aABs leads to immunopathological syndromes similar to the natural disease and
- immunization of test animals with the antigen leads to disease symptoms

Recently, different *in-vivo* passive-transfer animal models were established to demonstrate typical AE syndromes in experimental animals upon application of potentially pathogenic aABs to neuronal antigens. These animal models include intrathecal injections via catheters to the spinal cord (Werner et al. 2016, Geis et al. 2010), intraventricular or intraparenchymal injections of small volumes by microinjection (Saadoun et al. 2010), or intraventricular infusions by osmotic pumps (Planaguma et al. 2015).

Here, the methods of chronic intraventricular infusion and of intraparenchymal injection are explained in more detail since these were used and adapted for application of potential pathogenic patient IgG fractions or CSF in the following experiments.

1.2.2.1 Intraventricular infusions with osmotic pumps

Osmotic pumps are commercially available (Alzet, Germany), small, implantable compartments consisting of a semipermeable membrane, an osmotic layer (the so called salt sleeve), and a probe reservoir. Osmotic pumps are able to deliver samples with steady infusion rates over a long time span to test their impact on the tissue. The pumps are connected to the tissue by cannulas. Water pours through the semipermeable membrane into the osmotic layer due to the high osmolality of the salt sleeve. When water enters the osmotic layer it compresses the impermeable probe reservoir, pumping the probe solution with controlled flow rate through the cannula. The flow rate can be varied from 0.1 to 10 $\mu\text{l/h}$ and the duration of infusion can be varied from one day to six weeks depending on the construction of the pump (Theeuwes and Yum 1976). The advantage of this method is the steady flow rate which assures stable drug concentrations over a long time span. In comparison to other techniques, this prevents over- or underdosing of compounds by fluctuations in their concentrations between single administrations or their depletion (Fara and Urquhart 1984). Additionally, infusing samples into the ventricles leads to a widespread distribution within the whole brain.

1.2.2.2 Intraparenchymal injections

Direct injection of compounds into selected brain regions is a commonly used method. The simplest way is to use manual injection of substances using e.g. Hamilton syringes (Bouilleret et al. 1999). Later, electrically driven nanoliter injection systems for Hamilton syringes or glass capillaries were used to obtain a slow and continuous injection rate (Okada et al. 2003). It is possible to inject very small amounts of samples into the brain, with only marginal tissue destruction, by using these nanoliter injections systems. The tissue destruction is reduced in

comparison to catheter cannulas. The surgery is fast and no implanted material remains. Furthermore, it is possible to investigate the effect of compounds in a targeted, locally limited area by injection of small volumes.

The adaptation of these animal models set the stage for the investigation of the molecular effects of aAB derived from AE patients and the direct testing of their pathogenic effects.

1.3 aABs related to AE subtypes show a wide spectrum of synaptic antigens

Each subtype of AE is characterized by specific aABs to a distinct synaptic antigen. As mentioned above, the number of target antigens and therefore also the subtypes of AE syndromes are continuously increasing. Antigens can be located postsynaptically as well as presynaptically and consist of membrane receptors and their interaction partners. On the presynaptic site there exist aABs to metabotropic receptors (GABA-B), presynaptical located anchoring proteins (Neurexin-3 α), vesicular proteins (Amphiphysin) or catalytic intracellular proteins (glutamate decarboxylase 65 [GAD65]). On the postsynaptic site aABs to ionotropic receptors (NMDAR, AMPAR), metabotropic receptors (metabotropic glutamate receptor 1), and anchoring proteins (leucine-rich glioma inactivated 1 gene) have been identified. Each of these aABs defines a specific syndrome and may be responsible for different disease symptoms in patients. Therefore, pathomechanisms of AE associated aABs on synaptic transmission depend on the respective target antigen and have to be evaluated for each type of AE. The largest part of the work presented here is about the pathogenic mechanisms of patient IgG aABs to ionotropic glutamate receptors. In the following, the clinical syndromes associated with aABs to the AMPA and the NMDA receptors as well as the physiological function of these receptors are outlined in detail.

1.3.1 Autoimmune encephalitis associated with aABs to the AMPAR

Patients suffering from AE associated with AMPAR aABs develop a typical limbic encephalitis. AMPAR limbic encephalitis manifests with a rapid development of mood changes, depression, anxiety, short-term memory dysfunction, retrograde amnesia, temporal lobe seizures, and strong anterograde memory deficits. Additionally, patients often show temporal lobe seizures and EEG abnormalities as well as temporal lobe hyperintensities and swelling, and at later stages atrophy in MRI (Tuzun and Dalmau 2007). 64% of all patients are women with a median age of 62 years (range: 23 – 81). 40% of patients show additional symptoms such as rapidly progressive dementia or psychosis (Hoftberger et al. 2015). 70% of the patients have an underlying tumor (small cell lung cancer, thymoma, ovarian cancer,

breast cancer or teratoma) and about 70% respond to immunotherapy such as rituximab or cyclophosphamide. Early diagnosis of the disease with following immunotherapy is important to decrease the risk of relapses (Hoftberger et al. 2015). There exist aAB against two subunits of the AMPAR, the glutamate receptor 1 and 2 subunit (GluA1 and GluA2, respectively). The reported clinical characteristics of AE with either GluA1 or GluA2 aABs are similar. However, less than 30 cases have been reported in literature so far. Therefore, the clinical description is still limited. Analysis of the aAB epitope suggests the bottom lobe of the extracellular amino terminal domain of either subunit, but with certain variability in the antigenic region between different patients (Gleichman et al. 2014).

1.3.1.1 AMPAR

AMPARs are heterotetrameric ionotropic receptors composed of four subunits (GluA1 – GluA4) that mediate the vast majority of excitatory transmission in the brain (Hollmann and Heinemann 1994). GluA2/GluA3 and GluA1/GluA2 heteromeric AMPARs dominate in excitatory hippocampal synapses (Passafaro et al. 2001). All subunits have a flip/flop splicing site, whereby the flip variant is mostly expressed in young and the flop variant in mature animals (Monyer et al. 1991). Flop isoforms of AMPARs have a lower binding affinity for glutamate and faster desensitization kinetics (Sommer et al. 1990, Mosbacher et al. 1994). Additionally, there are different editing sites of the AMPAR. First, the R/G edited AMPARs show faster desensitization kinetics (Lomeli et al. 1994). Second, the GluA2 Q/R editing site mediates the Ca^{2+} -conductivity and inward rectification of AMPARs. Receptors of juvenile rodents are not Q/R edited and therefore Ca^{2+} -conductible (Burnashev et al. 1992). Edited GluA2 AMPARs are conductible only for K^+ and Na^+ , have a decreased single-channel conductivity in comparison to unedited AMPARs and are inward rectifying (Bowie and Mayer 1995, Sommer et al. 1991, Hollmann et al. 1991). GluA2-lacking and Ca^{2+} permeable AMPARs are important for long-term potentiation (LTP) in order to strengthen synaptic transmission. They mediate an increase in Ca^{2+} conductivity for second messenger activation (Malinow and Malenka 2002, Newpher and Ehlers 2008). Additionally, GluA2-lacking AMPARs are important for homeostatic plasticity to increase synaptic activity and restore synaptic function (Turrigiano and Nelson 2004, Hou et al. 2008). GluA1 homomeric AMPARs are not incorporated into the synapse under normal conditions but can be found in extrasynaptic compartments (Sans et al. 2003, Wenthold et al. 1996). Taken together, the GluA2 subunit plays a special role in AMPAR transmission since this subunit is responsible

for Ca^{2+} permeability, inward rectification, LTP induction, and regulation of AMPAR kinetics.

1.3.1.2 Research on autoimmune encephalitis associated with aABs to the AMPAR - state of the art

Incubation of dissociated hippocampal cultures with pooled IgG containing aABs to GluA1 and GluA2 led to a decrease of synaptic clusters of AMPARs and to a reduction of fluorescence intensity of the remaining AMPARs. Against this, NMDARs, post-synaptic protein 95 (PSD95), vesicular glutamate transporter (VGLUT), and stargazin clustering is unchanged (Lai et al. 2009, Peng et al. 2015). Western Blot analysis of preincubated hippocampal cell cultures showed a decrease of AMPAR surface expression but not of intracellularly located receptor subunits. This suggests a global reduction of synaptic AMPARs by internalization and degradation of AMPARs after aAB binding (Peng et al. 2015). In electrophysiological recordings of miniature excitatory postsynaptic currents (mEPSCs) in hippocampal cell cultures aAB incubation induced a reduction of AMPAR mEPSC amplitudes and frequencies. Moreover, GABA-A receptor mediated miniature inhibitory postsynaptic currents (mIPSCs) were also reduced (Peng et al. 2015, Gleichman et al. 2014). This observation was interpreted as a possible mechanism of compensation for the loss of AMPAR mediated transmission.

1.3.2 Autoimmune encephalitis associated with aABs to the NMDAR

In comparison to AMPAR AE, patients suffering from NMDAR AE show a distinct clinical syndrome and a different course of disease. The median age of patients with NMDAR AE is 22 years (approximately 40% with age < 18 years). 80% of all patients are women (Dalmau et al. 2017). In about 40% of patients (all females) teratomas of the ovaries are detected. Since these teratomas express ectopic neuronal tissue and also NMDARs, ovarian teratomas may serve as a trigger of NMDAR AE by inducing molecular mimicry. Another identified trigger is herpes simplex encephalitis as it has been shown that some patients after herpes encephalitis develop secondary symptoms of NMDAR encephalitis. These patients have been tested positive for NMDAR aABs and respond to immunotherapy (Pruss et al. 2012). However, in up to 60% of all cases with NMDAR AE no trigger can be identified (Titulaer et al. 2013).

The clinical spectrum of the disease presents with a rapidly progressing neuropsychiatric manifestations. Beginning with prodromal headache or fever patients develop psychiatric syndromes like anxiety, insomnia, delusional thinking, hallucinations, paranoid thoughts, pressured speech, mood disorder, aggressive behavior and episodes of extreme agitation and catatonia (Dalmau et al. 2011, Titulaer et al. 2013). Patients further progress with development of seizures, reduced verbal output, decreased levels of consciousness, rigidity and autonomic dysfunction (high blood pressure, hyperthermia, profuse salivation, hypoventilation) until they eventually become comatose (Titulaer et al. 2013, Irani et al. 2010, Sansing et al. 2007). Clinical MRI shows mild or transient cortical, subcortical, cerebellar, or brainstem abnormalities in some patients (40%). EEG can show epileptic activity and bursts of rhythmic 20-30 Hz beta frequency activity riding on rhythmic delta (1-3 Hz) waves, called “extreme delta brush” in several patients (Schmitt et al. 2012). About 80% of all patients respond to immunotherapy such as corticosteroids, intravenous immunoglobulins, plasma exchange, rituximab or cyclophosphamide. Tumor resection in case of a teratoma, symptomatic care, and physical therapy are also important completing the treatment strategies (Titulaer et al. 2013). Recovery from NMDAR AE usually takes several weeks to months although adequate immunotherapy and intensive care is conducted. It is suggested that this prolonged recovery is due to the continuous presence of pathogenic aABs synthesized by long-lived mature plasma cells within the CNS (Dalmau et al. 2017).

The epitope of NMDAR AE is a highly restricted region in the N-terminal domain of the N-methyl-D-aspartate receptor subunit (NR) 1. Mutants of NR1 with deletion of the N368/G369 region of the aminoterminal domain of the receptor show no aAB binding (Kreye et al. 2016, Gleichman et al. 2012).

1.3.2.1 NMDARs

NMDARs are heterotetrameric ionotropic glutamate receptors composed of three subunits (NR1, NR2 and NR3). There exist eight NR1 subunit splice variants, four different NR2 (A-D) and two NR3 (A, B) subunits (Dingledine et al. 1999). The NR1 subunit is obligatory for the expression of functional NMDARs (Forrest et al. 1994). NR2 assembles with NR1 and NR3 as ternary NR1/NR2/NR3 complexes (Sasaki et al. 2002, Karakas and Furukawa 2014). The agonist binding sites of NMDARs are located in the S1 and S2 domains, whereas NR1 and NR3 bind glycine as coagonist and NR2 binds glutamate (Yao and Mayer 2006,

Furukawa et al. 2005). NR2A and NR2B have an allosteric inhibitor binding site for Zn^{2+} and ifenprodil (Paoletti et al. 2000). Additionally, NMDARs are voltage-dependently blocked by Mg^{2+} . At membrane potential smaller than -40 mV external Mg^{2+} ions enter the NMDAR and block the pore due to the size of magnesium ions. With increasing depolarization the Mg^{2+} block resolves according to the magnesium driving force (Nowak et al. 1984, Mayer et al. 1984). In the hippocampus NR1/NR2B complexes are thought to be present in nascent synapses and extrasynaptic sites whereas NR2A-containing NMDARs predominantly exist in mature synapses (Thomas et al. 2006, Tovar and Westbrook 1999).

1.3.2.2 Research on autoimmune encephalitis associated with aABs to the NMDAR AE - state of the art

Previous studies on NMDAR AE revealed aAB driven NMDAR internalization and degradation. Incubation of dissociated cultured neurons with aABs caused an activity-independent decrease of NMDAR surface density and synaptic location after two hours with the greatest effect after 12 hours. AMPAR or GABAA receptor transmission was unaltered. Additional experiments, using fragment antigen binding (Fab)-Fragments that are unable of crosslinking NMDARs, showed no changes in NMDAR density and location (Hughes et al. 2010, Dalmau et al. 2008, Moscato et al. 2014). These experiments suggest that NMDAR aABs induce a pathogenic function by crosslinking mechanisms and internalization of the antigen. Recordings of NMDAR mEPSCs in neuronal cultured cells after NMDAR aAB incubation for 24 hours induced a reduction of the amplitudes, but not of their frequency, without altering AMPAR mEPSC amplitudes (Hughes et al. 2010). There was no difference in mEPSC amplitudes after incubation of cells with Fab-Fragments. These results corroborate the hypothesis of a reduction in NMDAR density (Moscato et al. 2014). Analysis of lateral diffusion by single molecule trafficking revealed dramatically increased NMDAR diffusion as compared to GluA1 or GABA-A receptors (Mikasova et al. 2012). This finding indicates a specific influence of NMDAR aABs on receptor trafficking in synaptic areas. As a potential target for inducing pathological NMDAR trafficking the Ephrin B2 receptor (EphB2) was identified. EphB2 is a tyrosine-kinase that modulates LTP by stabilization and clustering of NMDARs in the postsynaptic membrane (Kullander and Klein 2002, Lisabeth et al. 2013). Quantum dot tracking of EphB2 demonstrated an increased EphB2 diffusion rate at the synapse after NMDAR aAB incubation. Additionally, there was a reduction in co-immunoprecipitation of EphB2/NMDAR pointing to a disturbed interaction of EphB2 with the NMDAR. Importantly, EphB2 activation by application of its ligand ephrine B2 prevented

the increase in synaptic NMDAR diffusion. Injection of ephrine B2 ligand together with NMDAR aABs into the dorsal hippocampus of rats was able to rescue the aAB induced loss of NMDARs in immunostaining experiments (Mikasova et al. 2012).

Recently, a passive-transfer mouse model was developed by continuous application of NMDAR aABs over 14 days using bilateral intraventricular catheters connected to osmotic pumps (Planaguma et al. 2015). Animals with NMDAR aAB infusion showed impairments in recognition memory, anhedonic and depressive-like behavior but no change in locomotor activity. IgG deposition in the brain was maximal on day 18 after pump implantation and decreased at later time points when pump infusion has ended. Similarly, cell surface NMDAR density was also decreased with a maximum on day 18. There were no detectable inflammatory infiltrates after aAB infusion, thus, suggesting a pathomechanism exclusively mediated by aABs without other effector activation.

2 Objectives of this work

The field of AE is continuously growing and gives rise to many questions on disease pathophysiology that need to be addressed by experimental work. Furthermore, treatment options are currently insufficient; therefore, development of target-specific treatment options is needed. The goal of this work was to analyze the molecular pathomechanisms of different subtypes of AE characterized by aABs to AMPARs, NMDARs, GAD65, and amphiphysin.

In the first step several experimental procedures were developed to analyze aAB effects *in-vivo* and *in-vitro*. This includes the improvement of *in-vitro* techniques using dissociated hippocampal cell cultures and establishment of different passive transfer animal models.

Second, the effects of several aABs on synaptic transmission at post- and presynaptic sites were examined using electrophysiological patch-clamp or field potential recordings. aAB induced structural changes were investigated using immunofluorescence methods in combination with super-resolution imaging or confocal microscopy. Behavioral abnormalities were investigated using standardized behavioral testing, e.g. using tests for memory, anxiety, depressive like behavior, and motor function.

Third, based on those experimental results, novel treatment methods were tested that directly interfere with the aAb-induced synaptic dysfunction as a concept of hypothesis-driven targeted treatment beyond immunosuppressive therapy.

3 Manuscript overview

Manuscript I:

Stiff person-syndrome IgG affects presynaptic GABAergic release mechanisms

Werner C, Haselmann H, Weishaupt A, Toyka KV, Sommer C, Geis C

J Neural Transm (Vienna). 2015 Mar;122(3):357-62. doi: 10.1007/s00702-014-1268-1 (IF 2.59)

Date of acceptance: 25th June 2014

In this publication, we analyzed the action of stiff-person syndrome aABs using patch-clamp recordings in dissociated hippocampal neurons and confocal microscopy. We identified an increase of GABAergic mIPSC frequency but no structural changes. Since these cannot be explained by GAD65 aABs we propose an additional, yet unknown, antigen in stiff-person syndrome. This hypothesis is supported by intense immunoreactivity of synapses in neuronal cultures after GAD65 antibody depletion and application of the depleted IgG fraction to the neurons.

CW designed the study, did patch-clamp and microscopy experiments, including IgG preabsorption and immunocytochemistry, data analysis and prepared the manuscript. HH prepared neuronal hippocampal cell cultures, did patch-clamp recordings and contributed to the discussion. AW purified the IgG fractions and contributed to the discussion. KVT and CS contributed to the discussion. CG designed the study and wrote the manuscript.

Personal contribution: 20%

Prof. Dr. med. Christian Geis

Manuscript II:**Interactions of human autoantibodies with hippocampal GABAergic synaptic transmission – analyzing antibody-induced effects *ex vivo***

Haselmann H, Röpke L, Werner C, Kunze A, Geis C

Frontiers in Neurology. 2015 Jun 11;6:136. doi: 10.3389/fneur.2015.00136 (IF 3.18)

Date of acceptance: 28th May 2015

In this manuscript, we developed a new passive transfer mouse model in order to study the effects of patient-derived aABs in the CNS of experimental animals by intraparenchymal or intraventricular injections. This method provides a stable passive-transfer animal model which requires only small amounts of patient aAB material, which is often limited.

HH designed the study, did the stereotactic injections, immunohistological stainings, patch-clamp recordings of hippocampal brain slices, data analysis and prepared the manuscript. LR contributed to the discussion. CW did patch-clamp recordings of hippocampal brain slices, data analysis and contributed to the discussion. AK contributed to the discussion. CG designed the study and wrote the manuscript.

Personal contribution: 80%

Prof. Dr. med. Christian Geis

Manuscript III:**Human autoantibodies to amphiphysin induce defective presynaptic vesicle dynamics and composition**

Werner C, Pauli M, Doose S, Weishaupt A, Haselmann H, Grünewald B, Sauer M, Heckmann M, Toyka KV, Asan E, Sommer C, Geis C

Brain. 2016 Feb;139:365-379. doi: 10.1093/brain/awv324 (IF 10.29)

Date of acceptance: 25th September 2015

In this work, we investigated the structural effects of amphiphysin aABs using electron microscopy and direct stochastic optical reconstruction microscopy (*d*STORM). We were able to provide evidence for interference of human anti-amphiphysin aABs with clathrin-mediated endocytosis. This interaction leads to a reduction of the presynaptic vesicle pool, clathrin coated intermediates, and endosome-like structures. Synaptobrevin 2 as a marker for the ready-releasable pool was increased and synaptobrevin 7 as a marker for the vesicle reserve pool was reduced. These changes may induce synaptic dysfunction by run-out of presynaptic vesicles as a possible pathomechanism in amphiphysin aAB associated stiff-person syndrome.

CG, MH, CS, and KVT designed the study. CW performed electron microscopy and *d*STORM microscopy and was responsible for data acquisition and analysis. MP, SD, and MS supported *d*STORM analysis and contributed own data. AW purified the IgG fractions. HH was responsible for neuronal cell cultures and helped in conceptualization and discussion of the manuscript. BG performed animal experiments. MH. EA performed electron microscopy together with CW. CG, CW, KVT, and CS wrote the manuscript.

Personal contribution: 10%

Manuscript IV:**Ephrin-B2 Prevents N-Methyl-D-Aspartate Receptor Antibody Effects on Memory and Neuroplasticity**

Planagumà J*, Haselmann H*, Mannara F*, Petit-Pedrol M, Grünewald B, Aguilar E, Röpke L, Martín-García E, Titulaer MJ, Jercog P, Graus F, Maldonado R, Geis C[#], Dalmau J[#]

Annals of Neurology. 2016 Sep;80(3):388-400. doi: 10.1002/ana.24721 (IF 9.89)

Date of acceptance: 27th June 2016

In this publication, we demonstrated the effects of human NMDAR aABs on behavior of mice that received long term NMDAR aAB infusion by osmotic pumps. Furthermore, we evaluated structural and functional changes induced by NMDAR aABs leading to impaired memory, depressive like behavior, and decreased LTP in *ex-vivo* field potential recordings in CA1 region of the hippocampus. In addition, we developed a treatment strategy of NMDAR AE by administration of ephrin-B2 as agonist of EphB2 to prevent synaptic disturbance of NMDAR trafficking *in-vivo* and *in-vitro*.

JD and CG were responsible for conception and design of the study. FM, MP-P, EM-G, EA, and JD were responsible for acquisition and analysis of animal behavior. JP, MJT, PJ, FG, and JD were responsible for acquisition and analysis of immunohistochemistry and confocal microscopy. HH, BG, LR, and CG were responsible for acquisition and analysis of electrophysiological studies. JP, HH, CG, and JD were responsible for drafting of the manuscript and figures. JP, HH, and FM contributed equally (*). CG and JD shared seniority (#).

Personal contribution: 30%

Prof. Dr. med. Christian Geis

Manuscript V:**Human autoantibodies against the AMPA receptor subunit GluA2 induce receptor reorganisation and memory dysfunction**

Haselmann H*, Mannara F*, Werner C, Planagumà J, Grünewald B, Petit-Pedrol M, Kirmse K, Classen J, Demir, F, Klöcker N, Doose S, Dalmau J, Hallermann S, Geis C

Neuron (in revision; IF 14.02)

This publication demonstrates the functional and structural effects of patient's aABs against the GluA2 subunit of the AMPAR *in-vitro*, *ex-vivo* and *in-vivo*. Here, we used patch-clamp recordings, extracellular field potential recordings, *d*STORM analysis and behavioral tests and found a compensation for the aAB induced loss of GluA2 containing AMPAR by the synaptic insertion of extrasynaptic GluA1 homomeric receptors. Furthermore, in passive-transfer models with GluA2 aABs mice exhibited characteristic disease symptoms e.g. impaired recognition memory and anxiety.

HH designed the study, performed electrophysiological experiments, intraparenchymal IgG injections, behavioral studies, HEK cell transfections, immunohistochemical stainings, data analysis, prepared dissociated hippocampal neurons and wrote the manuscript. FM did intraventricular IgG infusions, behavioral studies and data analysis. CW and SD did immunocytochemical stainings and *d*STORM analysis and contributed to the discussion. KK performed data analysis and contributed to the discussion. JP and MP-P did immunohistochemical stainings, data analysis and contributed to the discussion. BG, JD and SD contributed to the discussion. JC and JD provided patient material. NK and FD did immunoprecipitation experiments and contributed to the discussion. SH provided analysis software and contributed to the discussion. CG designed the study and wrote the manuscript. HH and FM contributed equally (*).

Personal contribution: 70%

4 Manuscripts

4.1 Manuscript I

Stiff person-syndrome IgG affects presynaptic GABAergic release mechanisms

Werner C, Haselmann H, Weishaupt A, Toyka KV, Sommer C, Geis C

J Neural Transm (2015) 122:357–362
DOI 10.1007/s00702-014-1268-1

TRANSLATIONAL NEUROSCIENCES - SHORT COMMUNICATION

Stiff person-syndrome IgG affects presynaptic GABAergic release mechanisms

Christian Werner · Holger Haselmann ·
Andreas Weishaupt · Klaus V. Toyka ·
Claudia Sommer · Christian Geis

Received: 22 April 2014 / Accepted: 25 June 2014 / Published online: 3 July 2014
© Springer-Verlag Wien 2014

Abstract The majority of patients with stiff person-syndrome (SPS) are characterized by autoantibodies to glutamate decarboxylase 65 (GAD65). In previous passive-transfer studies, SPS immunoglobulin G (IgG) induced SPS core symptoms. We here provide evidence that SPS-IgG causes a higher frequency of spontaneous vesicle fusions. Sustained GABAergic transmission and presynaptic GABAergic vesicle pool size remained unchanged. Since these findings cannot be attributed to anti-GAD65 autoantibodies alone, we propose that additional autoantibodies with so far undefined antigen specificity might affect presynaptic release mechanisms.

Keywords Stiff person-syndrome · Glutamate decarboxylase 65 · GAD2 · Patch clamp · Synaptic transmission

Introduction

Gamma-aminobutyric acid (GABA), the major inhibitory transmitter in the central nervous system, is synthesized by two GAD isoforms. GAD65 is the rate-limiting enzyme for

vesicular GABA synthesis. It is predominantly located in presynaptic terminals and is reversibly anchored to the synaptic vesicle membrane. GAD65 knockout mice are susceptible to seizures (Kash et al. 1997), show abnormalities in anxiety behavior (Bergado-Acosta et al. 2014; Seidenbecher et al. 2003), and have reduced GABA release at sustained synaptic transmission (Tian et al. 1999). Autoantibodies (AB) targeting GAD65 are detected in several diseases including type 1 diabetes (Solimena 1998), cerebellar ataxia (Vianello et al. 2003), limbic encephalitis (Mata et al. 2010), Batten disease (Chattopadhyay et al. 2002) and in non-paraneoplastic stiff person-syndrome (SPS) (Solimena et al. 1988). Only recently, SPS-IgG containing AB to GAD65 was shown to induce motor dysfunction and increase fear-related behavior in experimental rats (Geis et al. 2011; Hansen et al. 2013; Manto et al. 2007). However, the pathogenic role of anti-GAD65 AB has been questioned due to the intracellular location of the target antigen and the clinical heterogeneity of GAD65 associated syndromes. To further elucidate the mechanism by which anti-GAD65-positive SPS-IgG may exert pathogenic effects we here investigated the influence of SPS-IgG on GABAergic synaptic transmission *ex vivo* using patch-clamp analysis of murine hippocampal granule cells and confocal microscopy of GABAergic vesicle pools.

Materials and methods

Purification of IgG fractions

IgG containing GAD65 AB from two SPS patients (SPS-IgG #1 and 2) with extremely high titer of anti-GAD65 AB in serum and cerebrospinal fluid (CSF) and control IgG from two patients (one with chronic inflammatory

C. Werner · H. Haselmann · C. Geis (✉)
Hans-Berger Department of Neurology, Jena University
Hospital, Erlanger Allee, 07747 Jena, Germany
e-mail: christian.geis@med.uni-jena.de

C. Werner · A. Weishaupt · K. V. Toyka · C. Sommer · C. Geis
Department of Neurology, University Hospital Würzburg,
Josef-Schneider Str. 11, 97080 Würzburg, Germany

H. Haselmann · C. Geis
Center for Sepsis Control and Care (CSCC), Jena University
Hospital, Erlanger Allee 101, 07747 Jena, Germany

polyneuropathy, one with tumor in the orbita, both without detectable AB in serum and CSF) were purified from therapeutic plasma exchange material as described previously (Sommer et al. 2005). Titer of anti-GAD65 AB was 508.900 mU/ml in the SPS patient #1 purified IgG, and 1.375.560 mU/ml in SPS patient #2 (normal value <70 mU/ml) determined by a commercial immunodot assay (Geis et al. 2011). Both patients were negative for other so far established antineuronal AB as tested by commercial available tests (Euroimmun, Luebeck, Germany). The IgG fractions were dialyzed, freeze dried and stored at -20°C . Lyophilized IgG was dissolved in normal saline before use.

IgG preabsorption with recombinant GAD65

SPS-IgG #2 was depleted off anti-GAD65 AB twice using affinity chromatography with recombinant human GAD65 (kindly provided by Diarect, Freiburg, Germany) as described previously (Geis et al. 2010).

Whole cell patch-clamp recordings

All experiments were approved by the Bavarian state authorities. As in SPS also the limbic system is involved (Henningsen and Meinck 2003) and the connectivity of hippocampal GABAergic basket cells and granule cells is well characterized (Kraushaar and Jonas 2000), we chose acute hippocampal slices as a model system for patch-clamp recordings. Hippocampal slices (300 μm) were cut from brains of 15–25 day old C57-B16-mice in ice cold extracellular solution (40 mM NaCl, 25 mM NaHCO_3 , 10 mM glucose, 150 mM sucrose, 4 mM KCL, 1.25 mM NaH_2PO_4 , 0.5 mM CaCl_2 , 7 mM MgCl_2 ; purged with 95 % CO_2 /5 % O_2). Slices were incubated with 100 $\mu\text{g}/\text{ml}$ SPS-IgG or control IgG at 32°C for at least 30 min. For recordings, slices were superfused with extracellular solution (125 mM NaCl, 25 mM NaHCO_3 , 25 mM glucose, 2.5 mM KCl, 1.25 mM NaH_2PO_4 , 2 mM MgCl_2 purged with 95 % CO_2 /5 % O_2). Inhibitory postsynaptic currents (IPSCs) were recorded with an EPC10 patch clamp amplifier (HEKA, Lambrecht, Germany). Recording electrodes pulled from borosilicate glass (Science Products, Hofheim, Germany) and filled with intracellular recording solution containing 140 mM KCl, 10 mM Hepes, 10 mM EGTA, 2 mM Na₂ATP, 2 mM MgCl_2 had a final resistance of 3–5 M Ω . Granule cells (GC) were clamped at -70 mV in whole cell configuration (Fig. 1a). Recordings were rejected if the resting potentials were more positive than -50 mV, changed during the experiments, or series resistance was higher than 20 M Ω . Evoked IPSCs were isolated by adding 10 μM Cyano-Nitroquinoxaline-Dione (CNQX) and 50 μM 2-amino-phosphonovaleric acid (AP-

5; Tocris Bioscience, Ellisville, USA). Application of 1 μM tetrodotoxin (TTX; Sigma Aldrich, Germany) was used for recording miniature IPSCs. Minimal evoked IPSCs were elicited as described previously (Allen and Stevens 1994; Edwards et al. 1990; Geis et al. 2010). In brief, GABAergic afferents of molecular layer basket cells were stimulated using a stimulus isolation unit (Isoflex, A.M.P.I., Jerusalem, Israel) by applying pulses of 200 μs at 0.3 Hz while IPSCs were recorded in GCs. Recordings were filtered at 2.9 and 10 kHz. Traces were analyzed by Igor Pro Software (Wavemetrics, Lake Oswego, OR, USA).

Primary hippocampal cell culture

Primary hippocampal neurons were prepared from C57Bl/6 E18 embryos as described (Byts et al. 2008). Primary neurons were cultivated in Neurobasal medium supplemented with glutamine (1 %), B27 (2 %) and penicillin/streptomycin (1 %; all from Life Technologies, Darmstadt, Germany) at a density of 30,000 cells on 12 mm diameter coverslips (Langenbrinck, Emmendingen, Germany) for 14 days before use.

Autoantibody treatment and immunocytochemistry

Primary neurons were incubated with patient IgG at a concentration of 100 $\mu\text{g}/\text{ml}$ for 6 h. The researcher was blinded to treatment conditions. Cells were fixed in ice-cold 4 % paraformaldehyde (PFA) for 10 min and permeabilized by 0.1 Triton-X. Unspecific binding sites were saturated with 10 % bovine serum albumin (BSA) for 30 min. Primary antibodies (1:1,000 each) to synaptophysin (rabbit polyclonal, AB9272, Chemicon, Darmstadt, Germany) and vesicular GABA transporter (VGAT; guinea pig polyclonal, 131004, Synaptic Systems, Göttingen, Germany) were incubated overnight at 4°C in 2 % BSA followed by Alexa 488 goat anti-rabbit (A21206, Life Technologies) and Rhodamin goat anti guinea-pig (Jackson Immunoresearch, West Grove, USA) as secondary antibodies for 2 h at room temperature. For binding studies of patient IgG preparations, primary neurons and coronal brain slices of mice perfused with ice-cold 4 % PFA were incubated with patient IgG in a concentration of 10 $\mu\text{g}/\text{ml}$ over night at 4°C followed by Cy3 goat anti-human secondary antibody (1:500, Dianova, #109165003) for 2 h at room temperature.

Confocal microscopy and image analysis

Cells and brain slices were viewed on a confocal microscope (Zeiss LSM 710, Jena, Germany) using a 40 \times objective, keeping laser power and photomultiplier tube

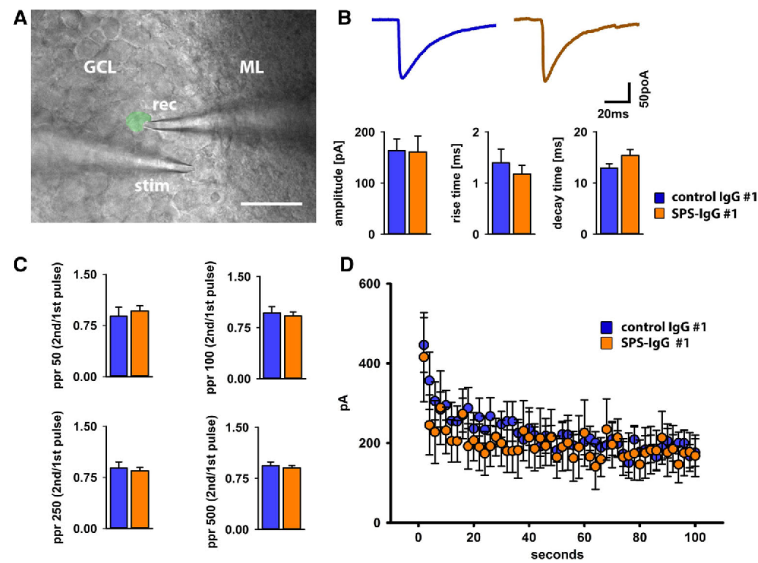


Fig. 1 SPS-IgG containing anti-GAD65 AB has no effect on evoked GABAergic IPSC. **a** Experimental setup for recording IPSCs in acute hippocampal slices. GABAergic afferents from inhibitory basket cells were stimulated in the inner third of the granule cell layer. IPSC evoked by minimal stimulation were recorded in granule cells that were monosynaptically connected. *GCL* granule cell layer, *ML* molecular layer, *rec* recording electrode, *stim* stimulation electrode; *scale bar* 20 μm . **b** Recordings from dentate gyrus granule cells after preincubation with control IgG or SPS-IgG revealed similar eIPSC amplitudes (control IgG #1 = 163.5 ± 23.1 pA; SPS-IgG #1 = 161.2 ± 31.2 pA; $p = 0.824$) and unchanged rise (control IgG #1 = 1.2 ± 0.2 ms; SPS-IgG #1 = 1.4 ± 0.3 ms; $p = 0.524$) and decay time (controls = 15.4 ± 1.1 ms, SPS-IgG #1 = 12.9 ± 0.9 ms; $p = 0.134$) in group comparison (n [control

IgG] = 15, n [SPS-IgG] = 10). *Upper traces* show averaged responses of representative individual neurons. **c** Paired pulse ratios showed a depression at 250 ms stimulus intervals (250 ms: control IgG #1 = 0.89 ± 0.09 , $n = 11$, SPS-IgG #1 = 0.84 ± 0.05 , $n = 13$, $p = 0.720$), but were not different between both groups at all tested inter-pulse intervals (50 ms: control IgG #1 = 0.97 ± 0.07 , $n = 6$; SPS-IgG #1 = 0.89 ± 0.14 , $n = 8$, $p = 0.645$; 100 ms: control IgG #1 = 0.92 ± 0.06 , $n = 11$; SPS-IgG #1 = 0.96 ± 0.01 , $n = 9$, $p = 0.761$; 500 ms: control IgG #1 = 0.90 ± 0.04 , $n = 6$; SPS-IgG #1 = 0.94 ± 0.04 , $n = 8$, $p = 0.652$). **d** IgG preincubation had no influence on IPSC peak amplitude during high frequency stimulation (10 Hz) of GABAergic basket cell afferences (bin size = 5; n [control IgG] = 9, n [SPS-IgG] = 6; *error bars* represent SEM)

voltage constant. Maximum projections of z-stacks were generated using FIJI image analysis software (Schindelin et al. 2012) and background signal subtraction was performed. Thresholds of VGAT and synaptophysin signals were determined, and area ratios were calculated by dividing the synaptophysin area by the VGAT area. VGAT positive areas served also as template for synaptophysin intensity quantification. Colocalization of signals was tested by applying FIJI's embedded Coloc2 plugin which performs pixel intensity correlation over space.

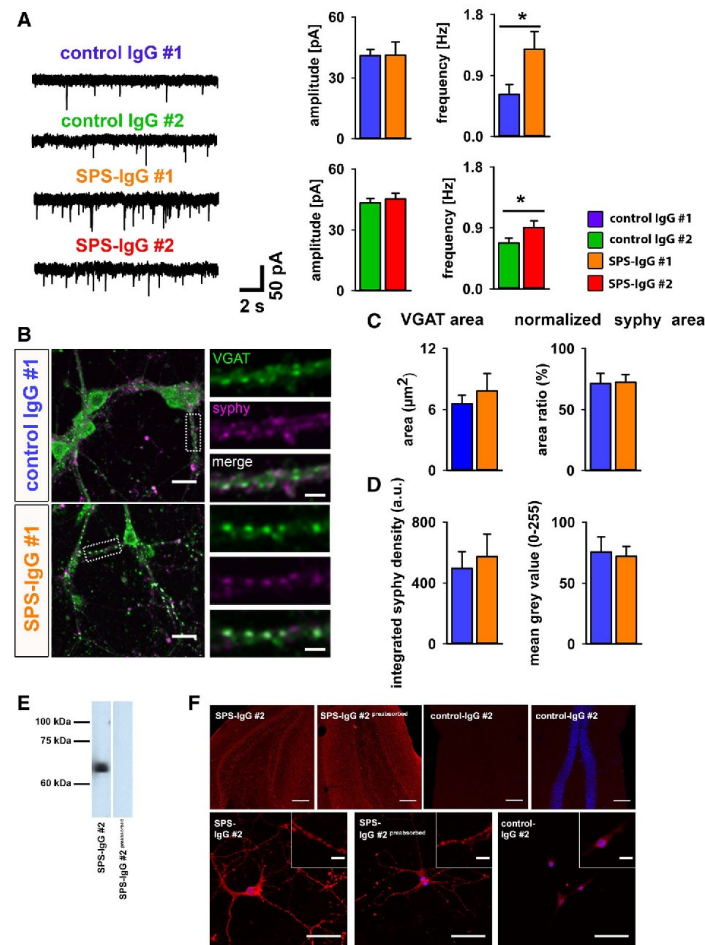
Data analysis

Statistical comparisons were made by applying Mann-Whitney U rank sum test using Sigmaplot 12 (Systat, Erkrath, Germany).

Results

Evoked GABAergic neurotransmission and short-term plasticity is not affected in the presence of SPS-IgG

The analysis of single evoked IPSC (eIPSC) in hippocampal granular cells after minimal stimulation of GABAergic afferences revealed similar amplitudes of eIPSC after incubation with SPS-IgG and control IgG. Moreover, eIPSC kinetics were not different between treatment groups (Fig. 1b). For evaluation of short-term plasticity and vesicular GABA loading at short inter-pulse intervals, we analyzed GABAergic transmission in a paired pulse paradigm. Both experimental groups showed paired pulse depression at 250 ms with no significant inter-group differences (Fig. 1c). Since autoantibodies may only have effects on GABAergic



transmission under sustained high synaptic activity, we performed high frequency train stimulation of GABAergic afferents at 10 Hz, revealing no change in depression rate by preincubation with SPS-IgG (Fig. 1d). Recovery of IPSC after trains of stimulation was also unchanged (not shown).

Higher frequency of spontaneous quantal IPSCs after SPS-IgG preincubation without changes in presynaptic vesicle pool size

We then investigated spontaneous quantal events (miniature IPSC, mIPSC) in the presence of TTX. mIPSC

frequency was significantly increased in hippocampal slices treated with SPS-IgG#1 and #2 (Fig. 2a). mIPSC amplitudes were unchanged indicating that individual vesicles had similar transmitter content in both experimental groups.

Next, we performed quantitative confocal microscopy in primary hippocampal neurons incubated with IgG-fractions to investigate if GABAergic vesicle pools have more vesicles available after SPS-IgG application allowing more frequent spontaneous vesicle fusions. We quantified the vesicle marker synaptophysin in VGAT positive GABAergic presynaptic terminals. The area of individual

Fig. 2 Higher frequency of spontaneous vesicle fusions in neurons preincubated with SPS-IgG than with control IgG. **a** Traces show representative mIPSC recordings of control IgG #1 and #2 and of SPS-IgG (patient #1 and patient #2) treated neurons. mIPSC amplitude was not different (control IgG #1 = 43.2 ± 2.2 pA, n [control IgG #1] = 8, SPS-IgG #1 = 40.9 ± 3.0 pA, n [SPS-IgG #1] = 7, $p = 0.977$; control IgG #2 = 43.2 ± 2.2 pA, n [control IgG #2] = 6, SPS-IgG #2 = 45.2 ± 2.8 pA, n [SPS-IgG #2] = 7; $p = 0.534$) while incubation with SPS-IgG led to a marked increase in the frequency of miniature potentials (control IgG #1 = 0.62 Hz \pm 0.14 Hz, n [control IgG #1] = 8, SPS-IgG #1 = 1.29 ± 0.26 Hz, n [SPS-IgG #1] = 7, $p = 0.038$; control IgG #2 = 0.68 ± 0.07 Hz, n [control IgG #2] = 6, SPS-IgG #2 = 0.91 ± 0.10 Hz, n [SPS-IgG #2] = 7; $p = 0.035$). **b** Representative confocal images of control IgG and SPS-IgG treated neurons. The overview microphotograph shows merged images of neurons after VGAT (green) and synaptophysin (syphy; magenta) double-staining. Standardized areas of proximal axonal synapses (dotted rectangle) were taken for further analysis (scale bar 20 μ m). High magnification images (right) of dotted areas in the overview images show individual and merged color channels demonstrating similar synaptophysin over VGAT signals in both treatment groups (scale bar 5 μ m). **c** The VGAT area (mean area per bouton) was unchanged (control IgG #1 = 6.55 ± 0.84 μ m², SPS patient-IgG #1 = 7.80 ± 1.72 μ m²; $p = 0.959$), in both experimental groups. Syphy areas normalized to VGAT areas were nearly identical (control IgG #1 = 71.2 ± 8.4 %, SPS-IgG #1 = 72.3 ± 6.3 %; $p = 0.798$) implicating a similar vesicle pool size in control IgG and SPS-IgG preincubated neurons. **d** Summated synaptophysin intensity (integrated signal density, control IgG #1 = 496.234 ± 108.459 bits/ μ m², SPS-IgG #1 = 573.3 ± 146.6 bits/ μ m²; $p = 0.878$) and mean grey values (control IgG #1 = 75.5 ± 12.4 , SPS-IgG #1 = 72.0 ± 8.2 , $p = 0.967$), both determined in VGAT positive presynaptic boutons, were similar in both experimental groups. Number of analyzed boutons: n [control IgG] = 109, n [SPS-IgG] = 69; number of independent coverslips analyzed n [control IgG] = 8, n [SPS-IgG] = 8. **e** Western blot (recombinant GAD65, 15 μ g per lane) showing efficient depletion of anti-GAD65 AB from SPS-IgG #2 by affinity chromatography; left lane = patient IgG #2, right lane = patient IgG #2 after preabsorption with recombinant human GAD65. **f** Positive synaptic immunostaining of primary hippocampal cells and mouse hippocampal slices with patient IgG #2 (red) before and after preabsorption. Control IgG #2 displayed no immunoreaction. Blue DAPI staining for cell nuclei. Insets show higher magnifications. Scale bar (top row, slices) = 100 μ m, scale bar (bottom row, cells) = 50 μ m, scale bar (insets) = 10 μ m

VGAT signals was stable without relevant variation in both groups (Fig. 2b, c). The area of synaptophysin immunoreactivity in GABAergic presynapses was similar in SPS-IgG treated neurons as compared to controls (Fig. 2b, c). Integrated density of synaptophysin signals and mean grey-scale values using VGAT as ROI also showed no differences in synaptophysin signal intensity (Fig. 2d). Accordingly, colocalization of VGAT and synaptophysin was not influenced by SPS-IgG (data not shown). Collectively, these results suggest that the size of presynaptic GABAergic vesicle pools is not changed by SPS-IgG and does not account for more frequent vesicle release.

Increased release probability of presynaptic GABAergic vesicles is not explained by AB to GAD65. Therefore,

we investigated whether SPS patient IgG may contain additional antineural AB other than anti-GAD65 IgG. SPS-IgG #2 depleted of AB to GAD65 (SPS-IgG^{preabsorbed}) was tested in comparison to native SPS-IgG #2 and control IgG on primary neurons and murine hippocampal brain slices. We found intense immunoreactivity to neuronal synapses in native SPS-IgG, but also in anti-GAD65 depleted SPS-IgG, thus supporting the assumption of additional AB to neuronal presynaptic antigens other than anti-GAD65 IgG.

Discussion

There is an ongoing debate if anti-GAD65 AB from SPS patients has an intrinsic pathogenic relevance. We found differences in presynaptic quantal release probabilities in granule cells between SPS-IgG and control IgG treated hippocampus slices. These findings cannot be directly attributed to effects brought about by AB targeting GAD65. In contrast, the interaction with GAD65 would likely result in reduced transmitter production and decreased GABAergic transmission during and after sustained stimulation, similar to experiments performed on GAD65 knockout mice (Tian et al. 1999). The present study is in support of the hypothesis that there may exist additional pathogenic AB in anti-GAD65-AB-positive SPS patient IgG fractions (Chang et al. 2013). As other candidates, AB to GABA-A receptor associated protein, to gephyrin, and to glycine receptors have been described in SPS patients (Butler et al. 2000; Raju et al. 2006). These targets are all located at the postsynaptic side of inhibitory synapses. However, our results here did not show any affection of postsynaptic GABAergic signaling suggesting a hypothetical IgG-AB specificity that is directed to an as yet undefined presynaptic target antigen. The observed increase of spontaneous vesicle release raises the hypothesis of a target antigen that is involved in regulating spontaneous vesicle fusion including calcium sensors (Martin et al. 2011; Pang et al. 2011; Walter et al. 2011) or a vesicle protein involved in spontaneous release mechanisms (Ramirez et al. 2012). Chronic increased spontaneous release of presynaptic GABA might evoke homeostatic downregulation and desensitization of postsynaptic GABA-A receptors leading to comparatively increased excitatory transmission. This is in line with previous reports showing reduced GABA-A receptor binding potential in SPS patients (Galldiks et al. 2008).

In our experiments we used a previously established concentration of IgG antibodies. Therefore we do not yet provide a dose-response relationship in the present study. Further studies are needed to investigate the specific functional role of SPS patient anti-GAD65 AB in more

detail using preabsorbed SPS patient IgG and reconstituted anti-GAD65 IgG (Geis et al. 2010) and to search for additional presynaptic antigens other than GAD65 that may exist in serum or cerebrospinal fluid of SPS patients.

Acknowledgments We thank B. Broll, B. Dekant, S. Hellmig, and C. Sommer (Jena) for providing expert technical assistance in animal care, cell culture experiments and IgG preparations. The authors declare no competing financial interest. This work was supported by the Deutsche Forschungsgemeinschaft (SFB 581 [TP A7], GE2519_3-1), by the IZKF and CSCC Jena (E-3.3), and by intramural University Research Funds (Würzburg and Jena).

References

- Allen C, Stevens CF (1994) An evaluation of causes for unreliability of synaptic transmission. *Proc Natl Acad Sci USA* 91:10380–10383
- Bergado-Acosta JR, Müller I, Richter-Levin G, Stork O (2014) The gaba-synthetic enzyme gad65 controls circadian activation of conditioned fear pathways. *Behav Brain Res* 260:92–100
- Butler MH et al (2000) Autoimmunity to gephyrin in stiff-man syndrome. *Neuron* 26:307–312
- Byts N, Samoylenko A, Fasshauer T, Ivanisevic M, Hennighausen L, Ehrenreich H, Siren AL (2008) Essential role for stat5 in the neurotrophic but not in the neuroprotective effect of erythropoietin. *Cell Death Differ* 15:783–792
- Chang T et al (2013) Immunization against gad induces antibody binding to gad-independent antigens and brainstem GABAergic neuronal loss. *PLoS One* 8:e72921
- Chattopadhyay S, Ito M, Cooper JD, Brooks AI, Curran TM, Powers JM, Pearce DA (2002) An autoantibody inhibitory to glutamic acid decarboxylase in the neurodegenerative disorder batten disease. *Hum Mol Genet* 11:1421–1431
- Edwards FA, Konnerth A, Sakmann B (1990) Quantal analysis of inhibitory synaptic transmission in the dentate gyrus of rat hippocampal slices: a patch-clamp study. *J Physiol* 430:213–249
- Galldikis N, Thiel A, Haense C, Fink GR, Hilker R (2008) 11c-flumazenil positron emission tomography demonstrates reduction of both global and local cerebral benzodiazepine receptor binding in a patient with stiff person syndrome. *J Neurol* 255:1361–1364
- Geis C et al (2010) Stiff person syndrome-associated autoantibodies to amphiphysin mediate reduced GABAergic inhibition. *Brain* 133:3166–3180
- Geis C et al (2011) Human stiff-person syndrome igg induces anxious behavior in rats. *PLoS One* 6:e16775
- Hansen N, Grunewald B, Weishaupt A, Colaco MN, Toyka KV, Sommer C, Geis C (2013) Human stiff person syndrome igg-containing high-titer anti-gad65 autoantibodies induce motor dysfunction in rats. *Exp Neurol* 239:202–209
- Henningsen P, Meinck HM (2003) Specific phobia is a frequent non-motor feature in stiff man syndrome. *J Neurol Neurosurg Psychiatry* 74:462–465
- Kash SF, Johnson RS, Tecott LH, Noebels JL, Mayfield RD, Hanahan D, Baekkeskov S (1997) Epilepsy in mice deficient in the 65-kDa isoform of glutamic acid decarboxylase. *Proc Natl Acad Sci USA* 94:14060–14065
- Kraushaar U, Jonas P (2000) Efficacy and stability of quantal gaba release at a hippocampal interneuron-principal neuron synapse. *J Neurosci* 20:5594–5607
- Manto MU, Laute MA, Aguera M, Rogemond V, Pandolfo M, Honnorat J (2007) Effects of anti-glutamic acid decarboxylase antibodies associated with neurological diseases. *Ann Neurol* 61:544–551
- Martin JA, Hu Z, Fenz KM, Fernandez J, Dittman JS (2011) Complexin has opposite effects on two modes of synaptic vesicle fusion. *Curr Biol* 21:97–105
- Mata S, Muscas GC, Cincotta M, Bartolozzi ML, Ambrosini S, Sorbi S (2010) Gad antibodies associated neurological disorders: incidence and phenotype distribution among neurological inflammatory diseases. *J Neuroimmunol* 227:175–177
- Pang ZP, Bacaj T, Yang X, Zhou P, Xu W, Sudhof TC (2011) Doc2 supports spontaneous synaptic transmission by a ca(2+)-independent mechanism. *Neuron* 70:244–251
- Raju R et al (2006) Autoimmunity to gaba-receptor-associated protein in stiff-person syndrome. *Brain* 129:3270–3276
- Ramirez DM, Khvotchev M, Trauterman B, Kavalali ET (2012) Vti1a identifies a vesicle pool that preferentially recycles at rest and maintains spontaneous neurotransmission. *Neuron* 73:121–134
- Schindelin J et al (2012) Fiji: an open-source platform for biological-image analysis. *Nat Methods* 9:676–682
- Seidenbecher T, Laxmi TR, Stork O, Pape HC (2003) Amygdalar and hippocampal theta rhythm synchronization during fear memory retrieval. *Science* 301:846–850
- Solimena M (1998) Vesicular autoantigens of type 1 diabetes. *Diabetes Metab Rev* 14:227–240
- Solimena M, Folli F, Denis-Domini S, Comi GC, Pozza G, De Camilli P, Vicari AM (1988) Autoantibodies to glutamic acid decarboxylase in a patient with stiff-man syndrome, epilepsy, and type i diabetes mellitus. *N Engl J Med* 318:1012–1020
- Sommer C, Weishaupt A, Brinkhoff J, Biko L, Wessig C, Gold R, Toyka KV (2005) Paraneoplastic stiff-person syndrome: passive transfer to rats by means of igg antibodies to amphiphysin. *Lancet* 365:1406–1411
- Tian N, Petersen C, Kash S, Baekkeskov S, Copenhagen D, Nicoll R (1999) The role of the synthetic enzyme gad65 in the control of neuronal gamma-aminobutyric acid release. *Proc Natl Acad Sci USA* 96:12911–12916
- Vianello M, Tavolato B, Armani M, Giometto B (2003) Cerebellar ataxia associated with anti-glutamic acid decarboxylase autoantibodies. *Cerebellum* 2:77–79. doi:10.1080/14734220309432
- Walter AM, Groffen AJ, Sorensen JB, Verhage M (2011) Multiple Ca²⁺ sensors in secretion: teammates, competitors or autocrats? *Trends Neurosci* 34:487–497

4.2 Manuscript II

Interactions of human autoantibodies with hippocampal GABAergic synaptic transmission – analyzing antibody-induced effects *ex vivo*

Haselmann H, Röpke L, Werner C, Kunze A, Geis C

Interactions of human autoantibodies with hippocampal GABAergic synaptic transmission – analyzing antibody-induced effects *ex vivo*

Holger Haselmann^{1,2*}, Luise Röpke¹, Christian Werner¹, Albrecht Kunze¹ and Christian Geis^{1,2}

¹Hans Berger Department of Neurology, Jena University Hospital, Jena, Germany, ²The Integrated Research and Treatment Center for Sepsis Control and Care (CSOC), Jena University Hospital, Jena, Germany

OPEN ACCESS

Edited by:

Christian E. Elger,
University of Bonn, Germany

Reviewed by:

Christoph Kleinschmitz,
University of Würzburg, Germany
Stefan Bittner,
University of Muenster, Germany

*Correspondence:

Holger Haselmann,
Hans Berger Department of
Neurology, Jena University Hospital,
Erfanger Allee 101, Jena 07747,
Germany
holger.haselmann@med.uni-jena.de

Specialty section:

This article was submitted to
Epilepsy, a section of the journal
Frontiers in Neurology

Received: 28 April 2015

Accepted: 28 May 2015

Published: 11 June 2015

Citation:

Haselmann H, Röpke L, Werner C,
Kunze A and Geis C (2015)
Interactions of human autoantibodies
with hippocampal GABAergic
synaptic transmission – analyzing
antibody-induced effects *ex vivo*.
Front. Neurol. 6:136.
doi: 10.3389/fneur.2015.00136

Autoantibodies (aAB) to the presynaptic located enzyme glutamate decarboxylase 65 (GAD65) are a characteristic attribute for a variety of autoimmune diseases of the central nervous system including subtypes of limbic encephalitis, stiff person-syndrome, cerebellar ataxia, and Batten's disease. Clinical signs of hyperexcitability and improvement of disease symptoms upon immunotherapy in some of these disorders suggest a possible pathogenic role of associated aAB. Recent experimental studies report inconsistent results regarding a direct pathogenic influence of anti-GAD65 aAB affecting inhibitory synaptic transmission in central GABAergic pathways. We here provide a method for direct evaluation of aAB-induced pathomechanisms in the intact hippocampal network. Purified patient IgG fractions containing aAB to GAD65 together with fixable lipophilic styryl dyes (FMdyes) are stereotactically injected into the hilus and the dentate gyrus in anesthetized mice. Twenty-four hours after intrahippocampal injection, acute hippocampal slices are prepared and transferred to a patch-clamp recording setup equipped with a fluorescence light source. Intraneural incorporated FMdyes show correct injection site for patch-clamp recording. Whole-cell patch-clamp recordings are performed from granule cells in the dentate gyrus and extracellular stimulation is applied in the border area of the dentate gyrus-hilus region to stimulate GABAergic afferents arising from parvalbumin positive basket cells. GABA-A receptor mediated inhibitory postsynaptic currents (IPSC) and miniature IPSC are recorded after blocking glutamatergic transmission. This approach allows investigation of potential aAB-induced effects on GABA-A receptor signaling *ex vivo* in an intact neuronal network. This offers several advantages compared to experimental procedures used in previous studies by *in vitro* AB preincubation of primary neurons or slice preparations. Furthermore, this method requires only small amounts of patient material that are often limited in rare diseases.

Keywords: autoantibody, stereotactic injection, hippocampus, patch-clamp recording, limbic encephalitis, GAD65, GABAergic inhibition

Introduction

IgG autoantibodies (aAB) to the glutamate decarboxylase 65 (GAD65) are increasingly recognized in neurological diseases of the central nervous system, e.g., in stiff person syndrome (SPS) (1, 2), limbic encephalitis (3), Batten's disease (4), or cerebellar ataxia (5). GAD65 is the rate limiting enzyme for GABA synthesis in presynaptic nerve endings of GABAergic interneurons (6). Signs of hyperexcitability or reduced central inhibition in these disorders point toward a potential pathogenic role of the associated aAB to GAD65 (7, 8). However, there are several concerns arguing against direct pathogenic mechanisms induced by the patient's aAB to GAD65. First, clinical syndromes are diverse and different regions and networks in the CNS seem to be afflicted, e.g., the hippocampus and amygdala in the subgroup of anti-GAD65 aAB positive limbic encephalitis, the brainstem and spinal cord in SPS, or the cerebellum in cerebellar ataxia (5). Second, GAD65 is an intracellular located enzyme that is less likely accessible to aAB compared to antigens on the neuronal surface. Third, in many of these syndromes exists a concurrent immune response to a variety of neuronal antigens in addition to GAD65. In SPS, patients with aAB to GAD65 develop often additional AB to the GABA-A receptor associated protein (GABARAP) (9). In Batten's disease, aAB to several antigens are described, e.g., to alpha-fetoprotein and further, still unknown neuronal antigens (10). So, if there are specific pathogenic mechanisms induced by aAB, it is uncertain which of the disease associated aAB causes disease symptoms. There are several experimental studies investigating patient derived IgG targeting GAD65 in neurons in different settings (8, 11, 12). However, results obtained from these studies are heterogeneous and sometimes contrasting. *In vitro* studies using dissociated neuronal cell cultures reported reduced GABAergic inhibitory synaptic transmission upon preincubation with patient IgG containing anti-GAD65 aAB (13). In a recent study, we could provide evidence patient IgG derived from patients with SPS induced disturbance of GABAergic transmission. However, this was not caused by associated aAB to GAD65 but by IgG to another, yet unknown presumably presynaptic antigen that is included in the IgG fraction of these patients (14). In animal studies, patient IgG with high titers of aAB to GAD65 was reported to induce disturbed GABAergic inhibition in the spinal cord, cerebellum, or cortical areas (8, 15, 16). However, the target-specificity of IgG-induced pathophysiology to GAD65 remains to be shown. This can be achieved by use of recombinant, specific IgG derived from isolated human plasma cells in animal passive-transfer models as shown before for aAB to aquaporin 4 in mouse models for neuromyelitis optica (17, 18). Another approach is the use of affinity-purified IgG aAB extracted of the polyclonal patient IgG fraction (19–21).

However, patient-derived material is often limited because many of these syndromes are rare diseases with only few affected patients. Invasive interventions required obtaining patient material, e.g., lumbar puncture for cerebrospinal fluid (CSF) cannot be performed repetitively in those patients for ethical reasons.

Here, we propose a method to investigate direct aAB induced effects *ex vivo* after stereotactic application of patient IgG preparations into the hippocampal compartment using only very limited amounts of patient material. We describe the possibility

of histological and electrophysiological analyses of GABAergic pathways in this passive-transfer mouse model.

Methods

Purification of Antibody-Containing IgG Fractions

IgG of an example patient with SPS and high titers of anti-GAD65 antibodies in serum and CSF as well as control IgG fractions without specific antineuronal reactivity were purified from therapeutic plasma exchange material by separation on exchange chromatography. Clinical details of the patients have been reported previously (16). The IgG fraction was concentrated by passage of the eluate through a Dialflo ultrafilter membrane (YM 100; Amicon, Witten, Germany) under nitrogen pressure to a volume of 50 ml. After dialysis against 10 l of water, the IgG sample was freeze-dried and stored at -20°C . Before use, lyophilized IgG was dissolved in 0.9M saline to a concentration of 5 mg/ml (16, 20).

Stereotactic Injections of Patient IgG Fractions into the Hippocampus of Mice

All animal experiments have been approved by the Thuringian state authorities (authorization # 02-059/13). Before surgery, the injection glass pipette (Glass Capillaries for Nanoliter 2000; Order# 4878; WPI, Sarasota, FL, USA) has been pulled with a long taper using a micropipette puller (Micropipette Puller P-1000; Sutter, Novato, CA, USA). The tip was then cut to a diameter of about 10 μm with a fine scissor. The injection pipette was attached to the head of a microprocessor-controlled nanoliter injector (Nanoliter 2000+ SYS-Micro4 Controller; WPI, Sarasota, FL, USA) and slightly filled with immersion oil to assure consistent pressure release onto the fluid by the injector. Thereafter, the pipette was completely filled with purified patient IgG fractions containing aAB against GAD65 (protein concentrations of 5 mg/ml in 0.9M saline). Together with the IgG fractions, 1 mM of FM1-43FX-dye (life technologies, Darmstadt, Germany) was added for fluorescent labeling of the area that has been targeted by the stereotactic intrahippocampal injection. A 6- (electrophysiological experiments) or 8-week-old (other experiments) wildtype C57BL/6 mice were anesthetized with 1.5–2.0% isoflurane/oxygen and their head was fixed to a stereotactic apparatus (Figure 1; Lab Standard™; Stoelting, Wood Dale, IL, USA). The temperature of the animals was monitored rectally and adjusted to 37°C by a heating pad with feedback control (FHC, Bowdoin, Canada). Eye ointment was used to prevent corneal drying during the surgery and the head was shaved with a razorblade. The skull was exposed by a small midline skin incision and the stereotactic injection sites were marked according to the respective coordinates (Table 1) determined according to the Paxinos mouse atlas (22). Holes were carefully drilled into the skull with a dentist driller (Foredom, Bethel, CT, USA) using drill heads of 0.47 mm diameter (Harvard Apparatus, Cambridge, UK) under visual control with an Olympus stereomicroscope (Olympus SZ 60, Tokyo, Japan). Care was taken not to penetrate the dura to avoid injury of the first cortical layers. For visual control of injection volumes, the initial maximum fluid level in the pipette was marked before each injection. The injection pipette was carefully moved to the respective injection point

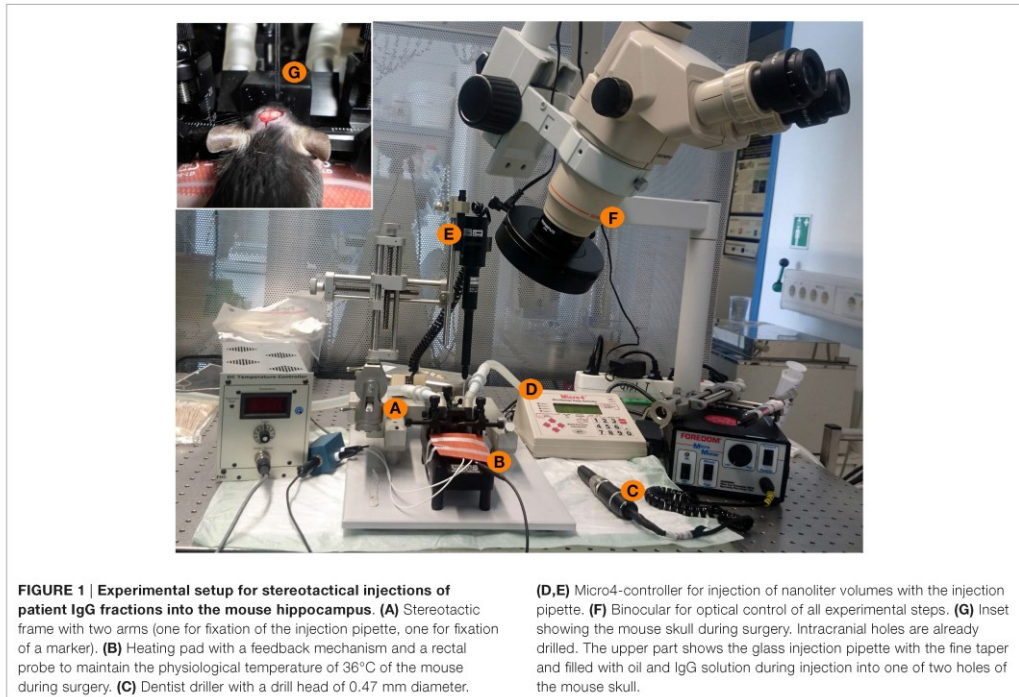


TABLE 1 | Coordinates for injections of IgG preparations in different parts of the hippocampal formation in mice (from bregma in mm).

| Target | Anterior-posterior | Medial-lateral | Distal-ventral |
|----------------------------------|--------------------|----------------|----------------|
| Middle dentate gyrus (front end) | 2.2 | 1.2 | 2.0 |
| Middle dentate gyrus (tale end) | 2.2 | 2.0 | 2.0 |
| End dentate gyrus (front end) | 2.5 | 1.5 | 2.0 |
| End dentate gyrus (tale end) | 2.5 | 2.5 | 2.5 |
| Middle CA1 region | 2.2 | 2.0 | 1.5 |
| End CA1 region | 2.5 | 2.3 | 2.0 |

according to the coordinates (Table 1; Figure 1). After waiting 1 min, 1 μ l of purified patient IgG solution together with fixable lipophilic styryl dyes (FMdyes) was injected into each hole with an injection speed of 4 nl/s. If the injection of solutions failed because the pipette was clogged by brain tissue, the injection pipette was removed and the injection was repeated with a new injection pipette. In some cases, minimal dorsal-ventral movement of the injection pipette was sufficient to perform proper injection without changing the pipette. After injection, the pipette was left in place for additional 5–10 min, before slowly being withdrawn. Thereafter, the skin was sutured with surgical suture (Covidien Sofilk 3-0, Dublin, Ireland) and the animals were monitored on a heating pad until complete recovery from anesthesia. All animals

were sacrificed 1–4 days after surgery for immunohistological or electrophysiological experiments.

In a subset of animals, we injected 1 μ l of a 0.4% trypan blue solution (Sigma-Aldrich, St. Louis, MO, USA) in the same way as described above to verify correct injection sites of stereotactical injection procedure (Figure 2). Here, 2–4 h after injection, the animals were sacrificed and the brain was cut in 1 mm slices with a tissue chopper (McIlwain Tissue Chopper, Mickle Laboratory Engineering Co Ltd., Guildford, UK) and the *ex vivo* slices were directly viewed under a stereomicroscope (Zeiss Stemi SV6, Zeiss, Jena, Germany).

Immunohistology of IgG-Injected Brain Slices

At 3–4 days post-injection, mice were deeply anesthetized, and intracardiac perfusion was performed. A catheter was placed into the left cardiac ventricle, and mice were perfused with 10 ml of phosphate buffered saline (PBS) followed by 4% paraformaldehyde (PFA) in phosphate buffer. Brains were extracted, afterfixed for 24 h in 4% PFA, dehydrated for 24 h in 10% sucrose, then further 24 h in 30% sucrose. Thereafter, 40 μ m serial sections were prepared on a freezing sliding microtome (HM 450 Sliding Microtome; Thermo Scientific, Waltham, MA, USA). Slices were stored in anti-freeze solution (30% ethylene glycol, 700 mM glucose, 3 mM sodium azide in phosphate buffer, pH 7.4) at -20°C until the day of staining. Slices were then defrosted at room temperature

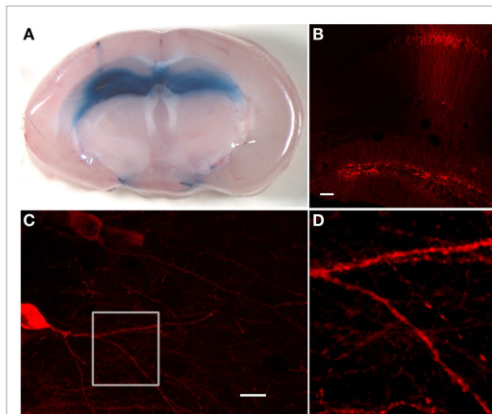


FIGURE 2 | Hippocampal stainings after stereotactic injections of trypan blue or anti-GAD65 aAB containing IgG preparations. (A) Injection of 1 μ l trypan blue in the dentate gyrus of each hemisphere shows uniform distribution exclusively in the hippocampal compartment. On the left side, the injection channel can be identified. (B) Immunohistological staining of injected anti-GAD65 aAB containing IgG preparation shows specific staining of cells in the dentate gyrus and around the injection channel (scale bar: 100 μ m). (C) Dendrites of a CA1 pyramidal cell can be analyzed after injection of anti-GAD65 aAB containing IgG preparations. The magnification of dendrites at the branching region of a CA1 neuron [white box shown in (D)] shows staining of human IgG deposits with distinct spots distributed along the dendrite (scale bar: 20 μ m).

and washed six times for 15 min in tris-buffered saline (TBS). Unspecific binding sites were blocked by 3% normal goat serum and 2% milk powder in TBS containing 0.1% of Triton-X100 for permeabilization of the membrane for 30 min. Slices were incubated with Cy3 goat anti-human antibodies (Dianova, Hamburg, Germany) as secondary antibodies to detect binding of the injected human aAB in 3% normal goat serum, 2% milk powder, and 0.1% TritonX-100 overnight at 4°C. After additional washing, steps in TBS for 10 min slices were placed on object slides, dried on air, stained for 5 min in DAPI solution (Sigma-Aldrich, St. Louis, MO, USA), washed three times in PBS for 5 min, and mounted with Fluoromount (Southern Biotech, Birmingham, AL, USA).

Confocal Microscopy

Cells were viewed on a confocal microscope (Zeiss LSM 710, Jena, Germany) using a 10 \times objective or a 63 \times oil objective, keeping laser power and photomultiplier tube voltage constant. Maximum projections of z-stacks were generated using FIJI image analysis software.

Acute Hippocampal Slice Whole-Cell Patch-Clamp Recordings

Separate groups of mice were used for *ex vivo* acute brain-slice recording. Twenty-four hours after intrahippocampal IgG injection, mice were deeply anesthetized and decapitated. The brain was removed in ice-cold extracellular artificial CSF (ACSF 1; 40 mM

NaCl, 25 mM NaHCO₃, 10 mM glucose, 150 mM sucrose, 4 mM KCl, 1.25 mM NaH₂PO₄, 0.5 mM CaCl₂, 7 mM MgCl₂; purged with 95% CO₂/5% O₂) and cut in two halves. The bulbus olfactorius was cut in a coronal manner and the brain was glued with the cut face onto the probe-holder with superglue (UHU, Bühl, Germany). Three hundred micrometer thick coronal slices were made with a vibratome (Leica, Wetzlar, Germany; Leica VT1200 S) with an amplitude of 1 mm and a velocity of 0.4 mm/s. Slices were transferred into an incubation beaker with extracellular ACSF suited for patch-clamp recording (ACSF 2; 125 mM NaCl, 25 mM NaHCO₃, 25 mM glucose, 2.5 mM KCl, 1.25 mM NaH₂PO₄, 2 mM MgCl₂; purged with 95% CO₂/5% O₂) and held at 34°C for at least 30 min. For recordings, slices were then transferred into a measurement chamber (Figure 3) superfused with extracellular ACSF 2 with 1.3–1.8 ml/min at room temperature. Recording electrodes pulled from thick-walled borosilicate glass (2.0 mm diameter; Science Products, Hofheim, Germany) were filled with intracellular recording solution containing 140 mM KCl, 10 mM HEPES, 10 mM EGTA, 2 mM Na₂ATP, 2 mM MgCl₂, pH 7.2, and an osmolarity of 300–330 mOsmol. Recording electrodes had a final resistance of 3–5 M Ω . Inhibitory postsynaptic currents (IPSCs) were recorded with an EPC10 patch clamp amplifier and Patch-Master Software (HEKA, Lambrecht, Germany). Whole-cell patches were performed of granule cells (GC) held at -70 mV. Recordings were rejected if the resting potential was more positive than -50 mV or changed during the experiments and if series resistance was higher than 20 M Ω . Acceptable membrane capacitance range is from 10 to 30 pF. Evoked IPSCs were isolated by blocking glutamatergic transmission using 10 μ M Cyano-Nitroquinoxaline-Dione (CNQX) and 50 μ M 2-amino-phosphonovaleric acid (AP-5; Tocris Bioscience, Ellisville, MO, USA). Application of 1 μ M tetrodotoxin (TTX; Sigma Aldrich, St. Louis, MO, USA) was used for recordings of miniature IPSCs (mIPSCs). Monosynaptic IPSCs were evoked as described previously (14, 20). Briefly, GABAergic synaptic inputs in whole-cell clamped GCs were evoked by another glass electrode filled with extracellular ACSF 2 that has been placed nearby a neighboring CG located toward the hilar region using a stimulus isolation unit (Isoflex, A.M.PI, Jerusalem, Israel) (Figures 3 and 4). In this configuration, GABAergic afferents arising from GABAergic basket cells (BC) located at the hilus border region are stimulated. Here, we applied pulses of 200 μ s duration at 0.3 Hz while measuring IPSCs of the postsynaptic clamped GCs. Paired-pulse recordings were obtained by stimulating the neurons with an inter-stimulus interval of 100 ms. Recordings were filtered at 2.9 and 10 kHz using the filters of the amplifier. Traces were analyzed by Igor Pro Software (Wavemetrics, Lake Oswego, OR, USA).

Results

Trypan Blue Injections Show Labeling of the Hippocampal Formation After Stereotactic Injection

For direct *ex vivo* verification of the distribution of injected substances within the mouse brain, we injected trypan blue solution at different stereotactic coordinates (Table 1) into the hippocampal formation of both hemispheres (Figure 1). The distribution of trypan blue is shown in Figure 2A. The trypan blue labeling was

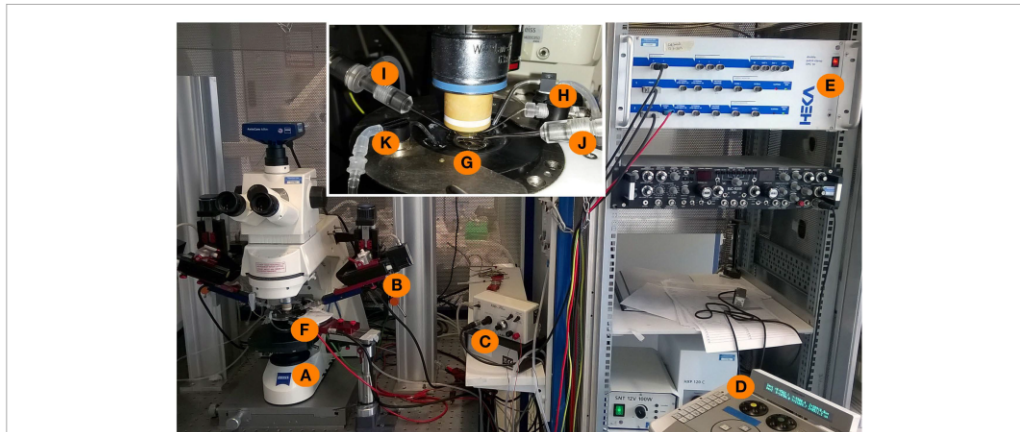


FIGURE 3 | Experimental setup for whole-cell patch-clamp measurements in acute brain slices. An upright microscope (A) is placed on a X–Y table and is now freely movable around the bath-chamber (F) and the micromanipulators (B), control unit: (D). The inset shows a magnification of the bath chamber with the perfusion system (K) of the bath and a grid holding

the brain slice in the middle of the chamber (G). The recording and stimulation electrodes are marked with (I, J), respectively. The recording electrode is connected to a grounding electrode (H) as well as to the amplifier (E). The stimulation electrode is connected to the stimulator (C) which is triggered by the amplifier with a 5 mV stimulus command.

apparent in most parts of the hippocampal formation including the dentate gyrus and major parts of the CA-regions. In this example, the injection channel can also be identified. This example also demonstrates that only minor lesions of the cortical and hippocampal tissue result by the injection procedure using thin glass pipettes. Beside a slight diffusion of trypan blue along the lateral ventricle, brain compartments surrounding the hippocampus were not labeled.

Detection of Human IgG Deposition After Stereotactic Intrahippocampal Injection

Deposition of human IgG was tested 1–3 days after stereotactic injection by using fluorescence coupled commercial antibodies directed to human IgG. Immunohistology was performed in brain slices after perfusion and fixation. Detection of the 10 μ g injected human IgG fractions with high titers of anti-GAD65 aAB resulted in exclusive hippocampal immunoreactivity (Figure 2B). Neuronal dendrites in the injection site showed synaptic staining (Figures 2C, D). Magnification of the dendrites as shown here by high-resolution confocal microscopy demonstrates that detailed morphological analysis and quantifications of dendritic structures including spines and synaptic spots are possible (Figure 2D). This method can also be combined with co-immunostaining of further synaptic markers. In comparison to the trypan blue stainings, the overall diffusion of the injected antibodies seems to be less widespread. This could be due to decreased concentrations of injected aAB in the more distant areas of the injection site, absorption of anti-GAD65 aAB by antigens near the injection site, or due to the higher viscosity of the IgG solution.

Electrophysiological Recordings and GABAergic Synaptic Transmission in the Perforans-Path – Granule Cell Synapse is not Affected by Stereotactic IgG Injection

Simultaneous injection of patient IgG fractions together with FM1-43FX-Dye allows precise control of the injection site in vital *ex vivo* acute brain slice preparations. FM1-43FX-Dye is fluorescent in contact with cellular membranes and gets incorporated by activity-dependent synaptic vesicle endocytosis. Therefore, the area of IgG injection can be determined in the vital hippocampal slices by localizing the FM1-43FX fluorescence (Figure 4A). The brain slices in this fluorescence labeled area seemed healthy without signs of swelling or tissue destruction. The neurons inside that region showed a healthy shape.

Electrophysiological measurements of IPSCs in GCs also showed reliable vitality in mice injected with control IgG fractions without specific antineuronal reactivity together with FM1-43FX dye. GC had the expected values of resting potential, input resistance, and membrane capacity. Figures 4B, C show averaged sample traces of evoked GABAergic IPSCs after single and paired-pulse stimulation of the perforant path with a time interval of 100 ms. The GABAergic currents in FM1-43FX-injected brain slices had similar amplitudes of 145 pA (mean of 30 sweeps) and kinetics (rise time = 1.27 ms; decay time = 20.05 ms) as in untreated animals. The paired-pulse experiments revealed a significant depression of IPSCs after the second pulse due to the expected short-term plasticity dependent on incomplete vesicle recycling 100 ms after the first induced IPSC (ratio A2/A1 = 0.84). This is in line with published findings on IPSC depression in normal brain slices after extracellular stimulation or in paired recordings of GCs and BCs

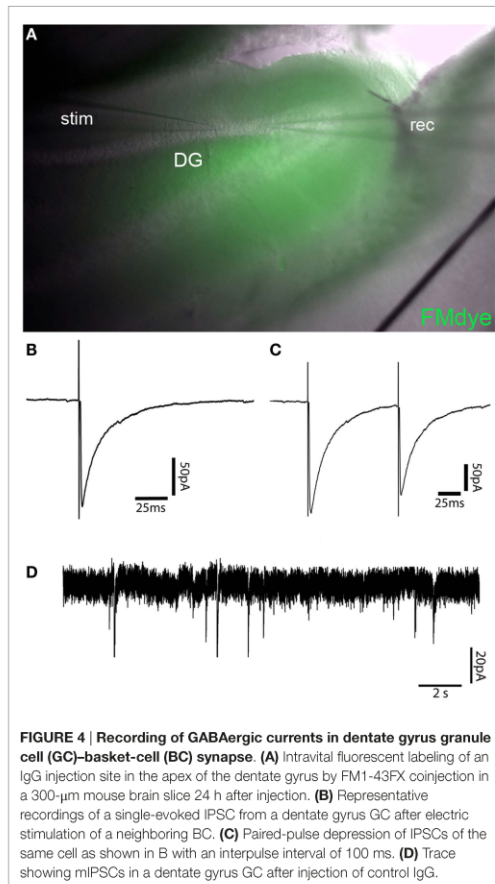


FIGURE 4 | Recording of GABAergic currents in dentate gyrus granule cell (GC)-basket-cell (BC) synapse. (A) Intravital fluorescent labeling of an IgG injection site in the apex of the dentate gyrus by FM1-43FX coinjection in a 300- μ m mouse brain slice 24 h after injection. **(B)** Representative recordings of a single-evoked IPSC from a dentate gyrus GC after electric stimulation of a neighboring BC. **(C)** Paired-pulse depression of IPSCs of the same cell as shown in B with an interpulse interval of 100 ms. **(D)** Trace showing mIPSCs in a dentate gyrus GC after injection of control IgG.

(14, 23). Recordings of mIPSCs in the control IgG injected brain slices show mean amplitude of 24 pA with a frequency of 0.41 Hz in a similar magnitude as mIPSCs of untreated animals (Figure 4D).

Discussion

The *in vivo* stereotactic intrahippocampal injection of small volumes offers several advantages in comparison to previously used passive-transfer methods of human IgG samples. First, this method is target-specific for the hippocampal formation as we could demonstrate by trypan blue staining and immunohistology detecting human IgG depositions. This selective delivery of IgG allows investigation of direct aAB effects on hippocampal function, e.g., learning and memory without interference of aAB-induced pathomechanisms in other regions of the CNS. Second, the surgical procedure is fast, and after completing the injections, animals are not affected by any implanted material as it is the case for

chronic application of IgG by intraventricular administration using osmotic pumps (24) or by repetitive application using implanted intrathecal (20, 21) or intraventricular (15) catheters. Third, the required amounts of rare human IgG samples are much lower as compared to the other passive-transfer techniques. Moreover, the tissue destruction due to the injection procedure using glass capillaries with thin taper is clearly less compared to implantation of intracerebral catheters.

The parallel application of FM1-43FX fluorescence dyes makes this procedure exceptional suited for *ex vivo* brain slice recordings. Injection sites can be easily identified using a conventional fluorescence light source on the recording setup. As mentioned, tissue destruction is minimal and extracellular as well as patch-clamp recordings can be performed without limitations in regions that have been visually identified by FM dye staining. However, one has to take into account that there might be a difference in the deposition of IgG and FM dye staining. Comparison of immunohistochemical detection of injected human IgG and fluorescent FM dyes are recommended in pilot experiments to test the co-distribution of FM dye and IgG in the injected brain areas. Example recordings shown here demonstrate that GABAergic pathways, e.g., the monosynaptic transmission from BC located in the hilus projecting to dentate gyrus GC can be investigated without any differences in parameters of evoked IPSC and mIPSC as compared to recordings obtained from sham animals that were not injected (20). Here, we used six to eight-week-old mice for injection and recording. In principle, also mice older than 8 weeks can be used in this procedure. Please note that patch-clamp neurophysiology may be more difficult in older animals due to more rigid connective tissue.

Certainly, there are also limitations of this procedure. Implantation of osmotic pumps or intrathecal catheters allows continuous or easy repetitive application in the subarachnoid space or into the brain parenchyma. Here, repetitive injections can be performed in principle but animals need to be anesthetized again. There is no need for additional trepanation but the skull has to be exposed and skin has to be opened and closed again which increases risk of infections. Further, optimal concentrations of IgG solutions are not determined and can only be varied within the small injection volumes. Preliminary experiments may be necessary to obtain a dose-response curve. It is possible to inject up to 3 μ l of IgG into one hemisphere (for example, three separate holes, 1 μ l into each) without relevant tissue destruction. Another possibility is to inject 2 μ l of IgG per hemisphere with repeated injections of IgG every day over total 3 days. The IgG concentrations can range from 2 to 10 mg/ml IgG. Even higher concentrations of IgG may be tested until clogging of the pipette tip occurs due to the increased viscosity of the solution.

Immunohistochemistry detecting human IgG may give first information of the magnitude and extent of intraparenchymal IgG deposition. Insufficient volume or less IgG concentration may result in only partial application in small areas in the hippocampus. To ensure adequate concentration and allocation of IgG solutions in most of the hippocampal compartment, at least two injection sites, e.g., in the CA3 region and in the dentate gyrus should be selected. As we tested, IgG deposits can be identified up to 1 week after injection. We did not observe any obvious immune cell infiltration or activation.

Together, we here describe a method of reliable, target-specific IgG application into the hippocampal compartment. This is suited for subsequent electrophysiological and histological analyses as an additional and complementary method of passive-transfer applications in mice. With this procedure, direct aAB-induced alternations of neuronal and synaptic activity can be investigated *in vivo* and in slice preparations. In case of aAB to GAD65, inhibitory transmission can be evaluated by recording the BC-GC synapse. In addition, this procedure can also be applied for investigation of aAB-induced dysfunction of excitatory transmission, e.g., induced by aAB to the NMDA- or AMPA receptor. For testing glutamatergic transmission, stimulation of perforant path fibers and recording in GC or stimulation of

Schaffer collaterals and recording from CA1 pyramidal neurons would be suitable. Moreover, field potential measurements for analysis of long term potentiation after IgG injection can be performed to obtain information about plasticity changes induced by aAB.

Acknowledgments

We thank C. Sommer for providing expert technical assistance in animal experiments and immunohistology, and A. Weishaupt and S. Hellmig for preparation of IgG solutions. This work was supported by the Deutsche Forschungsgemeinschaft (SFB 581 [TP A7], GE2519_3-1), the IZKF, and CSCC Jena (E-3.3).

References

- Solimena M, Folli E, Aparisi R, Pozza G, De Camilli P. Autoantibodies to GABAergic neurons and pancreatic beta cells in stiff-man syndrome. *N Engl J Med* (1990) 322(22):1555–60. doi:10.1056/NEJM199005313222202
- Holmoy T, Geis C. The immunological basis for treatment of stiff person syndrome. *J Neuroimmunol* (2011) 231(1–2):55–60. doi:10.1016/j.jneuroim.2010.09.014
- Malter MP, Helmstaedt C, Urbach H, Vincent A, Bien CG. Antibodies to glutamic acid decarboxylase define a form of limbic encephalitis. *Ann Neurol* (2010) 67(4):470–8. doi:10.1002/ana.21917
- Chattopadhyay S, Ito M, Cooper JD, Brooks AL, Curran TM, Powers JM, et al. An autoantibody inhibitory to glutamic acid decarboxylase in the neurodegenerative disorder Batten disease. *Hum Mol Genet* (2002) 11(12):1421–31. doi:10.1093/hmg/11.12.1421
- Saiz A, Blanco Y, Sabater L, Gonzalez F, Bataller L, Casamitjana R, et al. Spectrum of neurological syndromes associated with glutamic acid decarboxylase antibodies: diagnostic clues for this association. *Brain* (2008) 131(Pt 10):2553–63. doi:10.1093/brain/awn183
- Buddhala C, Hsu CC, Wu JY. A novel mechanism for GABA synthesis and packaging into synaptic vesicles. *Neurochem Int* (2009) 55(1–3):9–12. doi:10.1016/j.neuint.2009.01.020
- Koerner C, Wieland B, Richter W, Meinck HM. Stiff-person syndromes: motor cortex hyperexcitability correlates with anti-GAD autoimmunity. *Neurology* (2004) 62(8):1357–62. doi:10.1212/01.WNL.0000120543.65812.33
- Manto MU, Laute MA, Aguera M, Rogemond V, Pandolfo M, Honnorat J. Effects of anti-glutamic acid decarboxylase antibodies associated with neurological diseases. *Ann Neurol* (2007) 61(6):544–51. doi:10.1002/ana.21123
- Raju R, Rakocevic G, Chen Y, Hoehn G, Semino-Mora C, Shi W, et al. Autoimmunity to GABA_A-receptor-associated protein in stiff-person syndrome. *Brain* (2006) 129(Pt 12):3270–6. doi:10.1093/brain/awl245
- Castaneda JA, Pearce DA. Identification of alpha-fetoprotein as an autoantigen in juvenile Batten disease. *Neurobiol Dis* (2008) 29(1):92–102. doi:10.1016/j.nbd.2007.08.007
- Takenoshita H, Shizuka-Ikeda M, Mitoma H, Song S, Harigaya Y, Igeta Y, et al. Presynaptic inhibition of cerebellar GABAergic transmission by glutamate decarboxylase autoantibodies in progressive cerebellar ataxia. *J Neurol Neurosurg Psychiatry* (2001) 70(3):386–9. doi:10.1136/jnnp.70.3.386
- Ishida K, Mitoma H, Song SY, Uchihara T, Inaba A, Eguchi S, et al. Selective suppression of cerebellar GABAergic transmission by an autoantibody to glutamic acid decarboxylase. *Ann Neurol* (1999) 46(2):263–7. doi:10.1002/1531-8249(199908)46:2<263::AID-ANA19>3.3.CO;2-S
- Vianello M, Bisson G, Dal Maschio M, Vassanelli S, Girardi S, Mucignat C, et al. Increased spontaneous activity of a network of hippocampal neurons in culture caused by suppression of inhibitory potentials mediated by anti-gad antibodies. *Autoimmunity* (2008) 41(1):66–73. doi:10.1080/08916930701619565
- Werner C, Haselmann H, Weishaupt A, Toyka KV, Sommer C, Geis C. Stiff person syndrome IgG affects presynaptic GABAergic release mechanisms. *J Neural Transm* (2015) 122(3):357–62. doi:10.1007/s00702-014-1268-1
- Hansen N, Grunewald B, Weishaupt A, Colaco MN, Toyka KV, Sommer C, et al. Human stiff person syndrome IgG-containing high-titer anti-GAD65 autoantibodies induce motor dysfunction in rats. *Exp Neurol* (2013) 239:202–9. doi:10.1016/j.expneurol.2012.10.013
- Geis C, Weishaupt A, Grunewald B, Wulstsch T, Reif A, Gerlach M, et al. Human stiff-person syndrome IgG induces anxious behavior in rats. *PLoS One* (2011) 6(2):e16775. doi:10.1371/journal.pone.0016775
- Geis C, Ritter C, Ruschil C, Weishaupt A, Grunewald B, Stoll G, et al. The intrinsic pathogenic role of autoantibodies to aquaporin 4 mediating spinal cord disease in a rat passive-transfer model. *Exp Neurol* (2014) 265:8–21. doi:10.1016/j.expneurol.2014.12.015
- Bennett JL, Lam C, Kalluri SR, Saikali P, Bautista K, Dupree C, et al. Intrathecal pathogenic anti-aquaporin-4 antibodies in early neuromyelitis optica. *Ann Neurol* (2009) 66(5):617–29. doi:10.1002/ana.21802
- Geis C, Beck M, Jablonka S, Weishaupt A, Toyka KV, Sendtner M, et al. Stiff person syndrome associated anti-amphiphysin antibodies reduce GABA associated [Ca²⁺]_i rise in embryonic motoneurons. *Neurobiol Dis* (2009) 36(1):191–9. doi:10.1016/j.nbd.2009.07.011
- Geis C, Weishaupt A, Hallermann S, Grunewald B, Wessig C, Wulstsch T, et al. Stiff person syndrome-associated autoantibodies to amphiphysin mediate reduced GABAergic inhibition. *Brain* (2010) 133(11):3166–80. doi:10.1093/brain/awq253
- Geis C, Grunewald B, Weishaupt A, Wulstsch T, Toyka KV, Reif A, et al. Human IgG directed against amphiphysin induces anxiety behavior in a rat model after intrathecal passive transfer. *J Neural Transm* (2012) 119(8):981–5. doi:10.1007/s00702-012-0773-3
- Franklin KBJ, Paxinos G. *The Mouse Brain in Stereotaxic Coordinates*. San Diego: Elsevier Academic Press (2007).
- Kraushaar U, Jonas P. Efficacy and stability of quantal GABA release at a hippocampal interneuron-principal neuron synapse. *J Neurosci* (2000) 20(15):5594–607.
- Planaguma J, Leyboldt F, Mannara F, Gutierrez-Cuesta J, Martin-Garcia E, Aguilar E, et al. Human N-methyl D-aspartate receptor antibodies alter memory and behaviour in mice. *Brain* (2015) 138(Pt 1):94–109. doi:10.1093/brain/awu310

Conflict of Interest Statement: The authors declare that the research was conducted in the absence of any commercial or financial relationships that could be construed as a potential conflict of interest.

Copyright © 2015 Haselmann, Röpke, Werner, Kunze and Geis. This is an open-access article distributed under the terms of the Creative Commons Attribution License (CC BY). The use, distribution or reproduction in other forums is permitted, provided the original author(s) or licensor are credited and that the original publication in this journal is cited, in accordance with accepted academic practice. No use, distribution or reproduction is permitted which does not comply with these terms.

4.3 Manuscript III

Human autoantibodies to amphiphysin induce defective presynaptic vesicle dynamics and composition

Werner C, Pauli M, Doose S, Weishaupt A, Haselmann H, Grünewald B, Sauer M, Heckmann M, Toyka KV, Asan E, Sommer C, Geis C

Human autoantibodies to amphiphysin induce defective presynaptic vesicle dynamics and composition

Christian Werner,^{1,2} Martin Pauli,³ Sören Doose,⁴ Andreas Weishaupt,² Holger Haselmann,^{1,2,5} Benedikt Grünewald,^{1,2,5} Markus Sauer,⁴ Manfred Heckmann,³ Klaus V. Toyka,² Esther Asan,⁶ Claudia Sommer² and Christian Geis^{1,2,5}

See Irani (doi:10.1093/awv364) for a scientific commentary on this article.

Stiff-person syndrome is the prototype of a central nervous system disorder with autoantibodies targeting presynaptic antigens. Patients with paraneoplastic stiff-person syndrome may harbour autoantibodies to the BAR (Bin/Amphiphysin/Rvs) domain protein amphiphysin, which target its SH3 domain. These patients have neurophysiological signs of compromised central inhibition and respond to symptomatic treatment with medication enhancing GABAergic transmission. High frequency neurotransmission as observed in tonic GABAergic interneurons relies on fast exocytosis of neurotransmitters based on compensatory endocytosis. As amphiphysin is involved in clathrin-mediated endocytosis, patient autoantibodies are supposed to interfere with this function, leading to disinhibition by reduction of GABAergic neurotransmission. We here investigated the effects of human anti-amphiphysin autoantibodies on structural components of presynaptic boutons *ex vivo* and *in vitro* using electron microscopy and super-resolution direct stochastic optical reconstruction microscopy. Ultrastructural analysis of spinal cord presynaptic boutons was performed after *in vivo* intrathecal passive transfer of affinity-purified human anti-amphiphysin autoantibodies in rats and revealed signs of markedly disabled clathrin-mediated endocytosis. This was unmasked at high synaptic activity and characterized by a reduction of the presynaptic vesicle pool, clathrin coated intermediates, and endosome-like structures. Super-resolution microscopy of inhibitory GABAergic presynaptic boutons in primary neurons revealed that specific human anti-amphiphysin immunoglobulin G induced an increase of the essential vesicular protein synaptobrevin 2 and a reduction of synaptobrevin 7. This constellation suggests depletion of resting pool vesicles and trapping of releasable pool vesicular proteins at the plasma membrane. Similar effects were found in amphiphysin-deficient neurons from knockout mice. Application of specific patient antibodies did not show additional effects. Blocking alternative pathways of clathrin-independent endocytosis with brefeldin A reversed the autoantibody induced effects on molecular vesicle composition. Endophilin as an interaction partner of amphiphysin showed reduced clustering within presynaptic terminals. Collectively, these results point towards an autoantibody-induced structural disorganization in GABAergic synapses with profound changes in presynaptic vesicle pools, activation of alternative endocytic pathways, and potentially compensatory rearrangement of proteins involved in clathrin-mediated endocytosis. Our findings provide novel insights into synaptic pathomechanisms in a prototypic antibody-mediated central nervous system disease, which may serve as a proof-of-principle example in this evolving group of autoimmune disorders associated with autoantibodies to synaptic antigens.

1 Hans-Berger Department of Neurology, Jena University Hospital, Erlanger Allee 101, 07747 Jena, Germany

2 Department of Neurology, University of Würzburg, Josef-Schneider Str. 11, 97080 Würzburg, Germany

3 Department of Neurophysiology, Institute of Physiology, University of Würzburg, Roentgenring 9, 97070 Würzburg, Germany

4 Department of Biotechnology and Biophysics, Biocenter, University of Würzburg, Am Hubland, 97074 Würzburg, Germany

5 Center for Sepsis Control and Care (CSCC), Jena University Hospital, Erlanger Allee 101, 07747 Jena, Germany

6 Institute for Anatomy and Cell Biology, University of Würzburg, Koellikerstrasse 6, 97070 Würzburg, Germany

Correspondence to: Christian Geis, MD,
Hans-Berger Department of Neurology,
Erlanger Allee, 07747 Jena,
Germany
E-mail: christian.geis@med.uni-jena.de

Keywords: stiff-person syndrome; amphiphysin; dSTORM super-resolution microscopy; clathrin-mediated endocytosis; autoantibody

Abbreviations: dSTORM = direct stochastic optical reconstruction microscopy; IgG = immunoglobulin G; specAmph = specific anti-amphiphysin antibody eluates; syb2 = synaptobrevin 2; syb7 = synaptobrevin 7; vgat = GABAergic vesicular transporter; v-SNARE = vesicular soluble N-ethylmaleimide-sensitive-factor attachment receptor

Introduction

The discovery of autoantibody-mediated disorders in the CNS is one of the major achievements in neurology during the past decades. The list of identified target antigens is continuously growing, but our understanding of the pathomechanisms of disease and of characteristic disease symptoms is still at the beginning (Irani *et al.*, 2014; Leypoldt *et al.*, 2015). Stiff-person syndrome is the prototype of an autoantibody-mediated CNS disease with autoantibodies to a presynaptic antigen. In paraneoplastic stiff-person syndrome the dominant IgG autoantibodies are directed at the synaptic protein amphiphysin (encoded by *AMPH*; De Camilli *et al.*, 1993; David *et al.*, 1994). Amphiphysin is a N-BAR domain protein involved in clathrin-mediated endocytosis (Lichte *et al.*, 1992). It is important in various stages of clathrin-mediated endocytosis including membrane bending, clathrin coating, and recruitment of dynamin, then mediating membrane fission of newly retrieved presynaptic vesicles (Takei *et al.*, 1996; Arkhipov *et al.*, 2009).

The pathogenic role of autoantibodies to amphiphysin was previously demonstrated by systemic and intrathecal passive transfer to rats (Sommer *et al.*, 2005; Geis *et al.*, 2010). Using super-resolution stimulation emission depletion (STED) microscopy we could provide evidence that specific autoantibodies to amphiphysin bind to their antigen in spinal cord presynapses at the site of vesicle endocytosis (Geis *et al.*, 2010). In neuronal cell culture, preabsorption and autoantibody competition assays revealed an epitope-specific process of pathogenic autoantibody internalization. Symptoms of patients with stiff-person syndrome have been attributed to decreased GABAergic neurotransmission based on the observation that drugs enhancing GABAergic transmission, e.g. benzodiazepines induce clinical improvement (Vasconcelos and Dalakas, 2003; Murinson, 2004). Neurophysiological studies in patients and in experimental animals showed compromised tonic GABAergic inhibition as an underlying pathomechanism (Sandbrink *et al.*, 2000; Geis *et al.*, 2010). Despite progress in understanding the stiff-person syndrome pathophysiology, the molecular events at the ultrastructural level leading to autoantibody-induced dysfunction remain unclear. Acute blocking of the amphiphysin SH3 (Src homology 3) domain with inhibitory peptides

injected into reticulospinal lamprey synapses *in vitro* led to stimulus-dependent endocytic dysfunction with accumulation of endocytic intermediates and smaller releasable vesicle pools, thus resulting in defective neurotransmission at high synaptic activity (Shupliakov *et al.*, 1997; Evergren *et al.*, 2004). Congenital deficiency of amphiphysin in a mouse null mutant induces memory deficits and increases seizure susceptibility as a consequence of impaired vesicle recycling (Di Paolo *et al.*, 2002).

Synaptic vesicles differ in their molecular composition determining their affinity to the distinct vesicle pools within the presynapse. The essential vesicular soluble N-ethylmaleimide-sensitive-factor attachment receptor (v-SNARE) proteins synaptobrevin 2 (syb2, encoded by *VAMP2*) and synaptobrevin 7 (syb7, encoded by *VAMP7*) are known to be directed to the readily releasable and to resting pool vesicles, respectively (Hua *et al.*, 2011). This provides an opportunity to differentiate the vesicle pools by their v-SNARE composition (Fig. 1). The synaptic proteins endophilin and synaptojanin are direct binding partners of amphiphysin. Endophilin is involved in membrane bending, vesicle uncoating and has also been shown to be important in endocytic pathways independent of clathrin (Milosevic *et al.*, 2011; Boucrot *et al.*, 2015). Synaptojanin interacts with amphiphysin and endophilin (Dong *et al.*, 2015) and serves as an uncoating factor at the later steps in clathrin-mediated endocytosis (Fig. 1). In the context of the hypothetical anti-amphiphysin autoantibody-induced dysfunctional clathrin-mediated endocytosis, we aimed at elucidating if these interacting synaptic proteins are affected and if they may act as compensatory factors.

Using ultrastructural analyses we here provide evidence that affinity-purified pathogenic human autoantibodies targeting the SH3 domain of amphiphysin lead to a stimulus-sensitive reduction of releasable vesicles and clathrin-coated vesicles in spinal cord presynapses *in vivo*.

In primary neurons, super-resolution microscopy (direct stochastic optical reconstruction microscopy, dSTORM) revealed anti-amphiphysin autoantibody-induced changes of v-SNARE composition on presynaptic vesicles. Furthermore, molecular targeting of endophilin is affected by human anti-amphiphysin autoantibodies within GABAergic presynaptic terminals.

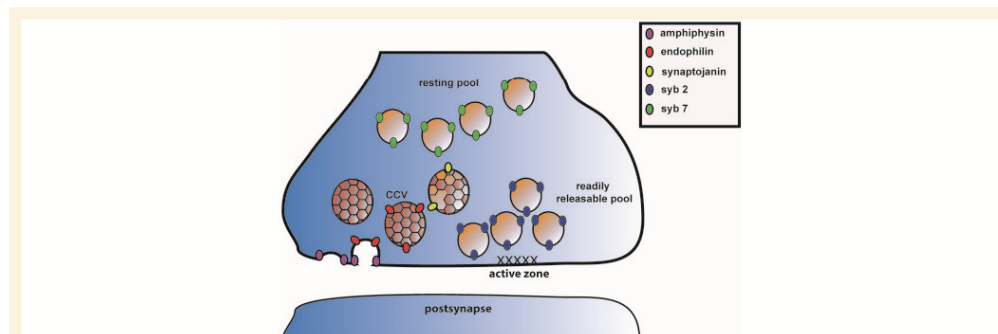


Figure 1 Schematic overview of investigated structural and molecular arrangements within the presynapse. Amphiphysin is involved in membrane bending to initiate the synaptic vesicle budding step in clathrin-mediated endocytosis. Amphiphysin has several interaction partners in these initial steps of endocytosis. Shown here is the interaction partner endophilin that is also involved in membrane bending and further in promoting the vesicle uncoating phase. Additionally, endophilin plays a role in clathrin-independent endocytosis. Synaptojanin initiates synaptic vesicle uncoating and interacts with amphiphysin and endophilin. Readily releasable vesicles are characterized by preferential molecular equipment with v-SNARE syb2 and resting vesicles are predominantly associated with syb7 isoforms. Further interaction partners of amphiphysin and other synaptic proteins are omitted for simplicity. Clathrin triskelions are illustrated as honeycombs on clathrin-coated vesicles (CCV).

Materials and methods

Patients and therapeutic plasma exchange

The clinical details of the patients with paraneoplastic stiff-person syndrome and high titres of anti-amphiphysin autoantibodies and a control patient suffering from peripheral neuropathy without CNS disease and without specific autoantibody reactivity to neuronal antigens have been reported (Wessig *et al.*, 2003). A commercial enzyme immunodot assay was used to determine titres of anti-amphiphysin autoantibodies with rabbit antisera raised against recombinant amphiphysin I as a positive control (H.P. Seelig). Serum titres before plasma exchange were $1\text{--}2 \times 10^8$.

Amphiphysin expression and IgG preparation

In this study, we exclusively used affinity purified human IgG specifically directed at the amphiphysin SH3 domain. Affinity purification of human IgG obtained from patient plasma filtrates was performed by capturing anti-amphiphysin autoantibodies from IgG fractions by affinity chromatography and reconstitution of specific anti-amphiphysin autoantibody eluates (specAmph) as previously described (Sommer *et al.*, 2005; Geis *et al.*, 2010). Expression and purification of human recombinant glutathione S-transferase (GST)-amphiphysin and of GST-SH3 domain fusion protein by using the gene encoding for amphiphysin and the construct containing its wild-type SH3 domain was performed as described (Grabs *et al.*, 1997). The IgG fractions were then dialyzed separately against distilled water, freeze dried, and stored at -20°C . Lyophilized IgG was dissolved in normal saline just before use and checked by western blotting. Affinity purification resulted in an IgG fraction with anti-amphiphysin specificity

of $>99\%$. To further test the binding specificity, we performed preabsorption experiments. SpecAmph autoantibodies ($0.4 \mu\text{g}/\text{ml}$) were preincubated using recombinant SH3 domain/GST fusion protein in ascending concentrations overnight at 4°C in blocking buffer. Mouse brain lysate ($100 \mu\text{g}$ total protein) was separated by gel electrophoresis and blotted. The blot was cut in 3-mm stripes and each was incubated overnight with the preabsorbed specAmph autoantibodies and GAPDH ($1:10\,000$, Cell Signaling Technology). For detection secondary HRP-conjugated antibodies ($1:2000$, Dako and Santa Cruz) were incubated for 2 h at room temperature and chemiluminescence images of stripes was captured at the same time (LAS 3000, FujiFilm). Analyses of preabsorbed specAmph autoantibodies by western blot showed complete deletion of the specific band detecting amphiphysin at 128 kDa when SH3 domain fusion protein was used in excess (Supplementary Fig. 1).

Intrathecal autoantibody delivery and tibial nerve stimulation

Female Lewis rats were obtained from Harlan-Winkelmann. All conducted experiments were approved by the respective State authorities and animal experiments were performed according to the ARRIVE guidelines (Kilkenny *et al.*, 2010). Catheters for intrathecal injection of IgG were placed as described (Geis *et al.*, 2010). Following a recovery period of 8 days, either specAmph autoantibodies or control IgG (1 mg) was injected intrathecally. Injections of $10 \mu\text{l}$ IgG solution following a flush of $10 \mu\text{l}$ saline were repeated daily for a period of 5 days, every second day for the following five injections, and every third day for the final two injections. This infusion protocol ensures fast saturation with IgG solutions and provides continuously high IgG concentration in the subarachnoid space over a longer time period as shown in previous studies (Geis *et al.*, 2010, 2012). Animals were deeply anaesthetized with Narcoren[®] (Merial) and Ia afferents of the right tibial

nerve were stimulated supramaximally (8–9 V, 10 Hz, 1 min) using a Grass S88 stimulator (Grass Technologies). Immediately at the end of stimulation, animals were perfused with 2.5% glutaraldehyde and 1% paraformaldehyde. After perfusion, lumbar spinal cord was removed post-fixed and washed with 0.1 M PBS.

Tissue processing for electron microscopy

Chemicals were obtained from Sigma Aldrich if not stated otherwise. The spinal cord was cut in hemi-segments using a razorblade. At the level L4-L5 from each hemi-segment 45- μ m sections were cut with a vibratome (Leica VT1000S) in 0.1 M PBS. Sections were further processed according to a published protocol with minor modifications (Weinberg and van Eyck, 1991). After fixation in 1% osmium tetroxide, sections were rinsed in maleate buffer (0.05 M; pH = 6.0) and stained *en bloc* with uranyl acetate (1% in 0.05 M maleate buffer). Dehydration included a rising ethanol concentration series with a final rinse in 100% propyleneoxide. Sections were flat embedded in epoxy resin on aclar foil (Serva). Ultrathin sections (70 nm; Ultracut E, Leica) were mounted on formvar-coated nickel grids (Plano).

Post-embedding immunolabelling for electron microscopy

GABA post-embedding immunolabelling procedures were adapted from established protocols (Watson and Bazzaz, 2001; Ranson *et al.*, 2006) using an affinity purified rabbit polyclonal autoantibody to GABA (1:1500, Sigma) detected with silver-enhanced subnanometer (Ultra Small) gold-conjugated secondary antibody (1:80, Aurion). Briefly, ultrathin sections were subjected to etching in periodic acid and sodium-metaperiodate (Watson and Bazzaz, 2001; Ranson *et al.*, 2006) for 30 s each. Rinsing in sterile PBS was followed by blocking of unspecific binding, primary antibody incubation (overnight at 4°C), secondary antibody incubation (2 h at room temperature), post-fixation in 2% glutaraldehyde and silver enhancement with R-Gent-SE-EM according to the manufacturer's recommendations (Aurion). In preparatory experiments, a silver enhancement time of 45 min was found to yield recognizable individual silver-gold particles while preventing particle fusion. After enhancement, sections were contrasted with uranyl acetate (2% in 70% ethanol) and Reynolds' lead citrate (Reynolds, 1963). Each GABA-immunostaining procedure included a negative control omitting the primary antibody.

Electron microscopy imaging

Electron micrographs were captured on a LEO 912 AB electron microscope or on a Leo 906 E electron microscope (Zeiss) with a ProScan Slow Scan CCD (ProScan) by a blinded investigator. Image acquisition and storage was performed with corresponding software iTEM (Olympus Soft Imaging Solutions).

For quantitative analyses, multiple square grids of 100 μ m² were randomly placed on a photograph taken next to a ventral horn motor neuron at the spinal cord L5 level.

These squares were screened for presynaptic boutons identified by the presence of presynaptic vesicles of 40–50 nm size and/or pre- and postsynaptic membrane specializations of the boutons and adjacent postsynaptic profiles. Silver-gold particles and presynaptic structures were counted by an experimenter blinded to the experimental conditions with MacBiophotonics ImageJ (Wayne Rasband, www.macbiophotonics.ca). Densities of silver-gold particles (representing GABA-immunolabelling intensity) and of vesicular structures were determined by dividing the respective counts by the area of the bouton (minus the area of mitochondria). For each GABA-immunolabelled section, bouton particle density was corrected for minor background labelling determined over non-synaptic areas (perikarya of motor neurons) of the same section. For analysis, particle density was related to quantitative GABA immunoreactivity. In addition, boutons were ranked according to particle density and the resulting histograms were divided into thirds. The upper third (threshold \geq rank 165) characterized 'GABA+' boutons with high density of GABA-immunogold labelling and the lower third (threshold \leq rank 82) 'GABA-' boutons with low immunolabelling intensity.

Primary neuronal cell culture

Reagents were obtained from Life Technologies if not stated otherwise. Cells were prepared from hippocampi of embryonic Day 18 embryos of pregnant C57Bl/6 mice (Harlan-Winkelmann). Hippocampi were dissected and separated from meninges and surrounding tissue before enzymatic digestion with 0.25% w/v trypsin EDTA for 5 min at 37°C. Following enzymatic treatment, trypsin was inactivated by two generous flushes of Hank's Balanced Salt Solution (HBSS) supplemented with penicillin/streptomycin and 10 mM HEPES. Hippocampi were subsequently triturated in Neurobasal[®] medium supplemented with glutamine (1%), B27[®] (2%) and penicillin/streptomycin (1%) with a narrowed glass pipette for further mechanical separation. Cells were counted with a haemocytometer (Hartenstein) and plated at a density of 50 000 cells on 18-mm diameter coverslips (Langenbrinck). Primary neurons were used for the experiments at *in vitro* Day 14.

In a separate set of experiments we tested specificity of specAmph autoantibody-induced pathomechanisms in amphiphysin-deficient neurons from knockout mice. Amphiphysin knockout mice were bred and genotyped as described (Geis *et al.*, 2010). Hippocampal cell cultures were prepared from embryonic Day 18 embryos of heterozygous breeding pairs. Genotyping was performed for each embryo and amphiphysin protein deficiency was confirmed in neuronal cultures at *in vitro* Day 14 using immunohistochemistry with a commercial antibody to amphiphysin (Acris, 13379-1-AP) and revealed complete loss of immunoreactivity in knockout cultures. All experiments were performed in triplicates.

Autoantibody treatment and stimulation of primary neurons

Primary hippocampal neurons were incubated with affinity purified specific patient autoantibodies targeting the SH3 domain of amphiphysin (specAmph) and control IgG for 6 h at 37°C (100 μ g/ml). The experimenter was blinded as to

treatment conditions (IgG application and stimulation protocols). Stimulation of cells was performed with a customized stimulation chamber RC-49FS (Warner Instruments). Platinum electrodes with a spacing of ~10 mm delivered electric fields of ~10 V/cm at a frequency of 10 Hz for 90 s (pulse duration = 1 ms). A Grass stimulator S88 (Grass Technologies) was used to deliver voltage at the stated parameters. Cells were stimulated in artificial CSF containing 119 mM NaCl, 2.5 mM KCl, 2 mM CaCl₂, 2 mM MgCl₂, 25 mM HEPES and 30 mM glucose.

For brefeldin A, treatment cells were first incubated with 100 µg/ml of specAmp for 6 h at 37°C and then brefeldin A (Sigma Aldrich, B5936-200UL) was added for the last 2 h of incubation time at a concentration of 10 µg/ml as described previously (Shetty *et al.*, 2013). The same volume of the solvent dimethyl sulphoxide (DMSO) served as control. After total incubation time of 6 h cells were processed for stimulation, immunostaining and imaging as described. All experiments were performed in triplicate.

Immunocytochemistry

Immediately after stimulation neurons were fixed with ice-cold 4% paraformaldehyde (PFA) for 20 min and permeabilized with 0.1% Triton™ X-100 for 30 min at room temperature. Primary antibodies were incubated for 1 h at room temperature in PBS containing 10% normal bovine and 10% normal goat serum (blocking solution), coverslips were washed six times for 10 min and subsequently incubated with secondary antibodies in blocking solution overnight at 4°C. Incubation was followed by washing steps as described above. Samples were kept in PBS until imaging in 100 mM mercaptoethylamine (MEA; pH 7.9) buffer.

Primary antibodies against synaptobrevin 2 (1:2000, #104211), synaptobrevin 7 (1:2000, #232011), endophilin (1:1000; #159002), synaptojanin (1:500, #145003), and vgat (1:1000, #131004) were obtained from Synaptic Systems. Secondary antibodies were from Life Technologies (Alexa Fluor® 647, goat anti-mouse, 1:500, A21237; Alexa Fluor® 647, goat anti-rabbit, 1:500, A21246) and Dianova (Cy3, goat anti-guinea pig, 1:500, #106-165-003).

dSTORM

Coverslips of immunostained neurons were mounted tightly on a custom built imaging chamber and placed on a customized Olympus IX71 inverted microscope. Samples were imaged in phosphate buffer containing 100 mM MEA adjusted to pH 7.9. Fluorophores were excited with an Ibeam Smart 640 s Laser (Toptica Photonics) at 640 nm and a Nano laser (Quioptiq photonics) at 532 nm while keeping laser powers [75 mW (640 nm) and 1 mW (532 nm)] constant during the experiment. Photons were collected using two EMCCD (Andor Ixon Ultra, BFI Optilas) cameras keeping detector gain and frame rate constant throughout the experiment. Resulting images were processed in rapidSTORM software (Wolter *et al.*, 2012) and saved as density matrices with z-dimensions representing localization counts. Matrices were rearranged by a custom written Python script kindly provided by Thorge Holm and fed into ImageJ as text image (Wayne Rasband, www.macbiophotonics.ca) for further analysis. For signal quantity calculations a region of interest was created in

ImageJ by applying a constant threshold of 45 bits (of maximum 256 bits on the colour scale) on the epifluorescent signal of GABAergic vesicular transporter (vgat). It has been shown previously that vgat serves as a reliable normalization factor without relevant fluctuations (Werner *et al.*, 2015). Variations of vgat thresholds were tested in subsets of presynaptic boutons resulting in confined region of interest leading to inaccuracy and missing signals in dSTORM localization count quantification (Supplementary Fig. 2). A binary mask was created and converted to regions of interest for quantification of integrated density in ImageJ. The reliability of density analysis in ImageJ was additionally checked by a parallel computation of raw values in Microsoft Excel. Localization count analysis (represented as signal quantity) is regarded as a direct measure of immunofluorescent molecules located in a distinct pre-defined area. It is not intended for counting molecules but serves as a proportional quantification of signals arising from fluorescent molecules.

Cluster analyses were performed by calculating the distances between each maximum residing in every singular vgat region of interest. Distances were calculated by a custom written script in Sigmaplot (Systat). Thus, shorter distances represent enhanced clustering and longer distances dispersed signal. Maxima were defined by ImageJ (FIJI distribution package) embedded 'find maxima' operation using a noise tolerance level of 2. Density of maxima within a presynaptic bouton, and density of the endophilin signal within a maximum were calculated by ImageJ using constant parameters for detection. Maxima within a presynaptic bouton are regarded as spots of several endophilin proteins and are used to evaluate distribution (signal distance) and the amount (maxima quantity) of these spots within a presynaptic compartment. Signal composition of endophilin within a single maximum is measured by localization counts and is regarded as a proportional measure of endophilin proteins located in this specific spot. Localization counts residing in endophilin maxima were calculated using the area from detected maxima defined as region of interest and applying the 'analyze particles' function in ImageJ.

Statistical analysis

For electron microscopy data, calculations were performed in Excel, dSTORM data were processed as described above. Statistical analysis was done in Sigmaplot 12. The non-parametric Mann-Whitney U-test was applied for comparing individual groups and one-way ANOVA with Tukey's *post hoc* test was used for statistical comparison of multiple groups.

Results

Sustained stimulation increases synaptic vesicle pool size in GABAergic spinal cord interneurons *in vivo*

First we examined the consequences of long-term high-frequency unilateral stimulation (10 Hz for 60 s) of sciatic nerve Ia afferents on the presynaptic vesicle pool of naïve spinal cord interneurons. Besides monosynaptic excitation

of motor neurons, this stimulation paradigm leads to a heterosynaptic activation of local GABAergic interneurons mediating presynaptic inhibition [Fig. 2A(i)]. We analysed structural changes in the presynaptic vesicle pool of boutons in the neuropil surrounding ventral horn motor neurons at the lumbar spinal cord (L4–5 level) by electron microscopy. Spinal cord presynaptic nerve endings are not restricted to a single type of neurotransmitter and may therefore contain both excitatory and inhibitory neurotransmitters (Somogyi, 2002). Boutons were identified as primarily GABAergic if they exceeded a preset upper threshold of GABA immunoreactivity as measured by post-embedding immunogold staining, whereas low GABA containing synapses had GABA immunoreactivity below a predefined lower threshold [Fig. 2A(ii) and ‘Materials and methods’ section]. These subgroups of boutons were compared in addition to analyses showing the dependence of vesicular structures on a continuous scale of GABA immunoreaction intensity in the respective boutons (Supplementary Fig. 3). Further, we quantified all boutons regardless of transmitter specificity. All investigated boutons were located in the vicinity of ventral horn motor neurons. Vesicle pool size, appearance of clathrin-coated vesicles and endosome-like structures, endocytic intermediates as recognized from studies on ultrafast endocytosis (Kittelmann *et al.*, 2013; Watanabe *et al.*, 2013) were then compared in presynaptic boutons in the two respective spinal cord hemi-segments at lumbar levels (L4–5; stimulated versus unstimulated). In control animals receiving non-reactive control patient IgG intrathecally, sustained stimulation profoundly increased the size of presynaptic vesicle pools (Fig. 2B). This effect was mediated primarily by GABAergic synapses whereas vesicle density was unchanged in synapses with low GABA content (Fig. 2B and Supplementary Fig. 3A). At resting conditions, only few endocytic intermediates (clathrin-coated vesicles and endosome-like structures) were observed. After prolonged stimulation, we found an increase of these intermediates in all boutons without preference for one of the subclasses analysed (Figs 2C, 4A and Supplementary Fig. 3B). Collectively, the findings yield ultrastructural evidence that spinal cord presynapses keep up with long-duration high-frequency stimulation by activity-induced formation of a large bulk of presynaptic vesicles including endocytic intermediates.

Pathogenic anti-amphiphysin autoantibodies induce activity-dependent presynaptic vesicle depletion

In contrast to control conditions, the vesicle density in spinal presynaptic boutons was markedly reduced upon sustained stimulation in rats that had been chronically injected intrathecally with specific affinity-purified pathogenic human autoantibodies to amphiphysin (specAmph)

and that showed characteristic disease signs of stiff-person syndrome (Geis *et al.*, 2010) (Fig. 3A). This reduction at stimulated synapses was seen in primarily GABAergic and non-GABAergic boutons. We found a higher incidence of presynaptic boutons with larger vesicle content in unstimulated compared to stimulated synapses (Fig. 3A). We then analysed vesicle density dependent on GABA immunolabelling intensity in these presynaptic boutons and found a reduction of vesicle density in boutons with low and high GABA density. However, in presynapses containing highest GABA density, vesicles were almost completely depleted (Supplementary Fig. 3A). Notably, the reduction of endocytic intermediates after stimulation was even more pronounced. Here, frequency distribution showed an almost complete depletion of clathrin-coated vesicles in boutons of stimulated synapses (Fig. 3B) and a reduction of endosome-like structures (Fig. 4B). Similar to the reduction of presynaptic vesicles, clathrin-coated vesicle depletion was apparent in boutons with low and high GABA density. Again, presynapses with the highest GABA density showed no remaining clathrin-coated vesicles after stimulation and preincubation with specAmph autoantibodies (Supplementary Fig. 3B). Thus, sustained high-frequency stimulation had an opposite effect on vesicle pool size and on endocytic intermediates in spinal boutons after application of pathogenic specAmph autoantibodies. Moreover, at resting conditions with only basal synaptic activity, presynaptic boutons of rats showed an increased density of vesicles ($54.0 \pm 3.8 \mu\text{m}^{-2}$) and clathrin-coated vesicles ($6.1 \pm 0.9 \mu\text{m}^{-2}$) after intrathecal application of specAmph autoantibodies as compared to control conditions ($32.5 \pm 3.6 \mu\text{m}^{-2}$; $P < 0.01$ and $3.2 \pm 0.6 \mu\text{m}^{-2}$; $P < 0.05$, respectively). Increased vesicle density may reflect compensatory vesicle recruitment including endocytic intermediates at basal activity levels, which is then nearly completely decompensated during sustained stimulation.

Altered v-SNARE composition of GABAergic vesicle pools induced by human anti-amphiphysin autoantibodies

Clathrin-mediated endocytosis depends on adaptor protein complex AP-2 (encoded by AP2A1 to AP2M1) (Kim and Ryan, 2009) and blockade of this endocytosis pathway involving the membrane interaction function of amphiphysin may lead to activation of compensatory pathways, e.g. clathrin-independent vesicle formation via AP-3 (encoded by AP3B1 to AP3S2), favouring production of different vesicle identities (Hua *et al.*, 2011; Shetty *et al.*, 2013). The endocytosis defect characterized by our electron microscopy findings led to the hypothesis that following exposure to anti-amphiphysin autoantibodies, presynaptic vesicle pools may consist of vesicle subtypes differing in

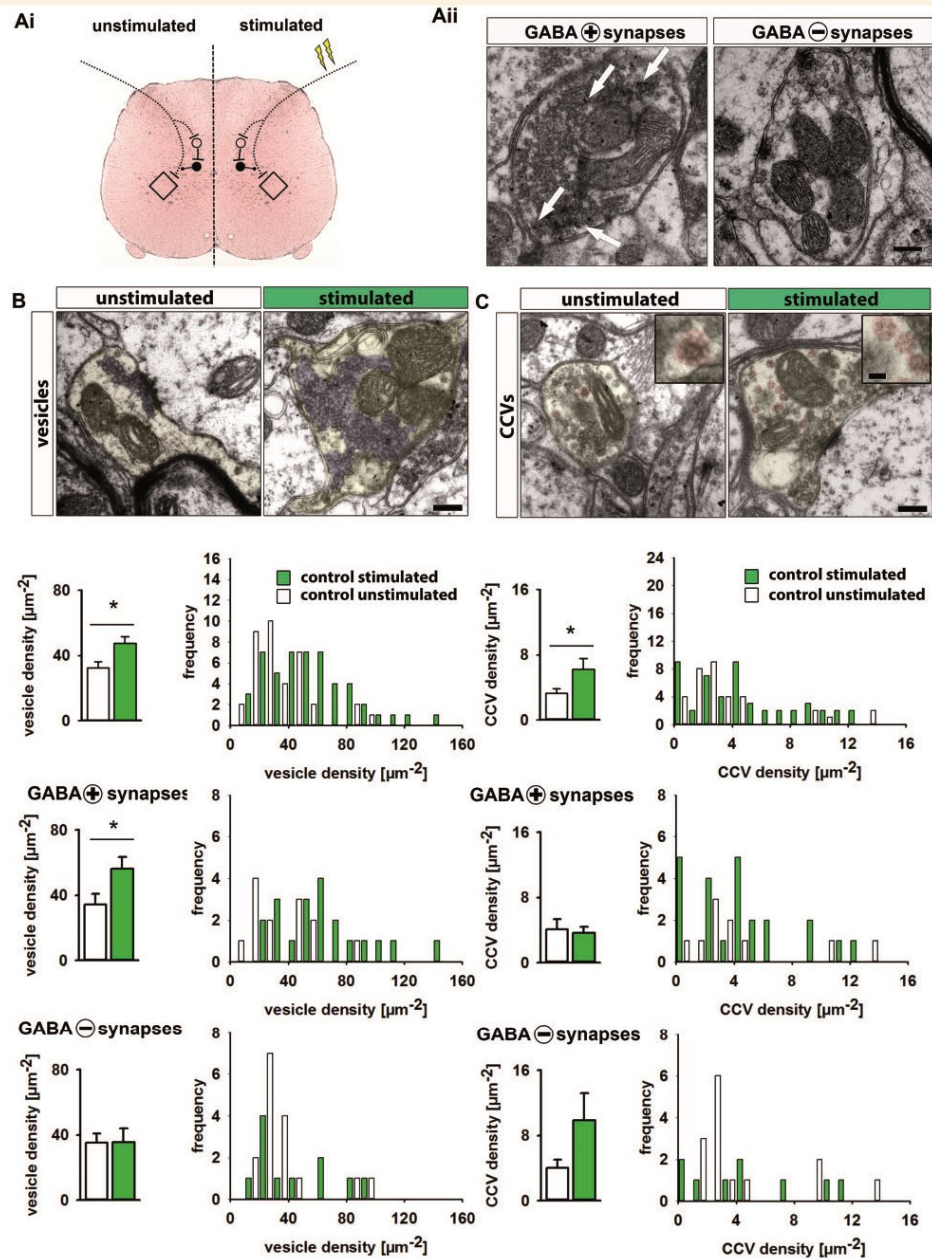


Figure 2 Sustained stimulation increases synaptic vesicle pool size and number of clathrin-coated intermediates in spinal control boutons. **[A(i)]** Scheme of experimental set-up depicting unilateral stimulation of Ia afferents in the peripheral sciatic nerve targeting ventral horn motor neurons. Stimulation leads to concurrent activation of local interneurons with last inhibitory interneuron projecting on terminal Ia afferent axons mediating presynaptic inhibition (rhombus = motor neuron; white circle = excitatory neuron; black circle = local (continued)

their composition of v-SNAREs from those under physiological conditions.

To test this hypothesis we used *d*STORM in primary neuronal cell cultures since this approach offers low complexity in synaptic connections and low background for quantifying fluorescent signals. Neurons were preincubated with purified IgG fractions and field stimulation paradigms were adapted to *in vivo* experiments. To determine vesicle identity and to quantify the size of the respective vesicle pools, we analysed the quantity of v-SNAREs syb2 and syb7 signals that are known to be directed to readily releasable and to resting pool vesicles, respectively (Hua *et al.*, 2011). We aimed at maximizing the accuracy of quantification by recording syb2 and syb7 signals as the sum of localization counts using a defined and constant amount of primary and secondary antibodies (for details see ‘Materials and methods’ section). To focus the analyses on GABAergic terminals, we defined the area of GABAergic presynaptic boutons by a fixed threshold on fluorescence signal of the presynaptic vesicular GABA transporter (vgat). This was tested for accuracy and then applied for all analysed boutons (Fig. 5A and Supplementary Fig. 2). Under control conditions, quantification of syb2 signal revealed nearly identical levels in GABAergic presynapses at high stimulation paradigms and basal activity (Fig. 5B). In contrast, sustained stimulation of GABAergic synapses pretreated with pathogenic specAmph autoantibodies led to an increase of syb2 quantity per unit of vgat positive area (Fig. 5B). This increase of quantitative syb2 signals was also significantly different from stimulated control presynapses by group comparisons. Moreover, this enhanced syb2 signal mainly arose from the border areas of presynaptic boutons located near the plasma membrane, since analysis of the central area of presynaptic boutons revealed lower signals of syb2 that were similar to control groups and to unstimulated conditions (Supplementary Fig. 2).

Next, we tested whether syb7, a v-SNARE protein typically present in vesicles of the presynaptic reserve pool, is deregulated by defective endocytosis. Analysis showed low overall syb7 signal densities, which is in line with reports of lower amounts of syb7 copies on synaptic vesicles in comparison to the syb2 isoform (Takamori *et al.*, 2006).

Quantitative analysis revealed that sustained stimulation does not significantly change syb7 signals in GABAergic presynapses under control conditions. However, after pretreatment with specAmph autoantibodies, syb7 quantity was markedly reduced upon sustained stimulation (Fig. 5C).

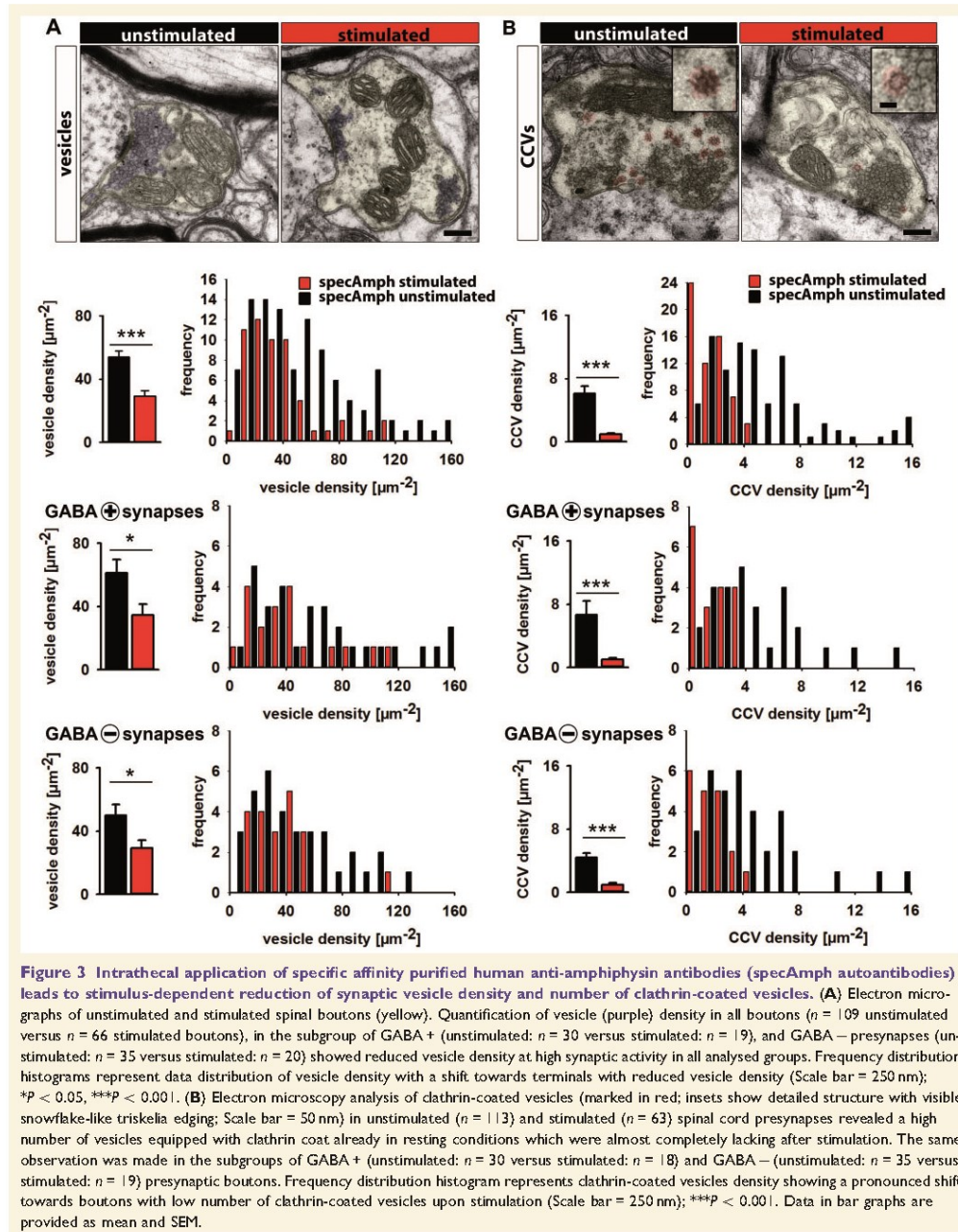
Specificity of autoantibody-induced changes in syb2 and syb7 synaptic regulation was tested with neurons deficient for amphiphysin. In amphiphysin knockout neurons preincubated with control IgG we found a slight but not significant upregulation of syb2 after sustained stimulation and no change of syb7 quantity (Supplementary Fig. 4). This change after stimulation was similar to that seen in wild-type neurons after incubation with specAmph (Fig. 5B and C), thus indicating analogous pathophysiological processes in the amphiphysin knockout situation *per se* and in wild-type neurons after acute specAmph autoantibody incubation. Importantly, in amphiphysin knockout neurons preincubation with specAmph autoantibodies did not further increase syb2 and has no impact on syb7 quantity as compared to control IgG preincubation (Supplementary Fig. 4), thus confirming that autoantibody-induced dysregulation in wild-type neurons is indeed mediated by autoantibodies to amphiphysin.

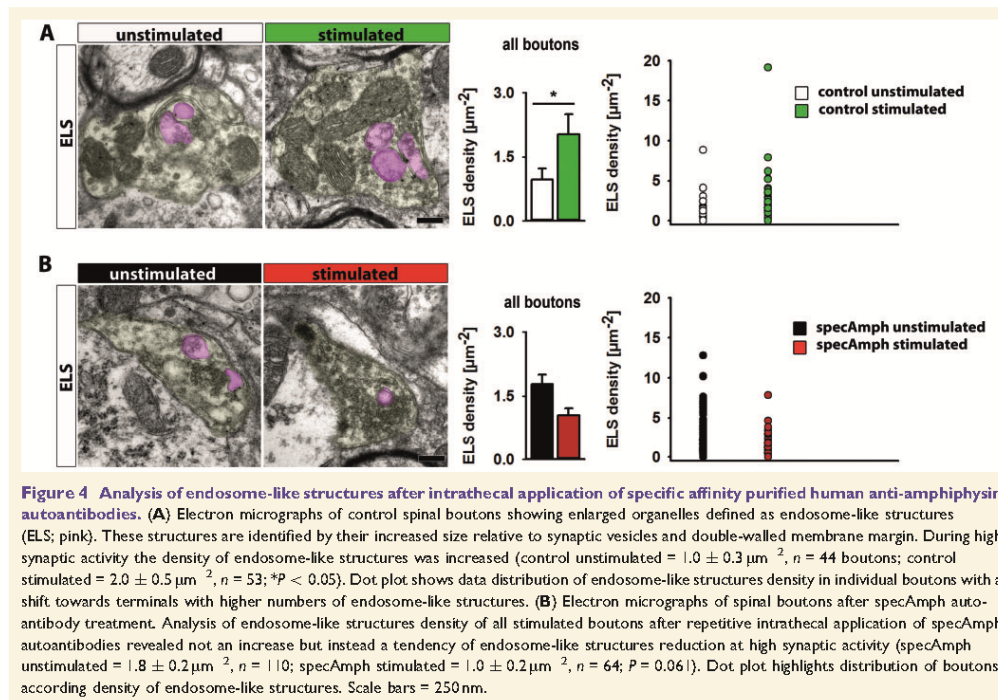
To further test the hypothesis of an autoantibody-induced switch to an AP-3 dependent pathway, we used brefeldin A, a fungal metabolite and inhibitor of protein transport from the endoplasmic reticulum that is known to block the AP-3 dependent pathway (Faundez *et al.*, 1998; Voglmaier *et al.*, 2006). Conversely to neurons only preincubated with specAmph autoantibodies, additional pretreatment with brefeldin A not only reversed the stimulation-induced effect of syb2 increase but also induced even reduced amounts of syb2 signal (Fig. 6A). Concordantly, the syb7 signal was increased in GABAergic boutons upon brefeldin A pretreatment in addition to specAmph incubation (Fig. 6B), indicating that the switch to the AP-3 dependent pathway may be blocked and AP-2 mediated vesicle formation increasingly reactivated.

Hence, endocytic dysfunction induced by anti-amphiphysin autoantibodies may influence synaptic vesicle pool dynamics and v-SNARE composition of GABAergic vesicle pools. The altered vesicle pool properties may underlie

Figure 2 Continued

GABAergic inhibitory neuron; flashes represent stimulation of peripheral Ia afferent. [A(ii)] Example micrographs of spinal boutons with high GABA immunoreactivity (arrows, GABA + synapses as defined by level of GABA immunoreactivity in the upper third spectrum of all synapses) or low reactivity (GABA – synapses with GABA immunoreactivity in the lower third spectrum). (B) Increased synaptic vesicle density in stimulated spinal boutons (control condition). Electron micrographs show unstimulated and stimulated spinal boutons (marked with light yellow). Quantification of vesicle (purple) density of all boutons ($n = 52$ stimulated versus 51 unstimulated boutons) and in the subgroup of primarily GABAergic presynapses ($n = 13$ versus 20) revealed larger synaptic vesicle pool size in stimulated conditions compared to basal neuronal activity. Frequency distribution histograms show a shift towards a higher number of boutons with high vesicle density. Vesicle density was unchanged in the subgroup of GABA – presynapses ($n = 16$ versus 11) following stimulation ($*P < 0.05$). (C) Increased clathrin-coated vesicles (CCVs) during high synaptic activity (control condition). Electron micrographs show increased numbers of CCVs (in red) during high-frequency stimulation ($n = 52$) compared to only few in unstimulated presynapses ($n = 40$). Insets present a detailed structure of clathrin coated vesicles with clearly visible triskelion surrounding the vesicle core structure. Low GABA containing synapses showed a similar trend but no significant changes in clathrin coated vesicles density ($n = 15$ versus 13), synapses predominantly using GABA as neurotransmitter were unchanged ($n = 11$ versus 23). Frequency distribution histogram represents data distribution of clathrin-coated vesicles density analysis ($P < 0.05$). Scale bars = 250 nm, insets = 50 nm. Data in bar graphs are provided as mean and SEM.





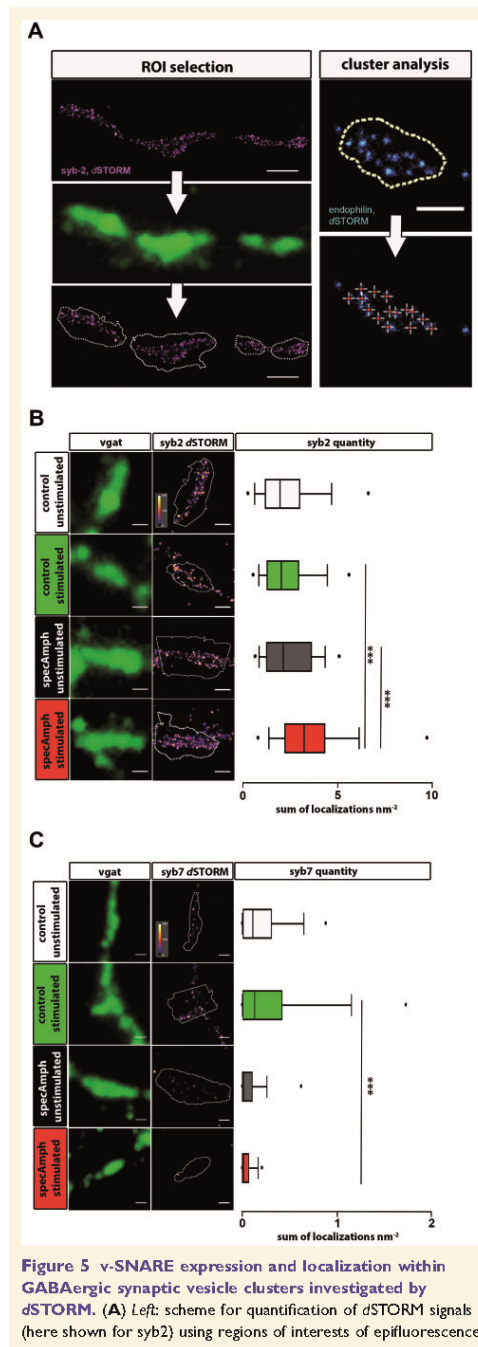
the high-frequency, stimulus-dependent defect of GABAergic transmission in the animal model of stiff-person syndrome reported previously (Geis *et al.*, 2010) and in characteristic clinical findings with motor hyperexcitability in patients with stiff-person syndrome (Meinck *et al.*, 2001; Dalakas, 2009).

Human autoantibodies to amphiphysin alter endophilin density and clustering in GABAergic presynaptic vesicle pools

Repetitive intrathecal application of specAmph autoantibodies in the animal model led to enhanced density of clathrin-coated vesicles at basal synaptic activity. This finding led us to investigate the direct amphiphysin interaction partners endophilin and synaptotagmin. Unlike dynamin, these proteins are not directly involved in membrane fission and the respective knockout mice show similar synaptic pathology as observed here in our passive-transfer model (Geis *et al.*, 2010; Milosevic *et al.*, 2011).

We first quantified endophilin signals over GABAergic vesicle pools in primary neurons. Under control conditions, sustained stimulation led to a decrease of total endophilin signal in individual GABAergic presynaptic boutons as revealed by

quantification of the localization counts (Fig. 7A). In addition to alterations of the amount of endophilin protein, changes in its localization may lead to disturbed endocytic function or may account for compensatory mechanisms. Endophilin signal distance of single maxima within an individual presynaptic bouton and localization counts within these signal maxima were unchanged under control conditions at both activity stages (Fig. 7B and D). However, sustained stimulation led to a significant reduction of individual maxima in single GABAergic presynaptic boutons (Fig. 7C), consistent to the reduction of total endophilin signal as revealed by quantification of localization counts (Fig. 7A). In neurons pretreated *ex vivo* with specAmph autoantibodies, the overall quantity of endophilin signal was not reduced throughout the individual GABAergic boutons upon stimulation (Fig. 7A). However, a significant reduction of endophilin localization count was evident in single maxima within these boutons (Fig. 7D). Accordingly, in comparison to stimulated synapses under control conditions, the dispersion of endophilin signal was increased upon pretreatment with specAmph autoantibodies (Fig. 7B). Individual endophilin clusters were reduced in unstimulated synapses after pretreatment with specAmph autoantibodies to a level similar to that of stimulated control synapses (Fig. 7C). Against these findings regarding quantity and distribution of endophilin in GABAergic presynapses, analyses of the uncoating factor



synaptotagmin showed no changes in signal quantity or synaptic localization (Supplementary Fig. 5).

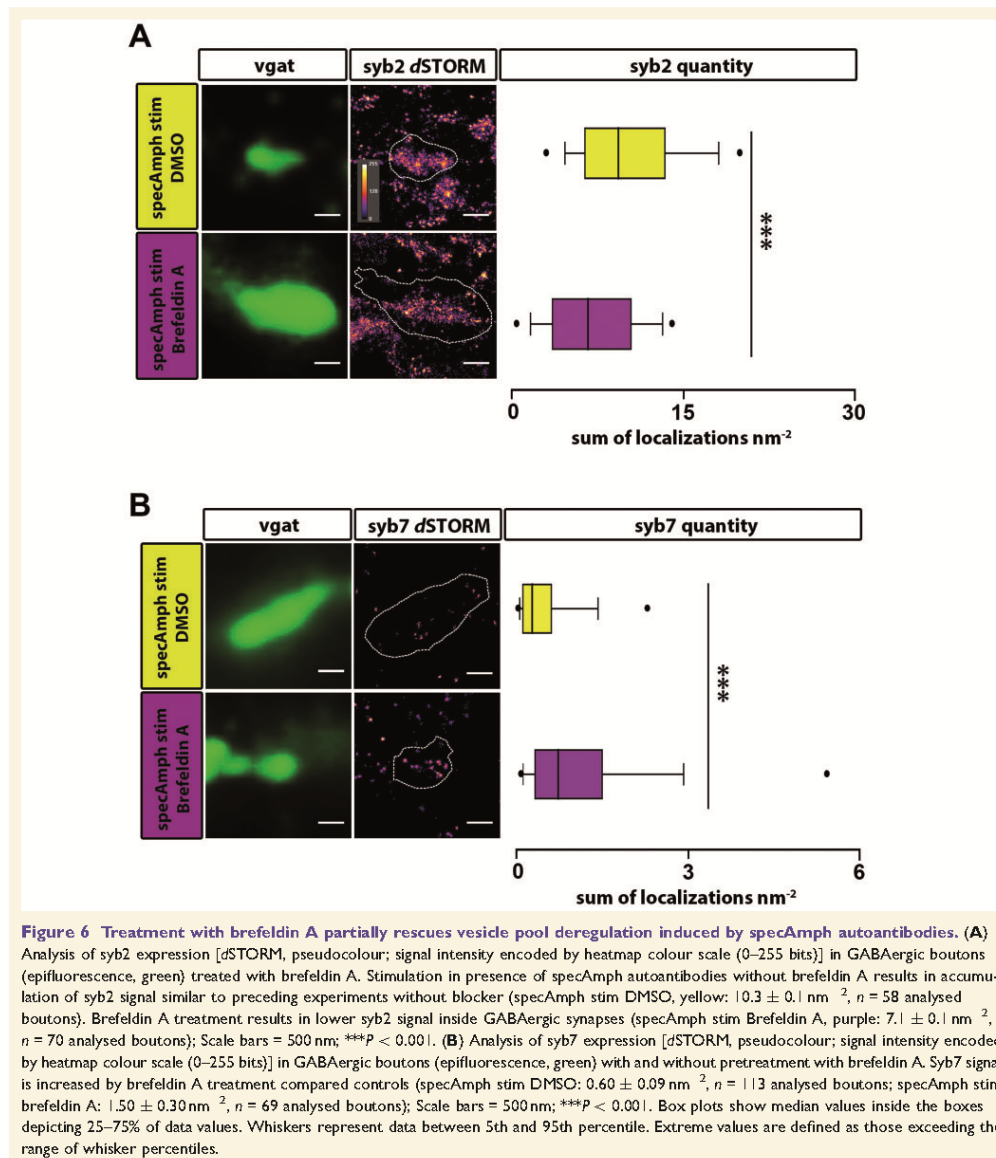
These findings indicate that endophilin localization is stimulus-dependent and more widespread with decreased clustering in GABAergic presynapses due to dysfunctional clathrin-mediated endocytosis on treatment with anti-amphiphysin autoantibodies.

Discussion

Stiff-person syndrome is an enigmatic autoimmune disease with key symptoms of motor hyperexcitability and increased anxiety. Previous experimental studies on paraneoplastic stiff-person syndrome with autoantibodies to amphiphysin have provided functional evidence for reduced GABAergic transmission (Sommer *et al.*, 2005; Geis *et al.*, 2010, 2012). Synaptic neurotransmission depends on reliable replacement of synaptic vesicles by clathrin-mediated endocytosis or budding of new vesicles from bulk endosomes. This is very important in GABAergic inhibitory

Figure 5 Continued

vgat signal (green). Dashed lines highlight calculated region of interest according to defined and constant signal properties. Right: scheme of dSTORM signals cluster analysis. Crosshairs depict signal maxima automatically detected by predefined parameters. Distances were measured between each maximum. Scale bars = 250 nm. (B) Human affinity purified anti-amphiphysin autoantibody-induced increase of syb2 signal within GABAergic presynapses during high synaptic activity. Images show signal of v-SNARE syb 2 [pseudocolour; dSTORM; signal intensity is encoded by heatmap colour scale (0–255 bits)] over vgat positive boutons (green, epifluorescence) of representative example boutons. Quantitative analyses of syb2 localization counts revealed similar amounts in control boutons regardless of synaptic activity (unstimulated: $2.4 \pm 0.3 \text{ nm}^{-2}$, $n = 51$ analysed boutons; stimulated: $2.3 \pm 0.1 \text{ nm}^{-2}$, $n = 100$). SpecAmph autoantibodies pretreated boutons showed an increased quantity of syb2 signal upon sustained stimulation compared to unstimulated specAmph autoantibodies pretreated terminals (unstimulated: $2.6 \pm 0.3 \text{ nm}^{-2}$, $n = 85$; stimulated: $4.8 \pm 1.1 \text{ nm}^{-2}$, $n = 70$) or to stimulated control terminals. Scale bars = 500 nm; $***P < 0.001$. (C) SpecAmph autoantibodies mediate decrease of syb7 signal in GABAergic presynapses. Analysis of signal quantity of v-SNARE syb7 [pseudocolour; dSTORM; heatmap colour scale (0–255 bits)] using vgat signal (green) as a mask for GABAergic boutons revealed a gradual increase of syb7 localization count in controls by stimulation (unstimulated: $0.22 \pm 0.03 \text{ nm}^{-2}$, $n = 79$; stimulated: $0.38 \pm 0.07 \text{ nm}^{-2}$, $n = 72$). Against this, in specAmph autoantibodies pretreated neurons syb7 quantity was markedly decreased (unstimulated: $0.16 \pm 0.06 \text{ nm}^{-2}$, $n = 98$; stimulated: $0.05 \pm 0.01 \text{ nm}^{-2}$, $n = 78$). In comparison to stimulated control conditions, analysis revealed a highly significant reduction of syb7 signal quantity in stimulated GABAergic boutons after specAmph autoantibodies application. Scale bars = 500 nm; $***P < 0.001$. Box plots show median values inside boxes depicting 25–75% of data values. Whiskers represent data between 5th and 95th percentile. Extreme values are defined as those exceeding the range of whisker percentiles.



synapses as these often serve as tonic synapses with a high turnover rate of presynaptic vesicles and therefore need for proper endocytic machinery (Ferguson *et al.*, 2007). Studies on clathrin-mediated endocytosis have so far focused on genetic knockout of clathrin-mediated endocytosis proteins (Milosevic *et al.*, 2011; Raimondi *et al.*, 2011; Soda *et al.*, 2012), on acute interference by inhibitory peptides, or on

the effects of small molecules blocking clathrin-mediated endocytosis proteins (Shupliakov *et al.*, 1997; Macia *et al.*, 2006; von Kleist *et al.*, 2011). Here we show that depending on synaptic activity, specific human pathogenic autoantibodies to amphiphysin may have striking effects upon morphological and molecular architecture of presynaptic vesicle pools. These autoantibody-mediated effects

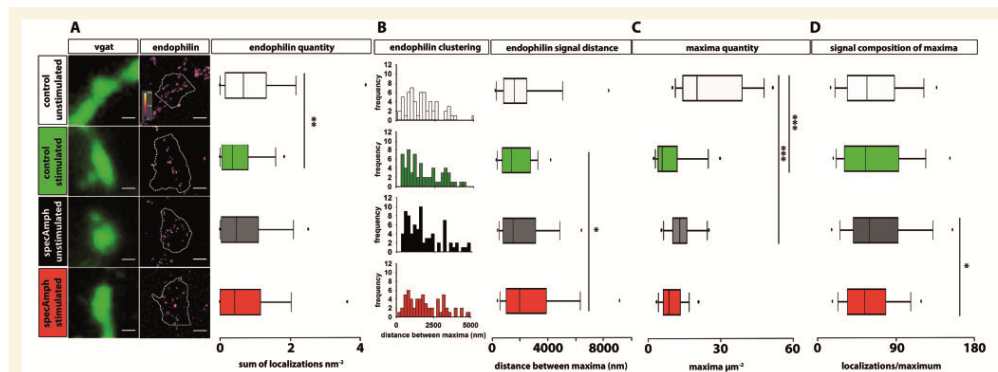


Figure 7 Disturbed expression of endophilin in GABAergic boutons induced by specific human autoantibodies to amphiphysin. (A) Analysis of endophilin expression [dSTORM, pseudocolour; signal intensity encoded by heatmap colour scale (0–255 bits)] in GABAergic boutons (epifluorescence, green). In control condition, sustained high frequency stimulation induced a reduction of total endophilin signal quantity over GABAergic vesicle pools (localization count analysis) (unstimulated: $1.0 \pm 0.1 \text{ nm}^{-2}$, $n = 107$ analysed boutons; stimulated: $0.6 \pm 0.1 \text{ nm}^{-2}$, $n = 106$). This reduction of total endophilin quantity was not present after pretreatment with specAmph autoantibodies (unstimulated: $0.8 \pm 0.1 \text{ nm}^{-2}$, $n = 154$; specAmph stimulated: $1.0 \pm 0.3 \text{ nm}^{-2}$, $n = 114$). Scale bars = 500 nm, $**P < 0.01$. (B) Stimulation-evoked dispersion of endophilin signal maxima in presence of specAmph autoantibodies as measured by clustering analysis. Sustained synaptic activity led to a significant dispersion of endophilin signal maxima in specAmph autoantibodies pretreated GABAergic boutons (maxima distance of $2962 \pm 325 \text{ nm}$, $n = 78$) compared to stimulated controls ($1770 \pm 158 \text{ nm}$, $n = 69$). Frequency distribution histograms and analysis of distance between endophilin signal maxima of unstimulated ($2386 \pm 343 \text{ nm}$, $n = 71$) versus stimulated control boutons revealed nearly equal distances. Scale bars = 500 nm, range of heatmaps: 0–255 bits; $*P < 0.05$. (C) Density of endophilin maxima was reduced in GABAergic boutons after pretreatment with specAmph autoantibodies. According to the analysis of absolute endophilin quantity as shown in (A), sustained stimulation reduced localized clustering of endophilin into single maxima in control condition. This dispersion of endophilin signal was already detected at basal activity in neurons pretreated with specAmph autoantibodies (maxima μm^{-2} : control unstimulated = 26.3 ± 4.2 , $n = 12$; control stimulated = 9.4 ± 2.1 , $n = 16$; specAmph unstimulated = 13.6 ± 1.4 , $n = 16$; specAmph stimulated = 10.2 ± 1.1 , $n = 20$, n depicts number of analysed boutons); $***P < 0.001$. (D) Endophilin maxima differ in quantity of localization counts. Endophilin signal quantity within the individual maxima was reduced in specAmph autoantibodies pretreated GABAergic boutons upon stimulation as determined by quantitative localization count analysis (localizations/maximum: control unstimulated = 65.2 ± 3.1 , $n = 168$; control stimulated = 66.4 ± 3.5 , $n = 160$; specAmph unstimulated = 71.2 ± 3.0 , $n = 218$; specAmph stimulated = 59.8 ± 2.3 , $n = 198$, n reflects number of analysed maxima); $*P < 0.05$. Box plots show median values inside boxes depicting 25–75% of data values. Whiskers represent data between 5th and 95th percentile. Extreme values are defined as those exceeding the range of whisker percentiles.

are best explained by dysfunctional clathrin-mediated endocytosis and may severely afflict the machinery for protein sorting and efficient preparation of vesicles for successive transmitter exocytosis. This consequently may impede fast replenishment of synaptic vesicles in presynaptic boutons, which is indispensable during sustained activity. We document that presynaptic vesicle pools and clathrin-coated vesicles are much reduced upon stimulation *in vivo* in spinal boutons. Together, these structural abnormalities support the proposition that application of specific human anti-amphiphysin autoantibodies *in vivo* induces slower endocytosis rates and faster synaptic exhaustion during high frequency firing of inhibitory neurons as reported previously (Geis *et al.*, 2010). Thus, these findings may represent the ultrastructural correlate of characteristic disease symptoms in patients with stiff-person syndrome consisting of reduced spinal inhibitory regulation (Sandbrink *et al.*, 2000; Wessig *et al.*, 2003).

Super-resolution dSTORM of GABAergic presynaptic vesicle pools in primary neurons revealed that specAmph

autoantibodies induced pathomechanisms include changes in the equipment of synaptic vesicles with v-SNARE isoforms as essential components of vesicle exocytosis. dSTORM offers precise antigen localization and accurate determination of signal components within small neuronal structures as shown here in presynaptic compartments. Recent reports could demonstrate that dSTORM is useful for characterizing synaptic dysfunction (Andreska *et al.*, 2014; Esbjorner *et al.*, 2014) and for investigating synaptic organization including quantification of synaptic proteins (Dani *et al.*, 2010; Ehmman *et al.*, 2014). In the present study we used the high localization precision of dSTORM to quantify protein distributions and to determine cluster properties. The protein composition of synaptic vesicles is generally believed to be different depending on which endocytic route is prevalent at a particular synapse (Voglmaier and Edwards, 2007). v-SNAREs were previously shown to characterize different vesicle pools. Syb2 is predominantly associated with the readily releasable pool whereas syb7 is mainly present on vesicles of the resting pool (Hua *et al.*,

2011). We found that *syb7* was strongly reduced in synapses upon exposure to specAmph autoantibodies during sustained stimulation. This is in line with our *ex vivo* observations of activity-dependent depletion of vesicles and clathrin-coated vesicles in spinal presynapses after specAmph autoantibody passive transfer. Besides changing location on presynaptic vesicles, v-SNAREs may also be trapped at the synaptic plasma membrane after fusion, which is caused by a slowed or inhibited endocytic machinery, as observed in a recent report investigating endocytic adaptor proteins (Shetty *et al.*, 2013). Differential distribution with preferential location at presynaptic bouton border areas and increase of *syb2* quantity may also result from its sorting by AP-180 (encoded by *SNAP91*; Koo *et al.*, 2011) for which we have previously shown a more intense clustering in the presence of specAmph autoantibodies (Geis *et al.*, 2010). Taken together, disturbed clathrin-mediated endocytosis may lead to maldistribution of essential v-SNAREs and this may challenge sustained exocytosis at high activity levels.

In this dysfunctional synaptic condition we provide evidence that the direct amphiphysin interaction partner endophilin (Micheva *et al.*, 1997) is differentially regulated within GABAergic vesicle pools and is abnormally localized. Similar to our present ultrastructural observations in spinal cord presynaptic boutons at basal activity levels after intrathecal specAmph autoantibody passive transfer, triple knockout of all endophilin isoforms was reported to lead to accumulations of clathrin-coated vesicles in resting conditions (Milosevic *et al.*, 2011). Endophilin seems especially important for high frequency neurotransmission (Llobet *et al.*, 2011). It is not yet clear if the more widespread distribution of endophilin in the presynapse during sustained stimulation and exposure to pathogenic specAmph autoantibodies as shown here is due to general reorganization of endocytic proteins or if it represents an early compensatory mechanism initiated by anti-amphiphysin autoantibody-induced clathrin-mediated endocytosis dysfunction. Similarly, the synaptic density of amphiphysin protein levels has been reported to be increased in endophilin triple knockout mice (Milosevic *et al.*, 2011).

In conclusion, our observations provide insights into molecular events of synaptic dysfunction underlying the effects of anti-amphiphysin autoantibodies in human stiff-person syndrome. This finding may serve as a proof-of-principle example for future research into the molecular pathophysiology of synaptopathies of autoimmune (Lai *et al.*, 2009; Gleichman *et al.*, 2012) and neurodegenerative aetiology (Trempe *et al.*, 2009; De Jesus-Cortes *et al.*, 2012) using electron microscopy and super-resolution microscopy in combination.

Acknowledgements

We thank B. Broll, B. Dekant, S. Hellmig, K. Reinfurt-Gehm, S. Schenk and C. Sommer (Jena) for providing

expert technical assistance in animal experiments, immunohistochemistry, IgG and electron microscopy preparations. The authors declare no competing financial interest.

Funding

This work was supported by the Deutsche Forschungsgemeinschaft (SFB 581 [TP A7], SFB/TR 166 [TP B2], GE2519_3-1), by the IZKF and CSCC Jena (E-3.3), and by intramural University Research Funds (Würzburg and Jena).

Supplementary material

Supplementary material is available at *Brain* online.

References

- Andreska T, Aufmkolk S, Sauer M, Blum R. High abundance of BDNF within glutamatergic presynapses of cultured hippocampal neurons. *Front Cell Neurosci* 2014; 8: 107.
- Arkhipov A, Yin Y, Schulten K. Membrane-bending mechanism of amphiphysin N-BAR domains. *Biophys J* 2009; 97: 2727–35.
- Boucrot E, Ferreira AP, Almeida-Souza L, Debarat S, Vallis Y, Howard G, et al. Endophilin marks and controls a clathrin-independent endocytic pathway. *Nature* 2015; 517: 460–5.
- Dalakas MC. Stiff person syndrome: advances in pathogenesis and therapeutic interventions. *Curr Treat Options Neurol* 2009; 11: 102–10.
- Dani A, Huang B, Bergan J, Dulac C, Zhuang X. Superresolution imaging of chemical synapses in the brain. *Neuron* 2010; 68: 843–56.
- David C, Solimena M, De Camilli P. Autoimmunity in stiff-Man syndrome with breast cancer is targeted to the C-terminal region of human amphiphysin, a protein similar to the yeast proteins, Rvs167 and Rvs161. *FEBS Lett* 1994; 351: 73–9.
- De Camilli P, Thomas A, Cofield R, Folli F, Lichte B, Piccolo G, et al. The synaptic vesicle-associated protein amphiphysin is the 128-kD autoantigen of Stiff-Man syndrome with breast cancer. *J Exp Med* 1993; 178: 2219–23.
- De Jesus-Cortes HJ, Noguera-Ortiz CJ, Gearing M, Arnold SE, Vega IE. Amphiphysin-1 protein level changes associated with tau-mediated neurodegeneration. *Neuroreport* 2012; 23: 942–6.
- Di Paolo G, Sankaranarayanan S, Wenk MR, Daniell L, Perucco E, Caldarone BJ, et al. Decreased synaptic vesicle recycling efficiency and cognitive deficits in amphiphysin 1 knockout. *Neuron* 2002; 33: 789–804.
- Dong Y, Gou Y, Li Y, Liu Y, Bai J. Synaptotagmin cooperates in vivo with endophilin through an unexpected mechanism. *Elife* 2015; 4.
- Ehmann N, van de Linde S, Alon A, Ljaschenko D, Keung XZ, Holm T, et al. Quantitative super-resolution imaging of Bruchpilot distinguishes active zone states. *Nat Commun* 2014; 5: 4650.
- Esbjorner EK, Chan F, Rees E, Erdelyi M, Luheshi LM, Bertoncini CW, et al. Direct observations of amyloid beta self-assembly in live cells provide insights into differences in the kinetics of Abeta(1-40) and Abeta(1-42) aggregation. *Chem Biol* 2014; 21: 732–42.
- Evergren E, Marcucci M, Tomilin N, Low P, Slepnev V, Andersson F, et al. Amphiphysin is a component of clathrin coats formed during synaptic vesicle recycling at the lamprey giant synapse. *Traffic* 2004; 5: 514–28.
- Faundez V, Horng JT, Kelly RB. A function for the AP3 coat complex in synaptic vesicle formation from endosomes. *Cell* 1998; 93: 423–32.

- Ferguson SM, Brasnjo G, Hayashi M, Wolfel M, Collesi C, Giovedi S, et al. A selective activity-dependent requirement for dynamin 1 in synaptic vesicle endocytosis. *Science* 2007; 316: 570–4.
- Geis C, Grunewald B, Weishaupt A, Wultsch T, Toyka KV, Reif A, et al. Human IgG directed against amphiphysin induces anxiety behavior in a rat model after intrathecal passive transfer. *J Neural Transm* 2012; 119: 981–5.
- Geis C, Weishaupt A, Hallermann S, Grunewald B, Wessig C, Wultsch T, et al. Stiff person syndrome-associated autoantibodies to amphiphysin mediate reduced GABAergic inhibition. *Brain* 2010; 133: 3166–80.
- Gleichman AJ, Spruce LA, Dalmau J, Seeholzer SH, Lynch DR. Anti-NMDA receptor encephalitis antibody binding is dependent on amino acid identity of a small region within the GluN1 amino terminal domain. *J Neurosci* 2012; 32: 11082–94.
- Grabs D, Slepnev VI, Songyang Z, David C, Lynch M, Cantley LC, et al. The SH3 domain of amphiphysin binds the proline-rich domain of dynamin at a single site that defines a new SH3 binding consensus sequence. *J Biol Chem* 1997; 272: 13419–25.
- Hua Z, Leal-Ortiz S, Foss SM, Waites CL, Garner CC, Voglmaier SM, et al. v-SNARE composition distinguishes synaptic vesicle pools. *Neuron* 2011; 71: 474–87.
- Irani SR, Gelfand JM, Al-Diwani A, Vincent A. Cell-surface central nervous system autoantibodies: clinical relevance and emerging paradigms. *Ann Neurol* 2014; 76: 168–84.
- Kilkenny C, Browne WJ, Cuthill IC, Emerson M, Altman DG. Improving bioscience research reporting: the ARRIVE guidelines for reporting animal research. *PLoS Biol* 2010; 8: e1000412.
- Kim SH, Ryan TA. A distributed set of interactions controls mu2 functionality in the role of AP-2 as a sorting adaptor in synaptic vesicle endocytosis. *J Biol Chem* 2009; 284: 32803–12.
- Kittelmann M, Liewald JF, Hegermann J, Schultheis C, Brauner M, Steuer Costa W, et al. *In vivo* synaptic recovery following optogenetic hyperstimulation. *Proc Natl Acad Sci USA* 2013; 110: E3007–16.
- Koo SJ, Markovic S, Puchkov D, Mahrenholz CC, Beceren-Braun F, Maritzen T, et al. SNARE motif-mediated sorting of synaptobrevin by the endocytic adaptors clathrin assembly lymphoid myeloid leukemia (CALM) and AP180 at synapses. *Proc Natl Acad Sci USA* 2011; 108: 13540–5.
- Lai M, Hughes EG, Peng X, Zhou L, Gleichman AJ, Shu H, et al. AMPA receptor antibodies in limbic encephalitis alter synaptic receptor location. *Ann Neurol* 2009; 65: 424–34.
- Leyboldt F, Armangue T, Dalmau J. Autoimmune encephalopathies. *Ann N Y Acad Sci* 2015; 1338: 94–114.
- Lichte B, Veh RW, Meyer HE, Kilimann MW. Amphiphysin, a novel protein associated with synaptic vesicles. *EMBO J* 1992; 11: 2521–30.
- Llobet A, Gallop JL, Burden JJ, Camdere G, Chandra P, Vallis Y, et al. Endophilin drives the fast mode of vesicle retrieval in a ribbon synapse. *J Neurosci* 2011; 31: 8512–9.
- Macia E, Ehrlich M, Massol R, Boucrot E, Brunner C, Kirchhausen T. Dynasore, a cell-permeable inhibitor of dynamin. *Dev Cell* 2006; 10: 839–50.
- Meinck HM, Faber L, Morgenthaler N, Seissler J, Maile S, Butler M, et al. Antibodies against glutamic acid decarboxylase: prevalence in neurological diseases. *J Neurol Neurosurg Psychiatry* 2001; 71: 100–3.
- Micheva KD, Ramjaun AR, Kay BK, McPherson PS. SH3 domain-dependent interactions of endophilin with amphiphysin. *FEBS Lett* 1997; 414: 308–12.
- Milosevic I, Giovedi S, Lou X, Raimondi A, Collesi C, Shen H, et al. Recruitment of endophilin to clathrin-coated pit necks is required for efficient vesicle uncoating after fission. *Neuron* 2011; 72: 587–601.
- Murinson BB. Stiff-person syndrome. *Neurologist* 2004; 10: 131–7.
- Raimondi A, Ferguson SM, Lou X, Armbruster M, Paradise S, Giovedi S, et al. Overlapping role of dynamin isoforms in synaptic vesicle endocytosis. *Neuron* 2011; 70: 1100–14.
- Ranson RN, Santer RM, Watson AH. The relationship between serotonin, dopamine beta hydroxylase and GABA immunoreactive inputs and spinal preganglionic neurones projecting to the major pelvic ganglion of Wistar rats. *Neuroscience* 2006; 141: 1935–49.
- Reynolds ES. The use of lead citrate at high pH as an electron-opaque stain in electron microscopy. *J Cell Biol* 1963; 17: 208–12.
- Sandbrink F, Syed NA, Fujii MD, Dalakas MC, Floeter MK. Motor cortex excitability in stiff-person syndrome. *Brain* 2000; 123 (Pt 11): 2231–9.
- Shetty A, Sytnyk V, Leshchynska I, Puchkov D, Hauke V, Schachner M. The neural cell adhesion molecule promotes maturation of the presynaptic endocytotic machinery by switching synaptic vesicle recycling from adaptor protein 3 (AP-3)- to AP-2-dependent mechanisms. *J Neurosci* 2013; 33: 16828–45.
- Shupliakov O, Low P, Grabs D, Gad H, Chen H, David C, et al. Synaptic vesicle endocytosis impaired by disruption of dynamin-SH3 domain interactions. *Science* 1997; 276: 259–63.
- Soda K, Balkin DM, Ferguson SM, Paradise S, Milosevic I, Giovedi S, et al. Role of dynamin, synaptojanin, and endophilin in podocyte foot processes. *J Clin Invest* 2012; 122: 4401–11.
- Sommer C, Weishaupt A, Brinkhoff J, Biko L, Wessig C, Gold R, et al. Paraneoplastic stiff-person syndrome: passive transfer to rats by means of IgG antibodies to amphiphysin. *Lancet* 2005; 365: 1406–11.
- Somogyi J. Differences in ratios of GABA, glycine and glutamate immunoreactivities in nerve terminals on rat hindlimb motoneurons: a possible source of post-synaptic variability. *Brain Res Bull* 2002; 59: 151–61.
- Takamori S, Holt M, Stenius K, Lemke EA, Grønborg M, Riedel D, et al. Molecular anatomy of a trafficking organelle. *Cell* 2006; 127: 831–46.
- Takei K, Mundigl O, Daniell L, De Camilli P. The synaptic vesicle cycle: a single vesicle budding step involving clathrin and dynamin. *J Cell Biol* 1996; 133: 1237–50.
- Trempe JF, Chen CX, Grenier K, Camacho EM, Kozlov G, McPherson PS, et al. SH3 domains from a subset of BAR proteins define a Ubl-binding domain and implicate parkin in synaptic ubiquitination. *Mol Cell* 2009; 36: 1034–47.
- Vasconcelos OM, Dalakas MC. Stiff-person Syndrome. *Curr Treat Options Neurol* 2003; 5: 79–90.
- Voglmaier SM, Edwards RH. Do different endocytic pathways make different synaptic vesicles? *Curr Opin Neurobiol* 2007; 17: 374–80.
- Voglmaier SM, Kam K, Yang H, Fortin DL, Hua Z, Nicoll RA, et al. Distinct endocytic pathways control the rate and extent of synaptic vesicle protein recycling. *Neuron* 2006; 51: 71–84.
- von Kleist L, Stahlschmidt W, Bulut H, Gromova K, Puchkov D, Robertson MJ, et al. Role of the clathrin terminal domain in regulating coated pit dynamics revealed by small molecule inhibition. *Cell* 2011; 146: 471–84.
- Watanabe S, Rost BR, Camacho-Perez M, Davis MW, Sohl-Kielczynski B, Rosenmund C, et al. Ultrafast endocytosis at mouse hippocampal synapses. *Nature* 2013; 504: 242–7.
- Watson AH, Bazzaz AA. GABA and glycine-like immunoreactivity at axoaxonic synapses on 1a muscle afferent terminals in the spinal cord of the rat. *J Comp Neurol* 2001; 433: 335–48.
- Weinberg RJ, van Eyck SL. A tetramethylbenzidine/tungstate reaction for horseradish peroxidase histochemistry. *J Histochem Cytochem* 1991; 39: 1143–8.
- Werner C, Haselmann H, Weishaupt A, Toyka KV, Sommer C, Geis C. Stiff person-syndrome IgG affects presynaptic GABAergic release mechanisms. *J Neural Transm* 2015; 122: 357–62.
- Wessig C, Klein R, Schneider MF, Toyka KV, Naumann M, Sommer C. Neuropathology and binding studies in anti-amphiphysin-associated stiff-person syndrome. *Neurology* 2003; 61: 195–8.
- Wolter S, Loschberger A, Holm T, Aufmkolk S, Dabauvalle MC, van de Linde S, et al. rapidSTORM: accurate, fast open-source software for localization microscopy. *Nat Methods* 2012; 9: 1040–1.

Supplementary Figure Legends

Supplementary Fig. 1: Anti-amphiphysin ABs (specAph ABs) are directed to the amphiphysin SH3 domain. Western blot demonstrating preabsorption of specAph ABs binding to brain lysate following preincubation with the recombinant SH3 domain. GAPDH serves as loading control.

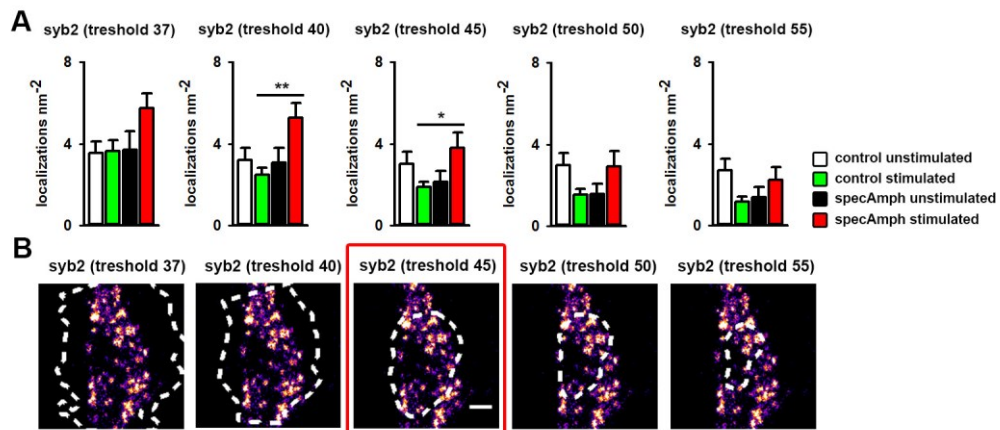
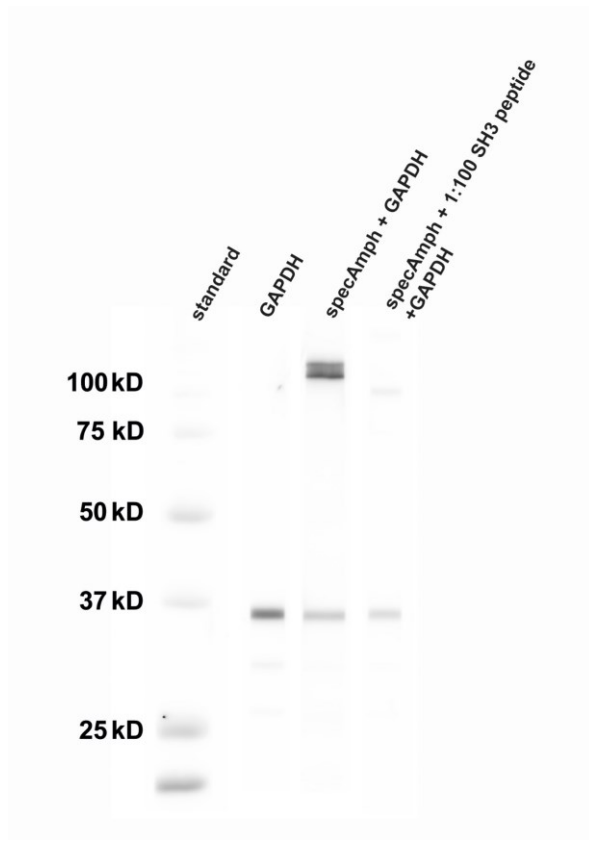
Supplementary Fig. 2: Determination of vgat signal threshold. Exemplary syb2 *d*STORM images demonstrating the impact of vgat thresholds variations on syb2 signal detection. Syb2 signal is displayed in pseudocolor, dashed lines represent ROIs, scale bar = 250 nm. (A) A group of boutons was analyzed for syb2 localization count quantification at different vgat thresholds of 37, 40, 45, 50, and 55 bits, respectively (control unstimulated: $n = 8$; control stimulated: $n = 17$; specAph unstimulated: $n = 9$; specAph stimulated: $n = 9$). vgat thresholds lower than 40 bits led to inadequate ROI selection exceeding the border areas of presynaptic boutons (shown in (B)) and absolute counts were increased in all groups. vgat signal thresholds higher than 45 bits (a threshold of 45 bits has been applied at the final experiments, for comparison see also Fig. 3) led to failure in determination of presynaptic ROI and missing values in syb2 signal quantification as exemplary shown here for quantification of syb2 localization count (B). Note the decrease of syb2 signal per nm^2 in specAph treated boutons at increasing vgat thresholds over 45 bits resulting from missing syb2 signal that is enriched at the plasma membrane areas of presynaptic boutons. $*P < 0.05$, $**P < 0.01$.

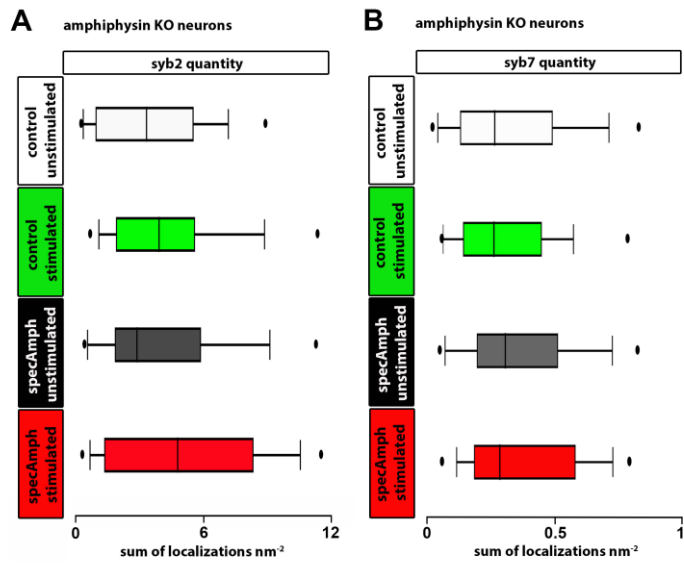
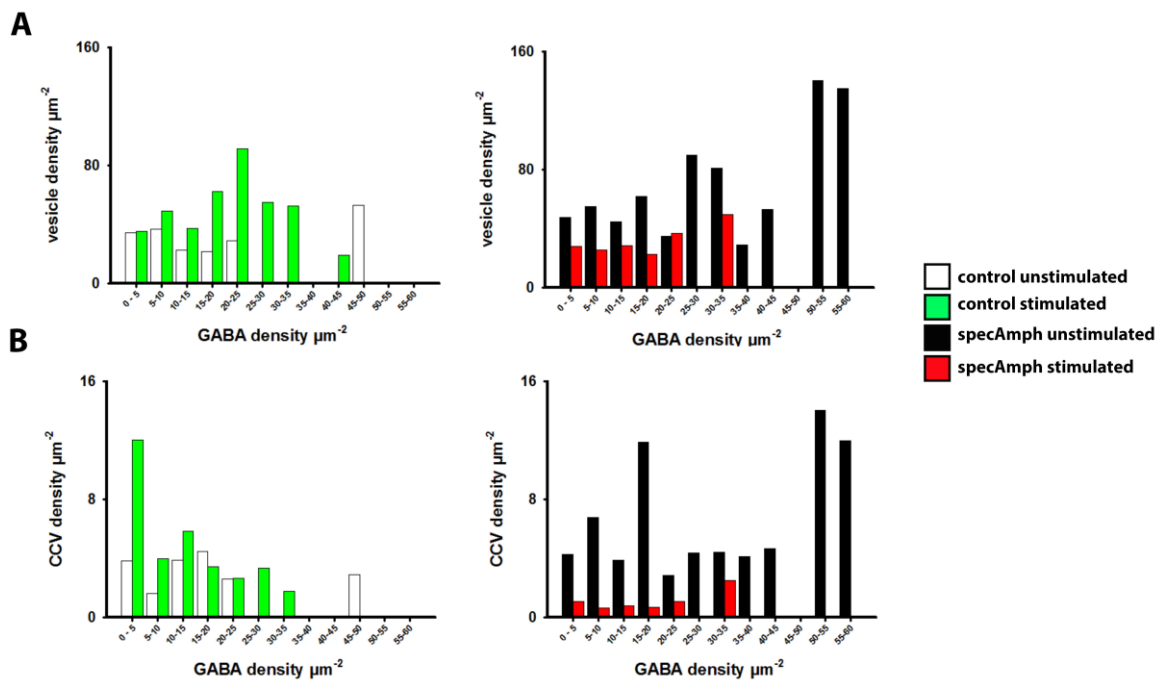
Supplementary Fig. 3: Correlation of GABA immunoreactivity with vesicle density and density of clathrin coated vesicles (CCV). (A) In animals injected with control IgG stimulation of Ia afferents led to an increase of vesicle density in presynapses of low and high

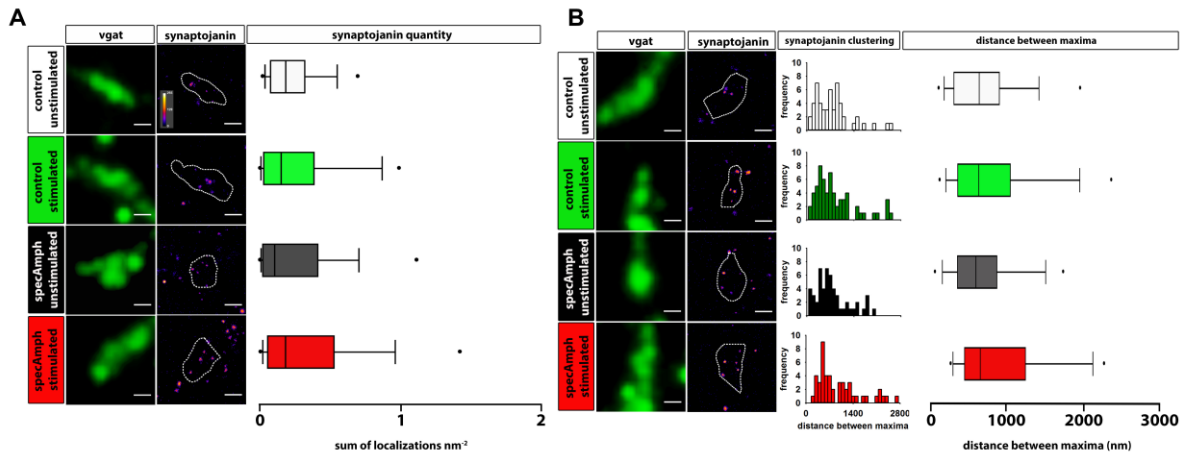
GABA density. I.th. injection of specAmph ABs induced general depletion of vesicles in synapses during sustained stimulation which is most pronounced in presynapses with high GABA density. (B) In control synapses amount of CCV was increased by sustained stimulation preliminary in synapses with low GABA content. In anti-amphiphysin AB injected animals stimulation induced massive depletion of CCV. In synapses with high GABA content CCV were completely absent.

Supplementary Fig. 4: SpecAmph ABs induce no off-target effects in amphiphysin knockout (KO) neurons. (A) Analysis of syb2 expression (*d*STORM, pseudocolor; signal intensity encoded by heatmap color scale [0 - 255 bits]) in GABAergic boutons lacking amphiphysin (epifluorescence, green). Sustained stimulation induces slight, not significant increase of syb2 expression inside GABAergic neurons in presence of both, specAmph ABs and control IgG (control unstimulated: $3.5 \pm 0.4 \text{ nm}^{-2}$, $n = 50$ analysed boutons; control stimulated: $4.4 \pm 0.4 \text{ nm}^{-2}$, $n = 56$, specAmph unstimulated: $4.1 \pm 0.5 \text{ nm}^{-2}$, $n = 50$; specAmph stimulated: $4.9 \pm 0.5 \text{ nm}^{-2}$, $n = 62$). Scale bars: 500 nm. (B) Analysis of syb7 expression (*d*STORM, pseudocolor; signal intensity encoded by heatmap color scale [0 - 255 bits]) in GABAergic boutons lacking amphiphysin (epifluorescence, green). Amphiphysin KO neurons have very low syb7 expression inside GABAergic boutons at comparable levels in all tested conditions (control unstimulated: $0.32 \pm 0.03 \text{ nm}^{-2}$, $n = 90$ analysed boutons; control stimulated: $0.31 \pm 0.03 \text{ nm}^{-2}$, $n = 60$, specAmph unstimulated: $0.36 \pm 0.04 \text{ nm}^{-2}$, $n = 45$; specAmph stimulated: $0.37 \pm 0.03 \text{ nm}^{-2}$, $n = 47$). Scale bars: 500 nm. Box plots show median values inside boxes depicting 25 - 75 % of data values. Whiskers represent data between 5th and 95th percentile. Extreme values are defined as those exceeding the range of whisker percentiles.

Supplementary Fig. 5: Expression and synaptic localization of synaptojanin is unaffected by human AB to amphiphysin. (A) Quantitative analysis of synaptojanin signal (pseudocolor, *d*STORM signal intensity encoded by heatmap color scale [0 - 255 bits]) in GABAergic synapses (green, epifluorescence) resulted in similar amount of synaptojanin signal localization count in GABAergic synapses in all experimental groups (controls unstimulated = $0.27 \pm 0.04 \text{ nm}^{-2}$, $n = 93$; controls stimulated = $0.30 \pm 0.04 \text{ nm}^{-2}$, $n = 135$, specAmph unstimulated = $0.33 \pm 0.06 \text{ nm}^{-2}$, $n = 141$; specAmph stimulated = $0.38 \pm 0.05 \text{ nm}^{-2}$, $n = 90$); (B) Clustering of synaptojanin was not affected by specAmph AB preincubation or synaptic activity (controls unstimulated = $711 \pm 74 \text{ nm}$, $n = 58$; controls stimulated = $827 \pm 85 \text{ nm}$, $n = 69$, specAmph unstimulated = $704 \pm 67 \text{ nm}$, $n = 59$; specAmph stimulated = $923 \pm 92 \text{ nm}$, $n = 54$); scale bars: 500 nm. Box plots show median values inside boxes depicting 25 - 75 % of data values. Whiskers represent data between 5th and 95th percentile. Extreme values are defined as those exceeding the range of whisker percentiles.







4.4 Manuscript IV

Ephrin-B2 Prevents N-Methyl-D-Aspartate Receptor Antibody Effects on Memory and Neuroplasticity

Planagumà J, Haselmann H, Mannara F, Petit-Pedrol M, Grünewald B, Aguilar E, Röpke L, Martín-García E, Titulaer MJ, Jercog P, Graus F, Maldonado R, Geis C, Dalmau J

RESEARCH ARTICLE

Ephrin-B2 Prevents N-Methyl-D-Aspartate Receptor Antibody Effects on Memory and Neuroplasticity

Jesús Planagumà, PhD,¹ Holger Haselmann, BS,^{2,3} Francesco Mannara, PhD,¹
 Mar Petit-Pedrol, BS,¹ Benedikt Grünewald, PhD,^{2,3} Esther Aguilar, BS,¹
 Luise Röpke, MD,² Elena Martín-García, PhD,⁴ Maarten J. Titulaer, MD, PhD,⁵
 Pablo Jercog, PhD,¹ Francesc Graus, MD, PhD,^{1,6} Rafael Maldonado, PhD,⁴
 Christian Geis, MD,^{2,3} and Josep Dalmau, MD, PhD^{1,7,8,9}

Objective: To demonstrate that ephrin-B2 (the ligand of EphB2 receptor) antagonizes the pathogenic effects of patients' N-methyl-D-aspartate receptor (NMDAR) antibodies on memory and synaptic plasticity.

Methods: One hundred twenty-two C57BL/6J mice infused with cerebrospinal fluid (CSF) from patients with anti-NMDAR encephalitis or controls, with or without ephrin-B2, were investigated. CSF was infused through ventricular catheters connected to subcutaneous osmotic pumps over 14 days. Memory, behavioral tasks, locomotor activity, presence of human antibodies specifically bound to hippocampal NMDAR, and antibody effects on the density of cell-surface and synaptic NMDAR and EphB2 were examined at different time points using reported techniques. Short- and long-term synaptic plasticity were determined in acute brain sections; the Schaffer collateral pathway was stimulated and the field excitatory postsynaptic potentials were recorded in the CA1 region of the hippocampus.

Results: Mice infused with patients' CSF, but not control CSF, developed progressive memory deficit and depressive-like behavior along with deposits of NMDAR antibodies in the hippocampus. These findings were associated with a decrease of the density of cell-surface and synaptic NMDAR and EphB2, and marked impairment of long-term synaptic plasticity without altering short-term plasticity. Administration of ephrin-B2 prevented the pathogenic effects of the antibodies in all the investigated paradigms assessing memory, depressive-like behavior, density of cell-surface and synaptic NMDAR and EphB2, and long-term synaptic plasticity.

Interpretation: Administration of ephrin-B2 prevents the pathogenic effects of anti-NMDAR encephalitis antibodies on memory and behavior, levels of cell-surface NMDAR, and synaptic plasticity. These findings reveal a strategy beyond immunotherapy to antagonize patients' antibody effects.

ANN NEUROL 2016;80:388–400

Anti-N-methyl-D-aspartate receptor (NMDAR) encephalitis is an inflammatory disorder of the brain that results in prominent neurological and psychiatric symptoms

in association with immunoglobulin G (IgG) antibodies against the GluN1 subunit of the receptor.¹ In recent years, several studies have provided evidence that the antibodies

View this article online at wileyonlinelibrary.com. DOI: 10.1002/ana.24721

Received Feb 27, 2016, and in revised form Jun 14, 2016. Accepted for publication Jun 27, 2016.

Address correspondence to Dr Josep Dalmau, IDIBAPS-Hospital Clínic, Universitat de Barcelona, Department of Neurology, c/ Villarroel 170, 08036 Barcelona, Spain. E-mail: jdalmau@clinic.ub.es

From the ¹Institut d'Investigacions Biomèdiques August Pi i Sunyer (IDIBAPS), Hospital Clínic, Universitat de Barcelona, Barcelona, Spain; ²Hans-Berger Department of Neurology, Jena University Hospital, Jena, Germany; ³Center for Sepsis Control and Care (CSCC), Jena University Hospital, Jena, Germany; ⁴Laboratori de Neurofarmacologia, Facultat de Ciències de la Salut i de la Vida, Universitat Pompeu Fabra, Barcelona, Spain; ⁵Erasmus Medical Center, Rotterdam, The Netherlands; ⁶Servei de Neurologia, Hospital Clínic, Universitat de Barcelona, Barcelona, Spain; ⁷Department of Neurology, University of Pennsylvania, Philadelphia, PA; ⁸Centro de Investigación Biomédica en Red Enfermedades Raras (CIBERER); and ⁹Institució Catalana de Recerca i Estudis Avançats (ICREA), Barcelona, Spain

Additional supporting information can be found in the online version of this article

alter synaptic function and likely result in the clinical syndrome.²⁻⁴ Approximately 80% of the patients improve with immunotherapy or sometimes spontaneously indicating that, despite the severity and protracted course of the disease, the altered NMDAR signaling is largely reversible.^{1,5-7} To date, the antibody effects have been mainly studied in cultured neurons exposed to patients' cerebrospinal fluid (CSF), demonstrating internalization of NMDAR and a decrease in their surface density and NMDAR-mediated currents.^{2,4} At the synapse, the antibodies disrupt the interaction between NMDAR and ephrin type B2 receptor (EphB2), displacing the NMDAR to extrasynaptic sites before they are internalized.³ This process of NMDAR internalization is antibody-titer dependent, reversible upon removing the antibodies, and highly specific for NMDAR, without per se affecting the density of α -amino-3-hydroxy-5-methyl-4-isoxazolepropionic acid receptor (AMPA).² Furthermore, antibody-treated neurons failed to increase the levels of AMPAR after chemical induction of long-term potentiation (LTP), suggesting that the mechanisms of plasticity were altered.³ Disruption of long-term plasticity was also suggested by a study in which the antibodies were applied for 5 minutes onto slices of normal mouse hippocampus.⁸ However, none of these studies determined whether long-term synaptic plasticity was altered in the brain of mice with symptoms related to NMDAR antibodies or whether the mechanisms of short-term plasticity were affected at the presynaptic level.

A definite link between development of memory and behavioral alterations and antibody-mediated decrease of NMDAR was recently established in a mouse model of cerebroventricular infusion of patients' CSF antibodies.⁹ The study showed a correlation between the intensity of the symptoms and the time course of antibody administration as well as between the reversibility of the symptoms and the restoration of levels of NMDAR after discontinuing the antibody infusion. In the current study, we first reproduced these findings using CSF from another group of patients and then applied the model to investigate whether the antibodies alter synaptic plasticity using electrophysiological paradigms of short- and long-term plasticity at the Schaffer collateral pathway. Additionally, given that previous work showed that ephrin-B2 antagonized the antibody-mediated changes in cell-surface dynamics of NMDAR,³ we have investigated *in vivo* whether this ligand prevents development of symptoms and antagonizes the mechanisms of disease in sets of experiments examining memory and behavioral responses, levels of cell-surface and synaptic NMDAR and EphB2, and synaptic plasticity in hippocampal networks. The results show a marked antibody-mediated impairment of the mechanisms of long-term synaptic plasticity, revealing a strategy to prevent the pathogenic effect of the antibodies that may lead to novel therapies.

Materials and Methods

Animals, Preparation of CSF, and Cerebroventricular Infusion of Antibodies

One hundred twenty-two male C57BL/6J mice (Charles River Laboratories, Wilmington, MA), 8 to 10 weeks old (25–30 g), were used for the studies. Some animals were used for more than one study (51 for memory and behavior, 60 for immunohistochemistry, and 29 for electrophysiological studies). Animal care, anesthesia, insertion of bilateral ventricular catheters (model 3280PD-2.0/SP; coordinates: 0.2mm anterior and 1.00mm lateral from bregma, depth 2.2mm; PlasticsOne Inc., Roanoke, VA), and connection of each catheter to a subcutaneous osmotic pump for continuous infusion of CSF (volume 100 μ l, flow rate 0.25 μ l/h for 14 days; Alzet, Cupertino, CA) have been reported.⁹ The CSF infused was pooled from samples of 34 patients with high-titer IgG GluN1 antibodies (all > 1:320) and 12 patients with normal pressure hydrocephalus without NMDAR antibodies (control samples). The patients used as controls had a history of rapidly progressive (median, 4 months; range, 2–9) memory deficits, cognitive decline, gait unsteadiness, or sphincter dysfunction; none of them had CSF inflammatory changes or autoantibodies.

To avoid the presence of other antibodies or small molecules that may have biological activity, patients' CSF samples were selected and prepared using the following studies: (1) confirmation that patients' CSF only had NMDAR antibodies by immunoadsorption of a representative sample of pooled CSF with HEK293 cells expressing the GluN1 subunit of the NMDARs showing abrogation of reactivity with mouse brain and NMDAR (tested in a cell-based assay [CBA]); (2) demonstration of the absence of antibodies against EphB2 receptor (confirmed by CBA, data not shown); and (3) CSF filtration (Amicon Ultracel 30K; Sigma-Aldrich, St. Louis, MO), dialysis against phosphate-buffered saline (PBS), and normalization to a physiological concentration of 2mg of IgG/dl, as reported.⁹

Four experimental groups were established: mice infused with patients' CSF without or with ephrin-B2 (50ng of ephrin-B2 added to the 100 μ l of CSF in each osmotic pump; two pumps per mouse; Sino Biological Inc, North Wales, PA), and mice infused with control CSF without or with ephrin-B2. The total dose of ephrin-B2 (100ng infused over 14 days) was based in a previous study using a single hippocampal injection (eg, 10ng/1 day).³ Animal procedures were conducted in accord with standard ethical guidelines (European Communities Directive 86/609/EU) and approved by the local ethical committees.

Cognitive Tasks and Locomotor Activity

These tasks were aimed to assess memory (novel object recognition [NOR]) discrimination index) and depressive-like behavior (tail suspension, and forced swimming tests) along with locomotor activity (local motor, horizontal and vertical activity). The selection and timing of these tasks were based on the findings of our previous study showing that patients' CSF antibodies, but not control CSF, caused memory deficits and depressive-like behaviors without

ANNALS of *Neurology*

significant change of locomotor activity.⁹ All behavioral tasks were performed by researchers blinded to experimental conditions.

Immunohistochemistry, Confocal Microscopy, and Immunoprecipitation

All techniques related to immunolabeling of live cultures of dissociated rodent hippocampal neurons,² immunoabsorption of patients' samples with antigen-expressing HEK cells,¹⁰ brain tissue processing, quantitative brain tissue immunoperoxidase staining, extraction of human IgG bound to mice brain, and determination of NMDAR specificity of brain-extracted IgG have been previously reported on.⁹ To quantify the effects of patients' antibodies on total cell-surface and synaptic NMDAR clusters and PSD95, nonpermeabilized 5- μ m brain sections were blocked with 5% goat serum, incubated with human CSF antibodies (1:20; used here as primary NMDAR antibody) for 2 hours at room temperature (RT), washed with PBS, permeabilized with Triton X-100 0.3% for 10 minutes at RT, and serially incubated with rabbit polyclonal anti-PSD95 (1:250, ab18258; Abcam, Cambridge, MA) overnight at 4°C and the corresponding secondary antibodies, Alexa Fluor 594 or 488 goat antihuman Fab-specific IgG (109-585-097 or 109-545-097; Jackson ImmunoResearch Laboratories, Inc., West Grove, PA) and Alexa Fluor 488 goat antirabbit IgG (A-11008; Thermo Fisher Scientific, Waltham, MA), all diluted 1:1,000, for 1 hour at RT. Clusters of EphB2 were identified using non-permeabilized tissue and a goat anti-EphB2 as primary antibody (1:100, AF467; R&D Systems, Minneapolis, MN) overnight at 4°C, followed by a secondary antibody, Alexa Fluor 594 donkey antigoat IgG (A-11058, 1:1000; Thermo Fisher Scientific), for 1 hour at RT. Slides were mounted and results scanned with a confocal microscope (Zeiss LSM710; Carl Zeiss GmbH, Jena, Germany) as reported.⁹ Standardized *z*-stacks including 50 optical images were acquired from 18 hippocampal regions per animal, including CA1, CA2, CA3, and dentate gyrus, as reported.⁹ For cluster density analysis, a spot detection algorithm from Imaris suite 7.6.4 (Bitplane, Zurich, Switzerland) was used. Density of clusters in each hippocampal region was expressed as spots/ μ m³. Synaptic localization is defined as colocalization of NMDAR with postsynaptic PSD95, and synaptic cluster density is expressed as colocalized spots/ μ m³. For animals treated with patients' CSF with or without ephrin-B2 or control CSF with ephrin-B2, the mean densities of all 18 hippocampal regions were calculated for total and synaptic NMDAR and EphB2, and normalized to the mean density of the 18 hippocampal regions in animals treated with control CSF (= 100%).

To demonstrate the binding of ephrin-B2 to EphB2, nonpermeabilized brain sections were obtained from animals infused for 5 days with patients' CSF with or without ephrin-B2, processed as above and sequentially incubated with rabbit anti-ephrin-B2 antibodies (1:500, ab131536; Abcam) for 2 hours at 4°C, washed, goat anti-EphB2 antibody (1:200, AF467; R&D Systems) overnight at 4°C, washed, and the secondary antibodies, Alexa Fluor 594 donkey antigoat followed by goat-anti-rabbit 488 (A-11058 or A-11008;

Thermo Fisher Scientific), all diluted 1:1,000, for 1 hour at RT. For each animal, three identical image stacks representing CA1 were examined. Intensity of ephrin-B2 immunostaining was calculated with ImageJ software (National Institutes of Health [NIH], Bethesda, MD), and colocalization of clusters of ephrin-B2 and EphB2 was determined with Imaris suite 7.6.4 (Bitplane). Results were normalized to the mean values obtained in animals treated with patients' CSF + ephrin-B2 (100%).

To determine the phosphorylation of EphB2 by ephrin-B2, permeabilized brain tissue sections were blocked as above and sequentially incubated with rabbit anti-phospho-EphB2 (dilution 1:50, E22-65BR; SignalChem, Richmond, British Columbia, Canada) overnight at 4°C and a secondary antibody, Alexa 488 goat anti-rabbit (1:1,000, A-11008; Thermo Fisher Scientific), for 1 hour at RT. Slides were then mounted and scanned with confocal microscope as above.

To demonstrate the specificity of neuronal-bound IgG, we used an immunoprecipitation method similar to that previously reported.¹¹ In brief, cultures of live hippocampal neurons were incubated for 1 hour with aliquots of the samples (patients' or control CSF with or without ephrin-B2) used for mice cerebroventricular infusion, washed, lysed, and neuronal-bound IgG precipitated with protein A and G sepharose beads. Immunoprecipitates were then run in a gel and incubated with a rabbit antibody specific for the NR1 subunit of the NMDAR (#G8913; Sigma-Aldrich), diluted 1:1,000, for 1 hour at room temperature, followed by a biotinylated anti-rabbit antibody (diluted 1:1,000, BA-1000; Vector Laboratories, Burlingame, CA), and the reactivity developed with the avidin-biotin peroxidase technique.

Electrophysiological Studies

Seventeen to 23 days after activation of osmotic pumps, mice were deeply anesthetized with isoflurane and decapitated. Brains were removed, placed in ice-cold, high-sucrose extracellular artificial fluid 1 (artificial CSF [aCSF] 1; 40mM of NaCl, 25mM of NaHCO₃, 10mM of glucose, 150mM of sucrose, 4mM of KCl, 1.25mM of NaH₂PO₄, 0.5mM of CaCl₂, and 7mM of Mg₂Cl; purged with 95% O₂/5% CO₂ [pH 7.35]) and subdivided into the hemispheres. Thick (400- μ m) coronal slices of hippocampus were obtained with a vibratome (VT1200 S; Leica Microsystems, Wetzlar, Germany) and transferred into an incubation beaker with extracellular aCSF 2 appropriate for electrophysiological recordings (aCSF 2; 124mM of NaCl, 26mM of NaHCO₃, 10mM of glucose, 3.4mM of KCl, 1.2mM of NaH₂PO₄, 2mM of CaCl₂, and 2mM of MgSO₄; purged with 95% O₂/5% CO₂ [pH 7.35]). Slices were kept at 34°C for 60 minutes and subsequently at RT for at least 60 additional minutes. For field potential measurements, single slices were then transferred into a measurement chamber perfused with aCSF 2 at 1.3 to 2.5ml/min at 32°C to 33°C (control CSF: number of acute slices: n = 7, prepared from brain hemisections of 4 mice; control CSF + ephrin-B2: n = 7, from hemisections of 6 mice; patients' CSF: n = 7, from

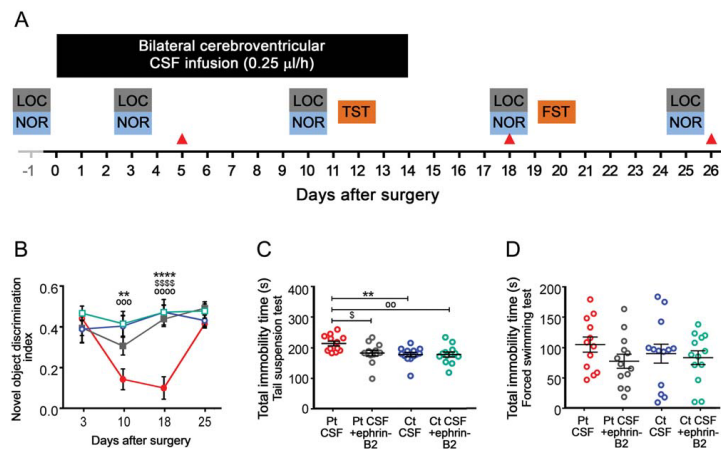


FIGURE 2: Intraventricular infusion of CSF from patients with NMDAR antibodies causes deficits in memory and depressive-like behavior that are prevented by ephrin-B2. (A) Schedule of cognitive testing and animal sacrifice. Memory (novel object recognition [NOR] discrimination index), depressive-like behavior (tail suspension test [TST] and forced swimming test [FST]), and locomotor activity (LOC) were assessed blinded to treatment at the indicated days. The NOR discrimination index was assessed in open field in four different cohorts of mice. Animals were habituated the day before surgery (baseline) to NOR and LOC. Red arrow heads indicate the days of sacrifice for studies of effects of antibodies in brain. (B) NOR index in open-field paradigm in animals treated with patients' CSF antibodies (Pt CSF; solid circles), Pt CSF + ephrin-B2 (open circles), control CSF (Ct CSF; solid squares), or Ct CSF + ephrin-B2 (open squares). A high index indicates better object recognition memory. (C) Total time of immobility in TST during the infusion period (day 12). (D) Total time of immobility in FST (day 20). Data are presented as mean \pm standard error of the mean (median \pm interquartile range IQR in C and D), n = number of animals: patients' CSF, n = 12; patients' CSF + ephrin-B2, n = 13; control CSF, n = 13; and control CSF + ephrin-B2, n = 13. Significance of treatment effect was assessed by repeated-measures two-way analysis of variance (ANOVA; $p = 0.0001$; B) with post-hoc testing with Bonferroni adjustment (asterisks), or one-way ANOVA ($p = 0.0032$) and Bonferroni post-hoc correction (C). Patients' CSF versus control CSF: ** $p < 0.01$; **** $p < 0.0001$; patients' CSF versus patients' CSF + ephrin-B2: $^{\$}p < 0.05$; $^{SSSS}p < 0.0001$; patients' CSF versus control CSF + ephrin-B2: $^{oo}p < 0.01$; $^{oooo}p < 0.0001$. CSF = cerebrospinal fluid; NMDAR = N-methyl-D-aspartate receptor.

hemisections of 4 mice; patients' CSF + ephrin-B2: n = 5, from hemisections of 5 mice). A custom made bipolar stimulation electrode was placed in the Schaffer collateral pathway. Recording electrodes were made with a puller (P-1000; Sutter Instrument Company, Novato, CA) from thick-walled borosilicate glass with a diameter of 2mm (Science Products, Hofheim, Germany). The recording electrode filled with aCSF 2 was placed in the dendritic branching of the CA1 region for local field potential measurement (field excitatory postsynaptic potential; fEPSP). A stimulus isolation unit (Isoflex; A.M.P.I., Jerusalem, Israel) was used to elicit stimulation currents between 70 and 260 μ A. Before baseline recordings for long-term potentiation (LTP) measurements, input-output curves were recorded for each slice at 0.03Hz (control CSF: n = 8 slices from N = 5 mice; control CSF + ephrin-B2: n = 8, N = 6; patients' CSF: n = 9, N = 5; patients' CSF + ephrin-B2: n = 7, N = 5). The stimulation current was then adjusted in each recording to evoke fEPSP at which the population spike could first be distinguished from the field potential and was then reduced by 10%.¹² The final intensities of stimulation ranged from 60% to 70% of maximum fEPSP slopes and were unchanged in between the experimental groups. After baseline recordings for

25 minutes with 0.03Hz, LTP was induced by theta-burst stimulation (TBS; 10 theta bursts of four pulses of 100Hz with an interstimulus interval of 200ms repeated 10 times with 0.03Hz).¹³ After LTP induction, fEPSPs were recorded for additional 65 minutes with 0.03Hz. Paired-pulse fEPSPs in the test pathway were measured directly before and 30 minutes after LTP induction with 0.03Hz and an interstimulus interval of 100ms. The fEPSP of the first paired-pulse stimulus was included in fEPSP analysis. All recordings were filtered at 2.9 and 10kHz using Bessel filters of the amplifier. Traces were analyzed by IGOR Pro software (WaveMetrics, Lake Oswego, OR).

Statistical Analysis

Behavioral tests with multiple time points (NOR, locomotor activity) were analyzed using repeated-measures two-way analysis of variance (ANOVA). The tail suspension test (behavioral paradigm with single time point) was analyzed with one-way ANOVA. All experiments were assessed for outliers, but none were identified, so measurements were pooled per time point and treatment (patient or control CSF). Human IgG intensity from different time points and electrophysiological data (LTP-induced changes in fEPSP slope and absolute fEPSP slope

values) were analyzed with two-way ANOVA. Intensity of reactivity of patients' antibodies with cultures of neurons, confocal cluster densities (GluN1, PSD95, and EphB2) at one time point, and assessment of fEPSP stimulation strength were analyzed using one-way ANOVA. Electrophysiological data from

the paired-pulse experiment were analyzed with repeated-measures two-way ANOVA. Post-hoc analyses for all experiments used Bonferroni correction for multiple testing. The EphB2 activation experiment was assessed by two-tailed *t* test. A *p* value of < 0.05 was considered significant. The α -error was

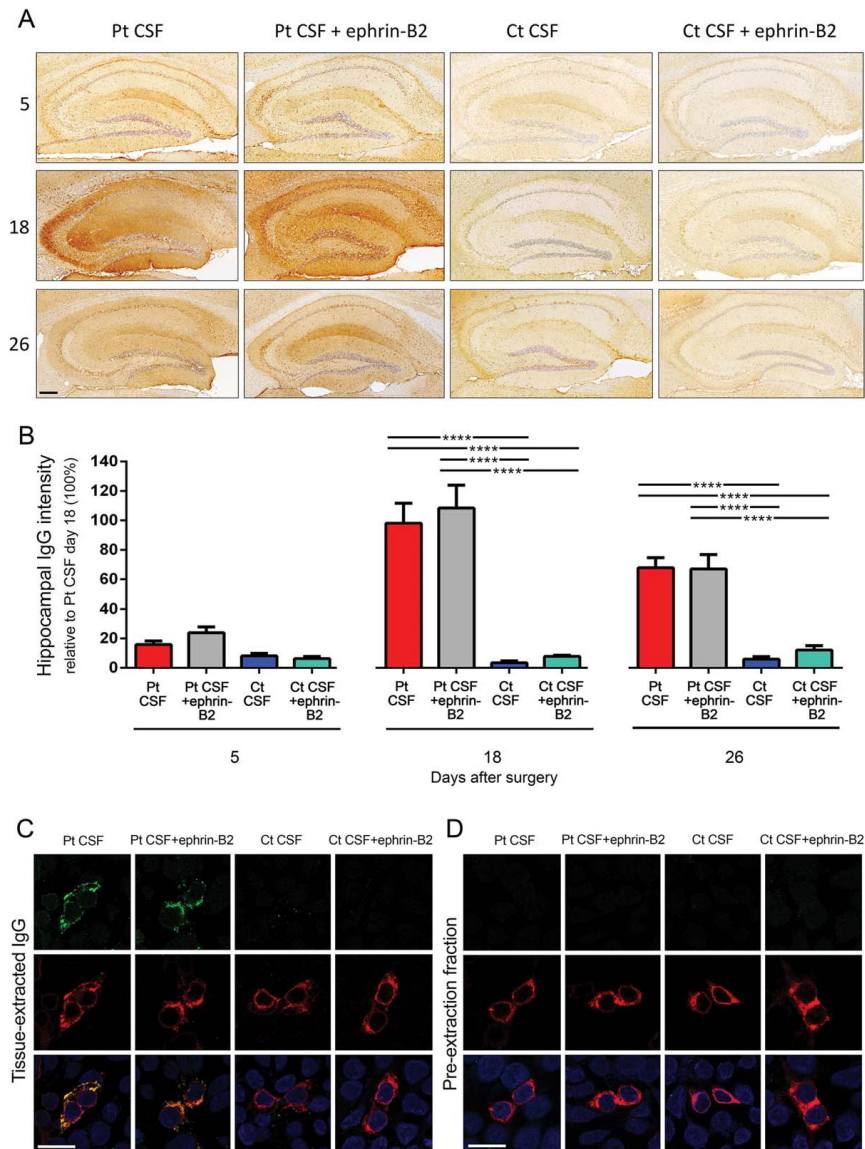


FIGURE 3.

ANNALS of *Neurology*

set at 0.05. All tests were done using GraphPad Prism software (version 6; GraphPad Software Inc., La Jolla, CA).

Results**Patients' Antibodies Cause Memory and Behavioral Deficits That Are Prevented by Ephrin-B2**

We first confirmed that (1) pooled patients' CSF only had GluN1 NMDAR antibodies (Fig 1A), (2) ephrin-B2 did not block binding of patients' antibodies (Fig 1B,C), and (3) binding of patients' antibodies to the neuronal surface was specific for NMDARs (eg, patients' antibodies precipitated this receptor; Fig 1D). We also confirmed in cultured neurons that patients' antibodies removed NMDARs from synapses causing their internalization² and that these effects were antagonized by ephrin-B2³ (Fig 1E–G). Next, we used patients' CSF samples for cerebroventricular infusions to mice. Animals infused for 14 days with patients' CSF antibodies, but not control CSF, showed a progressive impairment of memory (NOR discrimination index) that was maximal on day 18 and recovered on day 25 (Fig 2A,B). Compared with animals infused with control CSF, those infused with patients' CSF developed depressive-like behavior (longer time of immobility during the tail suspension test [TST] on day 10; Fig 2C) that recovered after the CSF infusion stopped (assessed by forced swimming test [FST] on day 20; Fig 2D). The reason for using two different tests to assess a similar task is that mice cannot be re-exposed to TST or FST test because of behavioral learning acquired during the first exposure. Although these tests are considered equivalent,^{14,15} future studies should confirm this in our model.

In contrast to the above-mentioned findings, mice that received patients' CSF along with ephrin-B2 showed a

mild, not significant, decrease of memory on day 10 and normal memory on day 18. In addition, mice that received ephrin-B2 did not develop depressive-like behavior (Fig 2B,C; Supplementary Table 1A,B). No significant difference in motor activity was noted among the different groups (Supplementary Table 2). Overall, these findings confirm those of our previous study and demonstrate, for the first time, that the alteration of memory and behavior caused by patients' NMDAR antibodies can be largely prevented by administration of ephrin-B2.

Ephrin-B2 Does Not Alter the Specific Binding of Patients' Antibodies to Mouse NMDAR

Mice infused with patients' CSF, but not control CSF, showed progressive accumulation of brain-bound human IgG, predominantly in the hippocampus (Fig 3A,B). Compared with mice not receiving ephrin-B2, those infused with this ligand showed increased density of ephrin-B2 bound to EphB2 and increased levels of EphB2 phosphorylated (data not shown). The dynamics and the degree of IgG binding to the brain were not altered by adding ephrin-B2 to patients' CSF (Fig 3A,B; Supplementary Table 3). NMDAR specificity of brain-bound human IgG (confirmed in immunosorption experiments before infusion in mice; Fig 1A) was further determined by acid extraction of the IgG bound to hippocampus and testing it with a CBA for NMDAR. IgG extracted from hippocampus of mice infused with patients' CSF with or without ephrin-B2, but not control CSF, was specific for NMDAR (Fig 3C). Confirmation that extracted IgG represented antibodies bound to the hippocampus and not unbound antibodies (eg, present in blood vessels) was provided by the absence of reactivity in the pre-extraction fraction (tissue wash fraction before applying acid; Fig 3D).

FIGURE 3: Animals infused with patients' CSF have a progressive increase of human anti-NMDAR IgG bound to hippocampus that is not altered by ephrin-B2. (A) Immunostaining of human IgG in sagittal hippocampal sections of mice infused with patients' CSF antibodies (Pt CSF), Pt CSF + ephrin-B2, control CSF (Ct CSF), and Ct CSF + ephrin-B2, sacrificed at the indicated experimental days. In animals infused with patients' CSF and patients' CSF + ephrin-B2, there is a gradual increase of IgG immunostaining until day 18, followed by a decrease of immunostaining. Scale bar: A = 200 μ m. **(B)** Quantification of intensity of human IgG immunostaining in hippocampus of mice infused with patients' CSF (red bars), patients' CSF + ephrin-B2 (gray bars), control CSF (blue bars), and control CSF + ephrin-B2 (cyan bars) sacrificed at the indicated time points. For all quantifications, mean intensity of IgG immunostaining in the group with the highest value (animals treated with patients' CSF and sacrificed at day 18) was defined as 100%. All data are presented as mean \pm standard error of the mean. For each time point, 5 animals of each experimental group were examined. Significance of treatment effect was assessed by two-way analysis of variance (ANOVA; time points, treatment, and interaction, all $p < 0.0001$), and post-hoc analyses were performed with Bonferroni correction; **** $p < 0.0001$. **(C and D)** Demonstration that the human IgG in mouse brain has NMDAR specificity: HEK293 cells expressing the GluN1 subunit of the NMDAR immunolabeled with acid-extracted IgG fractions (top row in C) or pre-extraction fractions (top row in D) from hippocampus of mice infused with patients' CSF antibodies (Pt CSF), Pt CSF + ephrin-B2, control CSF (Ct CSF), or Ct CSF + ephrin-B2 at day 18. The intense reactivity with GluN1-expressing cells was noted in acid-extracted IgG fractions from Pt CSF and Pt CSF + ephrin-B2 groups (C); none of the pre-extraction fractions from any animal group showed GluN1 reactivity (D). The second row in (C) and (D) shows the reactivity with a monoclonal GluN1 antibody, and the third row the colocalization of immunolabeling. Scale bars = 10 μ m. Pt CSF (n = 5), Pt CSF + ephrin-B2 (n = 5), Ct CSF (n = 5), and Ct CSF + ephrin-B2 (n = 5). CSF = cerebrospinal fluid; IgG = immunoglobulin G; NMDAR = N-methyl-D-aspartate receptor.

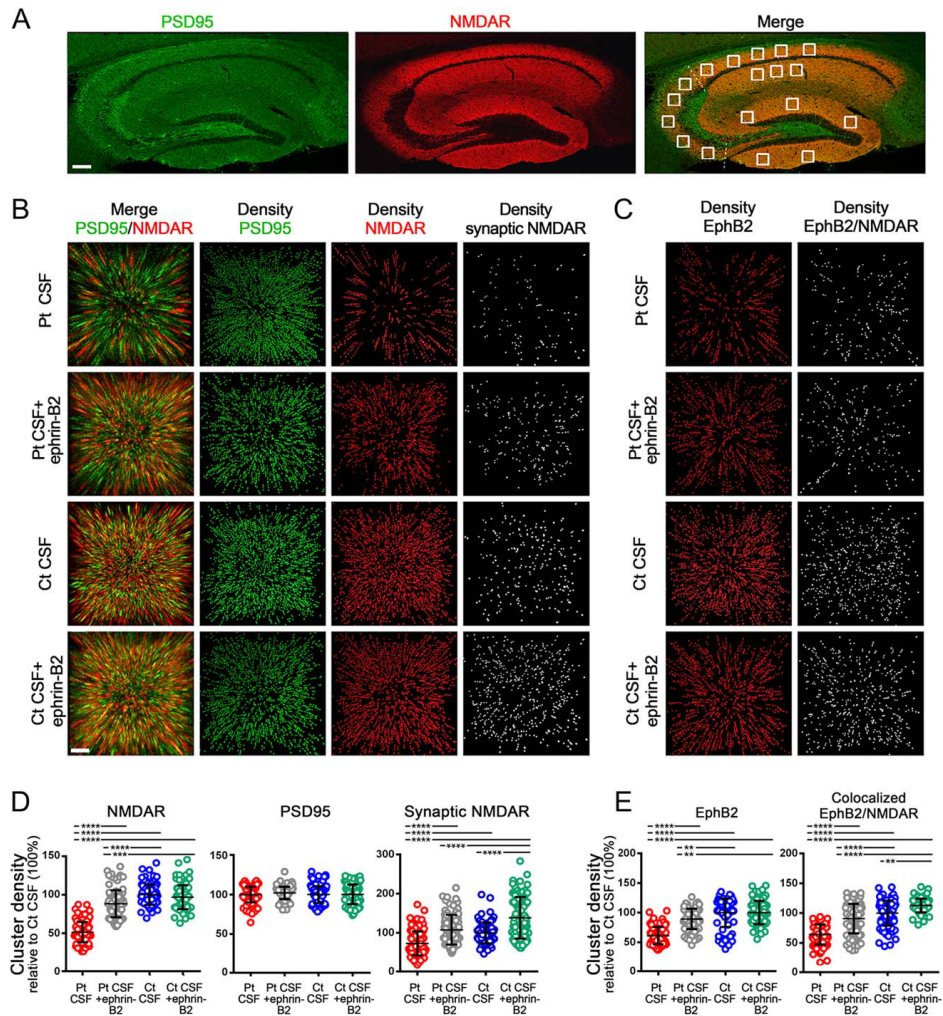


FIGURE 4: Soluble ephrin-B2 antagonizes the antibody-mediated reduction of NMDAR and EphB2 in mice hippocampus. (A) Hippocampus of mouse immunolabeled for PSD95 and NMDAR. Images were merged (merge) and postprocessed to demonstrate colocalizing clusters. Squares in "merge" indicate the analyzed areas in CA1, CA2, CA3, and dentate gyrus. Each square is a three-dimensional (3D) stack of 50 sections. Scale bar = 200 μm . (B) 3D projection and analysis of the density of total clusters of PSD95 and NMDAR, and synaptic clusters of NMDAR (defined as NMDAR clusters colocalizing with PSD95) in a CA3 region (square in A "merge") from a representative animal of each experimental group. Merged images (merge: PSD95 [green]/ NMDAR [red]) were postprocessed and used to calculate the density of clusters (density = spots/ μm^3). Scale bar = 2 μm . (C) Density of total clusters of EphB2 and EphB2 colocalizing with NMDAR. Scale bar = 2 μm . (D) Quantification of the density of total (left) and synaptic (right) NMDAR clusters, and (E) total EphB2 and EphB2 colocalizing with NMDAR at day 18 in a pooled analysis of hippocampal areas (CA1, CA2, CA3, and dentate gyrus) in animals treated with patients' CSF antibodies (Pt CSF; red), Pt CSF + ephrin-B2 (gray), control CSF (Ct CSF; blue), and control Ct CSF + ephrin-B2 (cyan). Mean density of clusters in control CSF treated animals was defined as 100%. Data are presented as scatterplot + mean \pm standard error of the mean. For each condition, 5 animals were examined (18 hippocampal areas per animal = 90 hippocampal areas per condition). Significance of treatment effect was assessed by one-way analysis of variance ($p < 0.0001$) and by post-hoc analysis with Bonferroni correction; ** $p < 0.01$; *** $p < 0.001$; **** $p < 0.0001$. CSF = cerebrospinal fluid; NMDAR = N-methyl-D-aspartate receptor.

ANNALS of Neurology

These experiments show that ephrin-B2 did not alter the specific binding of patients' antibodies to mouse hippocampal NMDAR, although it prevented the memory and behavioral deficits caused by the antibodies.

The Antibody-Mediated Reduction of Synaptic NMDAR and EphB2 Is Antagonized by Ephrin-B2

To determine whether the protective effects of ephrin-B2 occurred *in vivo*, we infused this ligand along with patients' antibodies into the cerebroventricular system of our mouse model. We then compared the effects of patients' antibodies on the density of total and synaptic NMDAR in the hippocampus of mice infused with patients' or control CSF, with or without ephrin-B2. Eighteen hippocampal areas with 50 z-sections per area, representing a total of 900 sections per animal (5 animals per group), were investigated (Fig 4A). Animals infused with patients' CSF antibodies, but not control CSF, showed a significant decrease of the density of total and synaptic NMDAR clusters. These effects were largely prevented when ephrin-B2 was coinjected with patients' antibodies (Fig 4B,D).

Patients' antibodies also caused a decrease of the density of EphB2 that was prevented by coinjection of ephrin-B2 (Fig 4C,E) similar to the results observed with cultured neurons (Fig 1F,H). Furthermore, we observed an increase in the density of colocalized EphB2/NMDAR in animals receiving ephrin-B2 either with patients' or control CSF (Fig 4E). This increase of colocalized EphB2/NMDAR, but not the total number of cell-surface EphB2 in the control group, is in line with studies showing that activation of EphB2 facilitates interaction with NMDAR and increases formation of EphB2/NMDAR clusters.¹⁶ Our findings confirm that CSF antibodies from patients with anti-NMDAR encephalitis cause a decrease of cell-surface and synaptic NMDAR *in vitro* and *in mice*, and show that these molecular effects as well as the resulting memory and behavioral deficits are prevented by the activation of EphB2 with ephrin-B2 *in vivo*.

Ephrin-B2 Antagonizes Antibody-Mediated Impairment of Hippocampal Long-Term Synaptic Plasticity

Acute brain slices from mice infused with patients' or control CSF, without or with ephrin-B2, were used to record fEPSPs in the CA1 region of the hippocampus (Fig 5A). Animals infused with patients' CSF showed a substantial reduction of LTP compared with animals infused with control CSF, as shown by analysis of fEPSP slope change (Fig 5B,C). Quantitative analysis comparing median changes in slope values of minutes 40 to 90 of the recordings (15

minutes after TBS) demonstrated a reduced potentiation of fEPSP in mice receiving patients' CSF in comparison to those receiving control CSF (Fig 5D). Coadministration of patients' CSF antibodies with ephrin-B2 partially abrogated the NMDAR antibody-mediated impairment of potentiation (Fig 5C,D; $p < 0.0001$). Administration of ephrin-B2 together with control CSF had no effects on the potentiation of fEPSP.

In contrast to severe reduction of hippocampal LTP, short-term plasticity was not affected in animals infused with patients' CSF antibodies. We performed a paired-pulse protocol before and after TBS in the CA3-CA1 synapse. As expected, fEPSP recordings showed significant paired-pulse facilitation (Fig 5E) according to increased presynaptic release probability. This effect was preserved in mice receiving patients' CSF regardless of the presence of ephrin-B2. Moreover, the fEPSP slope values of the first of the paired stimuli before and after TBS did not change in mice infused with patients' CSF, but they significantly increased in mice infused with patients' CSF and ephrin-B2, consistent with the antibody-induced impairment of LTP shown in Figure 5C. Input-output curves of fEPSPs reflecting glutamatergic transmission in the CA1/Schaffer collateral pathway at increasing stimulus intensities revealed an exponential rise of fEPSP slope values to a maximum plateau phase that is finally reached by complete stimulation of the fiber tract. In animals that received patients' CSF, absolute fEPSP slope values were reduced at nearly all stimulation intensities and also in the plateau phase compared to those of control animals. Coinjection of ephrin-B2 led to improvement of antibody-induced reduction of fEPSP slope (Fig 5F; $p = 0.001$ compared to patients' CSF). fEPSPs in slices of mice infused with control CSF and ephrin-B2 showed no differences compared to animals infused with control CSF alone. Thus, we found severe impairment of postsynaptic, but not presynaptic, plasticity after TBS in animals that received patients' CSF.

Discussion

We have used a mouse model of chronic cerebroventricular infusion of patients' NMDAR antibodies to demonstrate the antibody pathogenicity at multiple levels from behavior to synaptic plasticity, and that all antibody-mediated effects can be at least partially prevented by administration of ephrin-B2, suggesting a novel molecular intervention with potential therapeutic implications.

Our results with CSF from a new group of patients with anti-NMDAR encephalitis accurately reproduced those of our previous study,⁹ as expected, knowing the limited GluN1 epitope repertoire in patients with this disorder.¹⁷ A novel finding was that patients' antibodies

caused a reduction of EphB2, a receptor that stabilizes the NMDAR at the synapse.¹⁸

Previous work with cultured neurons showed that patients GluN1 antibodies interfered with NMDAR signaling by reducing NMDAR-mediated miniature excitatory postsynaptic currents (mEPSCs).^{2,17} GluN1 is the obligatory subunit for formation of functional NMDAR, and GluN1 knockout mice die within hours after birth.¹⁹ Hippocampal CA1 region-specific GluN1 knockouts show

impaired spatial and temporal learning with severe impairment of formation of LTP in the Schaffer collateral/CA1 synapse, demonstrating the role of NMDAR in establishing synaptic plasticity and memory formation.^{20,21} Our findings show that similar hippocampal network alterations occur when the NMDAR is targeted by GluN1 antibodies from patients with anti-NMDAR encephalitis. Indeed, LTP recordings in the CA3-CA1 synapses of acute brain slices of our mouse model showed severe impairment of

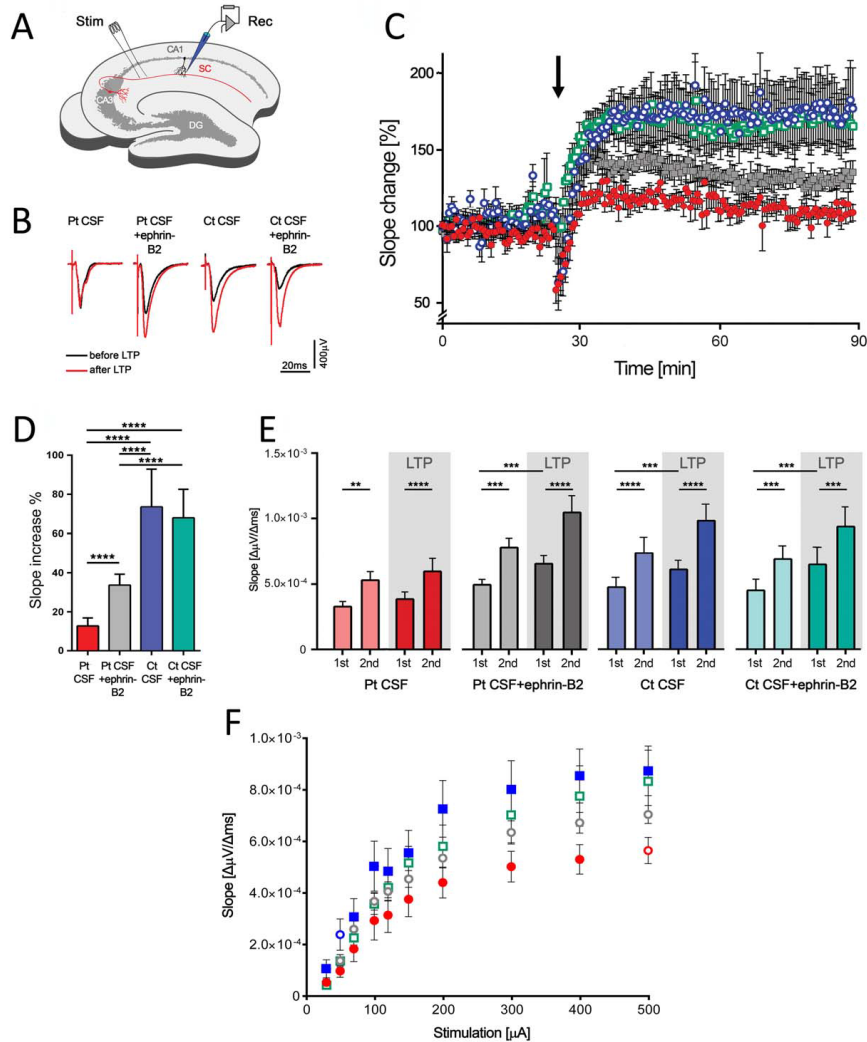


FIGURE 5.

ANNALS of *Neurology*

hippocampal synaptic plasticity. This finding possibly accounts for the memory and behavioral deficits observed in our animal model. Long-term impairment of synaptic plasticity by altered NMDAR function may result in reduction of activity-induced incorporation of high-conductance AMPARs in synaptic receptor fields, which is one of the main postsynaptic mechanisms of LTP.²² In contrast to these postsynaptic alterations, paired-pulse facilitation was unaffected accounting for largely intact presynaptic release mechanisms.²³

A study using bilateral single injection of patients' CSF into the dentate gyrus of rats showed impairment of spatial memory along with a reduction of NMDAR-evoked excitatory postsynaptic potentials and long-term potentiation.²⁴ However, these alterations appeared to be irreversible and similar to those of a commercial GluN1 antibody, the binding of which requires cell permeabilization, suggesting that antibody-independent factors may have been involved.⁴ Another study that aimed to model seizures in mice by single cerebroventricular injection of patients' IgG showed no spontaneous epileptic activity, but a decrease of seizure threshold.²⁵ The NMDAR specificity of these effects (eg,

change of synaptic NMDAR cluster density or NMDAR synaptic currents) was not investigated.

Eph receptors are a family of receptor tyrosine kinases that modulate LTP probably through their interaction with NMDAR and stabilization and clustering of this receptor in the postsynaptic membrane.^{16,26-28} Ephrin signaling, such as ephrin-B2 binding to the EphB2, is important to establish LTP in CA3-CA1 synapses for which downstream kinase signaling upon EphB activation is not critical as intracellular truncated forms of EphB do not interfere with LTP.^{26,29} In our mouse model, we hypothesize that autoantibody-induced disruption of the direct extracellular interaction of NMDAR with EphB2¹⁶ results in reduction of synaptically located NMDAR, leading to memory and behavioral deficits and reduced LTP. Moreover, ligand-dependent direct interaction of EphB2 and NMDAR may also influence phosphorylation status or subunit composition of NMDAR and, in this way, modulate synaptic plasticity.¹⁸ In cultured neurons, the antibody-mediated disruption of the cross-talk of NMDAR and EphB2 leading to NMDAR synaptic displacement and internalization is efficiently

FIGURE 5: Patients' antibodies cause severe impairment of long-term synaptic plasticity in the hippocampus that is partially prevented by ephrin-B2. (A) The Schaffer collateral pathway (SC, red) was stimulated (Stim) and field potentials were recorded in the CA1 region of the hippocampus (Rec). Long-term potentiation (LTP) was induced by theta-burst stimulation (TBS); DG = dentate gyrus; CA = Cornu Ammonis. **(B)** Example traces of individual recordings showing average traces of baseline recording before LTP induction (black traces) and after LTP (red traces). Slope and peak amplitude of fEPSPs are increased after TBS in mice infused with control CSF (Ct CSF) and Ct CSF + ephrin-B2, whereas manifestation of LTP is strongly impaired in animals infused with patients' CSF antibodies (Pt CSF). In mice infused with Pt CSF + ephrin-B2, the increase of slope is improved. Note that initial peak amplitude of fEPSP may vary within individual recordings. **(C)** Time course of fEPSP recordings demonstrating robust changes in fEPSP slope in the Ct CSF (n = 7 recordings, blue open circles) and Ct CSF + ephrin-B2 group (n = 7, cyan open squares), which is stable throughout the recording period after TBS (arrow). In animals chronically infused with Pt CSF (n = 7, red solid circles), the induction of synaptic LTP is markedly impaired. Recordings from the Pt CSF + ephrin-B2 group (n = 5, gray solid squares) show partially resolved effects on synaptic plasticity after LTP induction. **(D)** Quantitative analysis of LTP-induced changes in fEPSPs in the plateau interval after TBS depicted as comparison to each individual baseline value (slope increase as median values \pm standard error of the mean in the consolidation phase during the last 50 minutes of each recording, starting 15 minutes after TBS). Chronic application of Pt CSF results in marked reduction of LTP ($13.3 \pm 4.1\%$ slope increase vs $73.6 \pm 19.3\%$ and $68.3 \pm 14.7\%$ in Ct CSF and Ct CSF + ephrin-B2, respectively). Coadministration of soluble ephrin-B2 improved fEPSP potentiation to levels of $33.7 \pm 5.5\%$. Significance of treatment effect was assessed by two-way analysis of variance (ANOVA; $p < 0.0001$ for treatment group) and by post-hoc analysis with Bonferroni correction; $***p < 0.001$. **(E)** Patients' antibodies do not alter short-term plasticity, as revealed by paired-pulse facilitation. Short-term plasticity in the Schaffer collateral-CA1 synaptic region shows paired pulse facilitation as measured by mean slope values of the first (1st) and second (2nd) stimulus in the group of mice infused with control CSF (Ct CSF, blue), Ct CSF + ephrin-B2 (cyan), patients' CSF antibodies (Pt CSF, red), or Pt CSF + ephrin-B2 (grey) before (pale color) and after (dark color) LTP induction. Analysis of 2nd versus 1st stimulation reveals a significant increase of fEPSPs in all groups and at both time points before LTP induction (Ct CSF: $p < 0.0001$; Ct CSF + ephrin-B2: $p = 0.0002$; Pt CSF: $p = 0.0012$; Pt CSF + ephrin-B2: $p = 0.0004$) and after LTP (Ct CSF: $p < 0.0001$; Ct CSF + ephrin-B2: $p = 0.0009$; Pt CSF: $p < 0.0001$; Pt CSF + ephrin-B2: $p < 0.0001$). Comparison of fEPSPs after the first stimulus before and after LTP induction shows a significant increase in the Pt CSF + ephrin-B2 ($p = 0.0007$) and both control CSF groups (Ct CSF: $p = 0.0003$; Ct CSF + ephrin-B2: $p = 0.0004$), but not in the Pt CSF group ($p = 0.21$). Analysis was performed using repeated-measures two-way ANOVA ($p < 0.0001$ for treatment groups) and post-hoc analysis with Bonferroni correction; $**p < 0.01$; $***p < 0.001$; $****p < 0.0001$. **(F)** Analysis of fEPSP absolute slope values depending on stimulus amplitude. Increasing stimulation leads to higher slope values reaching a plateau phase at stimulation strength $> 400 \mu A$ (maximum slope and peak amplitude of fEPSP). The fEPSP slope is significantly reduced in mice infused with patients' CSF antibodies (Pt CSF; red circles). In the Pt CSF + ephrin-B2 group (gray circles), the fEPSP slope is partially restored in comparison to mice infused with Pt CSF. Blue and cyan squares indicate animals infused with control CSF (Ct CSF) and Ct CSF + ephrin-B2, respectively. Two-way ANOVA showed $p < 0.0001$ for increasing stimulation and treatment; post-hoc analysis with Bonferroni correction showed difference between the groups of mice infused with Pt CSF compared with Ct CSF with or without ephrin-B2 ($p < 0.0001$); Pt CSF compared with Pt CSF + ephrin-B2 ($p = 0.001$); and Pt CSF + ephrin-B2 compared with Ct CSF ($p = 0.0007$). CSF = cerebrospinal fluid.

antagonized by stimulation of EphB2.³ Here, we provide evidence that in mice receiving patients' antibodies, treatment with ephrin-B2 is able to partially prevent the antibody-induced impairment of LTP and glutamatergic transmission in the hippocampus.

Direct quantification of ephrin-B2-induced restoration of NMDAR-mediated individual currents awaits further experimental evidence by evaluating synaptic currents using patch-clamp experiments at the single-cell level. These effects *ex vivo* are supported by the morphological findings demonstrating abrogation of the antibody-induced reduction of NMDAR and EphB2 in the ephrin-B2-treated mice. Thus, stabilization of NMDAR expression in the postsynaptic receptor fields mediated by stimulation of Eph2B receptors may account for the rescue of memory and behavioral deficits in this animal model.

Different from the current model in which the antibodies are infused by a pump that stops after 14 days, in the human disease the exposure of brain to central nervous system (CNS) antibodies decreases slowly over months.^{30,31} A relevant source of CNS antibodies are the plasma cells demonstrated in pathological studies^{32,33} and associated with intrathecal synthesis of antibodies.^{1,6} Current treatments (plasma exchange, intravenous immune globulin, or rituximab) have limited efficacy on removing antibodies and plasma cells from the CNS. Thus, prolonged exposure of the human brain to NMDAR antibodies may disturb synaptic networks, as suggested by our observed decrease of synaptic NMDAR and alteration of synaptic plasticity in our model. It is important to keep in mind that a period of 14 days in 2-month-old mice is equivalent to 60 weeks in humans.³⁴ Additionally, in the human disease, the presence of inflammatory cells, mediators of inflammation, and frequent clinical complications (eg, intensive care unit complications, autonomic instability) may modify the outcome of the disorder.³⁵

An important finding of this study is that all antibody-mediated deficits, from memory to synaptic plasticity, were substantially prevented by ephrin-B2, providing a potential treatment strategy with peptides or small-molecule agonists of EphB2. There is precedence for the clinical use of agonists of other types of Ephrin receptors, such as the EphA2 agonist, doxazosin, which is used for treatment of benign prostate hypertrophy, but in experimental models also inhibits tumor cell migration and metastases.³⁶ In antibody-mediated disorders of the neuromuscular junction, such as myasthenia gravis or Lambert-Eaton syndrome, the discovery of the physiopathological underpinnings led to the development of drugs that antagonize the effects of the corresponding antibodies (eg, anticholinesterases and 3,4-diaminopyridine).³⁷ One envisions

a similar result in anti-NMDAR and perhaps other autoimmune encephalitis, in which the combined use of immunotherapy and small molecules crossing the blood-brain barrier and antagonizing antibody effects could represent a future treatment approach. For anti-NMDAR encephalitis, such drugs may lead to a faster control of the severe symptoms of the disease, stabilizing the function of the NMDAR in the synapses.

Acknowledgments

This study was supported, in part, by Instituto Carlos III/FEDER (FIS 15/00377 [to E.G.], FIS 14/00203 and CIBERER [to J.D.], and RETICS-RTA and RD12/0028/0023 [to R.M.]), NIH RO1NS077851 (to J.D.), MINECO (SAF2014-59648-P; to R.M.), European Commission (HEALTH-F2-2013-602891; to R.M.), Fundació Cellex (to J.D.), the Netherlands Organisation for Scientific Research (NWO, Veni incentive; to M.T.), an Erasmus MC fellowship (to M.T.), and the German Research Council (DFG; GE 2519/3-1 and CRC-TR 166/1 B2 [to C.G.]).

We thank Dr Melike Lakadamyali (ICFO-Institut de Ciències Fotòniques, Barcelona) and Dr Myrna Rosenfeld (IDIBAPS, University of Barcelona) for their critical review of the manuscript and useful suggestions and Dr Thaïs Armangué (IDIBAPS, University of Barcelona) for her comments on the statistical analysis.

Author Contributions

J.D. and C.G. were responsible for conception and design of the study. F.M., M.P.-P., E.M.-G., R.F., and J.D. were responsible for acquisition and analysis of animal behavior. J.P., M.J.T., P.J., E.G., and J.D. were responsible for acquisition and analysis of immunohistochemistry and confocal microscopy. H.H., B.G., L.R., and C.G. were responsible for acquisition and analysis of electrophysiological studies. J.P., H.H., C.G., and J.D. were responsible for drafting of the manuscript and figures. J.P., H.H., and F.M. contributed equally. C.G. and J.D. share seniority.

Potential Conflicts of interest

Dr Dalmau holds a patent for the use of NMDA receptor as an autoantibody test. Dr Dalmau has received a research grant from Euroimmun Inc.

References

1. Dalmau J, Gleichman AJ, Hughes EG, et al. Anti-NMDA-receptor encephalitis: case series and analysis of the effects of antibodies. *Lancet Neurol* 2008;7:1091–1098.

ANNALS of *Neurology*

2. Hughes EG, Peng X, Gleichman AJ, et al. Cellular and synaptic mechanisms of anti-NMDA receptor encephalitis. *J Neurosci* 2010;30:5866–5875.
3. Mikasova L, De Rossi P, Bouchet D, et al. Disrupted surface cross-talk between NMDA and Ephrin-B2 receptors in anti-NMDA encephalitis. *Brain* 2012;135:1606–1621.
4. Moscato EH, Peng X, Jain A, et al. Acute mechanisms underlying antibody effects in anti-N-methyl-D-aspartate receptor encephalitis. *Ann Neurol* 2014;76:108–119.
5. Titulaer MJ, McCracken L, Gabilondo I, et al. Treatment and prognostic factors for long-term outcome in patients with anti-NMDA receptor encephalitis: an observational cohort study. *Lancet Neurol* 2013;12:157–165.
6. Irani SR, Bera K, Waters P, et al. N-methyl-D-aspartate antibody encephalitis: temporal progression of clinical and paraclinical observations in a predominantly non-paraneoplastic disorder of both sexes. *Brain* 2010;133:1655–1667.
7. Viacoz A, Desestret V, Ducray F, et al. Clinical specificities of adult male patients with NMDA receptor antibodies encephalitis. *Neurology* 2014;82:556–563.
8. Zhang Q, Tanaka K, Sun P, et al. Suppression of synaptic plasticity by cerebrospinal fluid from anti-NMDA receptor encephalitis patients. *Neurobiol Dis* 2012;45:610–615.
9. Planaguma J, Leyboldt F, Mannara F, et al. Human N-methyl D-aspartate receptor antibodies alter memory and behaviour in mice. *Brain* 2015;138:94–109.
10. Petit-Padról M, Armangue T, Peng X, et al. Encephalitis with refractory seizures, status epilepticus, and antibodies to the GABA_A receptor: a case series, characterisation of the antigen, and analysis of the effects of antibodies. *Lancet Neurol* 2014;13:276–286.
11. Lai M, Hughes EG, Peng X, Dalmau J. AMPA receptor antibodies in limbic encephalitis alter synaptic receptor location. *Ann Neurol* 2009;65:424–434.
12. Grover LM, Kim E, Cooke JD, Holmes WR. LTP in hippocampal area CA1 is induced by burst stimulation over a broad frequency range centered around delta. *Learn Mem* 2009;16:69–81.
13. Raymond CR. LTP forms 1, 2 and 3: different mechanisms for the “long” in long-term potentiation. *Trends Neurosci* 2007;30:167–175.
14. Schmuckermair C, Gaburo S, Sah A, et al. Behavioral and neurobiological effects of deep brain stimulation in a mouse model of high anxiety- and depression-like behavior. *Neuropsychopharmacology* 2013;38:1234–1244.
15. Kordjazy N, Haj-Mirzaian A, Amiri S, et al. Involvement of N-methyl-d-aspartate receptors in the antidepressant-like effect of 5-hydroxytryptamine 3 antagonists in mouse forced swimming test and tail suspension test. *Pharmacol Biochem Behav* 2015;141:1–9.
16. Dalva MB, Takasu MA, Lin MZ, et al. EphB receptors interact with NMDA receptors and regulate excitatory synapse formation. *Cell* 2000;103:945–956.
17. Gleichman AJ, Spruce LA, Dalmau J, et al. Anti-NMDA receptor encephalitis antibody binding is dependent on amino acid identity of a small region within the GluN1 amino terminal domain. *J Neurosci* 2012;32:11082–11094.
18. Nolt MJ, Lin Y, Hruska M, et al. EphB controls NMDA receptor function and synaptic targeting in a subunit-specific manner. *J Neurosci* 2011;31:5353–5364.
19. Forrest D, Yuzaki M, Soares HD, et al. Targeted disruption of NMDA receptor 1 gene abolishes NMDA response and results in neonatal death. *Neuron* 1994;13:325–338.
20. Huerta PT, Sun LD, Wilson MA, Tonegawa S. Formation of temporal memory requires NMDA receptors within CA1 pyramidal neurons. *Neuron* 2000;25:473–480.
21. Tsien JZ, Huerta PT, Tonegawa S. The essential role of hippocampal CA1 NMDA receptor-dependent synaptic plasticity in spatial memory. *Cell* 1996;87:1327–1338.
22. Zamanillo D, Sprengel R, Hvalby O, et al. Importance of AMPA receptors for hippocampal synaptic plasticity but not for spatial learning. *Science* 1999;284:1805–1811.
23. Oertner TG, Sabatini BL, Nimchinsky EA, Svoboda K. Facilitation at single synapses probed with optical quantal analysis. *Nat Neurosci* 2002;5:657–664.
24. Würdemann T, Kersten M, Tokay T, et al. Stereotactic injection of cerebrospinal fluid from anti-NMDA receptor encephalitis into rat dentate gyrus impairs NMDA receptor function. *Brain Res* 2015;1633:10–18.
25. Wright S, Hashemi K, Stasiak L, et al. Epileptogenic effects of NMDAR antibodies in a passive transfer mouse model. *Brain* 2015;138:3159–3167.
26. Henderson JT, Georgiou J, Jia Z, et al. The receptor tyrosine kinase EphB2 regulates NMDA-dependent synaptic function. *Neuron* 2001;32:1041–1056.
27. Kullander K, Klein R. Mechanisms and functions of Eph and ephrin signalling. *Nat Rev Mol Cell Biol* 2002;3:475–486.
28. Lisabeth EM, Falivelli G, Pasquale EB. Eph receptor signaling and ephrins. *Cold Spring Harb Perspect Biol* 2013;5 pii: a009159. doi: 10.1101/cshperspect.a009159.
29. Grunwald IC, Korte M, Wolfert D, et al. Kinase-independent requirement of EphB2 receptors in hippocampal synaptic plasticity. *Neuron* 2001;32:1027–1040.
30. Gresa-Arribas N, Titulaer MJ, Torrents A, et al. Antibody titres at diagnosis and during follow-up of anti-NMDA receptor encephalitis: a retrospective study. *Lancet Neurol* 2014;13:167–177.
31. Leyboldt F, Hofberger R, Titulaer MJ, et al. Investigations on CXCL13 in anti-N-methyl-D-aspartate receptor encephalitis: a potential biomarker of treatment response. *JAMA Neurol* 2015;72:180–186.
32. Martínez-Hernández E, Horvath J, Shiloh-Malawsky Y, et al. Analysis of complement and plasma cells in the brain of patients with anti-NMDAR encephalitis. *Neurology* 2011;77:589–593.
33. Bien CG, Vincent A, Barnett MH, et al. Immunopathology of autoantibody-associated encephalitides: clues for pathogenesis. *Brain* 2012;135:1622–1638.
34. Flurkey K, Currer JM, Harrison DE. The mouse in aging research. In: Fox JGea, ed. *The Mouse in Biomedical Research*. Burlington, MA: American College Laboratory Animal Medicine (Elsevier); 2015:637–672.
35. Dalmau J, Lancaster E, Martínez-Hernández E, Rosenfeld MR, Balice-Gordon R. Clinical experience and laboratory investigations in patients with anti-NMDAR encephalitis. *Lancet Neurol* 2011;10:63–74.
36. Petty A, Myshkin E, Qin H, et al. A small molecule agonist of EphA2 receptor tyrosine kinase inhibits tumor cell migration in vitro and prostate cancer metastasis in vivo. *PLoS One* 2012;7:e42120.
37. Newsom-Davis J. Therapy in myasthenia gravis and Lambert-Eaton myasthenic syndrome. *Semin Neurol* 2003;23:191–198.

Suppl. Tab. 1

A

| Test | 2-way ANOVA analysis | | | Post-hoc analysis OR Index* | | | | | | | | | | | | | |
|----------------------------------------------|----------------------|-------------|----------|-----------------------------|--------|-----------------|-----------------|------------|-----------------|----------|------------------------------|------------------------------|------|-------|---------------|----------------|----------|
| | Source of variation | P-value | F-value | Pt CSF vs Ct CSF | | | | | | | | | | | | | |
| | | | | Mean | | difference | 95% CI | P-value | | | | | | | | | |
| Novel Object Recognition | OR Index | Interaction | < 0.0001 | 4.72 | Day | | | | Pt CSF | Ct CSF | | | | | | | |
| | | | | | 3 | 0.44 | 0.39 | 0.05 | -0.15 to 0.25 | > 0.5 | | | | | | | |
| | | | | | 10 | 0.14 | 0.40 | -0.26 | -0.46 to -0.060 | < 0.01 | | | | | | | |
| | | | | | 18 | 0.10 | 0.47 | -0.37 | -0.57 to -0.17 | < 0.0001 | | | | | | | |
| | OR Index | Time | < 0.0001 | 8.32 | Day | Pt CSF | Ct CSF | difference | 95% CI | P-value | | | | | | | |
| | | | | | | | | | | | | 25 | 0.42 | 0.43 | -0.015 | -0.21 to 0.19 | > 0.05 |
| | | | | | | | | | | | | Pt CSF vs Ct CSF + ephrin-B2 | | | | | |
| | | | | | | | | | | | | 3 | 0.44 | 0.47 | -0.025 | -0.23 to 0.18 | > 0.5 |
| | OR Index | Treatment | < 0.0001 | 8.63 | Day | Pt CSF | Ct CSF+EphrinB2 | difference | 95% CI | P-value | | | | | | | |
| | | | | | | | | | | | | 10 | 0.14 | 0.42 | -0.27 | -0.47 to -0.07 | < 0.01 |
| | | | | | | | | | | | | 18 | 0.10 | 0.47 | -0.37 | -0.47 to -0.07 | < 0.0001 |
| | | | | | | | | | | | | 25 | 0.42 | 0.48 | -0.06 | -0.26 to 0.14 | > 0.5 |
| Total time of exploration (internal control) | Interaction | 0.15 | 1.49 | Day | Pt CSF | Pt CSF+EphrinB2 | difference | 95% CI | P-value | | | | | | | | |
| | | | | | | | | | | | 3 | 0.44 | 0.40 | 0.05 | -0.16 to 0.25 | > 0.5 | |
| | | | | | | | | | | | 10 | 0.14 | 0.31 | -0.16 | -0.36 to 0.03 | > 0.5 | |
| | | | | | | | | | | | 18 | 0.10 | 0.44 | -0.33 | -0.54 to 0.14 | < 0.0001 | |
| Total time of exploration (internal control) | Time | 0.0001 | 7.35 | Day | Pt CSF | Pt CSF+EphrinB2 | difference | 95% CI | P-value | | | | | | | | |
| | | | | | | | | | | | 25 | 0.42 | 0.49 | -0.08 | -0.28 to 0.12 | > 0.5 | |
| | | | | | | | | | | | Pt CSF vs Pat CSF + EphrinB2 | | | | | | |
| | | | | | | | | | | | 3 | 0.44 | 0.40 | 0.05 | -0.16 to 0.25 | > 0.5 | |
| Total time of exploration (internal control) | Treatment | 0.97 | 0.076 | Day | Pt CSF | Pt CSF+EphrinB2 | difference | 95% CI | P-value | | | | | | | | |
| | | | | | | | | | | | 10 | 0.14 | 0.31 | -0.16 | -0.36 to 0.03 | > 0.5 | |
| | | | | | | | | | | | 18 | 0.10 | 0.44 | -0.33 | -0.54 to 0.14 | < 0.0001 | |
| | | | | | | | | | | | 25 | 0.42 | 0.49 | -0.08 | -0.28 to 0.12 | > 0.5 | |

B

| | Variable | N | | | | Mean (95% CI) | | | | F-value | P-value |
|------------------------|--------------------|--------|-------------------|--------|-------------------|---------------|------------------|---------------|-------------------|---------|---------|
| | | Pt CSF | Pt CSF +Ephrin B2 | Ct CSF | Ct CSF +Ephrin B2 | Pt CSF | Pt CSF +EphrinB2 | Ct CSF | Ct CSF +Ephrin B2 | | |
| Tail Suspension | Time of immobility | 12 | 13 | 13 | 13 | 209 (192-225) | 178 (159-198) | 173 (159-188) | 173 (156-191) | 5.27 | 0.0032 |
| Forced Swimming | Time of immobility | 12 | 13 | 13 | 13 | 108 (79-137) | 79 (53-106) | 93 (57-128) | 86 (60-111) | 0.81 | 0.49 |

* Post-hoc data for comparisons of Pt CSF + ephrin-B2 vs Ct CSF, Pt CSF + ephrin-B2 vs Ct CSF + ephrin-B2 and Ct CSF vs Ct CSF + ephrin-B2 revealed no significant differences.

Suppl. Table 2

| Test | <i>2-way ANOVA analysis</i> | | | |
|--------------------|-----------------------------|-------------|---------|-------|
| | Source of variation | p-value | F-value | |
| Locomotor Activity | Motor Activity | Interaction | 0.90 | 0.51 |
| | | Time | < | 26.92 |
| | | Treatment | 0.94 | 0.13 |
| | Horizontal Activity | Interaction | 0.86 | 0.58 |
| | | Time | < | 23.95 |
| | | Treatment | 0.47 | 0.85 |
| | Vertical Activity | Interaction | 0.81 | 0.63 |
| | | Time | < | 36.95 |
| | | Treatment | 0.82 | 0.30 |
| Weight | % Difference weight | Interaction | 0.16 | 1.35 |
| | | Time | < | 9.08 |
| | | Treatment | 0.26 | 1.36 |

Suppl. Tab. 3

| <i>2-way ANOVA analysis</i> | | | | <i>Post-hoc analysis OR Index *</i> | | | | | | |
|---------------------------------------------|-------------------------|-------------------------|-------------------------------------|-------------------------------------|-----------------|-------------------------|----------------|-----------------|-----------------|--|
| Source of variation | <i>P</i> -value | <i>F</i> -value | <i>Pt CSF vs Ct CSF</i> | | | | | | | |
| | | | Day | Mean Pt CSF | Mean Ct CSF | difference | 95% CI | <i>P</i> -value | | |
| IgG deposits | Interaction | < 0.0001 | 11.02 | 5 | 11.31 | 4.61 | 6.70 | -13.87 to 27.28 | > 0.05 | |
| | | | | 18 | 69.94 | 2.50 | 67.44 | 48.04 to 86.84 | < 0.0001 | |
| | | | | 26 | 48.33 | 4.25 | 44.09 | 24.69 to 63.49 | < 0.0001 | |
| | Treatment | < 0.0001 | 60.55 | <i>Pt CSF vs Ct CSF + ephrin-B2</i> | | | | | | |
| | | | | Day | Mean Pt CSF | Mean Ct CSF + ephrin-B2 | difference | 95% CI | <i>P</i> -value | |
| | | | | 5 | 11.31 | 4.03 | 7.28 | -12.12 to 26.29 | > 0.05 | |
| Time | < 0.0001 | 32.38 | 18 | 69.94 | 5.50 | 64.44 | 45.04 to 83.84 | < 0.0001 | | |
| | | | 26 | 48.33 | 8.60 | 39.74 | 20.33 to 59.14 | < 0.0001 | | |
| | | | <i>Pt CSF + ephrin-B2 vs Ct CSF</i> | | | | | | | |
| Day | Mean Pt CSF + ephrin-B2 | Mean Ct CSF | difference | 95% CI | <i>P</i> -value | | | | | |
| 5 | 17.02 | 4.61 | 12.41 | -8.16 to 32.99 | > 0.05 | | | | | |
| 18 | 77.40 | 2.50 | 74.91 | 55.51 to 94.31 | < 0.0001 | | | | | |
| 26 | 47.75 | 4.25 | 43.50 | 24.10 to 62.90 | < 0.0001 | | | | | |
| <i>Pt CSF + ephrin-B2 vs Ct + ephrin-B2</i> | | | | | | | | | | |
| Day | Mean Pt CSF + ephrin-B2 | Mean Ct CSF + ephrin-B2 | difference | 95% CI | <i>P</i> -value | | | | | |
| 5 | 17.02 | 4.03 | 12.99 | -6.41 to 32.39 | > 0.05 | | | | | |
| 18 | 77.40 | 5.50 | 71.90 | 52.50 to 91.30 | < 0.0001 | | | | | |
| 26 | 47.75 | 8.60 | 39.15 | 19.75 to 58.55 | < 0.0001 | | | | | |

* Post-hoc data for comparisons of Pt CSF vs Pt CSF + ephrin-B2 and Ct CSF vs Ct CSF + ephrin-B2 revealed no significant differences.

4.5 Manuscript V

Human autoantibodies against the AMPA receptor subunit GluA2 induce receptor reorganisation and memory dysfunction

Haselmann H*, Mannara F*, Werner C, Planagumà J, Grünewald B, Petit-Pedrol M, Kirmse K, Classen J, Demir, F, Klöcker N, Doose S, Dalmau J, Hallermann S, Geis C

Human autoantibodies against the AMPA receptor subunit GluA2 induce receptor reorganisation and memory dysfunction

Holger Haselmann^{1,2,§}, Francesco Mannara^{3,§}, Christian Werner^{1,4}, Jesús Planagumà³, Benedikt Grünewald^{1,2}, Mar Petit-Pedrol³, Knut Kirmse¹, Joseph Classen⁵, Fatih Demir⁶, Nikolaj Klöcker⁶, Sören Doose⁴, Josep Dalmau^{3,7,8}, Stefan Hallermann⁹, Christian Geis^{1,2,*}

¹Hans-Berger Department of Neurology, ²Center for Sepsis Control and Care (CSCC), Jena University Hospital, Am Klinikum 1, 07747 Jena, Germany; ³Institut d'Investigacions Biomèdiques August Pi i Sunyer (IDIBAPS), Hospital Clínic, Universitat de Barcelona, 08036 Barcelona, Spain; ⁴Department of Biotechnology and Biophysics, Biocenter, University of Würzburg, Am Hubland, 97074 Würzburg, Germany, ⁵Department of Neurology, University of Leipzig, Liebigstrasse 20, 04103 Leipzig, Germany, ⁶Institute of Neural and Sensory Physiology, Medical Faculty, University of Düsseldorf, Germany; ⁷Department of Neurology, University of Pennsylvania, Philadelphia, PA, 19104, USA; ⁸Institució Catalana de Recerca i Estudis Avançats (ICREA), Passeig de Lluís Companys, 23, 08010 Barcelona, Spain, ⁹Carl-Ludwig-Institute for Physiology, Medical Faculty, University of Leipzig, Liebigstrasse 27, 04103 Leipzig, Germany.

[§]These authors contributed equally

*lead contact

Corresponding author:

Christian Geis, MD

Hans-Berger Department of Neurology, Am Klinikum 1, 07747 Jena, Germany

email: christian.geis@med.uni-jena.de

phone: +49-3641-9323410

fax: +49-3641-9323422

Summary

AMPA receptors are essential for fast excitatory transmission in the central nervous system. Autoantibodies to AMPA receptors have been identified in humans with autoimmune encephalitis and severe defects of hippocampal function. Here, we analyze how specific human autoantibodies against the AMPA receptor subunit GluA2 affect receptor function and composition, synaptic transmission, and plasticity. Using passive transfer of purified human pathogenic antibodies to mice, electrophysiology, and super-resolution imaging, we show that anti-GluA2 antibodies induce a distinct pattern of changes in synaptic AMPA receptor composition. GluA2 subunits are replaced by GluA1 resulting in synaptic scaling due to synaptic incorporation of AMPA receptors with increased single channel conductance and reduced inward rectification. With passive transfer of human pathogenic antibodies to mice, we show that anti-GluA2 antibodies impair synaptic plasticity and memory. Our results identify a specific immune-neuronal rearrangement of AMPA receptor subunits providing a novel framework to explain disease symptoms.

Keywords

AMPA receptor, GluA2 subunit, autoimmune encephalitis, autoantibody, synaptic plasticity, synaptic scaling, passive-transfer, super-resolution microscopy, synaptic transmission, iontophoretic application

Highlights

- human GluA2 autoantibodies (ABs) cause changes in AMPA receptor subunit composition
- AB-mediated down-regulation of synaptic AMPA receptors leads to synaptic scaling

- passive-transfer of GluA2 ABs impairs synaptic plasticity and triggers disease symptoms *in vivo*
- AMPA receptor subunit rearrangement provides a novel framework to explain disease symptoms

Introduction

Autoimmune encephalitis represents a heterogeneous group of autoimmune disorders in the central nervous system that are characterized by autoantibodies (ABs) to neuronal targets localized at central synapses, such as ionotropic or G-protein coupled receptors, presynaptic proteins, or ion channels (Dalmau et al., 2017). Recently, α -amino-3-hydroxy-5-methyl-4-isoxazolepropionic acid receptors (AMPA receptors) have been described as targets for ABs in patients with a subtype of autoimmune encephalitis (Lai et al., 2009). Patients with anti-AMPA receptor encephalitis may harbor antibodies against either the GluA1 or GluA2 subunit of the AMPAR or against both subunits. Patients showing high titers of anti-AMPA receptor ABs in their cerebrospinal fluid (CSF) most often develop a syndrome of limbic encephalitis with dramatic impairment of the ability to build new memories, in addition to retrograde amnesia, anxiety, mood changes, psychosis and temporal lobe seizures (Hoftberger et al., 2015; Lai et al., 2009; Panzer et al., 2014). In two thirds of cases, autoimmune encephalitis with ABs to AMPARs is associated with malignancy most frequently lung tumor or thymoma (Hoftberger et al., 2015). Besides an effective therapy of the malignant tumor in paraneoplastic cases, patients with AMPAR encephalitis have been treated effectively with plasma exchange and/or immunosuppressive therapy (De Bruijn and Titulaer, 2016; Hoftberger et al., 2015; Lai et al., 2009).

First *in-vitro* experimental studies indicate that patient CSF containing AMPAR ABs to both GluA1 and GluA2 subunits decreases synaptic GluA2/3 clusters and miniature excitatory postsynaptic currents (mEPSCs) amplitude and frequency in cultures of primary hippocampal

neurons (Lai et al., 2009; Peng et al., 2015). However, the precise molecular mechanisms and the direct consequences of AMPAR ABs on network plasticity are unknown. Moreover, if human AMPAR ABs can induce disease symptoms in mice have yet to be shown.

AMPARs are heterotetrameric ionotropic glutamatergic receptors composed of the four pore-lining subunits GluA1 – GluA4 and several auxiliary subunits (Bredt and Nicoll, 2003; Hollmann and Heinemann, 1994; Malinow and Malenka, 2002; Schwenk et al., 2012). The GluA2 subunit plays a special role in the composition of AMPARs with consequences on AMPAR function in synaptic transmission and plasticity. In normal hippocampus, the majority of synaptic AMPARs are assembled as heteromeric receptors of GluA1 and GluA2 subunits. AMPARs containing GluA2 subunits conduct Na^+ and K^+ but not Ca^{2+} , whereas those lacking GluA2 are also permeable for Ca^{2+} , have a large single-channel conductance, and are inwardly rectifying due to a channel block by polyamines at positive membrane potentials (Bowie and Mayer, 1995; Isaac et al., 2007; Verdoorn et al., 1991). This change in receptor properties is mediated by the Q/R editing site in GluA2 subunits, where a neutral glutamine residue is replaced by a positively charged arginine (Burnashev et al., 1992; Sommer et al., 1991). Ca^{2+} permeable AMPARs, i.e. receptors lacking GluA2 subunits, can primarily be found at extrasynaptic sites. During synaptic long-term potentiation (LTP) Ca^{2+} permeable AMPARs are incorporated into synapses where they increase Ca^{2+} influx and strengthen synaptic transmission (Ehlers et al., 2007; Malinow and Malenka, 2002; Newpher and Ehlers, 2008; Tardin et al., 2003). Conversely, after long-lasting decreases in synaptic activity Ca^{2+} permeable AMPARs are incorporated at synapses thereby restoring synaptic function, a phenomenon termed homeostatic plasticity by synaptic scaling (Hou et al., 2008; Turrigiano and Nelson, 2004).

Since the GluA2 subunit is exceptionally important for AMPAR function, we sought to investigate whether autoimmune mechanisms involving ABs specifically targeting GluA2 directly influence basic properties of AMPAR function and if these processes are sufficient to induce characteristic disease symptoms of AMPAR encephalitis. Using purified patient

immunoglobulin G (IgG) ABs specifically directed against the GluA2 subunit we show that anti-GluA2 ABs lead to distinct changes in synaptic transmission by modifications in AMPAR composition and localization, and by synaptic scaling mechanisms involving enhanced synaptic incorporation of GluA1. These changes affect LTP in the hippocampus and induce characteristic behavioral changes *in-vivo*. Our results thus identify a novel immune-neuronal interaction that may underlie characteristic disease symptoms.

Results

Human autoantibodies against GluA2 induce synaptic insertion of inward rectifying AMPA receptors lacking GluA2

In this study, we used purified IgG fractions from plasma exchange material or serum samples of nine patients with autoimmune encephalitis and high-titer ABs against only the GluA2 subunit of the AMPAR (a-GluA2 IgG) and of a control patient without detectable antineuronal ABs (ct IgG). One IgG fraction was derived from an individual patient with very high titers of specific ABs to GluA2, and the other IgG fraction was derived from a group of eight patients (a-GluA2 IgG 1 and 2, respectively). According to previous reports, all patients presented with limbic encephalitis including severe memory dysfunction and seizures (Hoftberger et al., 2015; Lai et al., 2009). We tested the specificity of both purified IgG fractions and found exclusive plasma membrane binding of patient IgG on non-permeabilized GluA2:eGFP but not GluA1:eGFP transfected human embryonic kidney 293 (HEK293) cells and on synaptic spots of dissociated neurons. Patient IgG bound to the neuropil in the hippocampus of wildtype (wt) and GluA1 knockout (ko) mice, but not in GluA2 ko mice. Furthermore, affinity purification experiments with patient IgG in rat brain tissue combined with mass spectrometric analysis confirmed GluA2 as its main target (Figure S1). Thus, patient IgG fractions used in this study target the GluA2 subunit of the AMPAR at high specificity.

We first investigated the effect of a-GluA2 IgG on quantal AMPAR signaling by recording AMPAR mEPSCs in dissociated hippocampal neurons after 24 h preincubation with the purified IgG fractions. At a holding potential of -80 mV, mean mEPSC peak amplitudes and their cumulative probability were not significantly different between control preparations and a-GluA2 IgG treated preparations (ct IgG 44.4 ± 5.1 pA, a-GluA2 IgG 1 33.0 ± 4.3 pA, a-GluA2 IgG 2 42.7 ± 3.7 pA; mean \pm SEM, Figure 1A-C). At this holding potential, AMPARs of all subunit compositions contribute to the recorded miniature current. To selectively record currents from AMPARs containing the GluA2 subunit (non-inwardly rectifying AMPARs), neurons were depolarized and voltage clamped at a membrane potential of +40 mV. Under this condition, mEPSC amplitudes were decreased (ct IgG 21.0 ± 1.4 pA, a-GluA2 IgG 1 12.5 ± 0.5 pA, a-GluA2 IgG 2 14.7 ± 0.7 pA) and cumulative probability was shifted towards smaller amplitudes (Figure 2A, B, D) in neurons treated with a-GluA2 IgG fractions compared with control preparations. Under both conditions, the mean mEPSC frequency was reduced in a-GluA2 IgG incubated neurons (holding potential -80 mV: ct IgG 5.5 ± 1.0 Hz, a-GluA2 IgG 1 2.6 ± 0.6 Hz, a-GluA2 IgG 2 3.1 ± 0.5 Hz; +40 mV: ct IgG 2.0 ± 0.4 Hz, a-GluA2 IgG 1 0.8 ± 0.1 Hz, a-GluA2 IgG 2 0.9 ± 0.1 Hz) and the cumulative probability plots of inter-event intervals were shifted to greater values (Figure 1C and D). These findings, obtained in two independent a-GluA2 IgG samples, led us to hypothesize that a-GluA2 IgG results in a decrease of AMPARs containing the GluA2 subunit.

Next, we tested our hypothesis of reduced signaling derived from GluA2 containing AMPARs by adding 1-naphthyl acetyl spermine (NASPM). NASPM is a selective blocker of AMPARs lacking GluA2 that allows the differentiation between currents mediated by AMPARs with or without GluA2 at a holding potential of -80 mV (Koike et al., 1997). NASPM led to a significant reduction of the mean mEPSC peak amplitude of 31% and to a left-shift in the cumulative probability distribution towards smaller amplitudes in neurons that had been preincubated with a-GluA2 IgG (Figure 1E and F). This demonstrates that a significant proportion of AMPARs lacking GluA2 subunits contributes to AMPAR mEPSCs after preincubation with a-GluA2 IgG. In contrast, NASPM did not significantly alter mEPSCs in

control IgG treated neurons (Figure S2). These experiments suggest a compensatory synaptic incorporation of AMPARs lacking GluA2, most likely GluA1 homomers.

Antibodies against GluA2 lead to decrease of iontophoretically evoked AMPA receptor mediated EPSCs on the multisynaptic but not on the single-synapse level

To dissect pre- and postsynaptic mechanisms that might contribute to the observed changes in mEPSC amplitude and frequency, we performed iontophoretic application of L-glutamate to synapses of primary neurons using sharp electrodes with very thin openings. Depending on the stimulation strength, this procedure allows both, stimulation of single synapses and multi-synaptic stimulation of larger dendritic portions (Figure 2A and B; Figure S3). Single synapse stimulation revealed unchanged iontophoretically evoked AMPAR mediated EPSCs (ieEPSCs) at -80mV after pre-incubation with α -GluA2 IgG consistent with the analysis of the mEPSC amplitude. However, we found reduced ieEPSC amplitudes at increased stimulation strength when a multi-synaptic response was elicited (Figure 2B and C). These findings provide an explanation for the reduced frequency of spontaneous events, as they indicate a decrease in the number of glutamatergic synapses. This uncompensated loss of synapses may either be due to structural loss of glutamatergic synapses or due to 'silent' synapses without compensatory GluA1 incorporation and functional AMPAR signaling.

When we performed paired-pulse stimulation of individual synapses, we found rapid desensitization and prolonged monoexponential recovery from desensitization as a characteristic feature of AMPAR signaling. Preincubation with α -GluA2 IgG slowed the recovery from desensitization in the paired-pulse paradigm (Figure 2D) similarly to findings in neurons from GluA2 ko mice (Harvey et al., 2001) or in HEK293 cells with homomeric GluA1 receptors after transfection with only the GluA1 subunit (Grosskreutz et al., 2003). Thus, the altered recovery from receptor desensitization is consistent with a rearrangement of AMPAR subunits from GluA2 to GluA1.

Super-resolution imaging reveals a reduction in GluA2 but an increase in GluA1 subunits per synapse

To more directly test the hypothesis of a switch from GluA2 to GluA1 subunits, we analyzed the structural changes of synaptic AMPAR subunit composition and distribution in dissociated hippocampal neurons by direct stochastic optical reconstruction microscopy (dSTORM). Postsynaptic fields were identified by Homer1 staining and postsynaptic localizations of GluA1 or GluA2 expression were evaluated with respect to the Homer1 defined regions with a lateral resolution of about 20 nm (see methods and Figure S4 for detailed description). When we quantified the total dendritic postsynaptic spots as revealed by analysis of Homer1 regions, we found that upon incubation with α -GluA2 IgG the total mean areas of Homer1 regions were unchanged and the number of Homer1 density regions per dendrite length was slightly reduced (Figure 3A and B). Importantly, the amount of synaptic GluA2 localizations within the Homer1 defined regions was decreased after α -GluA2 IgG preincubation while the perisynaptic amount of GluA2 localizations was unchanged (Figure 3C and D). As synaptic AMPAR in the hippocampus regularly exist as GluA1/2 heterodimers (Henley and Wilkinson, 2016; Lu et al., 2009), we expected a similar reduction of GluA1 subunit expression due to AB-induced AMPAR internalization. By contrast, synaptic GluA1 density increased in synapses, with the perisynaptic amount of GluA1 localizations remaining unchanged (Figure 3E). Distance analysis of AMPAR subunits with respect to the nearest synaptic Homer region indicated that both GluA1 and GluA2 were more concentrated within a ~500 nm vicinity than would be expected if extrasynaptic receptor population were distributed homogeneously (Figure 3F). It was also in this vicinity that GluA2 receptor localizations were decreased and those of GluA1 were increased. Thus, in line with our functional experiments in primary neurons, these findings suggest AB-induced depletion of heteromeric synaptic AMPARs containing GluA2 along with an incorporation of GluA1 subunits.

Stereotactic intrahippocampal injection of human a-GluA2 IgG in mice induce AMPAR rearrangement as observed in dissociated hippocampal neurons

To elucidate the pathogenic mechanisms of GluA2 ABs in the brain, we evaluated AMPAR mediated synaptic transmission in the hippocampal network after stereotactic intrahippocampal injection of a-GluA2 IgG fractions in mice. The amount of injected human IgG detected in mice hippocampi was similar for control and a-GluA2 IgG (Figure S5A). Concomitant injection of FM1-43 dye that labels active synapses served as a marker in acute brain slices for verification that IgG fractions were applied to the correct recording site (Figure 4A). In some mice, specific binding of injected patient IgG fractions to the AMPAR GluA2 subunit *in vivo* was confirmed by immunoprecipitation of the bound human IgG. In the hippocampi of injected mice, human IgG reactivity to the AMPAR was exclusively found after a-GluA2 IgG injection (Figure S5B). Confocal analysis of AMPAR subunit expression in the hippocampal DG and CA1 region of mice after targeted intrahippocampal injection of purified IgG fractions confirmed the *in vitro* findings of synaptic downregulation of GluA2 obtained by super-resolution microscopy (Figure S5C-E).

In whole-cell patch-clamp recordings from granule cells (GC) in the dentate gyrus (DG) we electrically evoked EPSCs (eEPSCs) by stimulation of the lateral perforant path (LPP). Corroborating our cell culture findings, we did not find differences in the amplitudes of eEPSC between control and a-GluA2 IgG injected mice (ct IgG 109.8 ± 13.7 pA, a-GluA2 IgG 112.9 ± 13.8 pA; Figure 4B and C). Paired-pulse stimulation induced facilitation in the LPP-DG pathway, but showed no differences between the experimental groups, indicating unchanged presynaptic release probability (Figure 4D). However, when we analyzed large numbers of eEPSCs by peak scaled non-stationary fluctuation analysis (nsFA) that provides information on single-channel conductance (i) and the number of contributing channels (N), we found a decrease in the average number of channels from 56.4 ± 10.4 in control IgG to 30.8 ± 3.6 in slices from a-GluA2-IgG injected mice (Figure 4E) and an increase in single

channel conductance from 23.5 ± 3.5 pS in control IgG to 39.1 ± 6.6 pS in slices from a-GluA2 IgG injected mice. Similarly to our *in vitro* findings, mEPSC amplitudes in slices of a-GluA2 IgG injected mice but not in those of controls were decreased (ct IgG 10.1 ± 0.6 pA, a-GluA2 IgG 7.9 ± 0.4 pA) and cumulative probability plots were shifted to smaller amplitudes when slices were superfused with NASPM (Figure 4F and G and Figure S6). These results corroborate our findings in dissociated hippocampal neurons and indicate that hippocampal injection of pathogenic a-GluA2 IgG *in vivo* significantly increases the single channel conductance of the AMPAR, most likely resembling incorporation of AMPAR GluA1 homomers.

GluA1 knockout mice cannot compensate antibody-induced loss of GluA2 containing AMPA receptors

To test this hypothesis more rigorously, we used knockout mice lacking the GluA1 subunit (GluA1 ko) (Andrasfalvy et al., 2003). In contrast to wt mice, eEPSC amplitude in GluA1 ko mice was reduced upon intrahippocampal injection of a-GluA2 IgG (ct IgG 65.6 ± 8.1 pA, a-GluA2 IgG 42.1 ± 5.5 pA; Figure 5A and B). Facilitation induced by paired-pulse stimulation was unchanged confirming the postsynaptic origin of the observed decline of eEPSC amplitude (Figure 5C). Moreover, nsFA revealed a persistent decrease in active channels contributing to eEPSCs (ct IgG 34.9 ± 5.9 , a-GluA2 IgG 19.5 ± 3.5 ; Figure 5D) but the compensatory increase in single-channel conductivity observed in wt neurons was no longer present (ct IgG 33.5 ± 11.6 pS, a-GluA2 IgG 26.9 ± 7.7 pS). Corroborating these findings, mEPSC amplitudes were decreased in slices of GluA1 ko mice after a-GluA2 IgG injection (Figure 5E). These data substantiate the hypothesis of synaptic scaling in wt neurons induced by increased incorporation of GluA1 subunits resulting in AMPARs with increased channel conductance.

Antibodies against GluA2 impair long-term synaptic plasticity in the Schaffer-collateral-CA1 pathway

Defective memory and cognition are key features of patients suffering from autoimmune encephalitis with ABs to the AMPAR (Lai et al., 2009). We therefore analyzed synaptic plasticity by measuring long-term potentiation (LTP) in the Schaffer collateral (SC) – CA1 pathway of the hippocampus 24 h after stereotactic injection of IgG fractions in the CA1 region of the hippocampus (Figure 6A). Input-output local field excitatory postsynaptic potential (fEPSP) measurements of basal glutamatergic transmission in the SC – CA1 synapses before potentiation were unchanged in both experimental groups corroborating our findings in eEPSC recordings (Figure 6B). However, after induction of LTP by theta burst stimulation (TBS), we observed impaired potentiation of fEPSP slope in GluA2 IgG injected mice as compared to controls (Figure 6C). Quantification during the late phase (60 – 80 min after TBS) revealed strongly reduced slope values in these mice (ct IgG $41.3 \pm 9.0\%$, a-GluA2 $16.7 \pm 5.8\%$; Figure 6C) suggesting heavily impaired synaptic plasticity in the region of a-GluA2 IgG deposition. Paired-pulse facilitation after single stimuli (interstimulus interval 100 ms) was present in both conditions and unchanged before and after LTP induction (Figure 6D), thus underlining the postsynaptic nature of LTP impairment. These data demonstrate that stereotactic intrahippocampal microinjection of human a-GluA2 IgG fractions in mice severely impair LTP in the SC – CA1 pathway.

Mice develop memory deficits and increased anxiety-like behavior in different passive-transfer models using human antibodies to GluA2

Patients with AMPAR encephalitis are characterized by severely affected limbic system with strong memory impairment as a key symptom of disease. To analyze the impact of a-GluA2 ABs in behaving animals, we used two independent passive-transfer animal models: (i) stereotactic injections of patient IgG directly into the CA1 and CA3 region and the DG of the

hippocampus on both sides (Haselmann et al., 2015) (Figure 7A and B); (ii) continuous two week infusion of IgG fractions into both lateral ventricles (Planaguma et al., 2015) (Figure 7F and G). General locomotor activity and total time spent exploring the objects during the NOR test (internal control) was unchanged in animals of both experimental groups and both application procedures (Figure 7C and H and Figure S7). However, we consistently found memory impairment as revealed by a decrease of the object recognition index (Figure 7D and J). With chronic intraventricular infusion the experimental setting allowed testing at several time points during and after the pump infusion period. Here, we found progressive deterioration of memory function over time with a maximum at day 18 when pump infusion had just stopped few days before. With longer recovery (day 25) the object recognition had recovered with an index similar to normalized control group levels (Figure 7J). When we tested for anxiety-like behavior using an elevated plus maze (EPM) or a black-and-white (BW) maze, we found reduced time spent at and less entries into the open arm or white sector in the groups receiving α -GluA2 IgG, respectively, indicating increased anxiety-like behavior (Figure 7E and K and Figure S7). Thus, our two independent passive-transfer animal models for *in vivo* application of α -GluA2 ABs induce typical signs of disease in the recipient mice thus fulfilling the Koch-Witebsky criteria of an autoimmune disease (Rose and Bona, 1993).

Discussion

By combining various electrophysiological techniques, super-resolution imaging, and *in vitro* and *in vivo* analysis including passive-transfer experiments we here demonstrate that pathogenic human antibodies against GluA2 provoke a rearrangement of AMPAR subunits in mice. This AMPAR subunits rearrangement provides a unique and disease-relevant novel concept of direct immune-neuronal interaction to explain consequences of encephalitis and the impaired memory formation in the patients.

Synaptic scaling as a mechanism in AMPAR encephalitis

Here we show that human α -GluA2 ABs provoke a compensatory increase in GluA1 subunits. This conclusion is based on the following findings: first, only those neurons preincubated with anti-GluA ABs showed inward rectification and block by endogenous spermine upon depolarization which are characteristic properties of GluA1 homomeric AMPARs (Verdoorn et al., 1991). Second, normal mEPSC and single synapse ieEPSC amplitude indicate functional compensation. Third, the slowed recovery from desensitization in dissociated cells indicates receptor rearrangement as AMPARs lacking the GluA2 subunit show in general faster desensitization kinetics (Mosbacher et al., 1994). Fourth, *d*STORM analysis in primary neurons confirmed loss of synaptic GluA2 containing AMPARs and compensatory synaptic incorporation of GluA1 subunits. Fifth, the single channel conductance was increased in wt mice after intrahippocampal injection of anti-GluA2 ABs consistent with a large single channel conductance of GluA1 homomeric AMPARs (Sommer et al., 1991; Swanson et al., 1997). Finally, the hypothesis of compensatory synaptic accumulation of GluA1 homomeric AMPARs was most directly tested by analysis of stereotactic injection of antibodies against GluA2 in knock-out mice deficient for GluA1. In these knock-out mice the single channel conductance did not increase consistent with their inability to compensate by GluA1 homomeric AMPARs. Thus, human α -GluA2 ABs induce a compensatory synaptic incorporation of GluA1 homomeric AMPARs, resembling some aspects of synaptic scaling (Hou et al., 2008; Soares et al., 2013; Turrigiano, 2008).

Importantly, the increased conductance, greater permeability for Ca^{2+} , slower recovery after desensitization, and receptor rectification of the newly incorporated AMPAR may provoke pathological excitatory neurotransmission. This could thus provide an explanation for disease symptoms resulting from hyperexcitability such as epileptic seizures.

Pathophysiology of GluA2 antibodies and comparison to genetic interference with GluA2

In contrast to germline ko models of GluA2, cell-specific knockout or knockdown models of the AMPAR GluA2 subunit share striking similarities with the pathomechanisms induced by anti-GluA2 ABs reported here (Lu et al., 2009). In GluA2-deficient neurons, mEPSC amplitudes are largely preserved at resting membrane potential but their rectification index is strongly reduced (Altimimi and Stellwagen, 2013; Gainey et al., 2009). Moreover, similar to our recordings, the frequency of mEPSCs at resting membrane potential is reduced in GluA2-deficient neurons (Lu et al., 2009; Panicker et al., 2008).

Corresponding to our findings of reduced frequency of quantal currents and reduced Homer1 clusters, we found a decrease in ieEPSC amplitudes only when iontophoretic glutamate application stimulated adjacent synapses along the dendrite and not when it was restricted to an individual synapse in primary neurons. These observations are most likely caused by the loss of synaptic GluA2 containing AMPARs leading to a proportion of silent synapses or to a reduced total number of synapses. This observation is in good agreement with partial silencing of synapses and reduced absolute AMPAR expression in neurons deficient of GluA2 AMPAR subunits (Lu et al., 2009; Sans et al., 2003). In GluA2 deficient neurons, two different types of excitatory synapses have been described; one type that is silenced after losing GluA2 AMPARs and another type that can be rescued by mainly GluA1 homomeric AMPARs (Lu et al., 2009). Accordingly, after unselective depletion of more than 50% of AMPARs, neurons are able to maintain the amplitude of AMPAR quantal currents suggesting prevalent depletion of the extrasynaptic AMPAR reserve pool (Schroeter et al., 2015).

AMPA receptor autoantibodies and effects on synaptic plasticity and cognitive function

During synaptic LTP, activated synapses recruit extrasynaptic AMPARs to strengthen synaptic transmission (Bassani et al., 2013; Tardin et al., 2003). Previous studies have

demonstrated that the induction of LTP strongly depends on the number of available AMPARs in the membrane but is independent of their subunit composition (Granger et al., 2013). Since reduction of GluA2-containing AMPARs was probably compensated by synaptic incorporation of non-GluA2 AMPARs, the impairment of LTP formation in our experiments could be due to a reduction of readily available extrasynaptic AMPARs. Indeed, previous studies have provided evidence that a reduction of the extrasynaptic AMPAR reserve pool may significantly impair the capability of synaptic potentiation (Schroeter et al., 2015).

These deficits in synaptic plasticity (homeostatic and Hebbian) most likely account for the behavioral abnormalities observed in the two independent passive-transfer models using α -GluA2 ABs reported here. Continuous long-term application of GluA2 ABs with osmotic pumps and by repeated microinjection both consistently afflicted memory and cognition. Since all these behavioral alterations follow the microinjection to a rather confined local distribution of the applied IgG preparations in the hippocampus, the pathophysiology is likely linked to limbic structures. This is in line with the typical signs of confusion and difficulties in forming new memories as seen in patients with AMPAR-mediated autoimmune encephalitis (Hoftberger et al., 2015; Joubert et al., 2015).

Future studies need to evaluate if the concept of AB-induced pathogenic changes in receptor composition will also apply to other entities in the expanding spectrum of AB-associated CNS disorders.

Author contributions

Conceptualization, C.G., S.H., J.D.; Methodology, H.H., C.G., F.M., J.D., Software, S.D., Validation, S.D., S.H., C.G., Investigation, H.H., F.M., C.W., J.P., B.G., M.P-P., F.D., N.K., K.K., Writing – Original Draft, C.G., H.H., Writing – Review & Editing, C.G., H.H., S.H., J.D., S.D., N.K., Resources, C.G., J.C., J.D., Funding Acquisition, C.G., S.D., J.D.

Acknowledgements

We thank C. Sommer (Jena) for providing expert technical assistance in animal experiments, immunohistology, and cell culture preparation. We thank R. Sprengel for providing GluA1 and GluA2 knockout mice. We thank Klaus V. Toyka for critical reading this manuscript. This work was supported by the Deutsche Forschungsgemeinschaft (CRC-TR 166 [TP B2 to C.G. and S.D.], GE2519_3-1 to C.G.), by the IZKF and CSCC Jena to C.G.). The authors declare no conflict of interest.

References

- Altimimi, H.F., and Stellwagen, D. (2013). Persistent synaptic scaling independent of AMPA receptor subunit composition. *J Neurosci* 33, 11763-11767.
- Andrasfalvy, B.K., Smith, M.A., Borchardt, T., Sprengel, R., and Magee, J.C. (2003). Impaired regulation of synaptic strength in hippocampal neurons from GluR1-deficient mice. *J Physiol* 552, 35-45.
- Bassani, S., Folci, A., Zapata, J., and Passafaro, M. (2013). AMPAR trafficking in synapse maturation and plasticity. *Cell Mol Life Sci* 70, 4411-4430.
- Bowie, D., and Mayer, M.L. (1995). Inward rectification of both AMPA and kainate subtype glutamate receptors generated by polyamine-mediated ion channel block. *Neuron* 15, 453-462.
- Bredt, D.S., and Nicoll, R.A. (2003). AMPA receptor trafficking at excitatory synapses. *Neuron* 40, 361-379.
- Burnashev, N., Monyer, H., Seeburg, P.H., and Sakmann, B. (1992). Divalent ion permeability of AMPA receptor channels is dominated by the edited form of a single subunit. *Neuron* 8, 189-198.

- Dalmau, J., Geis, C., and Graus, F. (2017). Autoantibodies to Synaptic Receptors and Neuronal Cell Surface Proteins in Autoimmune Diseases of the Central Nervous System. *Physiol Rev* 97, 839-887.
- Dani, A., Huang, B., Bergan, J., Dulac, C., and Zhuang, X. (2010). Superresolution imaging of chemical synapses in the brain. *Neuron* 68, 843-856.
- De Bruijn, M.A., and Titulaer, M.J. (2016). Anti-NMDAR encephalitis and other glutamate and GABA receptor antibody encephalopathies. *Handb Clin Neurol* 133, 199-217.
- Ehlers, M.D., Heine, M., Groc, L., Lee, M.C., and Choquet, D. (2007). Diffusional trapping of GluR1 AMPA receptors by input-specific synaptic activity. *Neuron* 54, 447-460.
- Gainey, M.A., Hurvitz-Wolff, J.R., Lambo, M.E., and Turrigiano, G.G. (2009). Synaptic scaling requires the GluR2 subunit of the AMPA receptor. *J Neurosci* 29, 6479-6489.
- Geis, C., Weishaupt, A., Hallermann, S., Grunewald, B., Wessig, C., Wultsch, T., Reif, A., Byts, N., Beck, M., Jablonka, S., *et al.* (2010). Stiff person syndrome-associated autoantibodies to amphiphysin mediate reduced GABAergic inhibition. *Brain* 133, 3166-3180.
- Granger, A.J., Shi, Y., Lu, W., Cerpas, M., and Nicoll, R.A. (2013). LTP requires a reserve pool of glutamate receptors independent of subunit type. *Nature* 493, 495-500.
- Grosskreutz, J., Zoerner, A., Schlesinger, F., Krampfl, K., Dengler, R., and Bufler, J. (2003). Kinetic properties of human AMPA-type glutamate receptors expressed in HEK293 cells. *European Journal of Neuroscience* 17, 1173-1178.
- Grover, L.M., Kim, E., Cooke, J.D., and Holmes, W.R. (2009). LTP in hippocampal area CA1 is induced by burst stimulation over a broad frequency range centered around delta. *Learn Mem* 16, 69-81.
- Harmel, N., Cokic, B., Zolles, G., Berkefeld, H., Mauric, V., Fakler, B., Stein, V., and Klocker, N. (2012). AMPA Receptors Commandeer an Ancient Cargo Exporter for Use as an Auxiliary Subunit for Signaling. *Plos One* 7.
- Harvey, S.C., Koster, A., Yu, H., Skolnick, P., Baumbarger, P., and Nisenbaum, E.S. (2001). AMPA receptor function is altered in GLUR2-deficient mice. *J Mol Neurosci* 17, 35-43.

- Haselmann, H., Ropke, L., Werner, C., Kunze, A., and Geis, C. (2015). Interactions of Human Autoantibodies with Hippocampal GABAergic Synaptic Transmission - Analyzing Antibody-Induced Effects *ex vivo*. *Front Neurol* 6, 136.
- Henley, J.M., and Wilkinson, K.A. (2016). Synaptic AMPA receptor composition in development, plasticity and disease. *Nat Rev Neurosci* 17, 337-350.
- Hoftberger, R., van Sonderen, A., Leyboldt, F., Houghton, D., Geschwind, M., Gelfand, J., Paredes, M., Sabater, L., Saiz, A., Titulaer, M.J., *et al.* (2015). Encephalitis and AMPA receptor antibodies: Novel findings in a case series of 22 patients. *Neurology* 84, 2403-2412.
- Hollmann, M., and Heinemann, S. (1994). Cloned glutamate receptors. *Annu Rev Neurosci* 17, 31-108.
- Hou, Q., Zhang, D., Jarzylo, L., Haganir, R.L., and Man, H.Y. (2008). Homeostatic regulation of AMPA receptor expression at single hippocampal synapses. *Proc Natl Acad Sci U S A* 105, 775-780.
- Isaac, J.T., Ashby, M.C., and McBain, C.J. (2007). The role of the GluR2 subunit in AMPA receptor function and synaptic plasticity. *Neuron* 54, 859-871.
- Jensen, V., Kaiser, K.M.M., Borchardt, T., Adelman, G., Rozov, A., Burnashev, N., Brix, C., Frotscher, M., Andersen, P., Hvalby, O., *et al.* (2003). A juvenile form of postsynaptic hippocampal long-term potentiation in mice deficient for the AMPA receptor subunit GluR-A. *Journal of Physiology-London* 553, 843-856.
- Joubert, B., Kerschen, P., Zekeridou, A., Desestret, V., Rogemond, V., Chaffois, M.O., Ducray, F., Larrue, V., Daubail, B., Idbaih, A., *et al.* (2015). Clinical Spectrum of Encephalitis Associated With Antibodies Against the alpha-Amino-3-Hydroxy-5-Methyl-4-Isoxazolepropionic Acid Receptor: Case Series and Review of the Literature. *JAMA Neurol* 72, 1163-1169.
- Kilkenny, C., Browne, W.J., Cuthill, I.C., Emerson, M., and Altman, D.G. (2010). Improving bioscience research reporting: the ARRIVE guidelines for reporting animal research. *PLoS Biol* 8, e1000412.

- Koike, M., Iino, M., and Ozawa, S. (1997). Blocking effect of 1-naphthyl acetyl spermine on Ca²⁺-permeable AMPA receptors in cultured rat hippocampal neurons. *Neurosci Res* 29, 27-36.
- Lai, M., Hughes, E.G., Peng, X., Zhou, L., Gleichman, A.J., Shu, H., Mata, S., Kremens, D., Vitaliani, R., Geschwind, M.D., *et al.* (2009). AMPA receptor antibodies in limbic encephalitis alter synaptic receptor location. *Ann Neurol* 65, 424-434.
- Lu, W., Shi, Y., Jackson, A.C., Bjorgan, K., Doring, M.J., Sprengel, R., Seeburg, P.H., and Nicoll, R.A. (2009). Subunit composition of synaptic AMPA receptors revealed by a single-cell genetic approach. *Neuron* 62, 254-268.
- MacGillavry, H.D., Song, Y., Raghavachari, S., and Blanpied, T.A. (2013). Nanoscale scaffolding domains within the postsynaptic density concentrate synaptic AMPA receptors. *Neuron* 78, 615-622.
- Malinow, R., and Malenka, R.C. (2002). AMPA receptor trafficking and synaptic plasticity. *Annu Rev Neurosci* 25, 103-126.
- Mosbacher, J., Schoepfer, R., Monyer, H., Burnashev, N., Seeburg, P.H., and Ruppertsberg, J.P. (1994). A molecular determinant for submillisecond desensitization in glutamate receptors. *Science* 266, 1059-1062.
- Murnick, J.G., Dube, G., Krupa, B., and Liu, G. (2002). High-resolution iontophoresis for single-synapse stimulation. *J Neurosci Methods* 116, 65-75.
- Newpher, T.M., and Ehlers, M.D. (2008). Glutamate receptor dynamics in dendritic microdomains. *Neuron* 58, 472-497.
- Panicker, S., Brown, K., and Nicoll, R.A. (2008). Synaptic AMPA receptor subunit trafficking is independent of the C terminus in the GluR2-lacking mouse. *Proc Natl Acad Sci U S A* 105, 1032-1037.
- Panzer, J.A., Gleichman, A.J., and Lynch, D.R. (2014). Glutamatergic autoencephalitis: an emerging field. *J Neural Transm (Vienna)* 121, 957-968.

- Peca, J., Feliciano, C., Ting, J.T., Wang, W., Wells, M.F., Venkatraman, T.N., Lascola, C.D., Fu, Z., and Feng, G. (2011). Shank3 mutant mice display autistic-like behaviours and striatal dysfunction. *Nature* 472, 437-442.
- Peng, X., Hughes, E.G., Moscato, E.H., Parsons, T.D., Dalmau, J., and Balice-Gordon, R.J. (2015). Cellular plasticity induced by anti-alpha-amino-3-hydroxy-5-methyl-4-isoxazolepropionic acid (AMPA) receptor encephalitis antibodies. *Ann Neurol* 77, 381-398.
- Planaguma, J., Haselmann, H., Mannara, F., Petit-Pedrol, M., Grunewald, B., Aguilar, E., Ropke, L., Martin-Garcia, E., Titulaer, M.J., Jercog, P., *et al.* (2016). Ephrin-B2 prevents N-methyl-D-aspartate receptor antibody effects on memory and neuroplasticity. *Ann Neurol* 80, 388-400.
- Planaguma, J., Leypoldt, F., Mannara, F., Gutierrez-Cuesta, J., Martin-Garcia, E., Aguilar, E., Titulaer, M.J., Petit-Pedrol, M., Jain, A., Balice-Gordon, R., *et al.* (2015). Human N-methyl D-aspartate receptor antibodies alter memory and behaviour in mice. *Brain* 138, 94-109.
- Raymond, C.R. (2007). LTP forms 1, 2 and 3: different mechanisms for the "long" in long-term potentiation. *Trends Neurosci* 30, 167-175.
- Rose, N.R., and Bona, C. (1993). Defining criteria for autoimmune diseases (Witebsky's postulates revisited). *Immunol Today* 14, 426-430.
- Sans, N., Vissel, B., Petralia, R.S., Wang, Y.X., Chang, K., Royle, G.A., Wang, C.Y., O'Gorman, S., Heinemann, S.F., and Wenthold, R.J. (2003). Aberrant formation of glutamate receptor complexes in hippocampal neurons of mice lacking the GluR2 AMPA receptor subunit. *J Neurosci* 23, 9367-9373.
- Schikorski, T., and Stevens, C.F. (1997). Quantitative ultrastructural analysis of hippocampal excitatory synapses. *J Neurosci* 17, 5858-5867.
- Schroeter, A., Wen, S., Molders, A., Erlenhardt, N., Stein, V., and Klocker, N. (2015). Depletion of the AMPAR reserve pool impairs synaptic plasticity in a model of hepatic encephalopathy. *Mol Cell Neurosci* 68, 331-339.

- Schwenk, J., Harmel, N., Brechet, A., Zolles, G., Berkefeld, H., Muller, C.S., Bildl, W., Baehrens, D., Huber, B., Kulik, A., *et al.* (2012). High-resolution proteomics unravel architecture and molecular diversity of native AMPA receptor complexes. *Neuron* 74, 621-633.
- Shimshek, D.R., Bus, T., Kim, J., Mihaljevic, A., Mack, V., Seeburg, P.H., Sprengel, R., and Schaefer, A.T. (2005). Enhanced odor discrimination and impaired olfactory memory by spatially controlled switch of AMPA receptors. *Plos Biology* 3, 2017-2030.
- Soares, C., Lee, K.F., Nassrallah, W., and Beique, J.C. (2013). Differential subcellular targeting of glutamate receptor subtypes during homeostatic synaptic plasticity. *J Neurosci* 33, 13547-13559.
- Sommer, B., Kohler, M., Sprengel, R., and Seeburg, P.H. (1991). RNA editing in brain controls a determinant of ion flow in glutamate-gated channels. *Cell* 67, 11-19.
- Sommer, C., Weishaupt, A., Brinkhoff, J., Biko, L., Wessig, C., Gold, R., and Toyka, K.V. (2005). Paraneoplastic stiff-person syndrome: passive transfer to rats by means of IgG antibodies to amphiphysin. *Lancet* 365, 1406-1411.
- Swanson, G.T., Kamboj, S.K., and Cull-Candy, S.G. (1997). Single-channel properties of recombinant AMPA receptors depend on RNA editing, splice variation, and subunit composition. *J Neurosci* 17, 58-69.
- Tardin, C., Cognet, L., Bats, C., Lounis, B., and Choquet, D. (2003). Direct imaging of lateral movements of AMPA receptors inside synapses. *EMBO J* 22, 4656-4665.
- Traynelis, S.F., Silver, R.A., and Cull-Candy, S.G. (1993). Estimated conductance of glutamate receptor channels activated during EPSCs at the cerebellar mossy fiber-granule cell synapse. *Neuron* 11, 279-289.
- Turrigiano, G.G. (2008). The self-tuning neuron: synaptic scaling of excitatory synapses. *Cell* 135, 422-435.
- Turrigiano, G.G., and Nelson, S.B. (2004). Homeostatic plasticity in the developing nervous system. *Nat Rev Neurosci* 5, 97-107.

- Verdoorn, T.A., Burnashev, N., Monyer, H., Seeburg, P.H., and Sakmann, B. (1991). Structural determinants of ion flow through recombinant glutamate receptor channels. *Science* 252, 1715-1718.
- Zimmer, T., Biskup, C., Dugarmaa, S., Vogel, F., Steinbis, M., Bohle, T., Wu, Y.S., Dumaine, R., and Benndorf, K. (2002). Functional expression of GFP-linked human heart sodium channel (hH1) and subcellular localization of the α subunit in HEK293 cells and dog cardiac myocytes. *Journal of Membrane Biology* 186, 1-12.

Figures and Figure legends

Figure 1. Human autoantibodies against GluA2 induce synaptic insertion of inward rectifying AMPA receptors lacking GluA2

(A) Example traces showing mEPSCs from individual neurons preincubated 24 h with ct IgG, a-GluA2 IgG 1 and a-GluA2 IgG 2 at holding potential -80 (left) and +40 mV (right).

(B) Averaged single mEPSC traces from individual neurons preincubated with ct IgG, a-GluA2 IgG 1 and a-GluA2 IgG 2 at holding potential -80 and +40 mV.

(C) Mean mEPSC amplitudes at -80 mV are not different upon a-GluA2 IgG treatment whereas mEPSC frequency is reduced for a-GluA2 IgG 1 (ct vs. a-GluA2 1 $p = 0.024$) and interevent intervals are increased for both a-GluA2 IgGs (ct vs. a-GluA2 1 $p < 0.001$; ct vs. a-GluA2 2 $p < 0.001$); $n_{(ct\ IgG)} = 15$, $n_{(a-GluA2\ IgG\ 1)} = 16$, $n_{(a-GluA2\ IgG\ 2)} = 15$ for all bar graphs, $n_{(ct\ IgG)} = 450$, $n_{(a-GluA2\ IgG\ 1)} = 450$, $n_{(a-GluA2\ IgG\ 2)} = 450$ for cumulative probability plots with 30 randomly chosen mEPSCs per neuron.

(D) At depolarized membrane potential (+40 mV) mean mEPSC amplitudes (ct IgG vs. a-GluA2 IgG 1 $p < 0.001$; ct IgG vs. a-GluA2 IgG 2 $p = 0.006$) and frequencies (ct IgG vs. a-GluA2 IgG 1 $p = 0.012$; ct IgG vs. a-GluA2 IgG 2 $p = 0.044$) are reduced in neurons incubated in a-GluA2 IgG. Cumulative probability plots show an increased proportion of small amplitudes (ct vs. GluA2 1 and 2 $p < 0.001$) and longer interevent intervals in a-GluA2-IgG treated neurons (ct vs. GluA2 1 and 2 $p < 0.001$); $n_{(ct\ IgG)} = 15$, $n_{(a-GluA2\ IgG\ 1)} = 16$, $n_{(a-GluA2\ IgG\ 2)} = 15$ for all bar graphs, $n_{(ct\ IgG)} = 450$, $n_{(a-GluA2\ IgG\ 1)} = 450$, $n_{(a-GluA2\ IgG\ 2)} = 450$ for cumulative probability plots with 30 randomly chosen mEPSCs per neuron.

(E) Example traces showing mEPSCs from individual neurons preincubated 24 h with a-GluA2 IgG 1 or a-GluA2 IgG 1 + NASPM.

(F) In an independent experimental series, block of non-GluA2 containing receptors by NASPM leads to a further decrease of mean mEPSC amplitudes in a-GluA2 IgG 1 incubated neurons (blue) as compared to a-GluA2 IgG 1 incubation alone (red). Cumulative probability plot of mEPSCs shows an increased proportion of small amplitudes in a-GluA2 IgG 1 +

NASPM treated neurons ($p < 0.001$). Mean frequency of α -GluA2 IgG 1 and NASPM incubated neurons is not significantly different ($p = 0.070$) similar as cumulative probability of mEPSC interevent intervals ($p = 0.15$); $n_{(\alpha\text{-GluA2 IgG 1})} = 15$, $n_{(\alpha\text{-GluA2 IgG 1} + \text{NASPM})} = 14$, $n_{(\alpha\text{-GluA2 IgG 1})} = 420$, $n_{(\alpha\text{-GluA2 IgG 1} + \text{NASPM})} = 420$ for cumulative probability plots with 30 randomly chosen mEPSCs per neuron. Comparisons were performed using ANOVA on Ranks with Dunn's post-hoc correction for group comparisons and the Mann-Whitney U-test for comparison of two groups. Kolmogorov-Smirnov-test was used for cumulative probability plots.

See also Figure S2.

Figure 2. Antibodies against GluA2 lead to decrease of iontophoretically evoked AMPA receptor mediated EPSCs on the multisynaptic but not on the single-synapse level.

(A) Experimental setup to record (rec) iontophoretically evoked single synapse EPSCs (ieEPSCs) in primary hippocampal neurons. Synaptic spots are labeled by intravital FM1-43 dye staining (red). Glutamate (with Alexa555 dye) is applied to individual synaptic spots on proximal dendrites by iontophoretic stimulation (stim; 1 ms duration) using a sharp microelectrode with thin opening ($\sim 60\text{M}\Omega$; scale bar: $20\ \mu\text{m}$).

(B) Example traces of glutamate ieEPSCs from ct IgG (black) and α -GluA2 IgG incubated (red) neurons with 100 nA and 750 nA glutamate eject current for single synapse and multi-synapse stimulation, respectively.

(C) In hippocampal neurons with α -GluA2 IgG preincubation ieEPSC peak amplitudes are unchanged after single synapse stimulation (100 nA eject current) but are severely decreased after multisynaptic stimulation (750 nA eject current; $n_{(\text{ct IgG})} = 18$, $n_{(\alpha\text{-GluA2 IgG})} = 12$; $p = 0.004$, Mann-Whitney U test).

(D) Paired-pulse stimulation is performed at the indicated inter-pulse intervals (IPI) with 750 nA eject current. In neurons with GluA2 ABs preincubation recovery from desensitization is prolonged as compared to controls ($n_{(\text{ct IgG})} = 16$, $n_{(\alpha\text{-GluA2 IgG})} = 14$; $p < 0.001$, two-way-ANOVA with Holm-Sidak post-hoc analysis). Recovery after desensitization was fitted by a two exponential equation and τ was determined from the fitted curves as $1/e$ of recovery.

See also Figure S3.

Figure 3. Super-resolution imaging reveals a reduction in GluA2 but an increase in GluA1 subunits per synapse.

(A) *d*STORM recording of postsynaptic areas defined by Homer1 immunostaining expressing post-synaptic boutons along a primary hippocampal neuron dendrite (white line). Image depicts Homer1 clusters after alpha shape clustering ($\alpha = 40$). Scale bar: 2 μm .

(B) Homer1 area is unchanged upon preincubation with a-GluA2 IgG. $n_{(\text{ct-IgG})} = 907$ (synapses), $n_{(\text{a-GluR2-IgG})} = 1006$ (synapses); $p = 0.978$. Homer1 positive postsynaptic spots per dendrite length are reduced in presence of a-GluA2 IgG ($n_{(\text{ct-IgG})} = 31$ [dendrites], $n_{(\text{a-GluR2-IgG})} = 37$ [dendrites]; $p = 0.006$, Mann-Whitney U test).

(C) Two-color *d*STORM showing AMPAR GluA2 subunit localizations and postsynaptic spots (Homer1) along a dendrite (left; scale bar: 500 nm). Right: example of a Homer1 cluster that is isotropically extended by 50 nm to define postsynaptic area (see methods for detailed information). Spots in magenta represent GluA2 receptor localizations (scale bar: 200 nm).

(D) Synaptic GluA2 localizations are decreased after application of a-GluR2 antibodies whereas extrasynaptic density is unchanged ($n_{(\text{ct-IgG})} = 477$ [synapses], $n_{(\text{a-GluR2-IgG})} = 726$ [synapses], $p < 0.001$, Mann-Whitney U test); 5 independent experiments.

(E) Synaptic GluA1 localizations are increased after application of a-GluR2 IgG ($p < 0.001$, Mann-Whitney U test), whereas density of extrasynaptic GluR1 receptors is unchanged ($n_{(\text{ct-IgG})} = 529$ [synapses], $n_{(\text{a-GluR2-IgG})} = 473$ [synapses]); 5 independent experiments.

(F) Frequency distribution histogram of receptor-cluster distances shows how GluA2 and GluA2 receptor subunits are located with respect to the postsynaptic marker Homer1. a-GluA2 IgG preincubated synapses show reduced GluA2 expression in the area of Homer1 defined postsynaptic fields. Green (data from the ct-IgG group) and blue (data from the a-GluA2 IgG group) lines depict simulation how extrasynaptic signals would behave if distributed in a random fashion.

See also Figure S4.

Figure 4. Stereotactic intrahippocampal injection of human α -GluA2 IgG in mice induce AMPAR rearrangement as observed in dissociated hippocampal neurons

(A) Recording situation in acute hippocampal slices after stereotactic microinjection of purified IgG preparations. The location of human IgG deposition in the dentate gyrus (DG) is shown in green by labeling with co-injected FM1-43 dye. Stimulation (stim) is performed in the lateral perforant path (LPP) and eEPSCs are recorded (rec) from DG granule cells (GC) (scale bar: 200 μ m).

(B) Example traces and average of LPP – GC evoked eEPSCs with averaged trace from ct-IgG (grey) and α -GluA2 IgG 1 (red) injected mice at resting membrane potential. Note that average peak amplitude is similar but distribution and shape of individual traces are different in the experimental groups.

(C) At resting membrane potential quantitative analysis of eEPSC peak amplitude is unchanged in both experimental groups ($n_{\text{ct IgG}} = 15$, $n_{\alpha\text{-GluA2 IgG}} = 17$).

(D) Paired-pulse facilitation as indicated by the index of the second vs. the first pulse (PP ratio) is not different in both experimental groups ($n_{\text{ct IgG}} = 13$, $n_{\alpha\text{-GluA2 IgG}} = 15$).

(E) Non-stationary fluctuation analysis (nsFA) of peak-scaled eEPSCs. Exemplary plot of α -GluA2 (red) and ct (black) IgG injected animals (30 bins per condition, median \pm SD; $n_{\text{ct IgG}} = 137$ traces; $n_{\alpha\text{-GluA2 IgG}} = 139$). Slope indicating single-channel conductance is increased in recordings of the α -GluA2 IgG injected mouse, whereas the number of channels is reduced as revealed by the equation of the hyperbola. Quantification of nsFA reveals a decrease of active receptors in α -GluA2 IgG treated animals ($n_{\text{ct IgG}} = 15$, $n_{\alpha\text{-GluA2 IgG}} = 16$; $p = 0.017$; Mann-Whitney U test). nsFA estimated single channel conductance is increased in α -GluA2 IgG injected mice ($n_{\text{ct IgG}} = 15$, $n_{\alpha\text{-GluA2 IgG}} = 16$; $p = 0.038$; Mann-Whitney U test).

(F) Example traces of mEPSC recordings from α -GluA2 IgG injected brain slices treated with (blue) or without NASPM (red).

(G) Mean mEPSC amplitudes and cumulative probability plots at -80 mV of granule cells after a-GluA2-IgG injections before and after perfusion with NASPM. Decreased amplitudes ($n_{(a-GluA2\ IgG)} = 16$, $n_{(a-GluA2\ IgG + NASPM)} = 16$; $p=0.009$; t-test) and an increased proportion of small amplitudes in the cumulative probability plot after NASPM administration ($n_{(a-GluA2\ IgG)} = 480$, $n_{(a-GluA2\ IgG + NASPM)} = 480$ for cumulative probability plots with 30 randomly chosen mEPSCs per neuron; $p<0.001$; Kolmogorov-Smirnov-test) indicate block of AMPARs without GluA2 subunit in brain slices of these mice. mEPSC frequency is unchanged after IgG injections before and after perfusion with NASPM ($n_{(a-GluA2\ IgG)} = 16$, $n_{(a-GluA2\ IgG + NASPM)} = 16$ and $n_{(a-GluA2\ IgG)} = 480$, $n_{(a-GluA2\ IgG + NASPM)} = 480$ for cumulative probability plots with 30 randomly chosen mEPSCs per neuron).

See also Figure S5 and S6.

Figure 5. GluA1 knockout mice cannot compensate antibody-induced loss of GluA2 containing AMPA receptors

(A) Example traces and averages of LPP–GC eEPSCs from slices of GluA1 ko mice injected with ct IgG (grey) and a-GluA2 IgG (red), respectively.

(B and C) In GluA1 ko mice eEPSC amplitude is reduced after stereotactic a-GluA2 IgG microinjections ($n_{(ct\ IgG)} = 14$, $n_{(a-GluA2\ IgG)} = 21$; $p = 0.023$; Mann-Whitney U test) whereas paired-pulse facilitation is still unchanged ($n_{(ct\ IgG)} = 6$, $n_{(a-GluA2\ IgG)} = 14$).

(D) nsFA of peak-scaled eEPSC. Exemplary plot of GluA1 ko hippocampal slices after a-GluA2 IgG (red) and ct IgG (black) IgG injection (30 bins per condition, median \pm SD; $n_{(ct\ IgG)} = 112$ traces; $n_{(a-GluA2\ IgG)} = 120$). Slope indicating single-channel conductance is unchanged, whereas the number of channels given by the equation of the hyperbola is reduced in recordings of the a-GluA2 IgG injected mouse. Quantification of nsFA reveals a decrease of active channels in a-GluA2 IgG treated GluA1 ko mice ($n_{(ct\ IgG)} = 10$, $n_{(a-GluA2\ IgG)} = 10$; $p = 0.038$; Mann-Whitney U test) but single channel conductance is unchanged ($n_{(ct\ IgG)} = 10$, $n_{(a-GluA2\ IgG)} = 10$).

(E) mEPSC amplitude but not mEPSC frequency is reduced upon a-GluA2 IgG microinjection in GluA1 ko mice ($n_{(ct\ IgG)} = 13$, $n_{(ct\ IgG + NASPM)} = 12$; $p = 0.028$, Mann-Whitney U test).

Figure 6. Antibodies against GluA2 impair long-term synaptic plasticity in the Schaffer-collateral-CA1 pathway

(A) Recording situation in the CA1-Schaffer-collateral LTP recordings. Co-applied FM-dye (green) delineates the injection site of human IgG (CA1 targeted stereotactic microinjection). Stimulation (stim) is performed in the Schaffer-collateral (sc) pathway using a bipolar electrode. Field potentials are recorded (rec) in the CA1 region of the hippocampus (scale bar: 200 μ m).

(B) Input-Output relationship reveals no differences in fEPSPs slope between ct IgG (black)- and a-GluA2-IgG injected hippocampi (red; $n_{(ct\ IgG)} = 16$, $n_{(a-GluA2\ IgG)} = 17$).

(C) Time course of LTP after TBS (arrow) as shown by slope changes of fEPSPs. LTP is severely affected after a-GluA2 IgG injection (red) into the hippocampus as compared to ct IgG injection (black; $n_{(ct\ IgG)} = 8$, $n_{(a-GluA2\ IgG)} = 6$; $p < 0.001$; two-way-ANOVA repeated measurements with Holm-Sidak post-hoc analysis). Inset shows averaged sample traces of fEPSPs from ct IgG (black) and a-GluA2 IgG treated slices (red) before and after induction of LTP. Right: quantification of LTP induced changes in fEPSP slope in the consolidation phase (last 20 min of recording; $n_{(ct\ IgG)} = 8$, $n_{(a-GluA2\ IgG)} = 6$; $p = 0.013$; Mann-Whitney U test).

(D). Short-term plasticity is unchanged after a-GluA2 IgG microinjection as measured by CA1 fEPSP recordings. Paired-pulse stimulation (interstimulus interval 100 ms) was performed in the Schaffer collateral-CA1 pathway before and after induction of LTP by TBS. Paired-pulse facilitation is observed in both experimental groups (ct IgG and a-GluA2 IgG microinjection) before and after TBS ($n_{(ct\ IgG)} = 8$, $n_{(a-GluA2\ IgG)} = 6$; paired t-test). Note that ct IgG injected mice show LTP with increased slope values in comparison of the first stimuli before and after TBS. Against this, slope values of the first stimuli in a-GluA2 IgG injected mice before and after TBS are not significantly changed corroborating deficits in LTP; see also (C).

Figure 7. Mice develop memory deficits and increased anxiety-like behavior in different passive-transfer models using human antibodies to GluA2

(A and B) Experimental time course of the intrahippocampal injection passive-transfer model. Stereotactic microinjections (3 injection sites per hemisphere; time points indicated by syringes) were performed on 3 consecutive days. Test for locomotor activity (LOC), novel object recognition (NOR), elevated plus maze (EPM) were performed at the indicated time points (sacr: sacrifice; brain slice illustration is modified from Paxinos Mouse Brain Atlas).

(C) Mice injected with ct IgG or a-GluA2 IgG show no differences in horizontal motor activity ($n_{(ct\ IgG)} = 10$, $n_{(a-GluA2\ IgG)} = 10$).

(D) OR (object recognition) index in a-GluA2 IgG injected mice is greatly reduced as compared to controls ($p < 0.001$), indicating severe impairment of memory function. Note that there is a slight reduction of OR Index in ct IgG injected mice after injections in comparison to baseline which might be due to repetitive anesthesia and surgery before testing ($n_{(ct\ IgG)} = 10$, $n_{(a-GluA2\ IgG)} = 10$; $p = 0.048$; two-way-ANOVA repeated measurements with Bonferroni post-hoc analysis).

(E) a-GluA2 IgG injected mice spend less time in the open arm of the EPM ($n_{(ct\ IgG)} = 9$, $n_{(a-GluA2\ IgG)} = 9$; $p = 0.004$; t-test).

(F and G) Experimental time course of the intraventricular infusion passive-transfer model. Purified IgG was continuously infused in both lateral ventricles for 14 days as indicated. Behavioral testing was done at the indicated time points (BW: black-and-white test; brain slice illustration is modified from Paxinos Mouse Brain Atlas).

(H) Horizontal motor activity was unchanged in both experimental groups throughout the experimental period ($n_{(ct\ IgG)} = 11$, $n_{(a-GluA2\ IgG)} = 12$).

(J) OR index in a-GluA2 IgG injected mice is significantly lower with respect to controls at day 10 and day 18, while animals recover completely on day 25 ($n_{(ct\ IgG)} = 11$, $n_{(a-GluA2\ IgG)} = 12$; $p < 0.001$; two-way repeated measurements ANOVA with Bonferroni post-hoc analysis).

(K) a-GluA2 IgG injected mice spend less time in the white sector of the BW maze ($n_{(ct\ IgG)} = 11$, $n_{(a-GluA2\ IgG)} = 12$; $p = 0.017$; t-test). See also Figure S7.

Figure 1

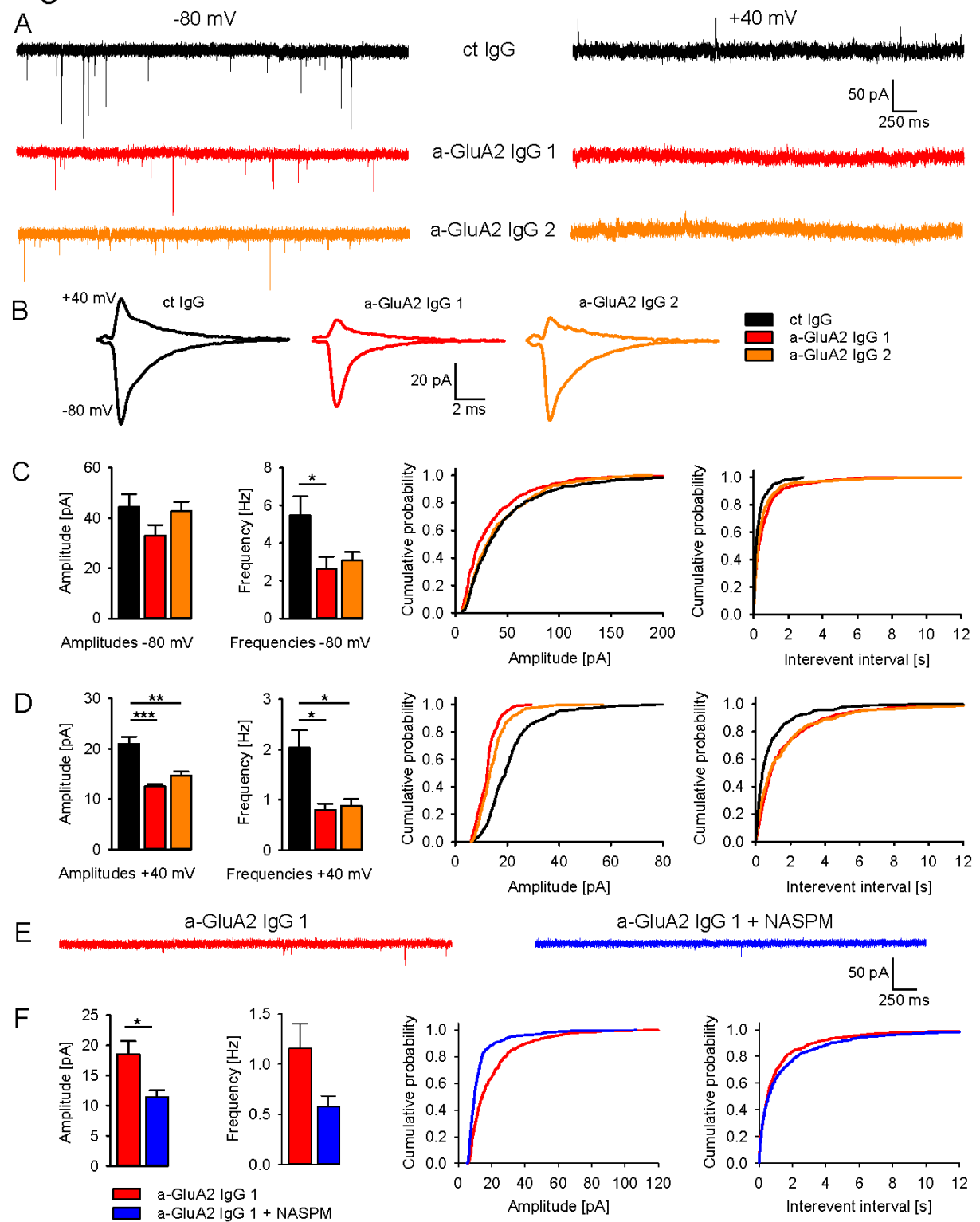


Figure 2

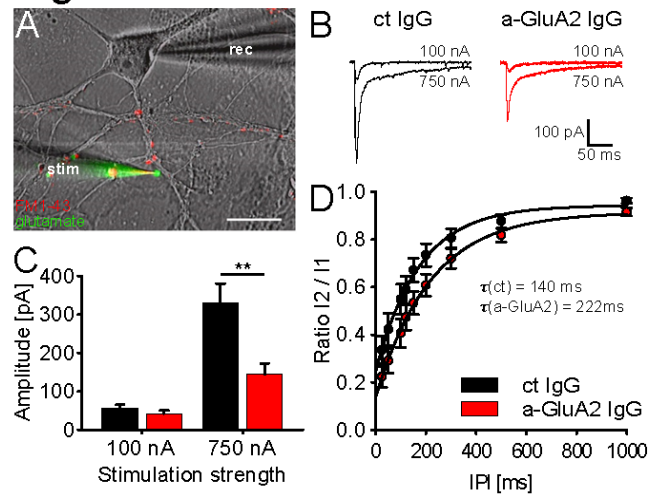


Figure 3

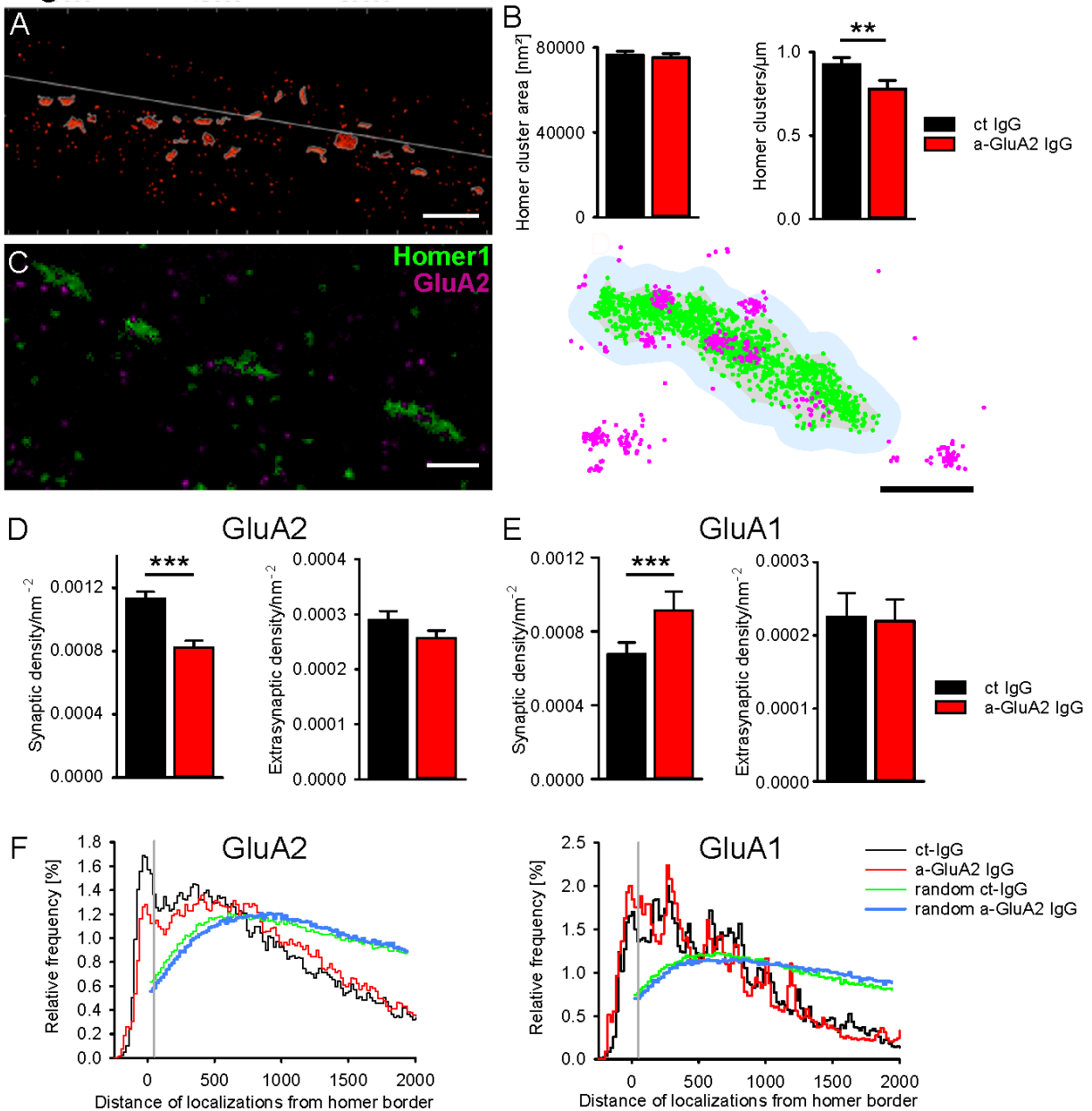


Figure 4

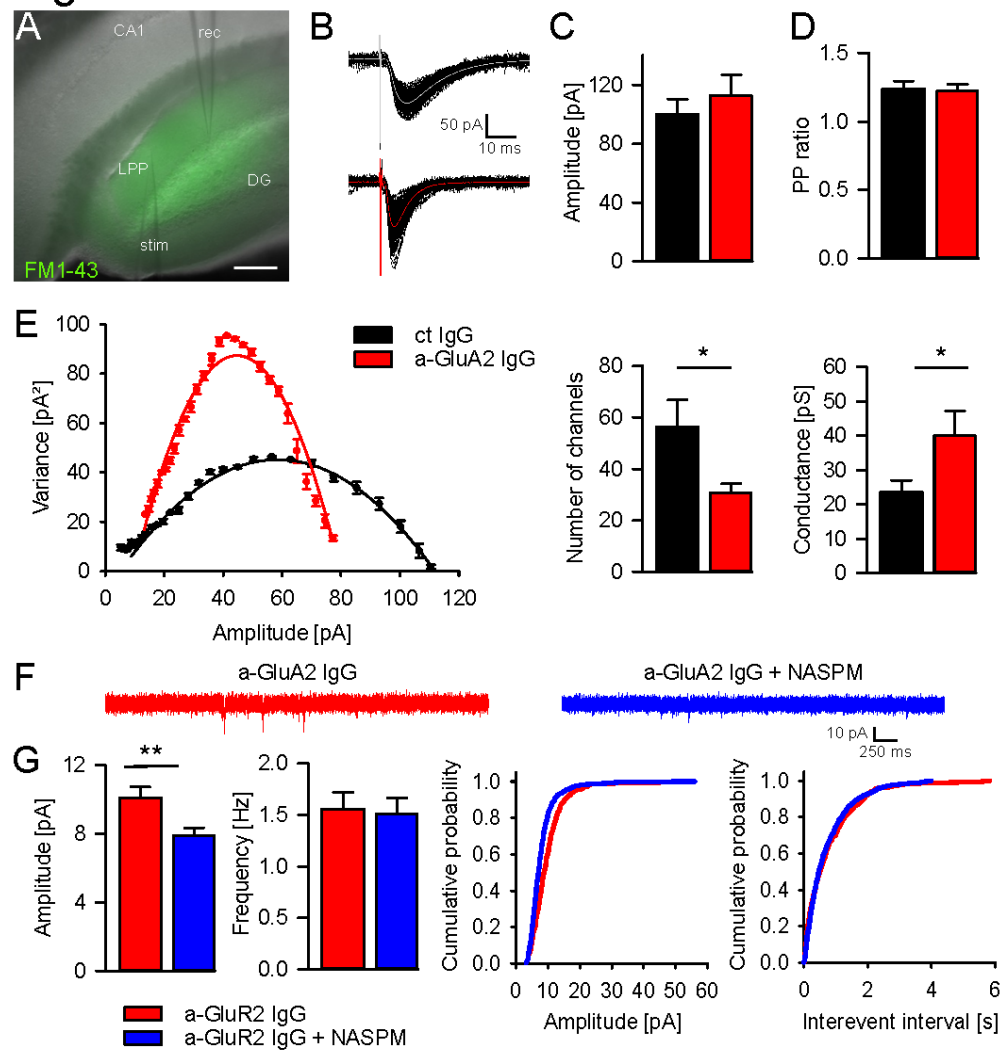


Figure 5

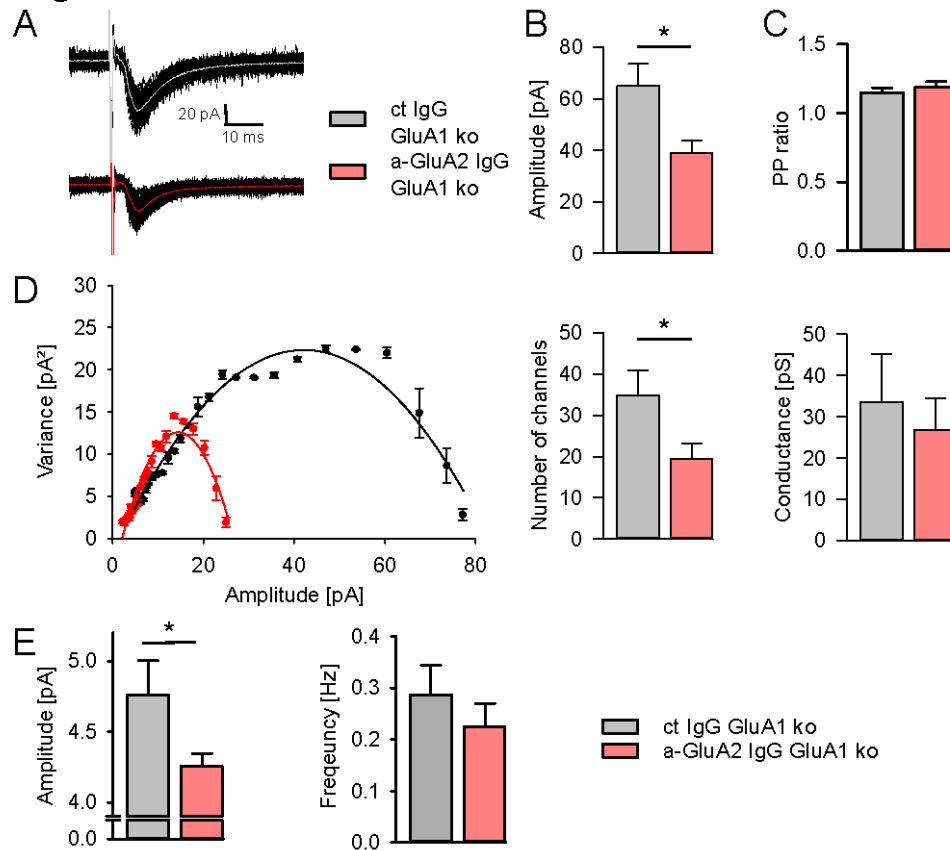


Figure 6

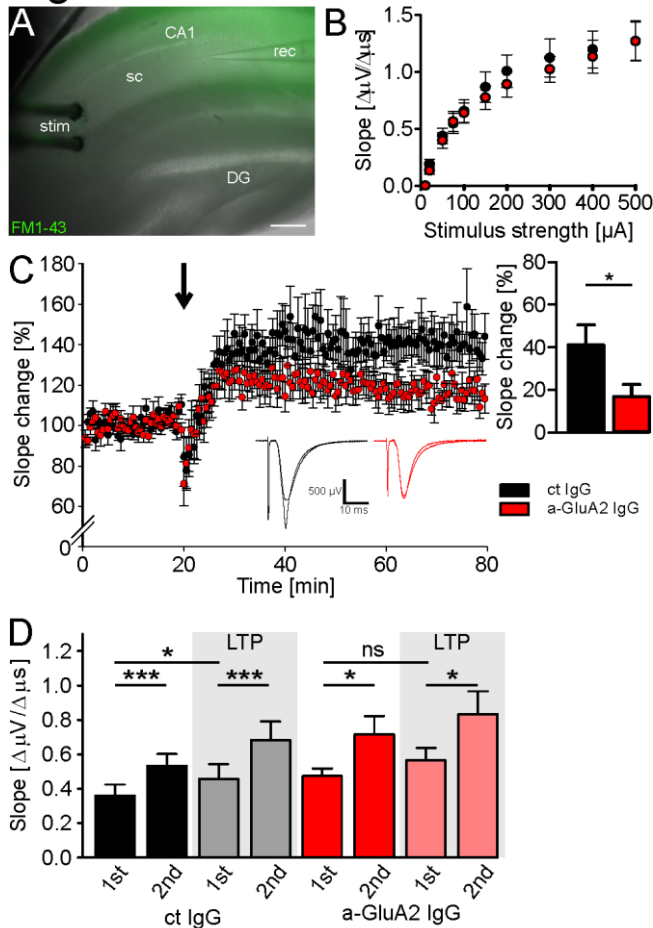
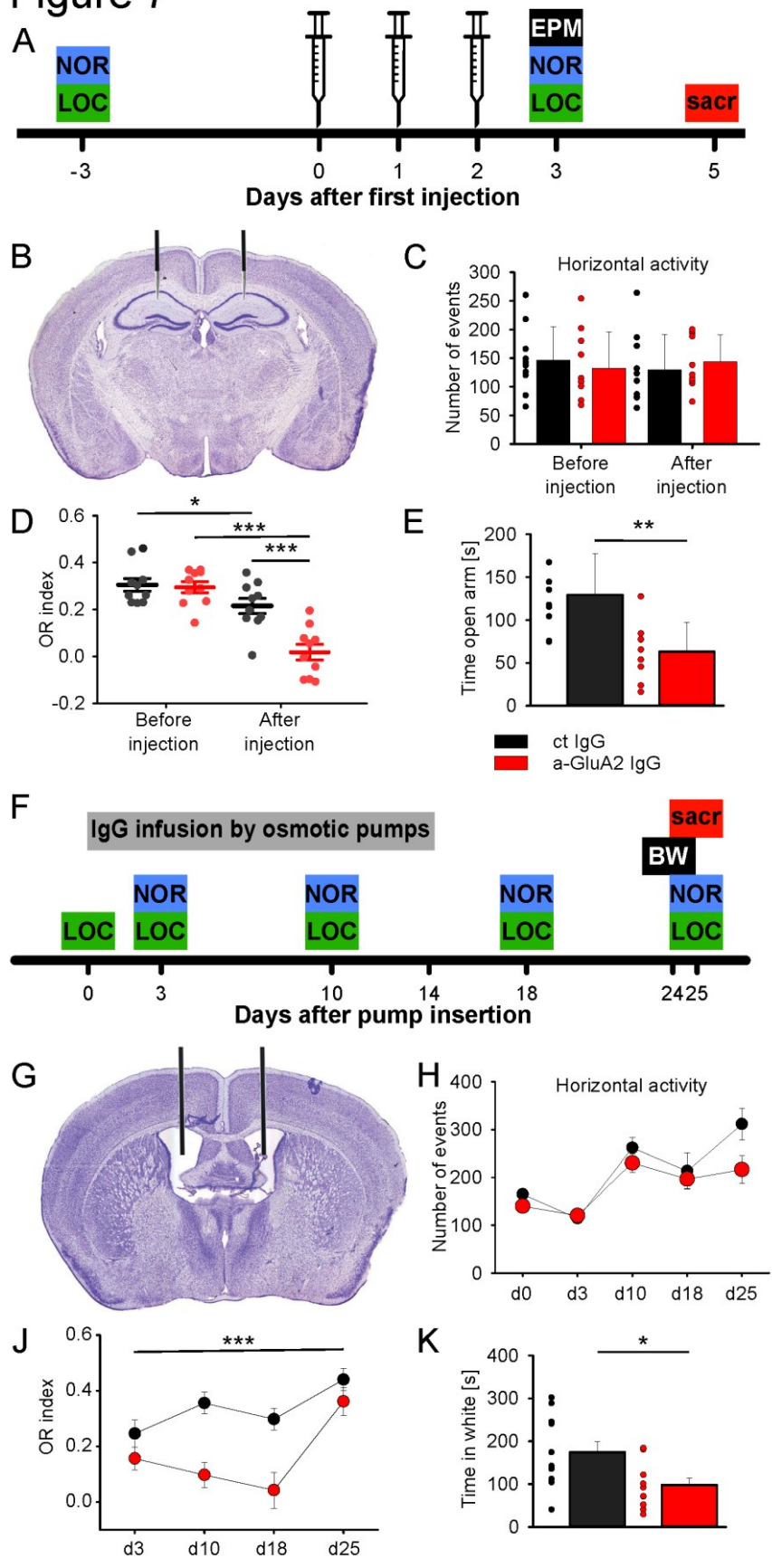


Figure 7



STAR Methods

Purification of IgG fractions

In the study we used the purified IgG fraction containing GluA2 ABs from an autoimmune encephalitis patient with high titer (> 1:320) of anti-GluA2 AB in serum and CSF, a pooled IgG fraction of further 8 patients with AMPAR encephalitis, and control IgG without detectable antineuronal ABs derived from a patient with chronic polyneuropathy. IgG fractions were purified from therapeutic plasma exchange material by separation on exchange chromatography as described previously (Sommer et al., 2005). All a-GluA2 AB IgG fractions also contained antinuclear antibodies (ANA) which is an unspecific sign of an active autoimmune state. This is a common finding in patients with AMPAR encephalitis suggesting a possible underlying predisposition to autoimmunity (Dalmau et al., 2017; Hoftberger et al., 2015; Lai et al., 2009). IgG fractions did not contain any other antineuronal or cell surface AB reactivity (see below and Figure S1 for detailed patient AB testing). The IgG fractions were dialyzed, freeze dried and stored at -20°C. Lyophilized IgG was dissolved to stock solutions of 5mg/ml or 10mg/ml in normal saline before use.

Binding specificities of patient IgG fractions

The binding specificity of purified patient IgG was evaluated by cell-based assays using transfected HEK293 cells, immunoprecipitation with CNS tissue, and immunohistochemistry using primary neurons and brain slices of wild-type, GluA1, and GluA2 deficient mice (Figure S1).

HEK293-cell transfection and immunocytochemistry

HEK293 cells were maintained in minimal essential medium (MEM; Life Technologies, Carlsbad, CA, USA) with 10% fetal bovine serum (Biochrom, Berlin, Germany), 1% antibiotic-antimycotic solution (Life Technologies) and 1% MEM non-essential amino acids (Life Technologies). Plasmid DNA for transfection was purified by the Plasmid Midi Kit (Qiagen, Venlo, Netherlands). 2-4 µg of rat GluA1i or GluA2i in pcDNA3.1 plasmid DNA (Harmel et al.,

2012) was cotransfected with 100 ng of pEGFP-N2 plasmid DNA (BD Biosciences, Heidelberg, Germany) by a standard calcium phosphate precipitation method (Zimmer et al., 2002). Briefly, after medium exchange, plasmid DNA containing BES buffered saline (BBS) (25 mM N,N-bis-(2-Hydroxyethyl)-2-aminoethanesulfonic Acid (BES, Calbiochem, San Diego, CA, USA), 140 mM NaCl, 0.75 mM Na₂HPO₄, pH 6.95) containing 125 mM CaCl₂ for plasmid precipitation was added to cultivated HEK293-cells for 24 h. Thereafter, cells were seeded onto PDL-coated coverslips until usage (up to 2 days after plating). GluA1:eGFP or GluA2:eGFP transfected HEK293-cells were fixated by 4% paraformaldehyde (PFA) for 20 min without permeabilization, washed in phosphate buffered saline (PBS) and incubated for 30min in blocking buffer 1 (BB 1; 5% milk powder, 5% bovine serum albumin (BSA) in PBS). Commercial antibodies and applied concentrations are listed in Table 1. Cells were incubated over night at 4°C with 10 µg/ml anti-GluA2 or control IgG fractions and 2% milk powder in PBS. After washing in PBS, HEK293 cells were incubated for 2 h with secondary Cy3 anti-human AB and 2% milk powder in PBS. After additional washing steps, cells were stained for 5 min with 4',6-Diamidin-2-phenylindo (DAPI) in PBS, washed again and mounted with Mowiol 4-88 (Calbiochem).

Affinity purification and mass spectrometry

Adult rat brain membrane fractions were solubilized for 30 min at 4 °C with 1 % Dodecanoylsucrose in 50 mM Tris/HCl pH 8.0, 150 mM NaCl at 1 mg protein/ml. Non-solubilized matter was removed by ultracentrifugation for 15 min at 125,000 g. Supernatants containing 3 mg solubilized membranes were incubated for 4 h at 4 °C with 30 µg human IgG fractions covalently immobilized on Protein G Dynabeads (Thermo Fisher). After three subsequent washes with solubilization buffer, immunoprecipitates were eluted in Laemmli buffer without dithiothreitol at 37 °C. Denatured eluates were analyzed by immunoblot using anti-GluA2/3 (Millipore #07-598) and anti-GluA1 (Millipore #AB1504) primary antibodies (each used at 1:1000) and goat anti-rabbit secondary antibodies (Santa Cruz #sc-2004, 1:20,000). Mass spectrometric (MS) analysis of whole eluates was performed using a nano-

LC-MS/MS system (LQT Orbitrap Velos, Thermo Fisher) by the Biomedizinisches Forschungszentrum (BMFZ), Heinrich-Heine Universität Düsseldorf. MS data was searched against the UniProt knowledgebase release 2017_02 rat reference proteome using MaxQuant (version 1.5.8.3) with standard settings (PSM and protein level FDR = 0.01 %) and the following variable modifications: methionine oxidation, acetylated protein N-termini, Glu/Gln → pyro-Glu. A minimum of two unique peptides was required for unambiguous protein identification.

GluA1 and 2 deficient mice and brain slice immunohistochemistry

Breeding pairs of heterozygous GluA1 and GluA2 deficient mice on a C57BL/6 background were kindly provided by Rolf Sprengel (Max Planck Institute, Heidelberg) and genotyped as described (Jensen et al., 2003; Shimshek et al., 2005). Homozygous ko mice and wt littermates were used in the experiments for comparison.

Mice were deeply anesthetized with isoflurane and perfused with 4% of PFA by cardiac puncture to obtain brain slices for immunohistochemistry. Brains were prepared, afterfixed for 24 h in 4% PFA, and dehydrated for 24 h in 10% and 24 h in 30% sucrose solution. Thereafter, free-floating 40 µm serial sections were prepared. Slices were blocked with BB 2 (3% normal goat serum, 2% milk powder and 0.1% Triton-X100 in TRIS buffered saline [TBS]) for 30 min. Thereafter, slices were incubated overnight at 4°C with primary AB (GluA2, GluA1) or patient IgG fractions in BB 2. After washing steps in TBS slices were incubated for 2h with secondary AB (Rhodamin anti-mouse, Rhodamin anti-rabbit, Cy3 anti-human). After additional washing in TBS slices were transferred to object slides with 0.5% gelatin, dried, stained for 5 min in DAPI solution, washed in PBS and mounted with Fluoromount (Southern Biotech, Birmingham, AL, USA).

Immunocytochemistry on cultured primary hippocampal neurons

Primary hippocampal neurons were prepared from C57BL/6 E18 embryos as described earlier (Haselmann et al., 2015). Briefly, embryonic brains were removed from the skull and

meninges were removed with a fine forceps. Hippocampi were separated, trypsinated in 0.25% Trypsin solution for 5 min at 37°C and triturated. Neurons were first plated on PDL-coated coverslips in plating medium (MEM, 0.5% glucose, 10% horse serum, 0.5% penicillin/streptavidin) with a density of 20.000 cells/cm². After 1 h plating medium was replaced by growth medium (Neurobasal, 2% B27 [Life Technologies], 1% glutamine, 0.5% penicillin/streptavidin) and neurons were cultured for 10 to 15 days before use.

After 14 days in vitro (DIV) neuronal cultures were fixed for 20 min with 4% PFA, washed with PBS and blocked for 30 min with BB 3 (10% BSA/PBS, 0.1% Triton-X100). Afterwards, cells were incubated with α -GluA2 IgG [1:500] and Homer1 AB overnight at 4° C. After washing steps in PBS cells were incubated with secondary AB (Cy3 anti-human for α -GluA2-IgG and Alexa488 anti-guinea pig for Homer1; see also Table 1) for 2 hours at room temperature. After repeated washing steps in PBS, neurons were stained in DAPI solutions for 5 min, washed again and mounted with Moviol.

Direct stochastic optical reconstruction microscopy (dSTORM)

Immunostaining for dSTORM

Primary hippocampal neurons were incubated with a 1:500 dilution of 5 mg/ml stock of anti-GluA2 IgG or control IgG for 24 h at 37 °C followed by paraformaldehyde fixation (PFA, 4% for 20 min at room temperature (RT)). Primary staining antibodies were then applied overnight at (4°C) in BB 4 (PBS, 10% bovine serum albumin, 10% normal goat serum, 10% normal donkey serum, 0.1 M glycine). Samples were washed in PBS+ (PBS + 0.1 M glycine) six times for 5 min, permeabilized 1 h (at RT) with BB 4 containing 0.1% Triton-X 100 and incubated with anti-Homer1 antibodies (2 h, at RT), washed again six times and subsequently incubated with secondary antibodies (2 h, RT). After immunostaining samples were washed with PBS+ and postfixed with 4% PFA at RT for 10 min. Samples were kept in PBS+ until recording.

dSTORM recordings

Samples were recorded in MEA buffer containing 100 mM mercaptoethylamine (pH adjusted to 7.9) with a Zeiss Elyra P.1 setup equipped with DPSS laser lines of 561 nm and 642 nm (Lasos Lasertechnik, Jena, Germany) and two EMCCD cameras (Ixon DU 897; Andor, Belfast, UK). All settings were kept constant throughout the experiments to allow relative quantification of experimental groups. Fluorophores were excited using the above laser lines starting with the longer wavelength excitation (sequential acquisition) using a 1.46 NA 100x TIRF oil objective (Zeiss, Jena, Germany). 90% of 561 nm laser and 14% of 642 nm laser line were constantly applied during experiments. Emission was filtered using appropriate filter sets. For each channel 15000 frames were recorded with a framesize of 320x320 px applying a camera exposure time of 25 ms and an in-software 250 detector gain. Sample z-drift was stabilized using Definite Focus© (Zeiss). Residual drift in x-y direction was corrected using a model based drift algorithm implemented in ZEN 2009 software (Zeiss). Chromatic aberration was corrected by performing a channel alignment using tetraspeck beads.

Image analysis

Localizations were calculated in Zeiss ZEN software by Gaussian fitting using a peak mask size of 9 pixel and a signal-to-noise threshold of 8 (receptor signals, Alexa 647) or 11 (Homer1 signal, CF568), respectively. Rarely, overlapping molecules localizations had to be discarded by the software. Localization raw data were further analyzed with a custom written Mathematica script. For Homer1 signal sparse localizations were excluded by a nearest neighbor analysis rejecting all localizations that have less than 10 neighbors within a radius of 40 nm to allow precise determination of PSD clusters. For characterization of postsynaptic Homer1 clusters an alpha shape algorithm (alpha = 40) was used. Preceding tests were performed with a series of alpha values that showed reliable reports of PSD size approaching areas measured with electron microscopy and PALM (MacGillavry et al., 2013; Schikorski and Stevens, 1997) (Figure 3 and S4C). We also compared this algorithm with the results from a density based clustering algorithm (DBSCAN; applied with parameters epsilon

= 40 and minPoints = 5) that yields similar synaptic GluA2 densities and trends in group comparisons (Figure S4C). Our selected cluster determination method (alpha shapes, alpha value = 40) showed no differences in PSD area between control and treatment group. Clusters were selected that were within a size range of 20.000 – 300.000 nm² and a minimum of 100 photons representing post-synaptic regions according to published PALM measurements of PSD size (Figure S4B) (MacGillavry et al., 2013). Resulting clusters were taken as regions of interest and localizations of receptors (second channel) were classified as intra- or extrasynaptic receptors according to the measured receptor-cluster distance. Previous studies estimated an average distance in the 2D projection between Homer1 signals and post-synaptic receptor localizations of about 50 nm using superresolution microscopy (Dani et al., 2010). We therefore classified all receptor localizations within 50 nm of Homer1 clusters as synaptic receptors and those with a cluster-receptor distance between 50 nm and 2000 nm as extrasynaptic receptors (Figure S4A). The number of synapses per dendrite length was estimated by dividing the number of detected Homer1 clusters by the longest distance within the dendrite region of interest (manually drawn). To interpret the distance distributions of measured data we used a Mathematica algorithm to simulate randomly located extrasynaptic receptor localizations within the extrasynaptic space. These random receptor distributions showed distributions without synaptic adherence as observed in our original measurements.

Stereotactic intravital IgG injections

All animal experiments have been performed according to the ARRIVE guidelines (Kilkenny et al., 2010) and were approved by the Thuringian state authorities (authorization # 02-059/13). Stereotactic injections of IgG fractions into the hippocampus were performed as previously described (Haselmann et al., 2015). Briefly, 129 eight week old C57BL/6 WT and 35 GluA1 deficient mice were deeply anesthetized by 1.5 to 2.0% of isoflurane/oxygen and head fixed into a stereotactic apparatus (Lab StandardTM, Stoelting, Wood Dale, IL, USA). The skull was exposed by a small midline incision, the stereotactic injection sites were

marked (for exact coordinates see Table 2), and holes were drilled with a dentist driller (Foredom, Bethel, CT, USA). Very thin injection pipettes were pulled from borosilicate glass (WPI, Sarasota, FL, USA, #4878) and filled with IgG solutions (concentration 5mg/ml; total volume 4 μ l). For electrophysiological measurements 1 mM of FM1-43-FX (Molecular Probes) was added to the IgG fractions for intravital visibility and verification of the injection site in acute slices. The injection pipette was placed at stereotactic coordinates as detailed in Table 2 and 1 μ l of IgG solution was injected with an injection speed of 0.4 nl/s by a microprocessor controlled nanoliter injector (Nanoliter 2000 + SYS-Micro4 Controller, WPI) per injection site. By using very thin glass application pipettes, low injection volume, and slow injection speed tissue damage in the target region is avoided. After injections the skin of the animals was sutured and mice were taken back to their home cage for at least 24 h for regeneration.

Placement of intraventricular catheters and osmotic pump application

23 male C57BL/6J mice were used for implantation of intraventricular catheters. Animal care, anesthesia, insertion of bilateral ventricular catheters (PlasticsOne, model 3280PD-2.0/SP; coordinates: 0.2 mm posterior and \pm 1.00 mm lateral from bregma, depth 2.2 mm), and connection of each catheter to a subcutaneous osmotic pump for continuous infusion of purified IgG fractions (Alzet 1002, Cupertino, CA; volume 100 μ l, flow rate 0.25 μ l/h for 14 days) was done as previously reported (Planaguma et al., 2016; Planaguma et al., 2015). Osmotic pumps were filled with IgG preparations the day before surgery (concentration 10mg/ml; 12 mice with anti-GluA2 AB, 11 mice with control IgG).

Behavioral tests

Novel object recognition (NOR) test

Animals were habituated for 45 minutes in a 45x45x40 cm open field arena (Panlab, Barcelona, Spain) two days before surgery. On the day of the test, animals were again placed in the arena and two identical objects were presented on the opposite corners. After 9

min of exploration, mice were taken back to their home cage. Three hours after the familiarization phase, animals were placed in the open field box, in which one familiar object was replaced by a novel one. Times of exploration of both familiar and novel object were manually recorded over 9 minutes. The novel object was presented in 50% of trials in the right side and in 50% of trials in the left side. Every nose poke or orientation of the nose to the object at less than 2 cm distance was considered an exploration event. The OR index was calculated as the difference between times of exploration of novel and familiar objects respectively, divided by the total time spent exploring both objects. Animals who received bilateral intrahippocampal injections were tested 72 hours before the first and 24 hours after the last injection. Animals that received intraventricular infusion by osmotic pumps were tested on days 3, 10, 18 and 25 after surgery, as described previously (Planaguma et al., 2016; Planaguma et al., 2015).

Locomotor activity test

Animals were assessed in locomotor activity boxes (11×21×18 cm; Imetric, Passac, France), equipped with 2 rows of photocell detectors, and placed in a dark environment, similarly to previously described protocols (Planaguma et al., 2016; Planaguma et al., 2015). The mouse locomotor activity was recorded for 60 minutes and differentially classified for local motor activity, horizontal activity and rearings. Animals were habituated to the apparatus the day before the surgery. Mice treated with bilateral intrahippocampal injections were tested 72 hours before the first and 24 hours after the last injection. Mice treated with continuous intraventricular infusion were tested on days 3, 10, 18 and 25 after surgery.

Elevated plus maze (EPM) test

The EPM was custom-made of grey Perspex (TSE Systems Inc., Bad Homburg, Germany) and had two sets of opposing arms (30x5 cm) extending from a central platform (5x5 cm). Two arms were enclosed by 15 cm high walls. The remaining two arms were open and surrounded by a slightly raised lip (0.25 cm). The apparatus was elevated 100 cm above

floor level and illuminated by a central 25 W light bulb. Illumination intensity was 70 lux in the open arms and 50 lux in the closed arms, respectively. Mice were placed in the center, facing to an open arm and were allowed to freely explore the maze for 10 min. The number of arm entries and the amount of time spent in the open and closed arms as well as the speed and the total distance travelled were recorded using a camera tracking system (EthoVision, Noldus, Wageningen, Netherlands). After each trial the EPM was cleaned with 70% ethanol ensuring identical experimental conditions for all subjects.

Black-and-white (BW) test

The protocol was adapted according to previously published methods (Planaguma et al., 2015). The BW maze consists of a black-painted wall compartment (16x25x24 cm) and a white-painted wall compartment (25x25x24 cm) connected by a 7 cm wide by 7 cm high opening (Panlab). Lighting in the black compartment was maintained at 30 lux, while the white compartment was brightly illuminated (500 lux), and subdivided in 3 sections (distal, medial and proximal), based on the distance from the opening. At the start of the session, mice were placed in the medial sector of white compartment, head facing one lateral side of the box. The distance travelled, the total number of entries and the time spent were calculated for both compartments for 5 min. The BW test was performed on day 24 after bilateral pump implantation.

Immunoprecipitation after microinjection of human IgG fractions

Under a dissection microscope (Zeiss stereomicroscope, Stemi 2000), the hippocampi were isolated, weighted, snap frozen and stored at -80°C. Tissue (12 mg) was placed in 0.5 ml ice-cold lysis buffer (NaCl 150mM, EDTA 1mM, tris (hydroxymethyl) aminomethane [Tris]-HCl 100mM, deoxycholate acid 0.5%, 1% Triton X-100, pH 7.5) with protease inhibitors (Sigma-Aldrich, 1:50) and homogenized through a 23G needle syringe. After 1h incubation at 4°C, tissue was centrifuged at 16000g for 5 min and supernatant incubated with protein A/G agarose beads (Pierce) for 2h at 4°C. Beads were then washed, resuspended in Laemmli

buffer, boiled for 5 minutes, separated in a 4 to 15% sodium dodecyl sulfate polyacrylamide gel electrophoresis, and transferred to a nitrocellulose membrane. The membrane was first incubated with a polyclonal rabbit antibody against GluR2/3 (1:200, Millipore) and a monoclonal mouse antibody against beta-Actin (1:20000, Sigma) overnight at 4°C. Then, membranes were incubated with secondary antibodies for 1 h at room temperature (anti-rabbit IgG HRP 1:1000, anti-mouse IgG HRP 1:1000) and analyzed by enhanced chemiluminescence (all Amersham GE Healthcare) on a LAS4000 (GE Healthcare).

Immunohistochemistry for determination of bound IgG upon stereotactic injection

For determination of IgG bound to brain tissue after stereotactic IgG injections using immunoperoxidase staining, 7 µm-thick tissue sections were sequentially incubated with 0.25% H₂O₂ for 10 minutes at 4°C, 5% goat serum for 15 minutes at room temperature (RT), biotinylated goat anti-human IgG (1:2000, Vector labs, Burlingame, CA, USA) overnight at 4°C, and the reactivity developed using avidin-biotin-peroxidase and diaminobenzidine. Sections were mildly counterstained with hematoxylin, and results photographed under a LSM710 Zeiss microscope equipped with a HRc Axiocam color CCD camera (Jena, Germany). Images were prepared creating a mask for diaminobenzidine color, converting the mask to grey scale intensities, and inverting the pixels using Adobe Photoshop CS6. Brain sections were manually outlined; intensity and area were quantified using the public domain Fiji ImageJ software (<http://fiji.sc/Fiji>). Values were normalized to the patients' IgG (defined as 100%, animals injected with a-GluA2 IgG).

Confocal analysis of hippocampal sections

To quantify the effects of patients' antibodies on total cell-surface and synaptic AMPAR clusters (GluA1 GluA2) and PSD95, non-permeabilized 5 µm brain sections were blocked with 5% goat serum, incubated with commercial anti-GluA1 or GluA2 antibodies for 2 hours at RT, washed with PBS, permeabilized with Triton X-100 0.3% for 10 minutes at RT, and serially incubated with rabbit polyclonal anti-PSD95 overnight at 4°C, and the corresponding

secondary antibodies, for 1 hour at RT (concentrations used for antibody staining see Table 1). Slides were mounted and results scanned with a confocal microscope (Zeiss LSM710). Standardized z-stacks including 50 optical images were acquired from 10 hippocampal regions per animal including CA1 and DG and deconvolved using the theoretical point spread function with AutoQuant software (Bitplane). For cluster density analysis a spot detection algorithm from Imaris suite 7.6.4 (Bitplane) was used. Density of clusters in each hippocampal region was expressed as spots/mm³. Synaptic localization was defined as co-localization of GluA1 or GluA2 with post-synaptic PSD-95, and synaptic cluster density was expressed as colocalized spots/mm³. The mean densities of all 10 hippocampal regions were calculated for total and synaptic GluR1 or GluR2.

Electrophysiological studies

All electrophysiological measurements were performed with a HEKA EPC10 amplifier with a sampling rate of 20 kHz. All recordings were filtered at 2.9 and 10 kHz using Bessel filters of the amplifier. Series resistance was compensated (60 - 80%) and monitored constantly. Cells with series resistance >30 MΩ or series resistance changes of >20% during measurement were discarded. Liquid junction potential of 10 mV was corrected offline for all whole-cell patch clamp recordings.

Whole-cell patch clamp recordings and single-synapse glutamate iontophoresis in dissociated hippocampal neurons

Primary hippocampal cultures of neurons 10 to 15 days *in-vitro* were used for whole-cell patch clamp recordings. Before recording, neuronal cultures were incubated with α-GluA2 or control IgG for 24 h (20 μg/ml). Recording electrodes were pulled from thick walled borosilicate glass (Science Products, Hofheim, Germany) and filled with intracellular recording solution containing 125 mM CsMeSO₃, 10 mM HEPES, 10 mM EGTA, 8 mM NaCl, 1 mM CaCl₂, 2 mM Mg-ATP, 0.3 mM Na-GTP, 5 mM QX-314 bromide (Tocris, Bristol, UK), 0.1 mM spermine tetrahydrochloride (Sigma-Aldrich) adjusted to pH 7,25 and an osmolarity

of 310 mOsmol and had a final resistance of 3 – 5 M Ω . For evaluation of AMPAR mediated mEPSCs whole cell voltage clamp measurements were performed for 100 s at holding potentials of -80 mV or +40 mV, respectively, in artificial cerebrospinal fluid 1 (ACSF 1; 125 mM NaCl, 25 mM NaHCO₃, 25 mM glucose, 2.5 mM KCl, 1.25 mM NaH₂PO₄, 1 mM MgCl₂, 2 mM CaCl₂, purged with 95% O₂/5% CO₂) containing 50 μ M AP-5 (Tocris), 20 μ M bicuculline (Sigma-Aldrich) and 1 μ M of TTX (Tocris). In some experiments 1-naphthyl acetyl spermine trihydrochloride (NASPM, Tocris) was added to block currents that were mediated by AMPARs without GluA2 subunits (Koike et al., 1997).

For evaluation of single-synapse evoked EPSCs, presynaptic boutons of the neurons were stained using 20 μ M of FM1-43-FX dye (Molecular Probes) and stimulation with high potassium ACSF (39 mM NaCl, 30 mM glucose, 25 mM HEPES, 90 mM KCl, 1 mM MgCl₂, 2 mM CaCl₂, pH7.4) for 60 seconds (Figure 2A). Thereafter neurons were perfused with ACSF1 containing 50 μ M AP-5 and 20 μ M bicuculline for at least 10 minutes. This results in clearly labelled synaptic spots that are visible in vital neurons during patch-clamp recordings (Geis et al., 2010). Neurons were voltage-clamped at -80 mV in whole cell configuration. ieEPSCs were evoked by single-synapse glutamate iontophoresis. FM1-43-FX stained synaptic terminals were stimulated by sharp thin-walled borosilicate glass pipettes (inner diameter 1.05; Science Products) filled with intracellular solution containing 150 mM sodium L-glutamate (Sigma-Aldrich) in ACSF1 with a final resistance of 40 – 60 M Ω . In some experiments Alexa 555 (Molecular Probes) was added for visualization of iontophoretic glutamate application. Stimulation was performed by a short iontophoretic application mimicking synaptic transmission using a MVCS-02 amplifier (NPI, Tamm, Germany) (Murnick et al., 2002). After the pipette was placed directly adjacent to the FM1-43-FX stained boutons, iontophoretic stimulation was performed for 1 ms with iontophoretic eject currents of -100 or -750 nA and a retain current in the range of 4 to 12 nA. For single- and multisynaptic recordings the mean of 10 consecutive trials was taken for further analysis. Recovery after desensitization was measured as the ratio between means of the 2nd and 1st eEPSCs at different interstimulus intervals ranging from 25 to 1000 ms at 750 nA eject current.

Preparation of acute hippocampal brain slices of adult mice

Mice with stereotactic injections into the dentate gyrus (DG) of the left hemisphere were decapitated. The brain was removed in ice-cold protective cutting ACSF (95 mM N-Methyl-D-glucamine, 30 mM NaHCO₃, 20 mM HEPES, 25 mM glucose, 2.5 mM KCl, 1.25 mM NaH₂PO₄, 2 mM thiourea, 5 mM sodium ascorbate, 3.0 sodium pyruvate, 10 mM MgSO₄, 0.5 CaCl₂, 12 mM N-acetylcysteine, adjusted to pH 7.3 and an osmolarity of 300 to 310 mOsmol, purged with 95% O₂/5% CO₂) (Peca et al., 2011) and cut into two halves. The olfactory bulb of the injected hemisphere was cut in the coronary plane and the hemisphere was glued with the cut face onto the probe-holder with superglue (UHU, Bühl, Germany). 300 µm thick coronal slices were made with a vibratome (Leica [Wezlar, Germany] VT1200S) with an amplitude of 1 mm and a velocity of 0.4 mm/s. Slices were given into an incubation beaker with protective cutting ACSF at 34°C for 10 to 15 min and then transferred into another incubation beaker with protective storage ACSF (125 mM NaCl, 25 mM NaHCO₃, 25 mM glucose, 2.5 mM KCl, 1.25 mM NaH₂PO₄, 1 mM MgCl₂, 2 mM CaCl₂, 2 mM thiourea, 5 mM sodium ascorbate, 3 mM sodium pyruvate, 12 mM N-acetylcysteine, adjusted to pH 7.3 and an osmolarity of 300 to 310 mOsmol, purged with 95% O₂/5% CO₂) until use. For LTP recordings in the Schaffer collateral (SC) – CA1 synapse the brain was cut into 400 µm thick coronal slices in high sucrose cutting ACSF (40 mM NaCl, 25 mM NaHCO₃, 10 mM glucose, 150 mM sucrose, 4 mM KCl, 1.25 mM NH₂PO₄, 0.5 mM CaCl₂, 7 mM Mg₂Cl; purged with 95% O₂/5% CO₂, pH 7.35), and transferred into ACSF2 (124 mM NaCl, 26 mM NaHCO₃, 10 mM glucose, 3.4 mM KCl, 1.2 mM NaH₂PO₄, 2 mM CaCl₂, 2 mM MgSO₄, purged with 95% O₂/5% CO₂, pH 7.35) for 1 h at 34°C and subsequently at RT for at least 60 additional minutes.

Patch-clamp recordings in acute brain slices

The injection site of the stereotactic application of AB solutions was identified by FM1-43-FX localization in the DG. Whole-cell recordings from granule cells were obtained with recording electrodes pulled from thick-walled borosilicate glass and filled with intracellular recording

solution. AMPAR mediated mEPSCs in hippocampal granule cells of WT and GluA1 deficient mice were recorded for 100 s at holding potentials of -80 mV in ACSF1 containing 50 μ M AP-5, 20 μ M bicuculline, and 1 μ M TTX. In some experiments NASPM was added to selectively block non-GluA2 containing AMPARs. For measurements of eEPSCs the lateral perforant path was stimulated by a theta glass bipolar stimulation electrode (Harvard Apparatus, Holliston, MA, USA) filled with ACSF1 and connected to a stimulus isolation unit (Isoflex, A.M.P.I, Jerusalem, Israel). eEPSCs were recorded at -80 mV holding potential. Supramaximal stimulation was determined when increasing stimulation did not result in increase of eEPSC and ranged from 300 – 500 μ A. Paired-pulse facilitation interstimulus interval of 50 ms was measured with supramaximal stimulation.

Non-stationary fluctuation analysis of granule cell eEPSCs

To estimate the single channel conductance and the number of AMPARs we performed peak-scaled non-stationary fluctuation analysis as previously described (Traynelis et al., 1993). In short, Igor Pro 6 or 7 was used to peak-scale EPSCs of 140 (wt slices) or 120 (ko slices) sweeps elicited by maximal stimulation, to filter the traces with a Gaussian low-pass filter with a -3 dB cut-off frequency of 500 Hz, and to calculate the average ($I(t)$) and the variance ($\sigma^2(t)$) of each time point of the EPSC. The analysis was restricted to the decay of the average EPSCs from ~80 to ~10% of the peak. The plot of $\sigma^2(t)$ versus $I(t)$ was fit with the equation

$$\sigma^2(I) = iI - \frac{I^2}{N} + \sigma_b^2,$$

where i is the single channel conductance, N the number channels, and σ_b^2 the baseline variance. We validated our approach with artificially generated EPSCs with realistic number of traces, single channel conductance, number of channels, and variance in the number of channels, which were superimposed with realistic Gaussian noise.

Field potential measurement in the Schaffer collateral – CA1 pathway

For field potential measurements single slices were transferred into a measurement chamber with perfusion of ACSF2 at 1.3 to 2.5 ml/min at 32-33°C. A custom made platinum stimulation electrode was placed in the SC pathway. Recording electrodes were filled with ACSF2 and placed in the stratum radiatum of the CA1 region for fEPSP recordings. A stimulus isolation unit (Isoflex, A.M.P.I.) was used to elicit stimulation currents between 25-400 μ A to record input-output characteristics. Stimulation was then adjusted in each recording to evoke fEPSP at which the population spike could first be distinguished from the field potential and was then reduced by 10% (Grover et al., 2009; Planaguma et al., 2016). After baseline recordings for 20 minutes with 0.03 Hz, LTP was induced by theta-burst stimulation (TBS; 10 theta bursts of 4 pulses of 100 Hz with an interstimulus interval of 200 ms repeated 10 times with 0.03 Hz) resulting in stable potentiation after short depression immediately after TBS (Planaguma et al., 2016; Raymond, 2007). After LTP-induction, fEPSPs were recorded for additional 60 minutes with 0.03 Hz. Slopes of all recordings were measured directly after fiber volley to the peak of the fEPSP or until the beginning of a clearly distinguishable population spike. Paired-pulse stimulation was performed before and after TBS with an interstimulus interval of 100 ms. For input-output and paired-pulse measurements the average slope of 5 fEPSPs was used for data analysis.

Analysis of electrophysiological recordings

Traces of electrophysiological recordings were analyzed by NeuroMatic plugin (<http://www.neuromatic.thinkrandom.com>) of Igor Pro Software (Wavemetrics, Portland, OR, USA). Erroneous traces (high noise, spontaneous input interfering with evoked inputs) were discarded manually before analysis. mEPSC data was analyzed by Mini Analysis software (Synaptosoft, Decatur, GA, USA) using AMPAR mediated mEPSC compatible templates. The automatically detected events were then visually examined and erroneous events were rejected from further analysis.

Data analysis

Electrophysiological and *d*STORM data were checked for normal distribution. Unless not otherwise stated the two-tailed Student's t-test or the non-parametric Mann-Whitney U-test were applied for comparing individual groups depending on normal distribution. For statistical comparison of multiple groups one-way ANOVA with Tukey's post hoc test or ANOVA on Ranks with Dunn's post hoc test was used according data distribution. For comparison of the time-course in LTP recordings we used repeated measurements two-way ANOVA test with Holms-Sidak post hoc test. Behavioral tests with multiple time points (NOR and locomotor activity) were analyzed using repeated measurements two-way ANOVA. Multiple comparisons were corrected using Bonferroni post-hoc test. Behavioral tests with single time point (BW and EPM) were analyzed using two-tailed Student's t-test or the non-parametric Mann-Whitney U-test. Confocal cluster density of total PSD-95, total and synaptic GluA1 and GluA2, and immunoperoxidase staining was analyzed by two-tailed Student's t-test. The statistical tests used for each analysis are indicated in the figure legends. A p-value of <0.05 was considered significant. The α -error was set at 0.05. In all figures p-values are indicated as follows: *: p<0.05; **: p<0.01; ***: p<0.001. Tests were done using SigmaPlot 13.0 (Systat, San Jose, CA, USA).

Table 1: commercial antibodies used for immunostains

| | article , number | species | company | concentration |
|-------------------------------------------------------|---------------------|------------|-------------------------------------|---------------------------------------------------------------------------|
| <i>primary antibodies</i> | | | | |
| GluA1 (cell culture stains) | AB1504 | rabbit | Millipore, Darmstadt, Germany | Cell culture: 1:500 <i>d</i> STORM: 1:250 |
| GluA1 (brain tissue stains) | AGP-009 | guinea pig | Alomone, Jerusalem, Israel | Brain tissue: 1:100 |
| GluA2 (cell culture and brain tissue stains) | MAB397 | mouse | Millipore, Darmstadt, Germany | Cell culture: 1:200 <i>d</i> StORM: 1:100 brain tissue: 1:100 |
| PSD-95 | Ab18258 | rabbit | Abcam, Cambridge, UK | Brain tissue: 1:250 |

| | | | | |
|-----------------------------|-------------|------------|--------------------------------------|--------------------------------------|
| Homer1 | #160004 | guinea pig | Synaptic systems, Göttingen, Germany | Cell culture: 1:1000 dSTORM 1:300 |
| secondary antibodies | | | | |
| anti-mouse Alexa 647 | A21237 | goat | Life technologies, Carlsbad, CA, USA | 1:200 |
| anti-rabbit Alexa 647 | A21246 | goat | Life technologies Carlsbad, CA, USA | 1:200 |
| anti-guinea pig CF 568 | 20108-1 | donkey | Biotium, Fremont, CA, USA | 1:200 |
| anti-human Cy3 | 109-165-003 | goat | Dianova, Hamburg, Germany | 1:500 |
| anti-rabbit Rhodamin Red-X | 711-297-003 | donkey | Dianova Hamburg, Germany | 1:500 |
| anti-mouse Rhodamin Red-X | 715-296-020 | donkey | Dianova Hamburg, Germany | 1:500 |
| anti-guinea pig Alexa 488 | A-11073 | goat | Molecular Probes, Eugene, OR, USA | 1:500 |

Table 2: stereotactic coordinates of IgG injections into the hippocampus (from bregma in mm)

| experiment | anterior-posterior | medial-lateral | dorso-ventral |
|------------------|--------------------|----------------|---------------|
| Whole-cell patch | -2.3 | -1.2 | -2.0 |
| clamp recordings | -2.3 | -2.2 | -2.0 |
| fEPSP recordings | -1.7 | -1.0 | -1.3 |
| | -2.3 | -2.0 | -1.5 |
| | -2.9 | -2.8 | -2.0 |

| | | | |
|------------------|------|---------|------|
| | -1.7 | +/- 1.0 | -1.3 |
| Behavioral tests | -2.3 | +/- 1.8 | -2.0 |
| | -2.9 | +/-2.8 | -2.0 |

Supplemental Information

Figure S1. Related to STAR Methods

Purified patient IgG is specifically directed to the GluA2 subunit of the AMPA receptor (a-GluA2 IgG).

(A) In wt primary neurons, patient IgG (GluA2 IgG1) shows strong synaptic staining and co-labeling with postsynaptic markers (Homer1; scale bar: 20 μ m; scale bar in magnification: 5 μ m).

(B) Patient IgG (GluA2 IgG1) binds selectively to non-permeabilized GluA2 transfected HEK293 cells showing strong and exclusive membrane staining (red) but not to GluA1 transfected HEK293 cells (scale bar: 10 μ m).

(C) Patient IgG binding on mouse hippocampus (wt, left column, and GluA2 ko, right column). Upper row: commercial antibody to GluA2; second row: patient IgG (GluA2 IgG1); third row: patient IgG (GluA2 IgG2); lower row: commercial antibody to GluA1. Note that patient IgG contains antinuclear antibodies (ANA) that exhibit strong nuclear staining; specific staining of neuropil is absent on GluA2 deficient tissue (*; scale bar: 200 μ m).

(D) Representative immunoblot analysis of GluA subunits in affinity purifications from solubilized rat brain membranes by control (ct) and patient (GluA2 IgG1) IgG (load is 5 %).

(E) MS analysis of the whole a-GluA2 IgG 1 eluate verifies GluA2 as the primary target of patient's IgG. GluA1 and GluA3 are co-purified as GluA complex constituents. Given are the Uniprot ID, the number of identified unique peptides, and the MaxQuant score of identification for respective proteins.

Figure S2. Related to Figure 1.

Synaptic AMPAR in primary neurons contain the GluA2 subunit as mEPSCs are not affected by NASPM

(A) Example traces showing mEPSCs from individual neurons preincubated 24 h with ct IgG or ct IgG + NASPM.

(B) Mean mEPSC amplitudes and frequencies in ct IgG incubated neurons are not affected by NASPM ($n_{(ct\ IgG)} = 16$, $n_{(ct\ IgG + NASPM)} = 14$).

(C) Cumulative probability plot of amplitudes and interevent intervals of mEPSCs reveals no change after NASPM application ($n_{(ct\ IgG)} = 510$, $n_{(ct\ IgG + NASPM)} = 380$ for cumulative probability plots with 30 randomly chosen mEPSCs per neuron).

Figure S3. Related to Figure 2.

Stimulation of individual FM1-43 stained synaptic boutons by iontophoretic glutamate application

(A) Stimulation pipette for iontophoretic glutamate application is located to a synaptic spot as identified by FM1-43 labeling (distance "0"). Lateral movement of the stimulation pipette along the dendrite leads to a distance-dependent decrease of ieEPSC amplitude (75 nA eject current, 1 ms stimulation time, averages of 50 stimulations per location \pm SD).

(B) In the range of single synaptic stimulation (small eject currents from 15 – 100 nA) increase of eject current leads to a linear increase of ieEPSC amplitude (averages of 50 stimulations per eject current \pm SD) thus demonstrating direct correlation of ieEPSC amplitude with the applied transmitter.

Figure S4. Related to Figure 3.

Validation of synaptic dSTORM recordings

(A) Inner and outer synaptic regions as derived from Homer1 clusters. Homer1 cluster are determined by an appropriate clustering algorithm (DBSCAN or alpha shapes). Homer1 clusters are isotropically extended by 50 nm (here 100 nm for illustration) thus defining the

inner synaptic region. Further extension by 2000 nm, unification and exclusion of all inner synaptic regions is used to define an outer synaptic (perisynaptic) region.

(B) Probability density function (PDF) of Homer1 areas showing cluster areas up to 300,000 nm² (n = 40685 synapses). Line indicates exponential distribution as estimated from areas ranging from 20,000 – 300,000 nm². The deviation from an exponential distribution for areas less than 20,000 indicates sparse homer proteins that are most likely not representing functional synapses.

(C) Series of alpha values showing robustness of observed effects independent of selection of a certain alpha value or clustering algorithm. Selected cluster algorithm settings (alpha shapes, alpha = 40) was compared with lower and higher alpha shape values and a density based clustering algorithm (DBSCAN; applied with parameters epsilon = 40 and minPoints = 5) resulting in similar results in group comparisons of GluA2 density data.

Figure S5. Related to Figure 4.

IgG deposition after repeated microinjections and immunoprecipitation of GluA2 subunits in the hippocampus

(A) Example stains of human IgG delivery after repeated stereotactic intrahippocampal microinjection. Quantification of IgG intensity demonstrates no difference between ct and a-GluA2 IgG in mouse brains. IgG intensity is normalized according to the mean of ct IgG injected mice ($n_{(ct\ IgG)} = 6$, $n_{(ct\ IgG + NASPM)} = 6$ scale bar: 2 mm)

(B) Immunoprecipitation of bound IgG after microinjection of human IgG fractions reveals detection of the GluA2 subunit exclusively a-GluA2 IgG (A – F) but not ct IgG (G – L) injected mice.

(C) Example stains of GluA2 (red) together with PSD-95 (green) in the hippocampus of an IgG injected animal. The right panel shows colocalization of GluA2 and PSD-95. The orange boxes indicate the region of quantitative analysis in the CA1 region and the dentate gyrus (scale bar: 200 μ m).

(D) Quantification of PSD-95 shows no changes in postsynaptic densities in a-GluA2 injected (red bars) as compared to ct IgG (black bars) injected mice. Overall GluA2 density ($p < 0.001$, Mann-Whitney U test) and less pronounced also overall GluA1 density ($p = 0.001$) is reduced upon intrahippocampal a-GluA2 application. Synaptic GluA2 clusters are severely reduced ($p < 0.001$, Mann Whitney U test) whereas synaptic GluA1 clusters are unchanged after a-GluA2 IgG injection ($n_{(ct\ IgG)} = 60$, $n_{(a-GluA2\ IgG)} = 60$ from 6 animals per condition). Note that confocal cluster analysis is well applicable to detect reduction of receptor spots in postsynaptic fields (marked by PSD-95), e.g. when immunostaining of the receptor is under the detection threshold. However, increase of receptor subunit density per synapse (as it is shown in primary neurons by super-resolution imaging in Figure 3) cannot be detected by this method.

(E) Three-dimensional projection of synaptic clusters of AMPAR subunits (defined as GluA2 or GluA1 clusters colocalizing with PSD95; colocalization = synaptic GluA2 or GluA1 white) in a representative CA1 region (square in (C) 'colocalization'). Merged images were post-processed and used to calculate the density of clusters (density = spots/ μm^3). Upper 2 images demonstrate localization studies for GluA2 subunits, lower 2 images for GluA1 subunits (scale bar: 2 μm).

Figure S6. Related to Figure 4.

mEPSC recordings after in-vivo microinjection of ct IgG

(A) Example traces showing mEPSCs from DG granule cells 24 h after microinjection of ct IgG with and without superfusion of NASPM.

(B) NASPM does not change mean mEPSC amplitudes and frequencies after intrahippocampal injection of ct IgG ($n_{(ct\ IgG)} = 15$, $n_{(ct\ IgG + NASPM)} = 15$).

(C) Cumulative probability plots of amplitudes and interevent intervals of mEPSCs after ct IgG microinjection are unchanged after NASPM application ($n_{(ct\ IgG)} = 450$, $n_{(ct\ IgG + NASPM)} = 450$ for cumulative probability plots with 30 randomly chosen mEPSCs per neuron).

Figure S7. Related to Figure 7.

Supplemental behavioral parameters from experiments with the hippocampal microinjection (A – C) and the ventricular infusion animal model (D – F).

(A) Local motor activity is unchanged in both experimental groups after microinjections of IgG preparations.

(B) Total time spent observing novel and familiar objects in the NOR test is similar after ct IgG and a-GluA2 IgG hippocampal microinjection ($n_{(ct\ IgG)} = 10$, $n_{(a-GluA2\ IgG)} = 10$).

(C) a-GluA2 injected mice show significantly less entries into the open arm ($p = 0.014$, t-test) and less travelled distance ($p = 0.004$, t-test) of the EPM whereas the total distance travelled is unchanged ($n_{(ct\ IgG)} = 9$, $n_{(a-GluA2\ IgG)} = 9$).

(D) Local motor activity is unchanged between both experimental groups during the experimental period of continuous intraventricular IgG delivery.

(E) Total time spent observing novel and familiar objects in the NOR test is unchanged in mice with ventricular infusion of ct IgG and a-GluA2 IgG throughout the experimental period ($n_{(ct\ IgG)} = 11$, $n_{(a-GluA2\ IgG)} = 12$).

(F) In the ventricular infusion model distance travelled in the white sector of the BW test is reduced in a-GluA2 IgG infused mice whereas entries into the white sector and the total distanced travelled are unchanged ($n_{(ct\ IgG)} = 11$, $n_{(a-GluA2\ IgG)} = 12$, $p = 0.034$, Mann-Whitney U test).

Figure S1

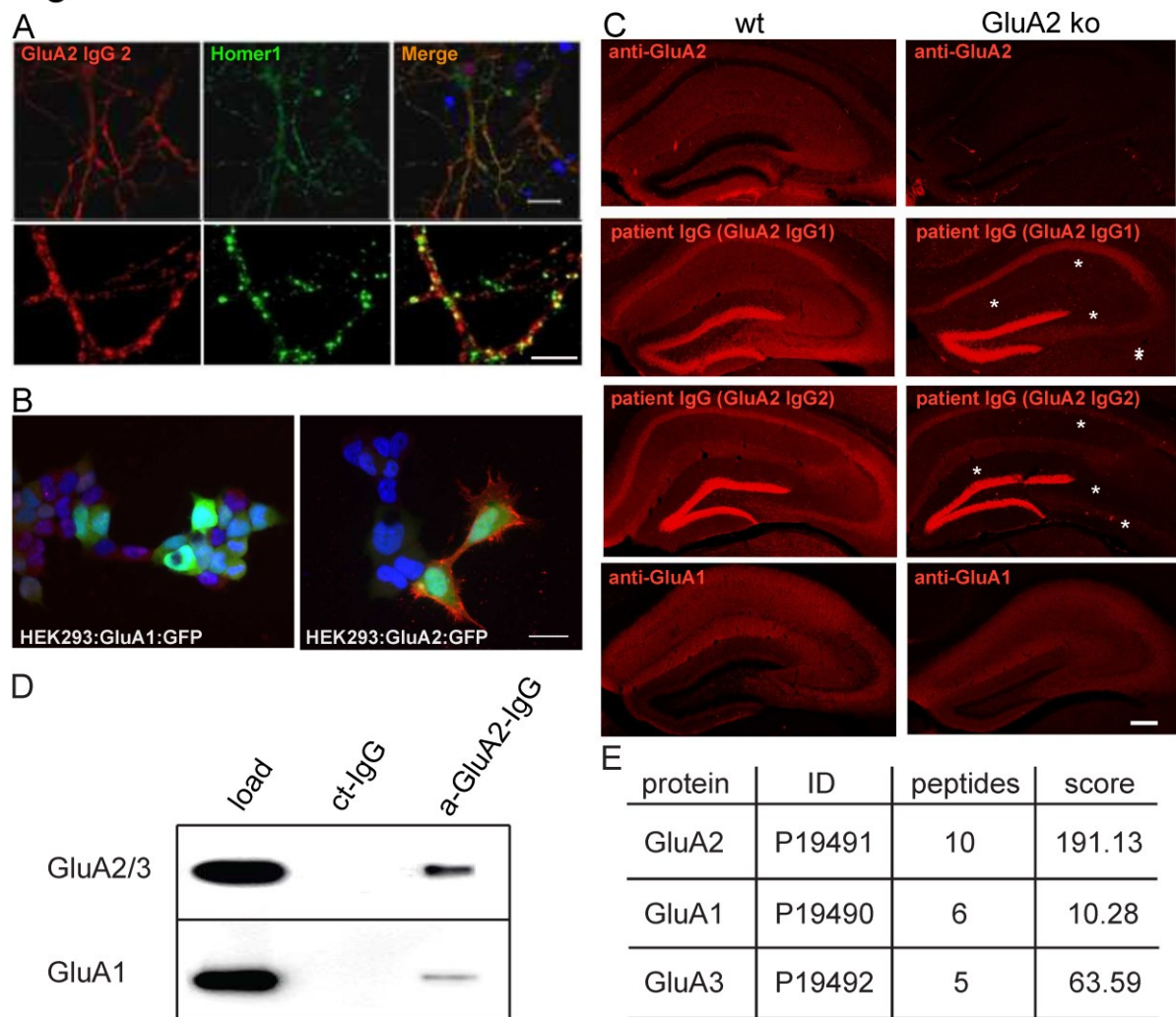


Figure S2

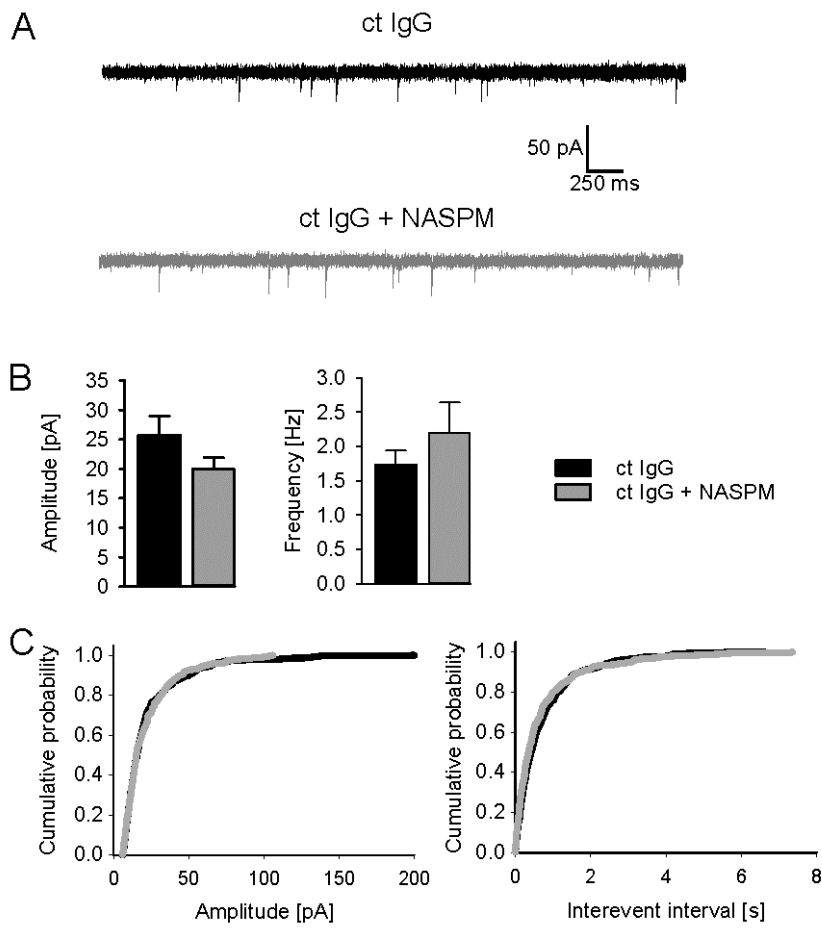


Figure S3

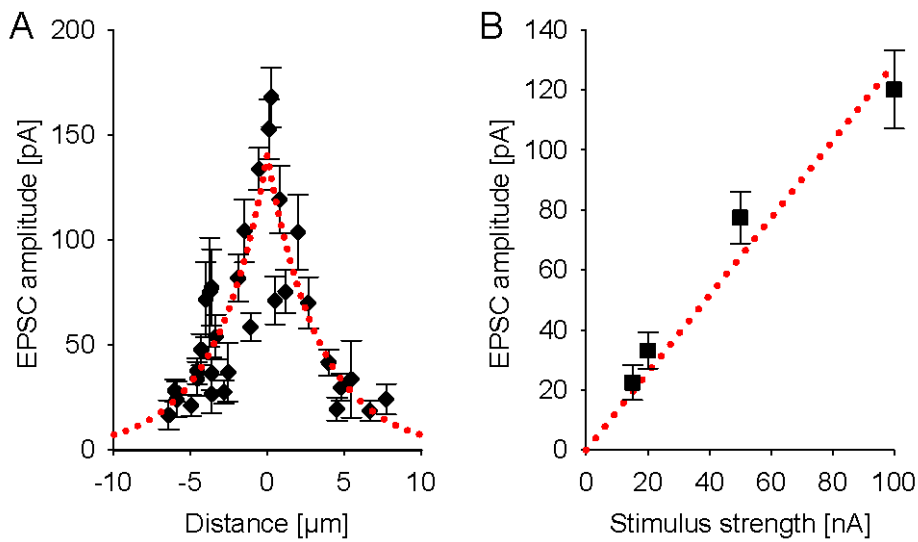


Figure S4

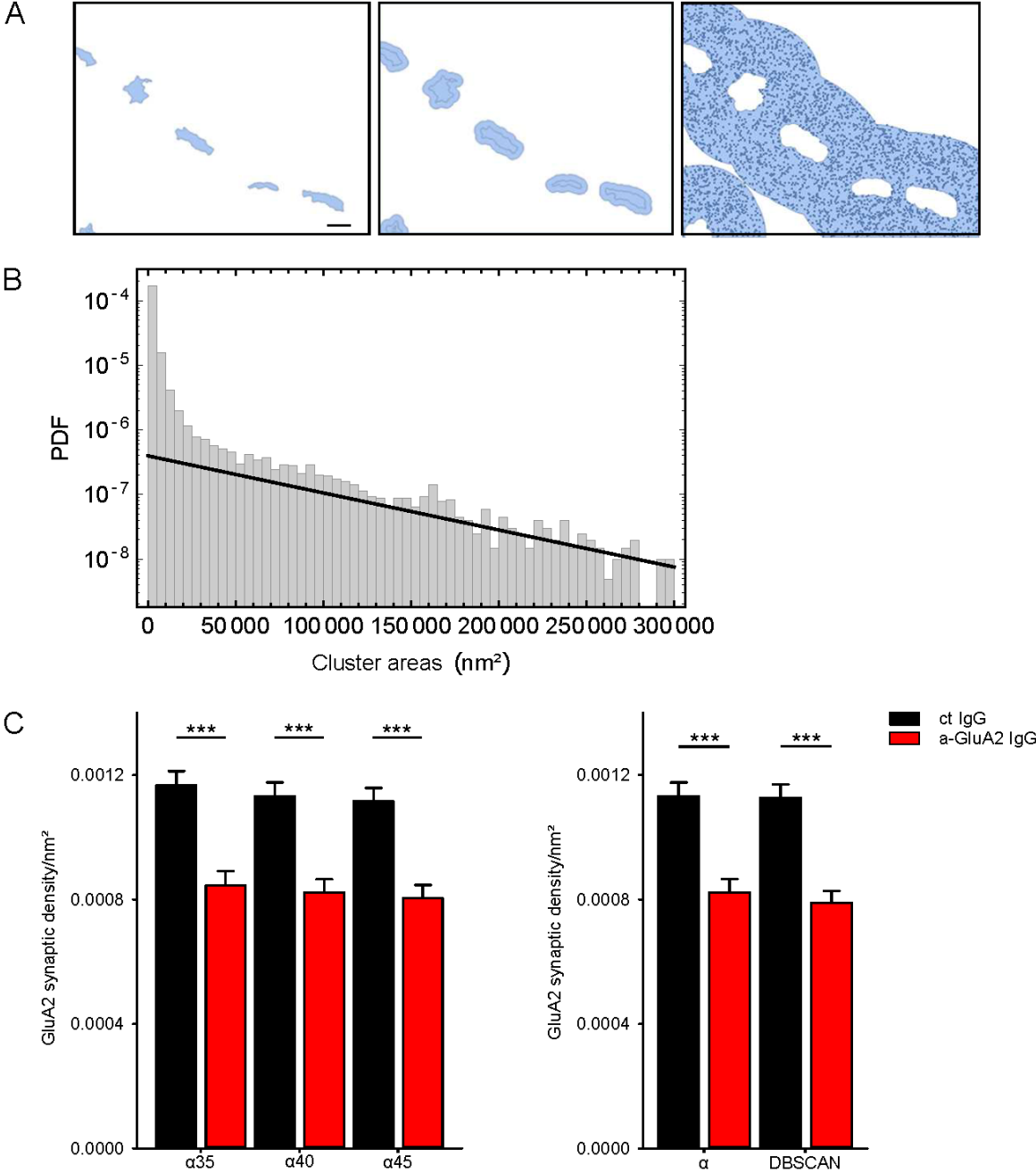


Figure S5

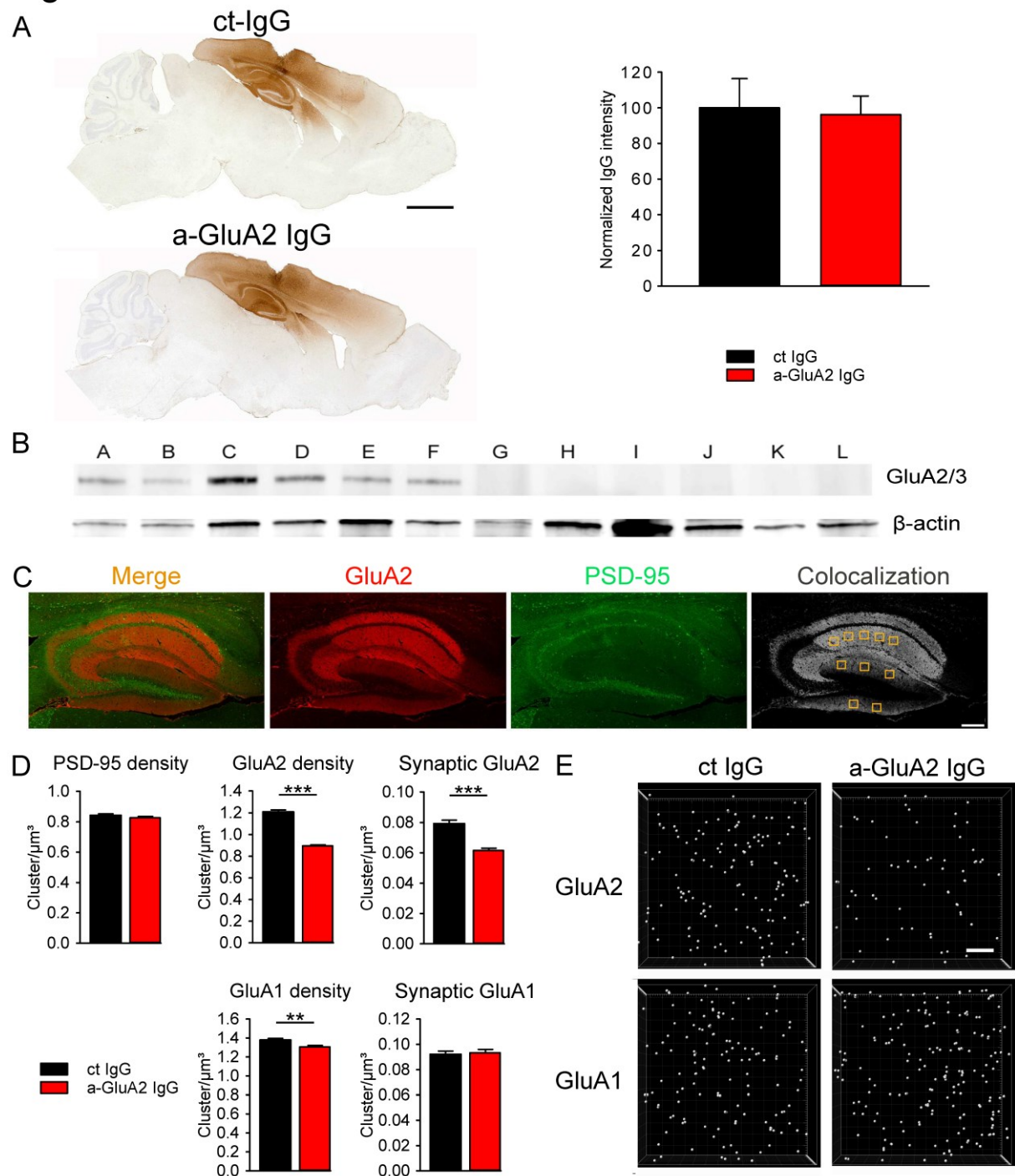


Figure S6

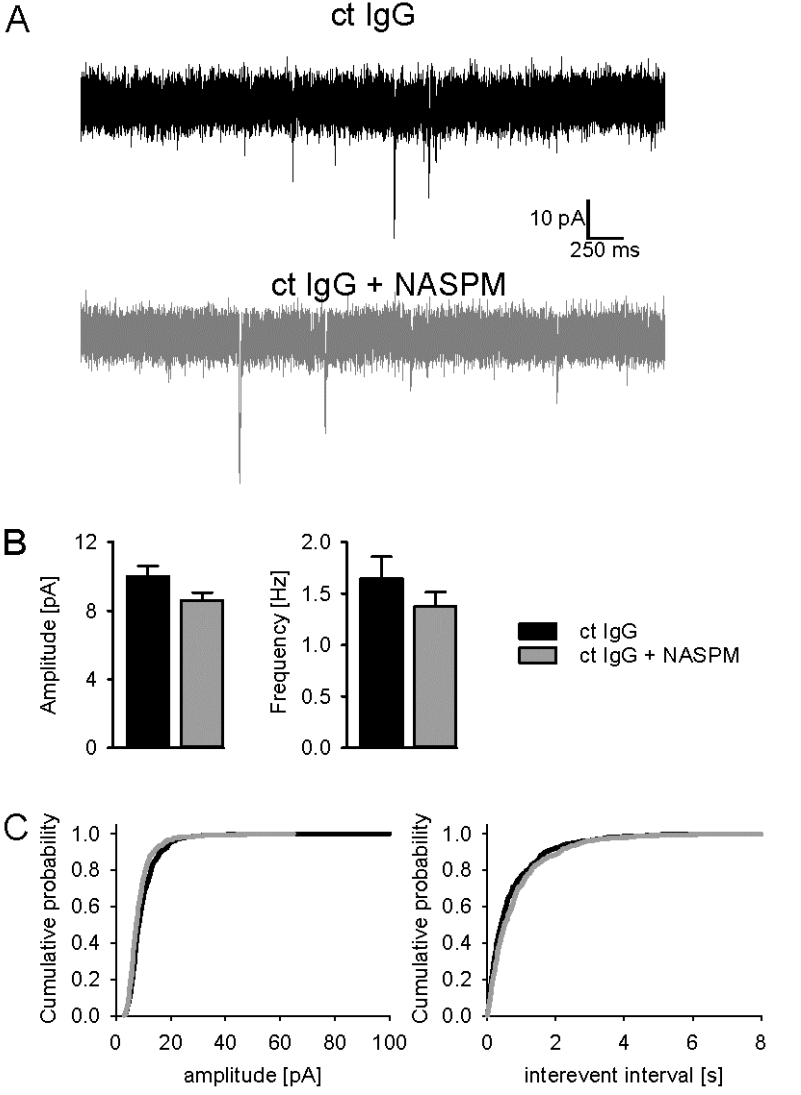
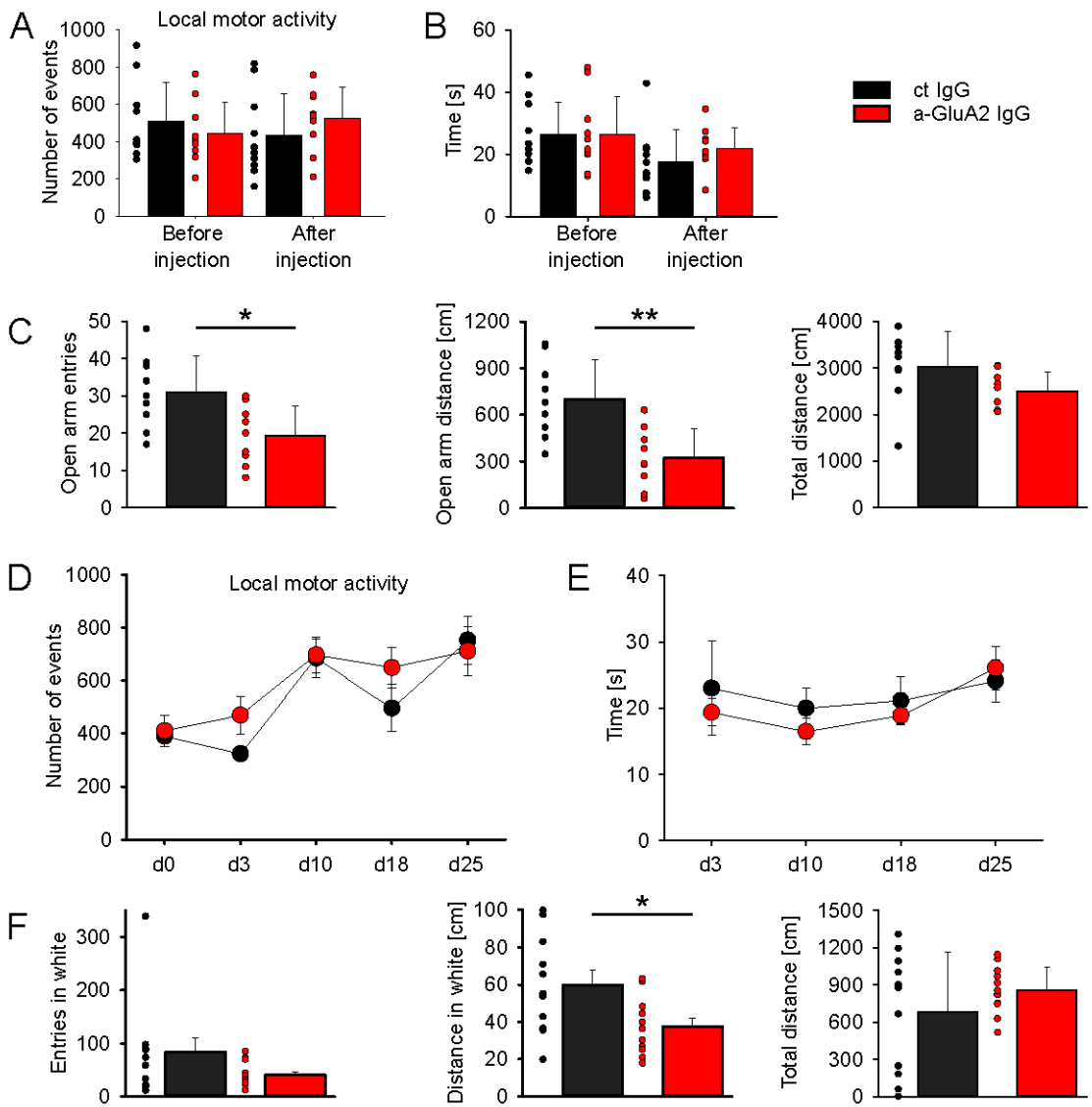


Figure S7



5 Discussion

In the last decade, the discovery of the spectrum of AE and the clinical characterization helped to identify patients suffering from these diseases and established the rationale that these patients should be treated with immunotherapy. Commercially available cell-based assays now allow fast diagnosis of the different subtypes of AE. These assays consist of cell lines that are transfected with the most common target antigens and can be applied for diagnostics using serum and CSF. When started early, immunotherapy often leads to substantial improvement even in very long phases of severe illness. This delayed response to treatment is most likely due to the long half-time of aABs in the CNS and due to long-life plasma cells that are difficult to attack by pharmacological means. Now, it is important to understand disease pathophysiology to understand disease symptoms and to develop target-specific treatment options that can be applied in addition to immunotherapy.

First experimental studies of the molecular mechanisms of aAB action in the brain provided insights into the pathomechanisms of AE. For example, aABs lead to the internalization of NMDARs by cross-linking mechanisms and the disruption of NMDAR - EphB2 interaction leading to impaired NMDAR trafficking to synapses in NMDAR AE (Hughes et al. 2010, Mikasova et al. 2012). These mechanisms then probably induce recognition and memory deficits, depressive-like, and anhedonic behavior in passive-transfer animal model using osmotic pumps to deliver pathogenic aABs into the lateral ventricles of mice. (Planaguma et al. 2015). However, in case of NMDAR AE it was not clear how these aABs interact with synaptic transmission *in-vivo* and if these aABs interfere with synaptic plasticity possibly underlying severe memory deficits. Moreover, to date more than 15 target antigens have been identified. For each of these antigens pathogenic mechanisms that are induced by the aABs may be different and remain to be investigated.

5.1 Experimental models for investigation of AE pathophysiology

One focus of this work was the investigation of aAB mediated deficits on the presynaptic as well as on the postsynaptic site of neuronal connections. Therefore, we generated different experimental models adapted to the respective experimental question. For the verification of aAB specificity we used transfected HEK cells. The cells were transfected with the target protein and specificity of purified human patient IgG was verified by immunocytochemical staining or preabsorption with transfected HEK cells (Planaguma et al. 2016, Werner et al. 2015, Haselmann et al. in revision).

For structural analysis of the pre- and postsynaptic organization of proteins we used dissociated hippocampal neurons. Thereby we were able to apply confocal microscopy or *d*STORM to reconstruct structural synaptic components and analyze protein density and clustering *in-vitro* (Werner et al. 2016, Werner et al. 2015, Haselmann et al. in revision). For cell culture experiments we only needed small amounts of patient IgG fractions for incubation of cells, the incubation procedure is experimentally easy, and answers to these experimental questions could be obtained without animal experiments. We were able to investigate the density and localization of presynaptic proteins and we could identify presynaptic disturbances in vesicle endocytosis induced by aABs to amphiphysin. Additionally, we were able to produce neuronal cell cultures from amphiphysin knockout (ko) mice as control for these structural presynaptic changes. Here, we used embryonic neuronal cultures from heterozygous amphiphysin mice with subsequent genotyping and control immunocytochemical staining against amphiphysin to select neuronal cultures from knockout embryos (Werner et al. 2016). Moreover, we used primary hippocampal neurons to perform electrophysiological patch-clamp studies for analysis of quantal and single synapse synaptic transmission (Werner et al. 2015, Haselmann et al. in revision). Here, among other findings, we could identify changes in quantal release frequency of neurons incubated with IgG fraction from patients with stiff-person syndrome (Werner et al. 2015).

For further evaluation of pathogenic mechanisms of aABs *in-vivo*, animal models are indispensable. For *in-vivo* behavioral and *ex-vivo* physiological experiments we used two different passive-transfer models. First, we established a mouse model with stereotactic intraparenchymal injections of patient IgG samples into different areas of the hippocampus. Using this model it is possible to analyze acute effects of aABs on synaptic function in a locally defined area. The injection site could be identified *ex-vivo* in vital slice preparations by fluorescence location of (*N*-(3-Triethylammoniumpropyl)-4-(4-(Dibutylamino) Styryl) Pyridinium Dibromide fixable (FM1-43FX) dyes added to the injected IgG fraction (Haselmann et al. 2015, Haselmann et al. in revision). This method was used mainly for electrophysiological patch-clamp and field potential recordings of acute hippocampal slices, since it allowed us to locally manipulate the neuronal network without disturbing other brain regions and with little destruction of brain tissue by the injection needle. By using a nanoliter injection device with glass pipettes with very small tip openings, lesions of brain tissue caused by the injection pipette could be reduced to a minimum. In addition, with this method a smaller amount of the patient IgG samples, which are often limited in rare diseases, was needed (Haselmann et al. 2015). Parenchymal injections are best suited for the investigation

of intermediate effects of aABs (up to 24h after injection) since the injected volume and the amount of aABs is small in comparison to the osmotic pump model (see below). Additionally, we used this injection model for behavioral studies by repetitive IgG injections at multiple hippocampal locations over several days, thus ensuring that the observed behavioral deficits on memory are caused by pathogenic effects of aABs exclusively in the hippocampal region.

However, the intraventricular osmotic pump infusion model is better suited for behavioral studies in general. In this model we subcutaneously implanted two osmotic pumps filled with patient IgG samples on the animals neck. These pumps were connected with small tubings on two implanted catheters that deliver IgG probes to both lateral ventricles. The flow rate of the used pumps was 25 μ l/h for total 14 days. As a consequence, investigation of the effects of long-term administration of IgG to the brain is possible and animals are able to recover from surgery over a long time period before maximal concentrations of intraventricular antibodies are reached. Furthermore, repetitive testing can be performed during the infusion period and also during the recovery period after the end of the infusion. We mainly used this model for analysis of structural and functional effects as well as for behavioral studies after long-term aAB administration to the brain (Planaguma et al. 2016, Haselmann et al. in revision).

With the use of both models in the same study testing the same IgG aAB preparation we were able to directly compare the two models with regard to the effects of aABs to the AMPAR in behavioral experiments. Based on these experiments, both models can be regarded as reliable methods for analysis of behavioral effects of AE aABs. In both models we found increased anxiety (EPM or black & white box) and decreased recognition memory (NOR) after administration of GluA2 aABs (Haselmann et al. in revision). In conclusion, the osmotic pump model is less stressful for the animals during experimental acquisition time and less time consuming for the experimenter because of the shorter surgery and there is no necessity for repetition of surgery to accumulate larger amounts of IgG in the brain. The osmotic pump model is able to reflect the long-term influence of IgG samples on brain function better than the injection model. It is also possible to exchange the osmotic pumps after the infusion time of 14 days and extend the long-term exposure of aABs to the time interval needed (Banach-Petrosky et al. 2007, Grathwohl and Jucker 2013). On the other side, the injection model is less material consuming in comparison to the osmotic pump model, since the amount of IgG sample needed is markedly lesser. Intraparenchymal injections are also better suited for investigations of effects of aABs in distinct brain areas.

5.2 aABs lead to internalization of the target antigen by cross-linking mechanisms

For some neuronal surface antigens it is commonly accepted that the binding of aABs leads to cross-linking of target proteins followed by internalization and degradation of these complexes. This has been shown by immunocytochemistry in primary neurons for aABs to the NMDAR, AMPAR, or glycine receptor (Moscato et al. 2014, Lai et al. 2009, Carvajal-Gonzalez et al. 2014). We confirmed these findings *ex-vivo* in brain slices of mice after osmotic pump infusion of NMDAR aABs by confocal microscopy showing reduced expression of NMDARs in the hippocampus (Planaguma et al. 2016). Additionally, we confirmed the findings of Lai et al. (2009) showing reduction of AMPAR expression in neuronal hippocampal cultures, but here with super-resolution microscopy. *d*STORM revealed a reduction of synaptically located GluA2 subunit localizations after 24h of anti-GluA2 IgG incubation (Haselmann et al. in revision). The *d*STORM technique is a powerful tool that is able to break the diffraction limit of normal light microscopy and dissolve structures of as little as 20-40 nm (Rust et al. 2006). This is achieved by photo-switching fluorophores between the on- and off-state, whereas most of the fluorophores are shifted to the off-state by special buffers containing mercaptoethylamine. After acquisition of several thousand pictures with different and separated fluorophores in the on-state it is possible to localize single molecules and compute an image from these single localizations with strongly increased resolution (van de Linde et al. 2011). Thus, *d*STORM enables the analysis of clusters of AMPARs in the subcompartment of the postsynaptic receptor field in hippocampal dissociated neurons. Moreover, measurements of synaptic protein densities are more accurate. Surprisingly, the synaptic GluA1 subunit densities after incubation with GluA2 aABs for 24h were increased, whereas no changes in extracellular GluA1 densities could be detected (Haselmann et al. in revision). When we evaluated the distribution of GluA1 AMPARs after aAB incubation we could show a shifted distribution of extracellular GluA1 AMPARs into synapses possibly compensating for the loss of GluA2 containing by homomeric GluA1 AMPARs. In addition, the number of Homer1 clusters is decreased after incubation with GluA2 aABs, indicating a decrease in the total number of synapses.

5.3 GluA2 AE leads to synaptic changes *in-vitro*

To verify this interesting result, we used functional whole-cell patch-clamp recordings of neuronal cell cultures to measure quantal synaptic inputs from single vesicle fusion (mEPSCs), spontaneous activity of the neuronal network (EPSCs), and evoked glutamatergic transmission by application of glutamate (ieEPSCs) on the level of a single synapse, a

defined group of synapses, and of all synapses projecting to the recorded neuron (Neher and Sakmann 1976, Brown and Greenberg 2016). AMPAR mediated mEPSCs were recorded after blocking action potentials (AP) with tetrodotoxin (TTX). There was no difference in mEPSC amplitude, but a decrease in the frequency of quantal events at resting membrane potentials. Together with our *d*STORM data this can be interpreted as a reduction of active synapses induced by GluA2 aABs or the presence of silent synapses lacking intrasynaptic AMPARs (Kullmann 2003).

Using the inward rectification properties of AMPARs (Bowie and Mayer 1995) we were able to show that mEPSC amplitude and frequency is decreased in GluA2 aAB incubated cells at positive holding potentials, consistent with studies on GluA2 deficient neurons (Lu et al. 2009). This is explained by the exchange of GluA2 containing heteromeric for GluA2 lacking AMPARs that are blocked at positive membrane potential by endogenous polyamines and have a higher single-channel conductance (Donevan and Rogawski 1995). The higher conductivity of the newly inserted AMPARs lacking GluA2 at resting membrane potential leads to a compensation of the mEPSC amplitude although the total number of receptors is reduced by aABs (Sommer et al. 1991). This synaptic AMPAR subunit exchange was corroborated by the use of the specific non-GluA2 AMPAR blocker 1-Naphthyl acetyl spermine (NASPM). mEPSC recordings with superfusion of NASPM led to similar results as compared to recordings at positive holding potentials (Koike et al. 1997). Together, these results are in good accordance with conditional GluA2 ko studies (Panicker et al. 2008, Altimimi and Stellwagen 2013, Lu et al. 2009).

Further, evaluation of the synaptic transmission in neuronal cultures by single synaptic glutamate iontophoresis revealed unchanged ieEPSCs. Here, single synaptic spots are identified with FM1-43FX, a fluorescent dye that is enriched in presynaptic vesicles upon stimulation and endocytosis (Geis et al. 2010). A glass pipette with very small tip opening filled with the negatively charged transmitter glutamate and connected to a iontophoretic device can release the transmitters for stimulation of the individual synapse when negative potential is given to the pipette for a very short time interval (1 ms) (Murnick et al. 2002, Liu et al. 1999). Increase of stimulation strength leads then to enhanced glutamate release and to multisynaptic stimulation along the dendrite. ieEPSC evoked by multisynaptic stimulation were decreased in GluA2 aAB preincubated cells (Haselmann et al. in revision). This observation suggests a reduction of AMPAR containing synapses consistent with immunocytochemical experiments as shown before (Lai et al. 2009). Moreover, partial

silencing of synapses or reduced absolute AMPAR expression was also reported in GluA2 deficient neurons (Lu et al. 2009, Sans et al. 2003). Corroborating these findings, the reduction of synaptic GluA2 containing AMPARs is also reflected in a decrease of recovery after desensitization in GluA2 aAB incubated neurons as it has been reported in GluA2 ko slice cultures (Harvey et al. 2001).

5.4 GluA2 aABs lead to synaptic scaling

Next, we injected human aABs into the dentate gyrus of the hippocampus of mice. FM1-43FX was co-injected for intravital identification of the correct application site in acute slice preparation. Stimulation of the lateral perforant path fibers revealed unchanged evoked excitatory currents (eEPSC) in dentate gyrus granule cells consistent with our results in neuronal cultures. With fixed experimental settings and a high number of stimulations we were able to perform non-stationary fluctuation analysis (nsFA) using the eEPSC recordings. With this method using a mathematical model it is possible to extract the single-channel conductivity and number of channels contributing to a synaptic response from the variation of this response (Benke et al. 2001). The readout of this method is a parabolic curve from which the single channel conductance is given by the initial slope and the number of channels by the equation of the parabola (Sigworth 1980). Analysis of nsFA data demonstrated increased single channel conductivities and decreased channel numbers in eEPSCs comparable to the results in mEPSC recordings in cultured neurons. The hypothesis of synaptic insertion of GluA2 lacking AMPARs was ultimately supported by recordings in GluA1 ko mice after GluA2 aAB administration. Here, eEPSC amplitudes were decreased with unchanged single channel conductance but decreased channel number (Haselmann et al. in revision). In GluA1 ko mice, the loss of GluA2 containing AMPARs cannot be compensated by insertion of GluA2 lacking AMPARs, e.g. GluA1 monomers. These mainly extrasynaptic located GluA1 homomeric AMPARs have increased single channel conductance (Sommer et al. 1991) and are blocked by NASPM (Koike et al. 1997) explaining the results of nsFA by insertion of GluA2 lacking AMPARs in wildtype mice (Soares et al. 2013). In GluA1 ko mice extrasynaptic homomeric GluA1 AMPARs are not available, therefore, single channel conductance in nsFA was unchanged, but the number of channels was decreased then leading to the reduction of eEPSC amplitude.

5.5 Recognition memory and anxiety like behavior is affected by GluA2 aABs

In the next step we tested for the pathogenic effects of GluA2 AE on the mouse behavior in our passive-transfer animal models. As behavioral readouts we used the novel object recognition test as a method for memory testing and the elevated plus maze test (EPM) or the black and white box as methods to assess anxiety related behavior. Additionally, we used an infrared (IR) actimeter for the analysis of locomotor activity. With this set of behavioral experiments we were able to reliably recognize behavioral changes of mice after aAB administration.

The IR actimeter is measuring motoric activity, including horizontal activity, local motor activity and rearings. Data from the IR actimeter were used to detect influence of the surgery on the activity of the animals. Moreover, this data can also be used to assess the direct influence of aAB administration on motoric behavior (Caille et al. 1999, Berrendero et al. 2005). As we expected, we did not find changes in locomotor activity since motor dysfunction is not a key symptom of the disease. This result also allows us to conclude that the surgeries had no influence on overall activity of test animals in the animal models (Planaguma et al. 2016, Haselmann et al. in revision).

The anxiety tests both measure the mice's natural aversion to open spaces and the tendency to be thigmotaxic. In the EPM there are two closed arms allowing the animal to hide in a dark zone and two open arms that are enlightened and allow the view over a wide area of the room. Dependent on anxiety level of the animal it will remain in the dark for a longer period (Walf and Frye 2007, Pellow et al. 1985). In the black and white box, the same paradigm is tested by using a black darkened box as a possibility to hide and an enlightened white box as a stimulus for anxiety (Gimenez-Llort et al. 2015). In contrast to the assumption that anxiety is nearly exclusively mediated by the amygdala, recent data revealed striking evidence that the ventral hippocampus is involved, too (Bannerman et al. 2014, Bannerman et al. 2004). In our experiments we could show that GluA2 aABs mediate increased anxiety in the hippocampal injection animal model in the EPM, as well as in the ventricular infusion animal model in the black and white box (Haselmann et al. in revision). Whereas the osmotic pump model could account for aAB induced pathomechanisms in the hippocampus as well as in the amygdala, the injection model is likely to induce anxiety related behavior especially in the hippocampus since the diffusion of locally injected aABs into the amygdala is not expected. Together, these findings are in line with further studies suggesting increased anxiety-like behavior after

benzodiazepine withdrawal induced deregulation of synaptic AMPAR composition (Van Sickel et al. 2004, Das et al. 2008).

We used the Novel Object Recognition (NOR) test in order to test the impact of anti-AMPA aABs on memory. This test uses the animals innate exploratory behavior without the need of other positive or negative stimuli (Antunes and Biala 2012). Another advantage of the NOR test is the possibility that it can be repeated several times with different objects without disturbing the performance of the animal. This allows the experimenter to test recognition memory before and after surgery to rule out effects of the surgery on brain function. The test measures the discrimination index, e.g. the time spent exploring the unknown object divided by the total time exploring both objects. A higher discrimination index is considered to reflect greater memory retention for the familiar object (Ennaceur and Delacour 1988). There is still discussion about the participating brain regions in NOR. On the one side, involvement of different brain regions in novel object preference and object location paradigms is suggested (Barker and Warburton 2011). Novel object preference may be mediated more by perirhinal cortex, whereas object location is mediated by the hippocampus. On the other side, also the hippocampus is identified to participate in novel object preference test (Broadbent et al. 2010, Cohen and Stackman 2015). Overall, the involvement of the hippocampus in object recognition memory seems to be dependent on the delay between the familiarization and the test phase (Cohen and Stackman 2015, Hammond et al. 2004). In our experiments we used two objects on a diagonal axis of the open field box for habituation and exchanged one of these objects for the acquisition (Puighermanal et al. 2009). Our experiments revealed a decrease in object recognition memory by GluA2 aABs in the microinjection model as well as the osmotic pump model. This reflects the characteristic anterograde memory deficit that is characteristic in patients with GluA2 AE (Tuzun and Dalmau 2007).

Of note, in the parenchymal injection model of GluA2 AE also control IgG injected mice showed slightly decreased performance in the NOR task in comparison to the baseline performance before surgery. This effect could be due to repetitive surgeries and anesthesia. Furthermore, repetitive injections at multiple injection sites might have effects on behavior due to small lesions of brain tissue. Another possible influence factor might be the short time (one day) of recovery after the last surgery. However, the decrease in recognition memory of these control mice was by far less pronounced than in GluA2 IgG injected animals. Based on these caveats the osmotic pump model might be better suited for behavioral testing whereas the injection model is possibly more suitable for electrophysiological recordings due to its

defined local application and the exact amount of injected aAB fractions to these targeted injection sites.

5.6 The effects of aABs to ionotropic glutamate receptors on synaptic long-term potentiation

By using aABs to the AMPAR (anti-GluA2 aABs) and to the NMDAR (anti-NR1 aABs) we first showed how disease-associated human aABs to neuronal antigens interfere with synaptic plasticity. As functional correlate for learning and memory we used *ex-vivo* hippocampal brain slice field excitatory postsynaptic potential (fEPSP) recordings to test long term potentiation (LTP) in the Schaffer collateral – CA1 synaptic pathway (Morris et al. 1986).

When anti-GluA2 aABs were injected into the CA1 region of the hippocampus, LTP after theta burst stimulation was heavily reduced as shown by the reduction of fEPSP slope values in comparison to control IgG injected animals (Haselmann et al. in revision). Induction of LTP drives the recruitment of extrasynaptic AMPARs to synapses (Bassani et al. 2013, Jacob and Weinberg 2015). Additionally, Granger et al. (2013) demonstrated that LTP formation is strongly dependent on the number of extrasynaptic receptors independently from their type or subunit composition. As we could show by electrophysiology and super-resolution microscopy, anti-GluA2 aABs mediate the internalization of AMPARs leading to the insertion of extrasynaptic AMPARs from the reserve pool. We therefore propose that the loss of extrasynaptic AMPARs after hippocampal GluA2 aAB injection leads to insufficient incorporation of AMPARs and finally to reduced LTP. Corroborating this hypothesis, basic synaptic transmission measured by input-output characteristics of fEPSPs during the same recording session is unaltered by anti-GluA2 aABs similar to eEPSC peak amplitudes in dentate gyrus granule cells as revealed by patch-clamp measurements (discussed above) (Haselmann et al. in revision).

In contrast, ventricular infusion of anti-NMDAR aABs and subsequent fEPSP recordings showed decreased basal synaptic transmission in the Schaffer collateral – CA1 pathway and decreased LTP after theta burst stimulation (Planaguma et al. 2016). For LTP the synaptical influx of Ca^{2+} and subsequent activation of Ca^{2+} /calmodulin-dependent protein kinase II is coercive. NMDAR aABs lead to the internalization of NMDARs. Consequently, this reduction of NMDARs leads to the impairment of LTP due to the decreased number of Ca^{2+} conductible channels (Lisman et al. 2012). These results show the differences of aAB interference with synaptic plasticity depending on the target antigen. Both aAB fractions lead

to the internalization of the respective receptors, but while in GluA2 AE AMPAR synaptic transmission can be rescued by extrasynaptic AMPAR that are then missing for induction of LTP, anti-NR1 aABs lead to disturbed synaptic anchoring of NMDARs by disruption of NMDAR – EphB2 interaction and therefore prevents appropriate synaptic transmission as well as LTP (Planaguma et al. 2016, Dalva et al. 2000).

5.7 Soluble ephrine-B2 is able to rescue the NMDAR AE phenotype in the osmotic pump model

Since Mikasova et al. (2012) could show that ephrine-B2 is able to prevent the loss of NMDARs in immunohistological stainings of brain slices, we aimed to test this observation as a treatment approach during long term aAB infusion by osmotic pumps in an *in-vivo* animal model. Therefore, we co-applied ephrine-B2 together with the aAB fractions during chronic intraventricular infusion. Indeed, ephrine-B2 was a potent inhibitor of the pathogenic effects on synaptic function and behavior mediated by anti-NR1 aABs. Behavioral deficits and structural abnormalities in receptor densities could be almost completely rescued by ephrine-B2 co-application whereas functional deficits of LTP and basic synaptic transmission were partially rescued. This beneficial effect is explained by the fact that the activation of EphB2 receptors by its ligand ephrine-B2 leads to an increased synaptic clustering of NMDARs (Dalva et al. 2000). According to these observations, application of EphB2 agonists might be an option for an alternative treatment approach of NMDAR AE in addition to immunosuppressive therapy (Planaguma et al. 2016). This dual therapeutic approach might be more effective in controlling disease symptoms. Importantly, it might also shorten the time of treatment response in this severe and long-lasting disorder.

5.8 The role of the target antigen in AE

This work shows the diversity of pathomechanisms in AE that depends on the target antigen of the associated aABs. Whereas some mechanisms seem to be present in several subtypes of AE (e.g. aAB-induced internalization of synaptic proteins), the outcome of this mechanism with respect to neuronal and network function may be diverse. The effects of aABs on the NR1 subunit of the NMDAR or to the GluA2 subunit of the AMPAR can serve as an example. For both subtypes of AE experimental evidence demonstrates aAB mediated crosslinking and internalization of the receptors leading to decreased receptor densities in neuronal cultures (Lai et al. 2009, Hughes et al. 2010). However, by using super-resolution microscopy we were able to elucidate the molecular mechanism in GluA2 AE more

accurately. We could show that the internalization of GluA2 containing receptors lead to the synaptic accumulation of GluA2 lacking AMPARs from extrasynaptic pools (Haselmann et al. in revision). Since the NR1 subunit of the NMDAR is obligatory for its membrane insertion and function such mechanism cannot be expected in NMDAR AE (Nakanishi 1992).

These differences are also reflected in the results of electrophysiological recordings. Anti-NR1 aABs lead to a reduction of synaptic NMDARs and therefore to a reduction of NMDAR but not AMPAR mediated mEPSC amplitudes (Hughes et al. 2010). On the other hand, AMPAR mEPSC amplitudes were unchanged after application of anti-GluA2 aABs at resting membrane potential due to the incorporation of AMPAR lacking GluA2 from extra- to intrasynaptic sites after GluA2 internalization (Haselmann et al. in revision).

In fEPSP recordings differences in the manifestation of defective LTP were elaborated. In mice injected with anti-GluA2 aABs reduction of LTP is mediated by the lack of an extrasynaptic reserve pool of AMPARs, but basal synaptic transmission was unaltered. By contrast, in mice after application of anti-NR1 aABs, reduced LTP is explained by globally reduced NMDARs after aAB-mediated internalization that also affected synaptic transmission on the multi-synaptic and cellular level (Planaguma et al. 2016, Haselmann et al. in revision, Hughes et al. 2010).

In behavioral tests aABs to GluA2 as well as to NR1 led to memory deficits in the NOR test, reflecting the dominant memory defects in patients. However, mice were affected differently in other behavioral tests. Whereas anti-AMPA-aAB infused animals showed increased anxiety in the EPM and the black and white box test, anti-NMDAR aAB infused animals were not susceptible for anxiety but had increased depressive-like behavior in tail suspension and forced swimming test.

These results elucidate the difference in the molecular mechanisms of disease-associated aABs in AE. These differences may be the underlying cause for diverse and characteristic symptoms in each subtype of disease and for different treatment response and time course of disease in patients (Tuzun and Dalmau 2007, Irani et al. 2010).

5.9 Conclusion and outlook

Taken together, the current work elucidates basic pathophysiological mechanisms in prototypic disorders of the newly discovered spectrum of AE. We could provide evidence for

aAB-induced synaptic dysfunction and defects in synaptic organization of important pre- and postsynaptic molecules. These changes most likely mediate characteristic disease symptoms in patients of AE, e.g. memory dysfunction and defective motor control. Moreover, we clearly demonstrate the diversity of synaptic pathomechanisms depending on the respective target antigen and depict the importance to explore detailed molecular mechanisms of the individual types of AE.

In case of Stiff person syndrome with aABs to amphiphysin we could show that vesicle endocytosis is altered by pathogenic aABs to amphiphysin leading to a depletion of reserve pool vesicles and disturbed vesicle release (Werner et al. 2016). This presynaptic defect might be causative for disturbed spinal GABAergic transmission and severe muscle hyperactivity as shown in a passive transfer model and in patients (Geis et al. 2010). In NMDAR encephalitis the NR1 – EphB2 interaction is disturbed by specific aABs leading to deficits in memory function and LTP (Mikasova et al. 2012, Planaguma et al. 2016). In AMPAR AE with aABs to GluA2 GluA1/GluA2 heteromeric AMPARs are internalized and synaptic incorporation of AMPARs with increased conductivity and inward rectification induce synaptic scaling. These changes are distinct from NMDAR encephalitis but may also induce behavioral deficits and impair synaptic plasticity (Haselmann et al. in revision).

Animal models are necessary tools for unequivocal confirmation of the pathological action of aABs according to the Witebsky criteria (Rose and Bona 1993). Together with *in-vitro* and *ex-vivo* studies and using a variety of advanced experimental techniques it is possible to analyze structural and functional changes of central synapses and to create a detailed picture of aAB induced pathomechanisms in the CNS. By uncovering these mechanisms new treatment approaches can be developed that act specifically and may extend immunotherapy. So far, immunotherapy is not able to eliminate aAB producing B-cells in the CNS. Thus, in near future alternative therapeutic approaches may be of great importance for treatment of AE in general (Furieux et al. 1990). The NMDAR – EphB2 interaction serves as a first example how such novel treatment approaches can be realized in experimental models. Further studies need to demonstrate if this approach has the potential to be translated for use in disease.

In AMPAR AE with aABs to GluA2 a possible novel treatment approach could be the interference with micro ribonucleic acid (miR) involved in AMPAR regulation. First, it has been shown that miR124 regulates the expression of GluA2, GluA3 and GluA4. Reduced expression of miR124 leads to increased GluA2, GluA3 and GluA4 expression in the frontal cortex (Gascon et al. 2014). In another study the increase of miR 124 lead to a reduction of

GluA1 and GluA2 AMPARs in the hippocampus as well as decreased memory performance in the Morris water maze (Arrant and Roberson 2014, Dutta et al. 2013). Therefore, downregulation of miR124 by an appropriate antagomir may induce overexpression of AMPARs that possibly counteracts the aAB mediated internalization of GluA2. Second, miR233 regulates the expression of GluA2 and NR2B. Downregulation of miR233 leads to increased GluA2 and NR2B levels in the hippocampus (Harraz et al. 2012). Third, miR181a expression leads to the reduction of GluA2 AMPAR leading to changes in synaptic organization and reduced mEPSC amplitude and frequency hippocampal neuronal cells (Saba et al. 2012, Zhang et al. 2016). Modulation of these miRNAs by antagomirs can be used as a tool for overexpression of GluA2 containing AMPARs and may serve as possible therapeutic target in GluA2 AE counteracting the deregulation of synaptic AMPARs.

In summary, we uncovered disease-relevant pathomechanism of Stiff-person syndrome with aABs to amphiphysin, of NMDAR AE with aABs to NR1, and of AMPAR AE with aABs to GluA2. For NMDAR AE a first treatment approach with ephrin-B2 in a passive transfer animal model successfully restored the functionality of synaptic transmission and performance in behavioral tests. Due to the diversity of antibody targets in AE it is of great importance to investigate the pathogenic effects of the respective aAB in detail. Specific alternative treatment approaches might be developed as complementary treatment approaches in addition to immunotherapy, thus leading to effective treatment and better disease control in patients with AE.

6 References

- Altimimi HF, Stellwagen D. 2013. Persistent Synaptic Scaling Independent of AMPA Receptor Subunit Composition. *Journal of Neuroscience*, 33 (29):11763-11767.
- Ances BM, Vitaliani R, Taylor RA, Liebeskind DS, Voloschin A, Houghton DJ, Galetta SL, Dichter M, Alavi A, Rosenfeld MR, Dalmau J. 2005. Treatment-responsive limbic encephalitis identified by neuropil antibodies: MRI and PET correlates. *Brain*, 128 (Pt 8):1764-1777.
- Antunes M, Biala G. 2012. The novel object recognition memory: neurobiology, test procedure, and its modifications. *Cognitive Processing*, 13 (2):93-110.
- Arrant AE, Roberson ED. 2014. MicroRNA-124 modulates social behavior in frontotemporal dementia. *Nature Medicine*, 20 (12):1381-1383.
- Banach-Petrosky W, Jessen WJ, Ouyang X, Gao H, Rao J, Quinn J, Aronow BJ, Abate-Shen C. 2007. Prolonged exposure to reduced levels of androgen accelerates prostate cancer progression in Nkx3.1; Pten mutant mice. *Cancer Research*, 67 (19):9089-9096.
- Bannerman DM, Sprengel R, Sanderson DJ, McHugh SB, Rawlins JNP, Monyer H, Seeburg PH. 2014. Hippocampal synaptic plasticity, spatial memory and anxiety. *Nature Reviews Neuroscience*, 15 (3):181-192.
- Bannerman DM, Rawlins JNP, McHugh SB, Deacon RMJ, Yee BK, Bast T, Zhang WN, Pothuizen HHJ, Feldon J. 2004. Regional dissociations within the hippocampus - memory and anxiety. *Neuroscience and Biobehavioral Reviews*, 28 (3):273-283.
- Barker GRI, Warburton EC. 2011. When Is the Hippocampus Involved in Recognition Memory? *Journal of Neuroscience*, 31 (29):10721-10731.
- Bassani S, Folci A, Zapata J, Passafaro M. 2013. AMPAR trafficking in synapse maturation and plasticity. *Cell Mol Life Sci*, 70 (23):4411-4430.
- Benke TA, Luthi A, Palmer MJ, Wikstrom MA, Anderson WW, Isaac JTR, Collingridge GL. 2001. Mathematical modelling of non-stationary fluctuation analysis for studying channel properties of synaptic AMPA receptors. *Journal of Physiology-London*, 537 (2):407-420.
- Berrendero F, Mendizabal V, Robledo P, Galeote L, Bilkei-Gorzo A, Zimmer A, Maldonado R. 2005. Nicotine-induced antinociception, rewarding effects, and physical dependence are decreased in mice lacking the preproenkephalin gene. *Journal of Neuroscience*, 25 (5):1103-1112.
- Bien CG, Vincent A, Barnett MH, Becker AJ, Blumcke I, Graus F, Jellinger KA, Reuss DE, Ribalta T, Schlegel J, Sutton I, Lassmann H, Bauer J. 2012. Immunopathology of autoantibody-associated encephalitides: clues for pathogenesis. *Brain*, 135 (Pt 5):1622-1638.
- Bouillere V, Ridoux V, Depaulis A, Marescaux C, Nehlig A, La Salle GL. 1999. Recurrent seizures and hippocampal sclerosis following intrahippocampal kainate injection in adult mice: Electroencephalography, histopathology and synaptic reorganization similar to mesial temporal lobe epilepsy. *Neuroscience*, 89 (3):717-729.
- Bowie D, Mayer ML. 1995. Inward rectification of both AMPA and kainate subtype glutamate receptors generated by polyamine-mediated ion channel block. *Neuron*, 15 (2):453-462.
- Broadbent NJ, Gaskin S, Squire LR, Clark RE. 2010. Object recognition memory and the rodent hippocampus. *Learning & Memory*, 17 (1):794-800.
- Brown APY, Greenberg HZE. 2016. Patch clamp. *British Journal of Hospital Medicine*, 77 (5):C74-C77.
- Burnashev N, Monyer H, Seeburg PH, Sakmann B. 1992. Divalent ion permeability of AMPA receptor channels is dominated by the edited form of a single subunit. *Neuron*, 8 (1):189-198.

- Caille S, Espejo EF, Reneric JP, Cador M, Koob GF, Stinus L. 1999. Total neurochemical lesion of noradrenergic neurons of the locus ceruleus does not alter either naloxone-precipitated or spontaneous opiate withdrawal nor does it influence ability of clonidine to reverse opiate withdrawal. *Journal of Pharmacology and Experimental Therapeutics*, 290 (2):881-892.
- Carvajal-Gonzalez A, Leite MI, Waters P, Woodhall M, Coutinho E, Balint B, Lang B, Pettingill P, Carr A, Sheerin UM, Press R, Lunn MP, Lim M, Maddison P, Meinck HM, Vandenberghe W, Vincent A. 2014. Glycine receptor antibodies in PERM and related syndromes: characteristics, clinical features and outcomes. *Brain*, 137:2178-2192.
- Cohen SJ, Stackman RW. 2015. Assessing rodent hippocampal involvement in the novel object recognition task. A review. *Behavioural Brain Research*, 285:105-117.
- Dalmau J, Geis C, Graus F. 2017. Autoantibodies to Synaptic Receptors and Neuronal Cell Surface Proteins in Autoimmune Diseases of the Central Nervous System. *Physiol Rev*, 97 (2):839-887.
- Dalmau J, Lancaster E, Martinez-Hernandez E, Rosenfeld MR, Balice-Gordon R. 2011. Clinical experience and laboratory investigations in patients with anti-NMDAR encephalitis. *Lancet Neurol*, 10 (1):63-74.
- Dalmau J, Gleichman AJ, Hughes EG, Rossi JE, Peng XY, Lai MZ, Dessain SK, Rosenfeld MR, Balice-Gordon R, Lynch DR. 2008. Anti-NMDA-receptor encephalitis: case series and analysis of the effects of antibodies. *Lancet Neurology*, 7 (12):1091-1098.
- Dalmau J, Tuzun E, Wu HY, Masjuan J, Rossi JE, Voloschin A, Baehring JM, Shimazaki H, Koide R, King D, Mason W, Sansing LH, Dichter MA, Rosenfeld MR, Lynch DR. 2007. Paraneoplastic anti-N-methyl-D-aspartate receptor encephalitis associated with ovarian teratoma. *Ann Neurol*, 61 (1):25-36.
- Dalva MB, Takasu MA, Lin MZ, Shamah SM, Hu L, Gale NW, Greenberg ME. 2000. EphB receptors interact with NMDA receptors and regulate excitatory synapse formation. *Cell*, 103 (6):945-956.
- Darnell RB, Posner JB. 2003. Paraneoplastic syndromes involving the nervous system. *N Engl J Med*, 349 (16):1543-1554.
- Das P, Lilly SM, Zerda R, Gunning WT, Alvarez FJ, Tietz EI. 2008. Increased AMPA Receptor GluR1 Subunit Incorporation in Rat Hippocampal CA1 Synapses During Benzodiazepine Withdrawal. *Journal of Comparative Neurology*, 511 (6):832-846.
- Dingledine R, Borges K, Bowie D, Traynelis SF. 1999. The glutamate receptor ion channels. *Pharmacological Reviews*, 51 (1):7-61.
- Donevan SD, Rogawski MA. 1995. Intracellular Polyamines Mediate Inward Rectification of Ca²⁺-Permeable Alpha-Amino-3-Hydroxy-5-Methyl-4-Isioxazolepropionic Acid Receptors. *Proceedings of the National Academy of Sciences of the United States of America*, 92 (20):9298-9302.
- Drachman DB, Adams RN, Josifek LF, Self SG. 1982. Functional activities of autoantibodies to acetylcholine receptors and the clinical severity of myasthenia gravis. *N Engl J Med*, 307 (13):769-775.
- Drachman DB, Angus CW, Adams RN, Michelson JD, Hoffman GJ. 1978. Myasthenic antibodies cross-link acetylcholine receptors to accelerate degradation. *N Engl J Med*, 298 (20):1116-1122.
- Dutta R, Chomyk AM, Chang A, Ribaldo MV, Deckard SA, Doud MK, Edberg DD, Bai B, Li M, Baranzini SE, Fox RJ, Staugaitis SM, Macklin WB, Trapp BD. 2013. Hippocampal Demyelination and Memory Dysfunction are Associated with Increased Levels of the Neuronal microRNA miR-124 and Reduced AMPA Receptors. *Annals of Neurology*, 73 (5):637-645.

- Ennaceur A, Delacour J. 1988. A New One-Trial Test for Neurobiological Studies of Memory in Rats .1. Behavioral-Data. *Behavioural Brain Research*, 31 (1):47-59.
- Fara J, Urquhart J. 1984. The Value of Infusion and Injection Regimens in Assessing Efficacy and Toxicity of Drugs. *Trends in Pharmacological Sciences*, 5 (1):21-25.
- Forrest D, Yuzaki M, Soares HD, Ng L, Luk DC, Sheng M, Stewart CL, Morgan JI, Connor JA, Curran T. 1994. Targeted Disruption of Nmda Receptor-1 Gene Abolishes Nmda Response and Results in Neonatal Death. *Neuron*, 13 (2):325-338.
- Furueux HF, Reich L, Posner JB. 1990. Autoantibody Synthesis in the Central-Nervous-System of Patients with Paraneoplastic Syndromes. *Neurology*, 40 (7):1085-1091.
- Furukawa H, Singh SK, Mancusso R, Gouaux E. 2005. Subunit arrangement and function in NMDA receptors. *Nature*, 438 (7065):185-192.
- Gascon E, Lynch K, Ruan H, Almeida S, Verheyden JM, Seeley WW, Dickson DW, Petrucelli L, Sun D, Jiao J, Zhou H, Jakovcevski M, Akbarian S, Yao WD, Gao FB. 2014. Alterations in microRNA-124 and AMPA receptors contribute to social behavioral deficits in frontotemporal dementia. *Nat Med*, 20 (12):1444-1451.
- Geis C, Weishaupt A, Hallermann S, Grunewald B, Wessig C, Wulsch T, Reif A, Byts N, Beck M, Jablonka S, Boettger MK, Uceyler N, Fouquet W, Gerlach M, Meinck HM, Siren AL, Sigrist SJ, Toyka KV, Heckmann M, Sommer C. 2010. Stiff person syndrome-associated autoantibodies to amphiphysin mediate reduced GABAergic inhibition. *Brain*, 133:3166-3180.
- Gimenez-Llort L, Ratia M, Perez B, Camps P, Munoz-Tonerreo D, Badia A, Clos MV. 2015. AVCRI104P3, a novel multitarget compound with cognition-enhancing and anxiolytic activities: Studies in cognitively poor middle-aged mice. *Behavioural Brain Research*, 286:97-103.
- Gleichman AJ, Spruce LA, Dalmau J, Seholzer SH, Lynch DR. 2012. Anti-NMDA Receptor Encephalitis Antibody Binding Is Dependent on Amino Acid Identity of a Small Region within the GluN1 Amino Terminal Domain. *Journal of Neuroscience*, 32 (32):11082-11094.
- Gleichman AJ, Panzer JA, Baumann BH, Dalmau J, Lynch DR. 2014. Antigenic and mechanistic characterization of anti-AMPA receptor encephalitis. *Annals of Clinical and Translational Neurology*, 1 (3):180-189.
- Granger AJ, Shi Y, Lu W, Cerpas M, Nicoll RA. 2013. LTP requires a reserve pool of glutamate receptors independent of subunit type. *Nature*, 493 (7433):495-500.
- Grathwohl SA, Jucker M. 2013. Replacement of osmotic minipumps to extend the intracerebral infusion time of compounds into the mouse brain. *Biotechniques*, 55 (2):75-78.
- Graus F, Titulaer MJ, Balu R, Benseler S, Bien CG, Cellucci T, Cortese I, Dale RC, Gelfand JM, Geschwind M, Glaser CA, Honnorat J, Hoftberger R, Iizuka T, Irani SR, Lancaster E, Leypoldt F, Pruss H, Rae-Grant A, Reindl M, Rosenfeld MR, Rostasy K, Saiz A, Venkatesan A, Vincent A, Wandinger KP, Waters P, Dalmau J. 2016. A clinical approach to diagnosis of autoimmune encephalitis. *Lancet Neurol*, 15 (4):391-404.
- Hammond RS, Tull LE, Stackman RW. 2004. On the delay-dependent involvement of the hippocampus in object recognition memory. *Neurobiology of Learning and Memory*, 82 (1):26-34.
- Harraz MM, Eacker SM, Wang XQ, Dawson TM, Dawson VL. 2012. MicroRNA-223 is neuroprotective by targeting glutamate receptors. *Proceedings of the National Academy of Sciences of the United States of America*, 109 (46):18962-18967.
- Harvey SC, Koster A, Yu H, Skolnick P, Baumbarger P, Nisenbaum ES. 2001. AMPA receptor function is altered in GLUR2-deficient mice. *Journal of Molecular Neuroscience*, 17 (1):35-43.

- Haselmann H, Ropke L, Werner C, Kunze A, Geis C. 2015. Interactions of human autoantibodies with hippocampal GABAergic synaptic transmission - analyzing antibody-induced effects ex vivo. *Frontiers in Neurology*, 6.
- Haselmann H, Mannara F, Werner C, Planaguma J, Grünewald B, Petit-Pedrol M, Kirmse K, Classen J, Demir F, Klöcker N, Doose S, Dalmau J, Hallermann S, Geis C. in revision. Human autoantibodies against the AMPA receptor subunit GluA2 induce receptor reorganisation and memory dysfunction. *Neuron*.
- Hoftberger R, van Sonderen A, Leypoldt F, Houghton D, Geschwind M, Gelfand J, Paredes M, Sabater L, Saiz A, Titulaer MJ, Graus F, Dalmau J. 2015. Encephalitis and AMPA receptor antibodies Novel findings in a case series of 22 patients. *Neurology*, 84 (24):2403-2412.
- Hollmann M, Heinemann S. 1994. Cloned Glutamate Receptors. *Annual Review of Neuroscience*, 17:31-108.
- Hollmann M, Hartley M, Heinemann S. 1991. Ca²⁺ permeability of KA-AMPA-gated glutamate receptor channels depends on subunit composition. *Science*, 252 (5007):851-853.
- Hou Q, Zhang D, Jarzylo L, Haganir RL, Man HY. 2008. Homeostatic regulation of AMPA receptor expression at single hippocampal synapses. *Proc Natl Acad Sci U S A*, 105 (2):775-780.
- Hughes EG, Peng XY, Gleichman AJ, Lai MZ, Zhou L, Tsou R, Parsons TD, Lynch DR, Dalmau J, Balice-Gordon RJ. 2010. Cellular and Synaptic Mechanisms of Anti-NMDA Receptor Encephalitis. *Journal of Neuroscience*, 30 (17):5866-5875.
- Hutchinson M, Waters P, McHugh J, Gorman G, O'Riordan S, Connolly S, Hager H, Yu P, Becker CM, Vincent A. 2008. Progressive encephalomyelitis, rigidity, and myoclonus: a novel glycine receptor antibody. *Neurology*, 71 (16):1291-1292.
- Irani SR, Bera K, Waters P, Zuliani L, Maxwell S, Zandi MS, Friese MA, Galea I, Kullmann DM, Beeson D, Lang B, Bien CG, Vincent A. 2010. N-methyl-d-aspartate antibody encephalitis: temporal progression of clinical and paraclinical observations in a predominantly non-paraneoplastic disorder of both sexes. *Brain*, 133:1655-1667.
- Jacob AL, Weinberg RJ. 2015. The organization of AMPA receptor subunits at the postsynaptic membrane. *Hippocampus*, 25 (7):798-812.
- Karakas E, Furukawa H. 2014. Crystal structure of a heterotetrameric NMDA receptor ion channel. *Science*, 344 (6187):992-997.
- Koike M, Iino M, Ozawa S. 1997. Blocking effect of 1-naphthyl acetyl spermine on Ca²⁺-permeable AMPA receptors in cultured rat hippocampal neurons. *Neuroscience Research*, 29 (1):27-36.
- Kreye J, Wenke NK, Chayka M, Leubner J, Murugan R, Maier N, Jurek B, Ly LT, Brandl D, Rost BR, Stumpf A, Schulz P, Radbruch H, Hauser AE, Pache F, Meisel A, Harms L, Paul F, Dirnagl U, Garner C, Schmitz D, Wardemann H, Pruss H. 2016. Human cerebrospinal fluid monoclonal N-methyl-D-aspartate receptor autoantibodies are sufficient for encephalitis pathogenesis. *Brain*, 139:2641-2652.
- Kullander K, Klein R. 2002. Mechanisms and functions of EPH and ephrin signalling. *Nature Reviews Molecular Cell Biology*, 3 (7):475-486.
- Kullmann DM. 2003. Silent synapses: what are they telling us about long-term potentiation? *Philos Trans R Soc Lond B Biol Sci*, 358 (1432):727-733.
- Lai MZ, Hughes EG, Peng XY, Zhou L, Gleichman AJ, Shu H, Mata S, Kremens D, Vitaliani R, Geschwind MD, Bataller L, Kalb RG, Davis R, Graus F, Lynch DR, Balice-Gordon R, Dalmau J. 2009. AMPA Receptor Antibodies in Limbic Encephalitis Alter Synaptic Receptor Location. *Annals of Neurology*, 65 (4):424-434.
- Lisabeth EM, Falivelli G, Pasquale EB. 2013. Eph Receptor Signaling and Ephrins. *Cold Spring Harbor Perspectives in Biology*, 5 (9).

- Lisman J, Yasuda R, Raghavachari S. 2012. Mechanisms of CaMKII action in long-term potentiation. *Nat Rev Neurosci*, 13 (3):169-182.
- Liu G, Choi S, Tsien RW. 1999. Variability of neurotransmitter concentration and nonsaturation of postsynaptic AMPA receptors at synapses in hippocampal cultures and slices. *Neuron*, 22 (2):395-409.
- Lomeli H, Mosbacher J, Melcher T, Hoyer T, Geiger JR, Kuner T, Monyer H, Higuchi M, Bach A, Seeburg PH. 1994. Control of kinetic properties of AMPA receptor channels by nuclear RNA editing. *Science*, 266 (5191):1709-1713.
- Lu W, Shi Y, Jackson AC, Bjorgan K, Doring MJ, Sprengel R, Seeburg PH, Nicoll RA. 2009. Subunit Composition of Synaptic AMPA Receptors Revealed by a Single-Cell Genetic Approach. *Neuron*, 62 (2):254-268.
- Malinow R, Malenka RC. 2002. AMPA receptor trafficking and synaptic plasticity. *Annu Rev Neurosci*, 25:103-126.
- Mayer ML, Westbrook GL, Guthrie PB. 1984. Voltage-Dependent Block by Mg²⁺ of Nmda Responses in Spinal-Cord Neurons. *Nature*, 309 (5965):261-263.
- Mikasova L, De Rossi P, Bouchet D, Georges F, Rogemond V, Didelot A, Meissirel C, Honorat J, Groc L. 2012. Disrupted surface cross-talk between NMDA and Ephrin-B2 receptors in anti-NMDA encephalitis. *Brain*, 135:1606-1621.
- Monyer H, Seeburg PH, Wisden W. 1991. Glutamate-Operated Channels - Developmentally Early and Mature Forms Arise by Alternative Splicing. *Neuron*, 6 (5):799-810.
- Morris RG, Anderson E, Lynch GS, Baudry M. 1986. Selective impairment of learning and blockade of long-term potentiation by an N-methyl-D-aspartate receptor antagonist, AP5. *Nature*, 319 (6056):774-776.
- Mosbacher J, Schoepfer R, Monyer H, Burnashev N, Seeburg PH, Ruppersberg JP. 1994. A molecular determinant for submillisecond desensitization in glutamate receptors. *Science*, 266 (5187):1059-1062.
- Moscato EH, Peng XY, Jain A, Parsons TD, Dalmau J, Balice-Gordon RJ. 2014. Acute Mechanisms Underlying Antibody Effects in Anti-N-Methyl-D-Aspartate Receptor Encephalitis. *Annals of Neurology*, 76 (1):108-119.
- Murnick JG, Dube G, Krupa B, Liu G. 2002. High-resolution iontophoresis for single-synapse stimulation. *J Neurosci Methods*, 116 (1):65-75.
- Nakanishi S. 1992. Molecular Diversity of Glutamate Receptors and Implications for Brain-Function. *Science*, 258 (5082):597-603.
- Neher E, Sakmann B. 1976. Single-Channel Currents Recorded from Membrane of Denervated Frog Muscle-Fibers. *Nature*, 260 (5554):799-802.
- Newpher TM, Ehlers MD. 2008. Glutamate receptor dynamics in dendritic microdomains. *Neuron*, 58 (4):472-497.
- Nowak L, Bregestovski P, Ascher P, Herbet A, Prochiantz A. 1984. Magnesium Gates Glutamate-Activated Channels in Mouse Central Neurons. *Nature*, 307 (5950):462-465.
- Okada T, Yamada N, Tsuzuki K, Horikawa HPM, Tanaka K, Ozawa S. 2003. Long-term potentiation in the hippocampal CA1 area and dentate gyrus plays different roles in spatial learning. *European Journal of Neuroscience*, 17 (2):341-349.
- Panicker S, Brown K, Nicoll RA. 2008. Synaptic AMPA receptor subunit trafficking is independent of the C terminus in the GluR2-lacking mouse. *Proc Natl Acad Sci U S A*, 105 (3):1032-1037.
- Paoletti P, Perin-Dureau F, Fayyazuddin A, Le Goff A, Callebaut I, Neyton J. 2000. Molecular organization of a zinc binding N-terminal modulatory domain in a NMDA receptor subunit. *Neuron*, 28 (3):911-925.
- Passafaro M, Piech V, Sheng M. 2001. Subunit-specific temporal and spatial patterns of AMPA receptor exocytosis in hippocampal neurons. *Nat Neurosci*, 4 (9):917-926.

- Pellow S, Chopin P, File SE, Briley M. 1985. Validation of Open - Closed Arm Entries in an Elevated Plus-Maze as a Measure of Anxiety in the Rat. *Journal of Neuroscience Methods*, 14 (3):149-167.
- Peng XY, Hughes EG, Moscato EH, Parsons TD, Dalmau J, Balice-Gordon RJ. 2015. Cellular Plasticity Induced by Anti-alpha-Amino-3-Hydroxy-5-Methyl-4-Isoxazolepropionic Acid (AMPA) Receptor Encephalitis Antibodies. *Annals of Neurology*, 77 (3):381-398.
- Planaguma J, Leyboldt F, Mannara F, Gutierrez-Cuesta J, Martin-Garcia E, Aguilar E, Titulaer MJ, Petit-Pedrol M, Jain A, Balice-Gordon R, Lakadamyali M, Graus F, Maldonado R, Dalmau J. 2015. Human N-methyl D-aspartate receptor antibodies alter memory and behaviour in mice. *Brain*, 138 (Pt 1):94-109.
- Planaguma J, Haselmann H, Mannara F, Petit-Pedrol M, Grunewald B, Aguilar E, Ropke L, Martin-Garcia E, Titulaer MJ, Jercog P, Graus F, Maldonado R, Geis C, Dalmau J. 2016. Ephrin-B2 prevents N-methyl-D-aspartate receptor antibody effects on memory and neuroplasticity. *Annals of Neurology*, 80 (3):388-400.
- Pruss H, Finke C, Holtje M, Hofmann J, Klingbeil C, Probst C, Borowski K, Ahnert-Hilger G, Harms L, Schwab JM, Ploner CJ, Komorowski L, Stoecker W, Dalmau J, Wandinger KP. 2012. N-methyl-D-aspartate receptor antibodies in herpes simplex encephalitis. *Ann Neurol*, 72 (6):902-911.
- Puighermanal E, Marsicano G, Busquets-Garcia A, Lutz B, Maldonado R, Ozaita A. 2009. Cannabinoid modulation of hippocampal long-term memory is mediated by mTOR signaling. *Nature Neuroscience*, 12 (9):1152-U1118.
- Rose NR, Bona C. 1993. Defining criteria for autoimmune diseases (Witebsky's postulates revisited). *Immunol Today*, 14 (9):426-430.
- Rust MJ, Bates M, Zhuang XW. 2006. Sub-diffraction-limit imaging by stochastic optical reconstruction microscopy (STORM). *Nature Methods*, 3 (10):793-795.
- Saadoun S, Waters P, Bell BA, Vincent A, Verkman AS, Papadopoulos MC. 2010. Intracerebral injection of neuromyelitis optica immunoglobulin G and human complement produces neuromyelitis optica lesions in mice. *Brain*, 133:349-361.
- Saba R, Storchel PH, Aksoy-Aksel A, Kepura F, Lippi G, Plant TD, Schrott GM. 2012. Dopamine-Regulated MicroRNA MiR-181a Controls GluA2 Surface Expression in Hippocampal Neurons. *Molecular and Cellular Biology*, 32 (3):619-632.
- Sabater L, Gaig C, Gelpi E, Bataller L, Lewerenz J, Torres-Vega E, Contreras A, Giometto B, Compta Y, Embid C, Vilaseca I, Iranzo A, Santamaria J, Dalmau J, Graus F. 2014. A novel non-rapid-eye movement and rapid-eye-movement parasomnia with sleep breathing disorder associated with antibodies to IgLON5: a case series, characterisation of the antigen, and post-mortem study. *Lancet Neurol*, 13 (6):575-586.
- Sans N, Vissel B, Petralia RS, Wang YX, Chang K, Royle GA, Wang CY, O'Gorman S, Heinemann SF, Wenthold RJ. 2003. Aberrant formation of glutamate receptor complexes in hippocampal neurons of mice lacking the GluR2 AMPA receptor subunit. *J Neurosci*, 23 (28):9367-9373.
- Sansing LH, Tuzun E, Ko MW, Baccon J, Lynch DR, Dalmau J. 2007. A patient with encephalitis associated with NMDA receptor antibodies. *Nature Clinical Practice Neurology*, 3 (5):291-296.
- Sasaki YF, Rothe T, Premkumar LS, Das S, Cui JK, Talantova MV, Wong HK, Gong XD, Chan SF, Zhang DX, Nakanishi N, Sucher NJ, Lipton SA. 2002. Characterization and comparison of the NR3A subunit of the NMDA receptor in recombinant systems and primary cortical neurons. *Journal of Neurophysiology*, 87 (4):2052-2063.

- Schmitt SE, Pargeon K, Frechette ES, Hirsch LJ, Dalmau J, Friedman D. 2012. Extreme delta brush A unique EEG pattern in adults with anti-NMDA receptor encephalitis. *Neurology*, 79 (11):1094-1100.
- Sigworth FJ. 1980. The Variance of Sodium Current Fluctuations at the Node of Ranvier. *Journal of Physiology-London*, 307 (Oct):97-129.
- Smitt PS, Kinoshita A, De Leeuw B, Moll W, Coesmans M, Jaarsma D, Henzen-Logmans S, Vecht C, De Zeeuw C, Sekiyama N, Nakanishi S, Shigemoto R. 2000. Paraneoplastic cerebellar ataxia due to autoantibodies against a glutamate receptor. *New England Journal of Medicine*, 342 (1):21-27.
- Soares C, Lee KFH, Nassrallah W, Beique JC. 2013. Differential Subcellular Targeting of Glutamate Receptor Subtypes during Homeostatic Synaptic Plasticity. *Journal of Neuroscience*, 33 (33):13547-13559.
- Sommer B, Kohler M, Sprengel R, Seeburg PH. 1991. Rna Editing in Brain Controls a Determinant of Ion Flow in Glutamate-Gated Channels. *Cell*, 67 (1):11-19.
- Sommer B, Keinänen K, Verdoorn TA, Wisden W, Burnashev N, Herb A, Kohler M, Takagi T, Sakmann B, Seeburg PH. 1990. Flip and Flop - a Cell-Specific Functional Switch in Glutamate-Operated Channels of the Cns. *Science*, 249 (4976):1580-1585.
- Theeuwes F, Yum SI. 1976. Principles of the design and operation of generic osmotic pumps for the delivery of semisolid or liquid drug formulations. *Ann Biomed Eng*, 4 (4):343-353.
- Thomas CG, Miller AJ, Westbrook GL. 2006. Synaptic and extrasynaptic NMDA receptor NR2 subunits in cultured hippocampal neurons. *Journal of Neurophysiology*, 95 (3):1727-1734.
- Titulaer MJ, McCracken L, Gabilondo I, Armangue T, Glaser C, Iizuka T, Honig LS, Benseler SM, Kawachi I, Martinez-Hernandez E, Aguilar E, Gresa-Arribas N, Ryan-Florance N, Torrents A, Saiz A, Rosenfeld MR, Balice-Gordon R, Graus F, Dalmau J. 2013. Treatment and prognostic factors for long-term outcome in patients with anti-NMDA receptor encephalitis: an observational cohort study. *Lancet Neurology*, 12 (2):157-165.
- Tovar KR, Westbrook GL. 1999. The incorporation of NMDA receptors with a distinct subunit composition at nascent hippocampal synapses in vitro. *Journal of Neuroscience*, 19 (10):4180-4188.
- Toyka KV, Brachman DB, Pestronk A, Kao I. 1975. Myasthenia gravis: passive transfer from man to mouse. *Science*, 190 (4212):397-399.
- Turrigiano GG, Nelson SB. 2004. Homeostatic plasticity in the developing nervous system. *Nat Rev Neurosci*, 5 (2):97-107.
- Tuzun E, Dalmau J. 2007. Limbic encephalitis and variants: Classification, diagnosis and treatment. *Neurologist*, 13 (5):261-271.
- van de Linde S, Loschberger A, Klein T, Heidbreder M, Wolter S, Heilemann M, Sauer M. 2011. Direct stochastic optical reconstruction microscopy with standard fluorescent probes. *Nature Protocols*, 6 (7):991-1009.
- Van Sickle BJ, Xiang K, Tietz EI. 2004. Transient plasticity of hippocampal CA1 neuron glutamate receptors contributes to benzodiazepine withdrawal-anxiety. *Neuropsychopharmacology*, 29 (11):1994-2006.
- Walf AA, Frye CA. 2007. The use of the elevated plus maze as an assay of anxiety-related behavior in rodents. *Nature Protocols*, 2 (2):322-328.
- Waterman SA, Lang B, Newsom-Davis J. 1997. Effect of Lambert-Eaton myasthenic syndrome antibodies on autonomic neurons in the mouse. *Ann Neurol*, 42 (2):147-156.
- Wenthold RJ, Petralia RS, Blahos J, II, Niedzielski AS. 1996. Evidence for multiple AMPA receptor complexes in hippocampal CA1/CA2 neurons. *J Neurosci*, 16 (6):1982-1989.

- Werner C, Haselmann H, Weishaupt A, Toyka KV, Sommer C, Geis C. 2015. Stiff person-syndrome IgG affects presynaptic GABAergic release mechanisms. *Journal of Neural Transmission*, 122 (3):357-362.
- Werner C, Pauli M, Doose S, Weishaupt A, Haselmann H, Grunewald B, Sauer M, Heckmann M, Toyka KV, Asan E, Sommer C, Geis C. 2016. Human autoantibodies to amphiphysin induce defective presynaptic vesicle dynamics and composition. *Brain*, 139 (Pt 2):365-379.
- Witebsky E, Rose NR, Terplan K, Paine JR, Egan RW. 1957. Chronic Thyroiditis and Autoimmunization. *Jama-Journal of the American Medical Association*, 164 (13):1439-1447.
- Yao YN, Mayer ML. 2006. Characterization of a soluble ligand binding domain of the NMDA receptor regulatory subunit NR3A. *Journal of Neuroscience*, 26 (17):4559-4566.
- Zhang K, Wang QZ, Jing XX, Zhao Y, Jiang HF, Du J, Yu SY, Zhao M. 2016. miR-181a is a negative regulator of GRIA2 in methamphetamine-use disorder. *Scientific Reports*, 6.

7 Appendix

Danksagung

In erster Linie möchte ich meinem Betreuer Prof. Dr. Christian Geis für die hervorragende Unterstützung bedanken, die er mir während dieser Arbeit entgegengebracht hat. Christian hat immer ein offenes Ohr für neue Ideen und jegliche Art von Problemen. Ohne seine Geduld und sein Vertrauen wäre diese Arbeit nicht möglich gewesen.

Ich möchte Prof. Dr. Klaus Benndorf für die Bereitschaft danken, sich als Betreuer meiner Doktorarbeit zur Verfügung zu stellen.

Ich danke allen Mitarbeitern der experimentellen Neurologie für das angenehme Arbeitsklima. Besonders Christian, Mihai, Lars, Josefine, Luise, Jonathan und Julius, den Mitgliedern der Arbeitsgruppe „Neuroimmunologie und Synaptopathie“, möchte ich herzlich danken. Besonderer Dank gilt Benedikt Grünwald der mir bei allen technischen und biologischen Problemen tatkräftig zur Seite stand und mich in das Feld der Elektrophysiologie eingeführt hat.

Dank gilt außerdem Claudia Sommer, Svetlana Tausch, Ina Ingrisch, Madlen Günther und Karin Schoknecht, die mich in eine Vielzahl molekularbiologischer Methoden eingelernt haben und mir in organisatorischen Fragen stets von großer Hilfe waren.

Bedanken möchte ich mich auch bei Stefan Hallermann für die Hilfe bei der Auswertung meiner elektrophysiologischen Messungen und die Bereitstellung seiner Software.

Mein Dank gilt auch allen Kooperationspartnern, die dazu beigetragen haben die Qualität der hier vorliegenden Arbeit deutlich zu erhöhen. Danke an Prof. Dr. Josep Dalmau für die Möglichkeit eines Forschungsaufenthalts in seinem Labor und an alle seine Mitarbeiter für die herzliche Aufnahme in dieser Zeit.

Besonderer Dank gilt Stephanie Graser für die seelische und tatkräftige Unterstützung, aber vor allem für die tiefe freundschaftliche Verbindung, die wir seit unserem Studium pflegen.

Zuletzt möchte ich meiner Familie für die Unterstützung und das Verständnis danken, die sie mir stets entgegenbringen.

Dem „Center for Sepsis Control and Care“ sowie dem SFB „Receptor Light“ danke ich für die finanzielle Unterstützung während meiner Doktorarbeit.

Ehrenwörtliche Erklärung

Hiermit erkläre ich, dass mir die Promotionsordnung der Medizinischen Fakultät der Friedrich-Schiller-Universität bekannt ist,

ich die Dissertation selbst angefertigt habe und alle von mir benutzten Hilfsmittel, persönlichen Mitteilungen und Quellen in meiner Arbeit angegeben sind,

mich bei der Auswahl und Auswertung des Materials sowie bei der Herstellung der Manuskripte nur die Co-Autoren - Asan Esther, Auguilar Esther, Classen Joseph, Dalmau Josep, Demir Fatih, Doose Sören, Geis Christian, Graus Francesc, Grünwald Benedikt, Hallermann Stefan, Heckmann Manfred, Jercog Pablo, Kirmse Knut, Klöcker Nikolaj, Kunze Albrecht, Maldonado Rafael, Mannara Francesco, Martín-García Elena, Pauli Martin, Petit-Pedrol Mar, Planagumà Jesús, Röpke Luise, Sauer Markus, Sommer Claudia, Titulaer Maarten, Toyka Klaus, Weishaupt Andreas, Werner Christian – der entsprechenden Manuskripte unterstützt haben,

die Hilfe eines Promotionsberaters nicht in Anspruch genommen wurde und dass Dritte weder unmittelbar noch mittelbar geldwerte Leistungen von mir für Arbeiten erhalten haben, die im Zusammenhang mit dem Inhalt der vorgelegten Dissertation stehen,

dass ich die Dissertation noch nicht als Prüfungsarbeit für eine staatliche oder andere wissenschaftliche Prüfung eingereicht habe und

dass ich die gleiche, eine in wesentlichen Teilen ähnliche oder eine andere Abhandlung nicht bei einer anderen Hochschule als Dissertation eingereicht habe.

Ort, Datum

Unterschrift des Verfassers

Circulum Vitae

Haselmann, Holger

Address: Friedenstraße 13d, 07743 Jena
Phone: +49 3641 9 396631
Email: holger.haselmann@med.uni-jena.de
Date of birth: 23/03/1985
Nationality: german

Education

Since July 2012 PhD-thesis “Pathomechanisms of AMPA receptor signalling in chronic CNS inflammation”, Supervisor: Prof. Dr. Christian Geis, University Hospital Jena
 Member of the “Center for Sepsis Control and Care Research Training Group”

March 2012 Diploma thesis in biology
 “The influence of AMPA-receptor autoantibodies on the synaptic transmission”, Supervisor: Prof. Dr. Christian Geis, Julius Maximilian University of Würzburg

June 2005 German University Entrance Qualification (Allgemeine Hochschulreife)

List of publications (* contributed equally)

Haselmann H, Ropke L, Werner C, Kunze A, Geis C. 2015. Interactions of human autoantibodies with hippocampal GABAergic synaptic transmission - analyzing antibody-induced effects ex vivo. *Frontiers in Neurology*, 6.

Haselmann H*, Mannara F*, Werner C, Planaguma J, Grunewald B, Petit-Pedrol M, Kirmse K, Classen J, Demir F, Klöcker N, Doose S, Dalmau J, Hallermann S, Geis C. in revision. Human autoantibodies against the AMPA receptor subunit GluA2 induce receptor reorganisation and memory dysfunction. *Neuron*.

Planaguma J*, **Haselmann H***, Mannara F*, Petit-Pedrol M, Grunewald B, Aguilar E, Ropke L, Martin-Garcia E, Titulaer MJ, Jercog P, Graus F, Maldonado R, Geis C, Dalmau J. 2016. Ephrin-B2 prevents N-methyl-D-aspartate receptor antibody effects on memory and neuroplasticity. *Annals of Neurology*, 80 (3):388-400.

Werner C, **Haselmann H**, Weishaupt A, Toyka KV, Sommer C, Geis C. 2015. Stiff person-syndrome IgG affects presynaptic GABAergic release mechanisms. *Journal of Neural Transmission*, 122 (3):357-362.

Werner C, Pauli M, Doose S, Weishaupt A, **Haselmann H**, Grunewald B, Sauer M, Heckmann M, Toyka KV, Asan E, Sommer C, Geis C. 2016. Human autoantibodies to amphiphysin induce defective presynaptic vesicle dynamics and composition. *Brain*, 139 (Pt 2):365-379.